CDF Study Report

GaiaNIR

Study to Enlarge the Achievements of Gaia with NIR Survey

Further information and/or additional copies of the report can be requested from:

L. Puig
ESA/ESTEC/SCI-FMA
Postbus 299
2200 AG Noordwijk
The Netherlands
Tel: +31-(0)71-5658675
Fax: +31-(0)71-5655985
Ludovic.Puig@esa.int

For further information on the Concurrent Design Facility please contact:

M. Bandecchi
ESA/ESTEC/TEC-SYE
Postbus 299
2200 AG Noordwijk
The Netherlands
Tel: +31-(0)71-5653701
Fax: +31-(0)71-5656024
Massimo.Bandecchi@esa.int

FRONT COVER

Study Logo Showing Stylised Star Shot with
Gaia Spacecraft

STUDY TEAM

This study was performed in the ESTEC Concurrent Design Facility (CDF) by the following interdisciplinary team:

TEAM LEADER			
AOCS		PAYLOAD	
COMMUNICATIONS		POWER	
CONFIGURATION		PROGRAMMATICS/ AIV	
COST		PROPULSION	
DATA HANDLING		RISK	
DETECTORS		STRUCTURES	
GS&OPS		SYSTEMS	
MECHANISMS			
OPTICS		THERMAL	

Under the responsibility of:

L. Puig, SCI-FMA Study Manager

With the scientific assistance of:

Lund Observatory, GaiaNIR lead scientist

SCI-S, Study Scientist

SCI-S, Study Scientist

With the technical support of:

OPS-GFA, Mission Analysis

SCI-ODE, Science Operations

SCI-OOO, Science Operations

IPL-IPS, Observer

TEC-EFA, Communications

SCI-PRP, former Gaia System Engineer

TEC-QQM, former Gaia PA & Safety Engineer

The editing and compilation of this report has been provided by:

TEC-SYE, Technical Author

This Page Intentionally Blank

TABLE OF CONTENTS

This Page Intentionally Blank

1 INTRODUCTION

1.1 Background

GaiaNIR (Gaia Near Infra-Red) was one of the proposals received from the D-SCI New Science Ideas call in 2016 RD[1]. Of the 26 proposals received, 3 key themes of potential interest were identified:

- Quantum physics
- Planetary science
- High-accuracy astrometry in the NIR

The GaiaNIR proposal fits into the last of these categories and is to:

- Enlarge the astrometric achievement of Gaia to the astronomical sources which are only visible in NIR
- Maintain the accuracy of the Gaia optical reference frame
- Improve the star parallax and proper motion accuracy by revisiting the astronomical sources a number of years after Gaia.

Requested by SCI-FM and funded by the General Studies Programme, the study was carried out in the ESA Concurrent Design Facility (CDF) by an inter disciplinary team of experts from ESA in 8 sessions, starting with a kick-off on the 19th September and ending with an Internal Final Presentation on the 23rd October 2017.

1.2 Objective

The objectives of the study as stated by the study customer are as follows:

- To make the GaiaNIR proposal fit the boundaries of an Medium-class (M-class) mission:
  - o ESA Cost at Completion (CaC) ≤ 550 M€[2017], covering the entire mission including the Payload Instruments (i.e. the same scope as for Gaia)
  - o Re-use of existing equipment as far as possible, with TRL ≥ 6 ("model demonstrating the critical functions of the element in a relevant environment" as per ISO scale) for mission adoption
  - o Implementation phase to last 6-7 years (after 4-5 years for Phase A/B1)
  - o Possible option for M6 or M7 (call not before 2020)
- Design a mission using a step & stare approach with conventional NIR detectors, and trade this with the NIR Time Delay Integration (TDI) detector solution suggested in the proposal.
- Identify technology development activities needed to make this mission concept feasible.

1.3 Scope and Initial Considerations

The GaiaNIR science proposal makes the case for what would effectively be a "copy" of Gaia with advanced NIR TDI instead of Visible light detectors (and the related

spacecraft design impacts on Thermal, DHS etc.) but otherwise "Gaia-like performance", to be flown some two decades later.

The study request however asked for a step & stare design that is compatible with conventional NIR detectors, rather than a Gaia-like slow-spin solution that would require TDI NIR detectors. The main reason for this is that the technical feasibility of TDI NIR detectors is questionable, and that the technology would most likely specifically need to be developed for the GaiaNIR mission, possibly at great expense.

The Gaia design and development philosophy was found not to be directly applicable to GaiaNIR, even for a slow-spin GaiaNIR solution, for the following reasons:

- GaiaNIR needs to fit inside a Cosmic Vision M-class mission budget that is well below the CaC of Gaia
- Gaia was launched with Soyuz, which at the time of GaiaNIR's tentative launch date will have been replaced by Ariane 62
- GaiaNIR would not necessarily involve the exact same Prime Contractor and Subcontractors as Gaia (although currently the sintered silicon carbide (SiC) technology required for the PLM is EADS proprietary)
- The use of NIR detectors (conventional or TDI) will have significant design impacts w.r.t. Vis detectors
- GaiaNIR does not need a Radial Velocity Spectrometer
- Some technology that was newly developed for Gaia is now available at high TRL, such as the Phased Array Antenna (PAA) and sintered SiC Optical Bench structure
- Much of the Gaia equipment will be obsolete by the time GaiaNIR will be implemented, and even some technology used on Gaia may not be maintained sufficiently long to be directly available for GaiaNIR (for cold gas micro propulsion, BAM and the PAA, for example)
- Improved technologies and equipment under development today may be available at the time of implementation of GaiaNIR
- Several Gaia "lessons learned" can/need to be taken into account for GaiaNIR, such as the origin of the stray light problem and the need for more thermal sensors on the PLM, among others.

1.4 Document Structure

The layout of this report of the study results can be seen in the Table of Contents. The Executive Summary chapter provides an overview of the study; details of each domain addressed in the study are contained in specific chapters.

Due to the different distribution requirements, only cost assumptions and qualitative results excluding figures are given in this report. The costing information is published in a separate document.

2   EXECUTIVE SUMMARY

2.1   Study Flow

The study involved 8 CDF sessions and a large number of splinter meetings, starting with a kick-off on September 19 and formally ending with an Internal Final Presentation on October 23. The first sessions focussed on system level trades as well as optical layout and detectors (type, number and arrangement on the FPA), based on which the rest of the PLM and SVM could then be designed.

A major system level trade-off was that between a true step & stare spacecraft solution and a Gaia-like slow-spin concept with a de-spin Mirror Mechanism, both potentially enabling the use of conventional detectors. The step & stare spacecraft concept was found to be unfeasible due to the far too-long time required between each observation step and the prohibitive amount of propellants needed, after which the study focussed on the design of a slow-spin spacecraft with de-spin Mirror Mechanism. No immediate show-stoppers were found for this concept, although there remain many related questions to be answered that were beyond the scope of this study.

2.2   Requirements and Design Drivers

The study objectives can be summarised as:

- To make the GaiaNIR proposal fit the boundaries of a Medium-class (M-class) mission
- Design a mission using a step & stare approach with conventional NIR detectors, and trade this with the NIR Time Delay Integration (TDI) detector solution suggested in the proposal
- Identify technology development activities needed to make this mission concept feasible.

The mission requirements for the study are listed below:

- The mission shall use NIR detectors to perform high accuracy astrometric and photometric measurements
- The nominal science operations (lifetime) of GaiaNIR shall be 5 years
- The mission and system design shall be compatible with a launch in 2035
- The satellite should be launched by a European launch vehicle
- The cost to ESA shall not exceed 550M€[2017], including:
  o Platform, Payload, System Integrator
  o Launcher
  o Operations (MOC, SOC)
  o ESA internal activities.

Identified system requirements are:

- o The astrometric measurement principle shall be based upon a continuous scanning or a step-stare mode which discretely approximates continuous scanning of the sky with at least two fields-of-view

- o The S/C shall be compatible with an Ariane 6-2/Ariane 6-4 launch vehicle
- o The S/C shall maximise reuse of existing Gaia technology with a TRL of at least 6 at the start of Phase B
- o The component of the rotation vector around the S/C X axis shall not be less than equivalent 60 arcsec/s (the goal is a nominal value equivalent to 96 arcsec/s).

2.3 Mission

A summary of the CDF GaiaNIR mission design and spacecraft concept can be found in the following tables.

Mission description		
Launch	Launcher	Ariane 6.2, Kourou
	Launch date	2035
Orbit	Orbit type	Small amplitude Lissajous orbit around Sun-Earth L2
Operations	Ground stations	ESTRACK 35m core ground stations
	Mission operations centre	ESOC
Lifetime	Nominal lifetime 5 years, plus 1 year extension.	
Overall system characteristics		
Mass	Dry mass	1891 kg, including margins, excl. adapter
	Wet mass	2253 kg, including margins, excl. adapter
		2328 kg, including margins, incl. adapter
Delta-V	278 m/s from main propulsion system, with geometrical efficiency resulting in 441 m/s.	
Dimensions	Stowed	Diameter 4.242 m
		Height 3.614 m
	Deployed (sun shield)	Diameter 10.8 m
		Height 2.9 m

Table 2-1: GaiaNIR Mission and system summary

Payload and Subsystems	
Payload	Single telescope classical Korsch configuration based on simple conics, with 2 FoV
	60 Teledyne Hawaii-2rg NIR detectors
AOCS	3-axis stabilised spacecraft
	Actuators: Cold Gas Micro Propulsion System (TAS-I/Leonardo)

	Sensors: • 2 Star Trackers (Leonardo AA-STR) • 3 Fine Sun Sensors (TNO/Bradford) • 1 Gyroscope incl. Accelerometers (Astrix 200+) • 2 Coarse Rate Sensors (Arietis-1 Innalabs)
Communications	2 X-Band Deep Space Transponder 1 RFDN 2 LGA 1 PAA (derived from Gaia PAA)
DHS	Service Module: • 1 OBC (OSCAR, from Airbus DS) • 1 RTU (from Airbus DS, with propulsion and AOCS submodules) • 1 DPU (4 video processing boards based on Xilinx Zynq Ultrascale+ System on Chip) • 1 SSMM of 8 Tbit Payload Module: • 1 ICU (4 boards with Xilinx Virtex-5QV FPGAs)
Power	28V Regulated Bus Solar panels: 8.4 m² of GaAs cells on the bottom of the SVM and Sun Shield 1 Battery, Li-ion, 144 Ah 1 PCDU, S3R (Terma Modular Medium Power Unit)
Propulsion	MON/MMH bipropulsion with • 2 x Eurostar 2000 propellant tank • 1 Helium pressurant tank • 16 x 10 N thrusters
Structure	SVM: Aluminium honeycomb panels, tank support brackets and launcher interface ring. PLM: SiC Torus and various support structures
Thermal	MLI and SLI 6.0 m² cold radiator for the FPA detectors 0.4 m² hot radiator for FEE and DHS PLM Thermal Tent Thermal Screens Thermal Straps Paints and Coatings Heaters, Thermistors and Wiring

Table 2-2: GaiaNIR spacecraft overview

2.4 Technical Conclusions and Options

The CDF study has shown that a Gaia-like slow-spin concept with a de-spin Mirror Mechanism, using conventional (non-TDI) NIR detectors, is in principle feasible and within the currently expected launch performance of the Ariane 62 to L2 via direct ascent. However, this concept exhibits several unfavourable characteristics:

- A total CaC well over the 550 M€[2017] limit set, in spite of several large cost-limiting measures such as the implementation of a single telescope instead of Gaia's two, and limiting the number of detectors to a minimum

- The incorporation of equipment with a TRL well below 6:
  - Mirror De-Spin Mechanism
  - Instrument Control Unit (ICE)
  - Data Processing Unit (DPU)

- The inclusion of a de-spin Mirror Mechanism that will inevitably result in thermal and mechanical noise, of which the impact on the quality of the scientific return remains to be evaluated

In final conclusion, there appears to be only two principal solutions for the GaiaNIR mission, both involving significant low-TRL equipment, high development and implementation risk, and potentially costly pre-developments:

- A Gaia-like slow-spin concept with a de-spin Mirror Mechanism and conventional detectors
- A Gaia-like slow-spin concept with TDI detectors.

For either case a total mission budget well over the limit for an M-class mission is to be expected; to make the mission fit within the budget constraint while maintaining sufficient scientific performance will require significant sharing of the cost with National Agencies and/or through international cooperation.

3 MISSION OBJECTIVES

3.1 Background & Lessons Learnt from Gaia

GaiaNIR (Gaia in the Near Infra-Red) was submitted as a proposed science idea following the New Science Ideas call in 2016 (https://www.cosmos.esa.int/web/new-scientific-ideas). The aim of this call was for scientists to propose new and innovative science ideas that could be relevant for future space missions within the ESA Science Programme. As a result, 26 proposals were received and from these, three key themes of potential interest emerged:

- Quantum physics
- Planetary science
- High-accuracy astrometry in the NIR.

GaiaNIR is addressing the third bullet, proposing to:

- Enlarge the astrometric achievement of Gaia to those astronomical sources which are only visible in the NIR and which have therefore not been observed by Gaia
- Improve the star parallax and proper motion accuracy of Gaia sources by revisiting them a number of years after Gaia (aiming at a possible launch ~2035)
- Maintain the accuracy of the Gaia optical reference frame by re-observing the majority of Gaia stars a few decades after Gaia (this is possible since the spectral energy distributions of the majority of Gaia stars cover both the optical and the NIR parts of the spectrum)

As this proposal is based on the Gaia mission, a main aspect of the CDF study was to benefit from the lessons learned from this mission. A summary of the main points is presented in Appendix A.

3.2 Mission Justification

Since the launch of Gaia in December 2013 and the first release of data, Gaia DR1 in 2016, more than 300 scientific papers were published using this Gaia data and Europe entered a new era of space astrometry. Gaia is the successor of Hipparcos and is two orders of magnitude more accurate in the five astrometric parameters and is also surveying four orders of magnitude more stars in a vast volume of the Milky Way.

However, both Gaia and Hipparcos operate in the optical wavelength range but much of the Galactic centre, Galactic disk, and the spiral arm regions are obscured by interstellar extinction, making objects in those regions almost invisible to Gaia and Hipparcos. To overcome this limitation, observations in the near infrared are needed, which could be provided by GaiaNIR. Thus, the main scientific motivations for this new mission are to:

1. Penetrate obscured regions and observe intrinsically red objects.
2. Obtain proper motions with ten times smaller (tbc) errors than from Gaia alone, by combining positions from two epochs with a ca. 20-year interval. In addition, the parallaxes, especially of binaries, could be much improved when astrometric data from two missions with a long temporal baseline are combined. This new

mission would also allow maintaining the accuracy of the Gaia optical reference frame that is degrading slowly over time.

3.3 Science Objectives

The science case for GaiaNIR is to build on the Gaia results of all-sky absolute astrometry for more than one billion stars. Expanding into the NIR allows to probe the dusty obscured regions of the Galaxy with high-precision astrometry.

A detailed description of the GaiaNIR science objectives is given in the GaiaNIR proposal (RD[1]).

3.4 Mission Requirements

The main mission requirements, as derived in this CDF study, are summarised in the following table:

Reference	Type of requirement	Statement
MIS-010	Payload	The mission shall use NIR detectors to perform high accuracy astrometric and photometric measurements
MIS-020	Mission duration	The nominal science operations (lifetime) of GaiaNIR S/C shall last 5 years
MIS-030	Mission timeline	The mission and system design shall be compatible with a launch in 2035
MIS-040	Launcher	The satellite shall be launched by a European launch vehicle
MIS-050	Mission cost	The cost to ESA shall not exceed €550M, including: • Platform, Payload (tbc), System integrator • Launcher • Operations (OGS, SGS) • ESA internal • Margin
SYS-010	Science operations	The astrometric measurement principle shall be based upon a continuous scanning or a step-stare mode which discretely approximates continuous scanning of the sky with at least two fields-of-view
SYS-020	Launcher	The S/C shall be compatible with an Ariane 6-2/Ariane 6-4 launch vehicle
SYS-030	Risk	The S/C shall maximise reuse of existing Gaia technology with TRL at least 6 at the start of Phase B
SYS-040	Mission operations	The component of the rotation vector around the S/C X-axis shall not be less than equivalent 60"/s. (The goal is a nominal value of equivalent 96"/s)

Table 3-1: Main mission and system requirements

3.5 CDF Objectives

The CDF was tasked by SCI-FM to perform a preliminary mission design for the GaiaNIR concept. The main objectives of this CDF study were:

1. To analyse how the GaiaNIR proposal could fit in the M-class boundaries. This required identifying which modifications need to be applied to achieve this objective with respect to technological as well as programmatic and financial aspects. For M-class missions the TRL is required to be at least 6 at the time of mission adoption; this satellite should be able to be launched in the 2035 time-frame, allowing for 4-5 years definition phase and 6-7 years implementation phase, after an M-class mission call in ca. 2020; and finally, there is a strict cost cap on these missions of 550 MEur.

2. To make a trade-off between the GaiaNIR proposal mission concept, based on the NIR TDI concept and a scanning mission, with a step-and-stare approach based on "standard" detectors. It should be noted that this was actually not part of the proposal but it became clear early on that in order to reach objective 1, a broader space needed to be explored. An additional reason for this trade-off is also that the NIR TDI detectors are considered to have very low TRL.

3. To identify technology development activities needed to make this mission concept feasible.

This Page Intentionally Blank

4   MISSION ANALYSIS

4.1   Requirements and Design Drivers

The following requirements derived from the Mission and Systems Requirements are relevant to Mission Analysis:

SubSystem Requirements		
Req. ID	**Statement**	**Parent ID**
MA-010	Sun SpaceCraft Earth angle (SSCE) of operational orbit less than 15 deg. Note: The value guarantees that the Earth is maximally 15 deg away from the boresight of the phased-array antenna, which is used for science data transmission.	MIS-010
MA-020	Stochastic residual accelerations of the S/C less than $1 \cdot 10^{-12}$ km/s^2	

Table 4-1: Mission Analysis Requirements

4.2   Assumptions and Trade-Offs

The operational orbit for GaiaNIR was a-priori defined as an orbit about the Sun-Earth Libration Point 2 (SEL2). Other orbit options were not considered for the mission during this CDF study.

The launch is envisioned on an Ariane 62 from the Kourou spaceport in French Guiana. The Ariane 62 launcher can lift more than 2,160 kg (payload + payload adapter) into the transfer orbit towards SEL2 utilising an intermediate circular parking orbit with an inclination of 15 Deg. This value has not been confirmed by the launch service provider or by numerical optimisation, but is simply based on the general statement that Ariane 62 shall be better or equivalent to the corresponding performance of a Soyuz-ST launch vehicle from Kourou, so the value stated here is the one of Soyuz-ST.

The duration of the initial powered ascent phase is about 1510 seconds, followed by an upper-stage re-orientation phase in case a specific separation attitude is required during the drift phase in the circular parking orbit. The upper stage might require the stack to spin. Then a re-orientation takes place and a second burn by the upper stage will propel the S/C stack towards SEL2.

The ΔV values presented in this Chapter are so called geometric or impulsive ΔV values. They do not take any losses into account, e.g. manoeuvre decomposition losses, ramping losses or gravity losses are not accounted for. The so called effective ΔV depends on the propulsion system design. On spacecraft with attitude limitations such a loss in efficiency can be drastic, e.g. some manoeuvre direction on the original Gaia S/C had efficiencies as low as 30 %.

In addition the ΔV values in this Chapter do not contain any margins. Applicable margins must be added to the different types of ΔV.

4.3 Baseline Design

The baseline orbit for GaiaNIR is a small amplitude Lissajous orbit about the collinear Sun-Earth Libration Point 2 (SEL2). A typical example of such an orbit is shown in Figure 4-1. Libration Point orbits are best depicted in a rotating coordinate frame. Here the x-axis is along the Sun-Earth line, the z-axis is normal to the ecliptic plane and the y-axis supplements the system to be a right-hand coordinate system. The origin of the system is located in the Earth's centre.
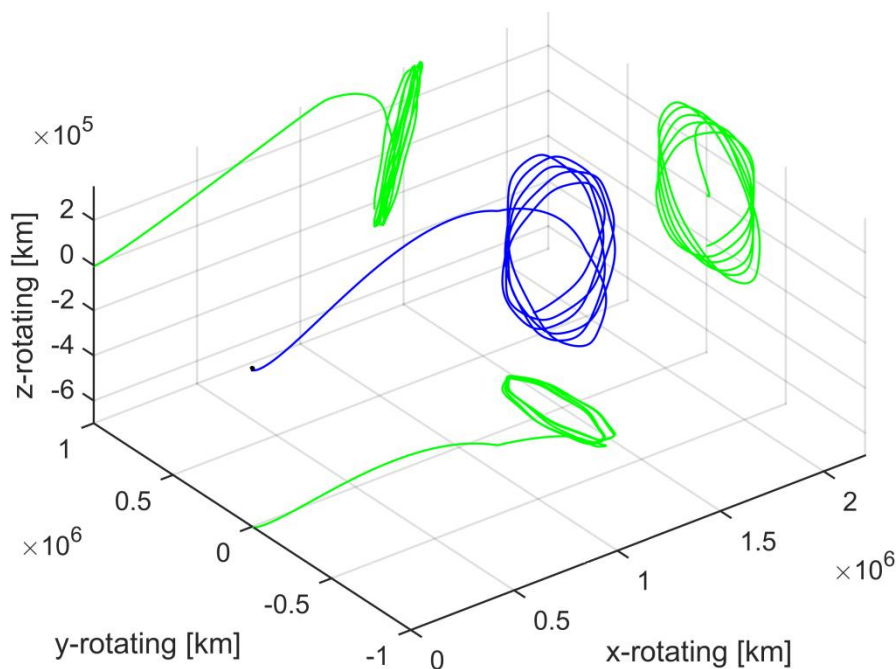
Figure 4-1 : Example of a small amplitude Lissajous orbit about the Sun-Earth Libration Point 2 (blue) and the projection on the axes (green)

The advantages of orbits about SEL2 are a constant thermal environment, since they can be designed to be eclipse free for a longer period of time, and a limited communication distance. Another advantage for astronomy missions is that the Sun, Earth and Moon are all located in one hemisphere as seen from the S/C.

Such a small Lissajous orbit cannot be reached via a so called "free" transfer trajectory and is thus requiring a deterministic orbit insertion manoeuvre after Earth departure. After this insertion manoeuvre the S/C travels on the so called stable manifold toward its operational orbit about SEL2. A typical transfer trajectory with an injection onto the stable manifold of the target orbit is depicted in Figure 4-2. The full stable manifold of the target orbit is shown. Different from large amplitude quasi-Halo orbits as e.g. used for Herschel, Lisa Pathfinder or JWST no parts of the manifold intersect with the near-Earth environment (the Earth is at the origin) and thus a free transfer injection is not possible.
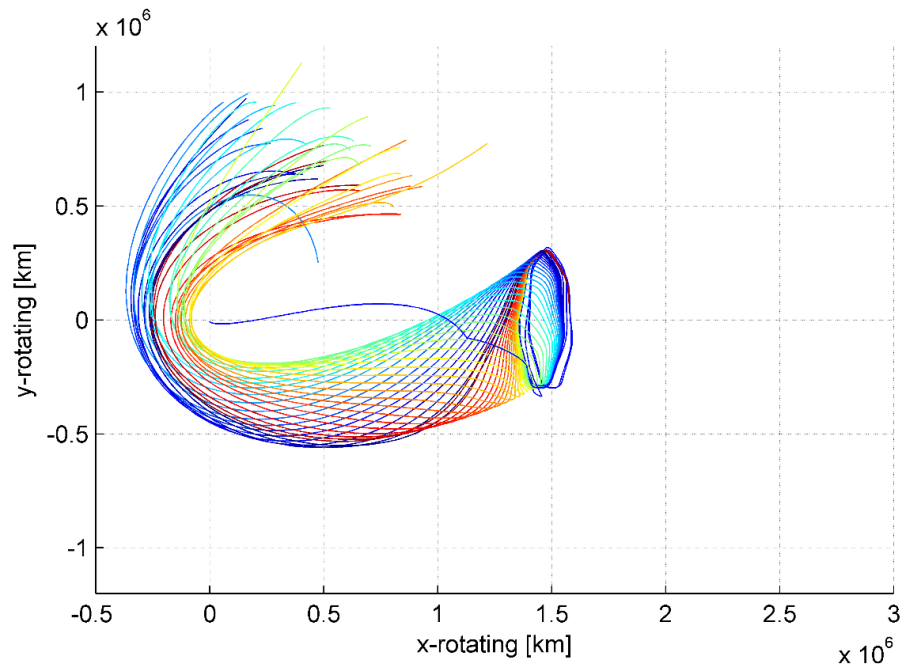
Figure 4-2: Stable manifold and transfer trajectory to an SEL2 example orbit. The transfer trajectory is the single blue line passing through the inner libration point orbit region

It is assumed that the launch vehicle will initially launch into a circular parking orbit with an inclination of 15 deg. The S/C and upper stage stack will then drift to the required departure point and a second burn will raise the apogee altitude to almost escape velocity. The drift duration in the circular parking orbit will determine the final departure argument of perigee. This allows placing the line-of-apses close to the ecliptic plane all year long, which is required to limit the orbit insertion ΔV on the S/C.

The target apogee altitude will not be the one required for an injection into an L2 orbit, but will be down-biased by the launcher dispersion to ensure that GaiaNIR only accelerates away from the Sun. This biasing of the trajectory doubles the allocation for the transfer correction manoeuvre, but the firing of thrusters into the Sun direction only prevents contamination on the payload side and also simplifies the propulsion system design.

After three transfer correction manoeuvres an injection onto the stable manifold of the operational orbit will take place. The in-and out-of-plane amplitudes (Ay and Az) of the SEL2 orbit are then not prescribed, but depend on the launch date and launch hour. The size of a SEL2 orbit is often described by the so called Sun-S/C-Earth angle (SSCE). For GaiaNIR a SSCE angle of 15 deg shall not be exceeded. This simplifies the antenna design and also prevents straylight issues for the selected Sun Aspect Angle (SAA) of the S/C (angle between the Spin direction of the S/C and the Sun direction as seen from the S/C).

For 3-axis stabilised missions as Athena/Herschel/Euclid/Plato/Ariel/JWST there is usually no strict constraint on the SSCE angle, however, for many missions an upper limitation of 33 deg SSCE has been proposed to limit design parameters as e.g. the

maximum declination with respect to the Earth's equator, which is important to ensure visibility from ground stations (GS) in the Northern and Southern hemisphere.

For GaiaNIR, solutions with an eclipse in the transfer trajectory are excluded from the launch window. The reached SEL2 Lissajous orbit is eclipse free for about 5.5 year after which an eclipse avoidance manoeuvre is required.

With a fixed launcher program the perigee velocity of the transfer orbit is also fixed. However, for each day of the year the optimal transfer requires a specific perigee velocity. In addition the launcher has a certain dispersion in the final osculating perigee velocity. The S/C will therefore initially not travel on the correct trajectory to reach the stable manifold of the Lissajous orbit and thus a small manoeuvre is required to correct the S/C attitude and put it onto the correct transfer trajectory. This manoeuvre is time critical and is thus performed as soon as possible after the launch. In order to have enough time to track the spacecraft and estimate the state vector an execution 24 hours into the mission is envisioned, but to account for any problems with the S/C or ground segment an execution on day-2 (48 hours into the mission) is budgeted. Inaccuracies in this manoeuvre will be corrected on day-5 and day-20. The third manoeuvre concludes the transfer navigation prior to the operational orbit insertion manoeuvre.

The orbit insertion manoeuvre is usually split into two parts to again account for manoeuvre execution errors. The two manoeuvres are executed separated by about a week. The S/C can now be assumed to be on the SEL2 orbit, where station-keeping continues.

The SEL2 operational orbit is inherently unstable and requires regular but small maintenance manoeuvres. The total ΔV allocated for the orbit maintenance manoeuvre depends on the station-keeping interval and the capability of the AOCS to deliver pure torque or torque only together with a change in the spacecraft's velocity.

Station-keeping manoeuvres are assumed in the unstable direction of the linear theory. This direction is depicted in Figure 4-3.
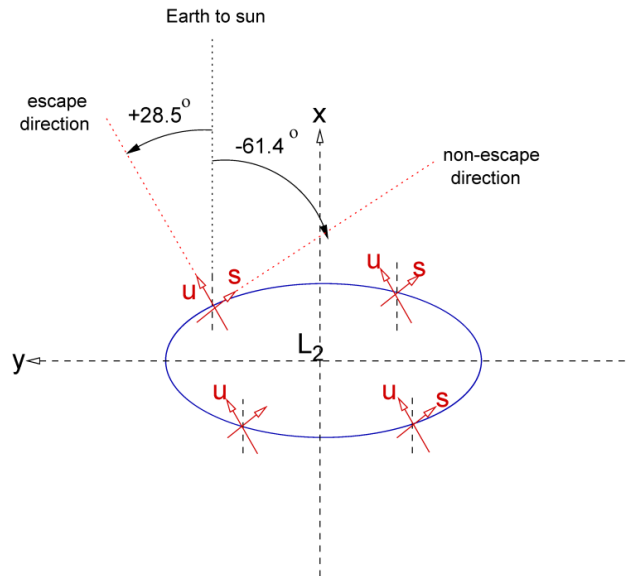
Figure 4-3: Stable and unstable direction derived from linear theory for station-keeping considerations

A typical station-keeping ΔV evolution example is provided in Figure 4-4. The yearly station-keeping ΔV highly depends on the residual accelerations of the S/C. To be more precise, it depends on the unknown residual acceleration of the S/C, since known components can be taken into account, similar to the solar radiation pressure. The difference in the allocation can easily be different by orders of magnitude. E.g. the largest station-keeping manoeuvre of Herschel was larger than the station-keeping allocation of Gaia for an entire year. Gaia, being a spinning S/C, had well predictable residual acceleration, while the attitude of 3-axis stabilised Herschel could by definition not be known a-priori.
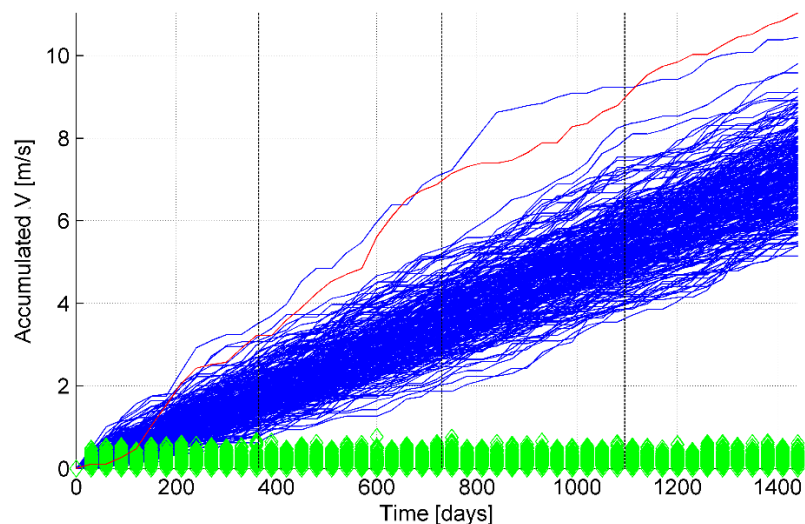
Figure 4-4: Example of station keeping ΔV evolution for 4 years. The blue curve shows the accumulated ΔV and the green diamonds indicate the size of each individual station-keeping manoeuvre. The red curve depicts the worst case trajectory out-of the monte-carlo simulation set

4.4 Budgets

ΔV budget will strongly depend on assumptions for the Launcher dispersion, affecting the first transfer correction manoeuvre TCM#1. There is currently no data available for a launch on Ariane-62, but it is assumed the launcher is equal or better than the Soyuz launcher used for Gaia.

A further point which can significantly affect the ΔV budget are the residual accelerations of S/C in operational orbit as discussed above in the station keeping section. These residual accelerations excite the unstable component of the libration point orbit that need to be cancelled by the station-keeping.

The thruster layout together with attitude constraints can also significantly affect the ΔV as well as the propellant budget. A biasing of the trajectory as for Gaia and assumed for GaiaNIR doubles the ΔV allocation for the transfer correction manoeuvres. Only the station-keeping manoeuvres were small enough to be executed with a ΔV into the Sun direction. On Gaia attitude constraints caused ΔV efficiencies as low as 30% and thus significantly more propellant needed to be carried on the S/C to achieve ΔV vectors in specific directions.

Manoeuvre	ΔV (m/s)	Comment
Launcher Dispersion and Perigee velocity correction	70	Doubled compared to a "nominal" injection due to required biasing of the trajectory
Midcourse corrections	20	Doubled compared to a "nominal" injection due to required biasing of the trajectory
Orbit insertion manoeuvre	165	Reduction of the SSCE to <= 15 Deg
Station-keeping	11	5.5 years (highly depends on residual accelerations and only valid for Gaia design)
Eclipse avoidance	15	Required after 5.5 years
Disposal	0.5-max.	10 m/s minimum suggested, no requirements

Table 4-2: Gaia ΔV budget also applicable to GaiaNIR

5 PAYLOAD

5.1 PLM Optics

5.1.1 Introduction

The initial request for the optical concept of GaiaNIR was for an instrument similar to Gaia but with a reduced field of view, a split entrance pupil, a shared image plane and individual entrance pupil areas of about 50% of Gaia's. The suggestion was to explore a concept similar to the Hipparcos optics, in which a single telescope looks at two different directions in the sky by means of a split mirror at the entrance pupil RD[2]. In the Hipparcos design this was easily achieved because the Schmidt telescope has a remote entrance pupil at the centre of curvature of the mirror where the corrector plate is placed. In the classical Schmidt design, the corrector plate is a refractive component, but it can be replaced by a tilted mirror with the aspheric shape adapted to the non-radially symmetric use.

The concept presented for GaiaNIR is based on a Korsch telescope, as it is in Gaia, which is also an off-axis system. But it differs from Gaia with regard to two important optical features described below. These advantageous features are possible because of the reduced entrance pupil and size of the field of view, together with the longer wavelength of operation:

The mirror surfaces are simple conics. This simplifies manufacturing alignment and test.

The entrance pupil is at the flat folding mirror in front of the primary instead of on the primary mirror itself. This does not have a significant effect on image quality.

Gaia's mirrors are conics with high order aspheric coefficients and used off axis, which made manufacture and test of these elements very challenging.

Note that the aim of the design presented here is not to give a definitive solution for the telescope which complies with all the requirements of GaiaNIR, as this would be an impossible goal given that further refinement will be required following the CDF study. Instead, it is intended to identify a viable starting concept with the potential to be the ultimate design solution. This is why only one single optical concept has been downselected and evaluated. In addition, the performance of the proposed optical design is quite close to compliance with the requirements. It will also be easy to add new degrees of freedom and improve the design if necessary (e.g. aspheric coefficients on some of the mirrors).

It must be mentioned at this point that there are aberrations in the design that might require additional optical surfaces for correction, such as is the case for the image-rotation-compensation induced defocus. This assertion will be explained in a dedicated section.

A final important remark is that during the CDF study, it became clear that there was the need for an additional optical requirement which did not appear in the original set. This is that there shall be a real and accessible pupil image. There are two reasons for this: one is the desire to potentially accommodate a sky mapper, the other is to

compensate for the spinning spacecraft, which like Gaia spins at 1 revolution every 6 hours, driven by its observing strategy. This demands an internal de-rotation of the sky image with a scan mirror. The de-rotation of the image is necessary to comply with the detector characteristics and to avoid (or simplify) the associated technology developments. In contrast with the Gaia detectors which use a Time Domain Integration (TDI) to track stellar images as they move across the focal plane, the NIR detector technology proposed for Gaia-NIR does not have this capability.

The sky mapper concept is based on a relative shear of the two fields at the detector and requires a splitting of the light where it is physically separated, thus at a pupil image (see Figure 5-5, Figure 5-12 and Figure 5-13 below for illustrations of how this concept works). The de-rotation is realised with an internal scanning mirror, which should be at a pupil image in order to avoid vignetting and lateral movements of the image footprint on the detector as a function of the pointing angle on the sky, which occurs in any optical scanning system. Fortunately, the concept selected has a real and accessible pupil, as this was already needed to combine the two fields of view of the telescope onto a single focal plane.

5.1.2 Telescope Requirements: Starting Point and Evolution

The initial requirements were based on one telescope with two fields of view on the sky which shared a common image plane (detector). It was suggested to use the Hipparcos concept with a split folding mirror at the entrance pupil making use of two plane mirrors pointing in two different directions on the sky.

For each pointing direction field of view, the initial requirements were as follows:

- Entrance pupil area should be equivalent to 720 x 520 mm²
- FoV: smaller than 1.4º x ± 0.7º (total)
- Effective Focal Length (EFL): similar to Gaia (about 35 m)
- Image quality: PSF as in Gaia but for longer wavelengths (TBD) and low image field distortion.

There was an evolution of these requirements during the CDF (mainly related to entrance pupil shape, FoV and EFL) and new requirements appeared. The final set used in the design is the following:

- Entrance pupil area should be equivalent to 1600 x 250 mm²
- Long side of entrance pupil in the direction of sky rotation
- FoV: 0.6 º x 0.47º
- EFL: 35 m
- Image quality: PSF as in Gaia but for 900 nm and small field distortion
- Compensation of sky rotation over 2 arc min by internal scanning (translates into accessible and real image pupil)
- Inclusion of a sky mapper
- Low field distortion.

Special attention should be paid to the image quality requirements. In the course of the CDF, the requirements for spatial resolution were not completed. It was required to

have a diffraction limited PSF at 900 nm in order to ensure that the PSF scales by a factor 2 at 1800nm. However, there is still an uncertainty about what the PSF at shorter wavelengths should be. It is unclear how this uncertainty impacts the rest of the system. The detector design and performance for a minimum increase in pixel numbers, and therefore read out noise and read out frequency over the wavelength range, can be affected. The risks associated with having a PSF requirement below 900 nm are not yet fully considered, for example having a PSF that is not adequate to meet the science requirements over the full NIR operational spectral bandwidth.

5.1.3   Trade Offs

In order to select a viable design concept for evaluation, an initial trade-off between four possible off-axis configurations was made, in which the starting pupil dimensions were used. These four configurations are represented as simple pupil projections in Figure 5-1

Originally, configuration 1 was selected on the basis of image quality, volume and compactness considerations. It is useful to check how the two beams from each entrance pupil direction on the sky merge or separate as they propagate through the Korsch telescope, in order to understand the design of the sky mapper as presented later. This can be done by looking at the footprint of the light paths from several field objects on the telescope mirrors and pupils, as depicted in Figure 5-2.
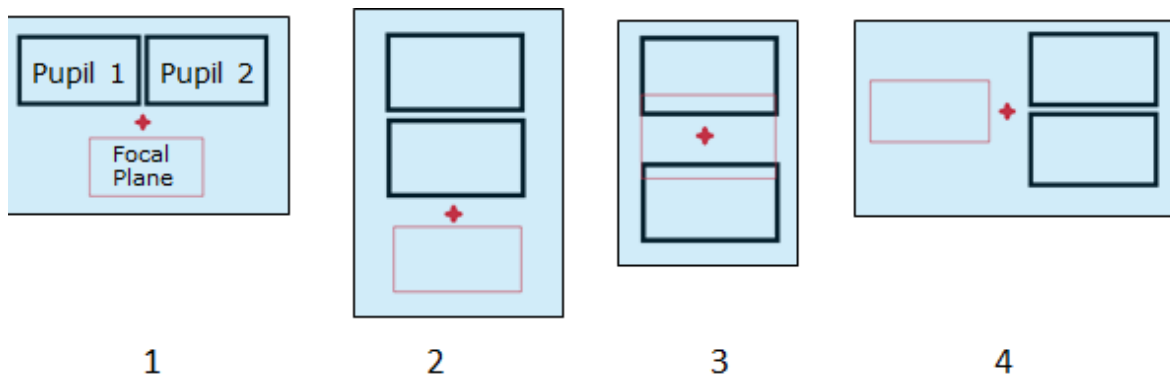
Figure 5-1: The four different off axis configurations used in the trade off. The black rectangles represent the two entrance pupils, the red cross is the axis of symmetry of the telescope mirrors and the red rectangle is the detector

Primary Mirror M1 | Secondary Mirror M2 | Tertiary Mirror M3 | Exit pupil | Focal plane
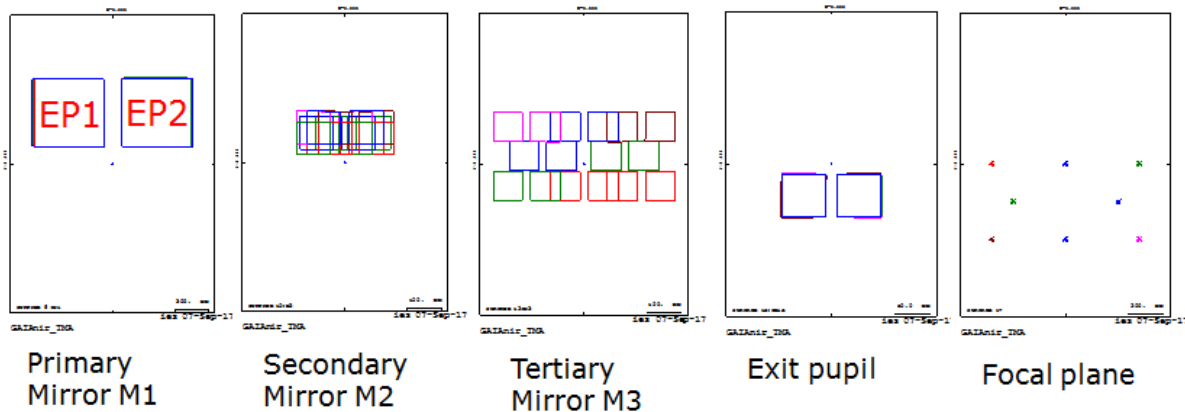
Figure 5-2: Evolution of the shape and overlap of the optical beam footprints of the light from several field objects as they propagate through the telescope mirrors from the separate entrance pupils to the focal plane. This corresponds to the originally adopted concept of option 1 in Figure 5-1 above.

In the end, however, the selected baseline had to be changed from configuration 1 to 2 when the entrance pupil shape was revised to be 1600 x 250 mm². The projection of the pupils, telescope axis of symmetry and detector positions for this final selection are shown in Figure 5-3. It should be noted that the resulting overall telescope geometry of configuration 1 and configuration 2 remained basically the same when the entrance pupil shape was changed, which makes the achievable image quality very similar in both cases.
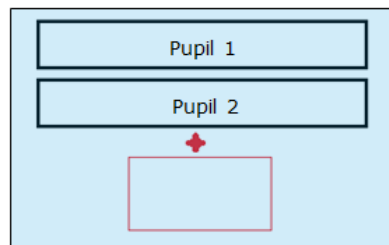
Figure 5-3: A projection of the entrance pupils and detector relative positions for the selected GaiaNIR off axis design configuration finally chosen (Option 2). Black rectangles represent the two entrance pupils, the red cross is the axis of symmetry of the telescope and the red rectangle, the detector

5.1.4 Sky Mapper

The sky mapper is a part of the instrument used to image the individual fields of view, in order to identify the target stars to be used in each astrometry (science) field. It requires that each image is focussed on two different detectors. That is the concept used in Gaia. It was requested to study and evaluate the impact on the Gaia-NIR telescope design of implementing this additional optical channel RD[3]. The optics needed therefore to be modified with respect to that of the basic astrometric telescope. These sky mapper images must have the same plate scale (e.g. telescope of the same focal length) and brightness (e.g. telescope entrance pupil area) as the science images.

Three possible solutions were considered and evaluated:

1. A completely independent optical system.
2. Separation of the two fields at the intermediate focus of the Korsch configuration.
3. Separation of beams at the exit pupil of the Korsch configuration

The first option was discarded as the required optics would be an independent telescope of similar entrance pupil area, and so with identical or very similar dimensions as the astrometric telescope. This could not be physically accommodated.
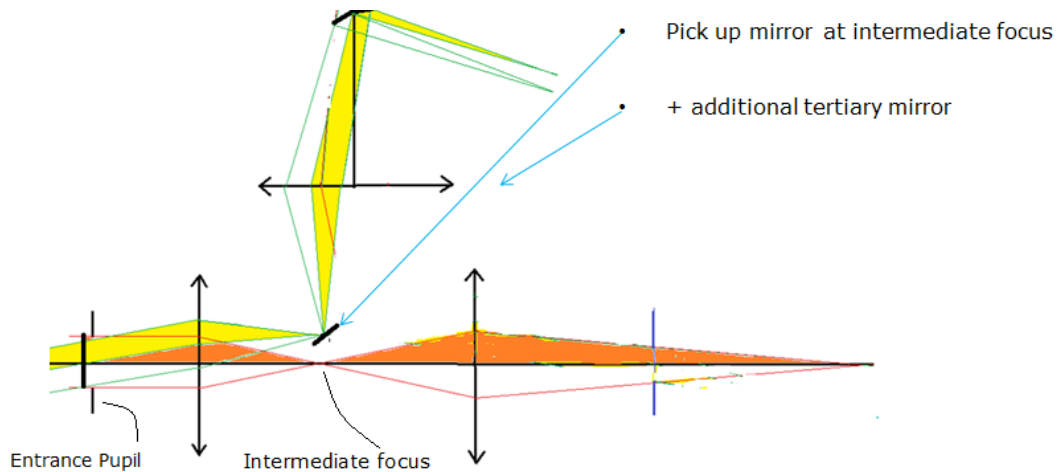
Figure 5-4: Diagram of a thin lens representation of the second sky mapper design

For the second option some optical elements of the Korsch telescope need to be duplicated and some new ones added. This can be seen in the thin lens equivalent representation of the telescope in Figure 5-4. The horizontal beam (orange rays) corresponds to the science (astrometry) path and the folded beam (green rays) with the sky mapper. The beam going through one of the entrance pupils is colourless whereas the beam through the other entrance pupil is highlighted in colour, with yellow for the sky mapper and orange for the astrometry/science channel.

The optical elements in the figure are: the first lens behind the entrance pupil is equivalent to the primary and secondary mirrors of the Korsch telescope yielding an intermediate focus, the second thin lenses in both optical paths are equivalent to the tertiary mirror of the Korsch telescope with the exit pupil and the image planes behind them. A flat pick off mirror (added to the Korsch) at the intermediate focus separates that part of the field to be imaged, on to the sky mapper detectors through a separate thin lens (duplication of the tertiary mirror). At the sky mapper channel exit pupil, the beams from the two sky directions are physically separated, which makes it possible to put two mirrors there and send the light in separate directions to reach two individual detectors, just the opposite of what is done at the entrance pupil.
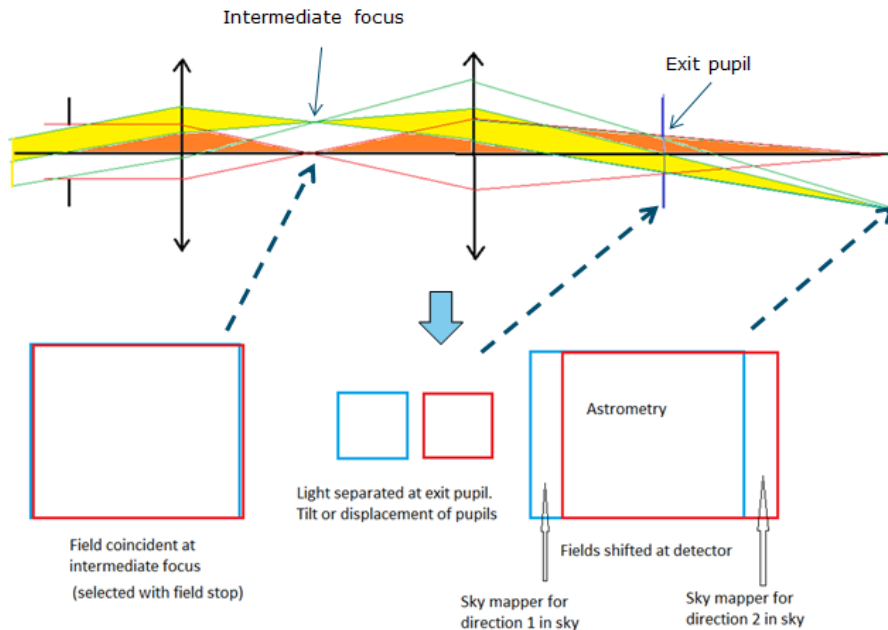
Figure 5-5: Diagram of thin lenses representing the third option of the sky mapper design. See also Figure 5-12 and Figure 5-13 below

In the third option (see Figure 5-5) the science and sky mapper beams share all the optical components up to the detector. As in the second option, two mirrors placed at the images of the entrance pupil mirrors send the light in two directions. Now, both science and sky mapper beams from one pupil (that is to say one direction on the sky) are separated from the other. The separation arranged is such that at the image plane, part of the field of view of the two pupils overlap (the astrometry/science detectors), and part does not (the sky mapper detectors). This is illustrated on the lower right of Figure 5-5, by the overlapping but displaced blue and red rectangles.

It should be noted that if this separation of the light from the two pupils is done with a single reflection, the image planes are tilted with respect each other, thus a defocus is introduced. A second reflection can correct this tilt and defocus while still shifting image surfaces with respect to each other.

The third option was finally chosen as a viable baseline for the sky mapper channel. However it was not implemented in the current Gaia-NIR telescope design (see Appendix B).

5.1.5 Telescope Design Concept

As mentioned in the introduction, the telescope baseline design chosen is a Korsch configuration with the entrance pupil some distance in front of the primary. As well as the three powered mirrors of the basic Korsch, three flat mirrors are added in the light path for each pupil. These are: a mirror at the entrance pupil to point in the chosen sky direction, a mirror at the exit pupil with a scanning mechanism, and a folding mirror after the exit pupil located to the side of the Korsch tertiary mirror to make the overall mechanical envelope more compact. From the last flat mirror the light can be folded into a convenient direction so that the detector focal plane array may be adequately and conveniently integrated within the telescope structure. Figure 5-6 shows the top and

side views of the optical system ray trace and Figure 5-7 shows two different 3D views of the system.
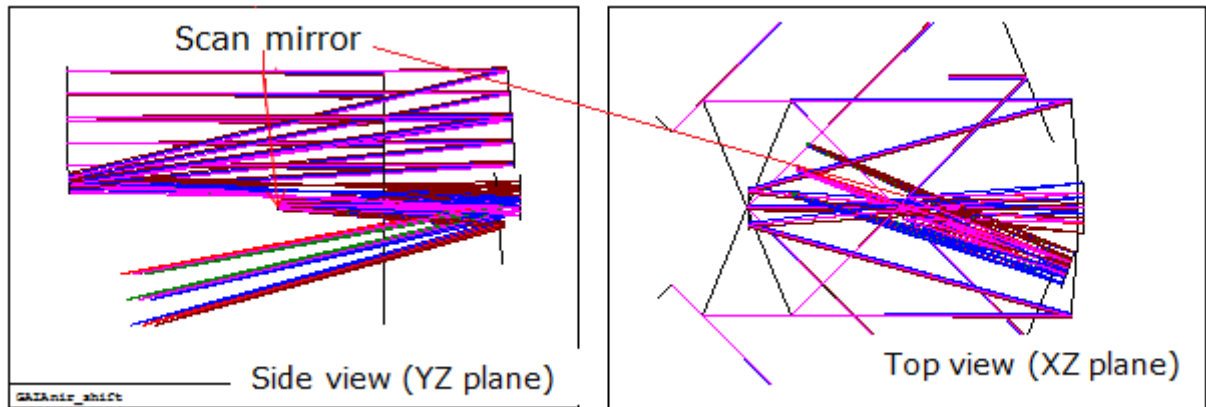
Figure 5-6: Top and side views of GaiaNIR baseline telescope
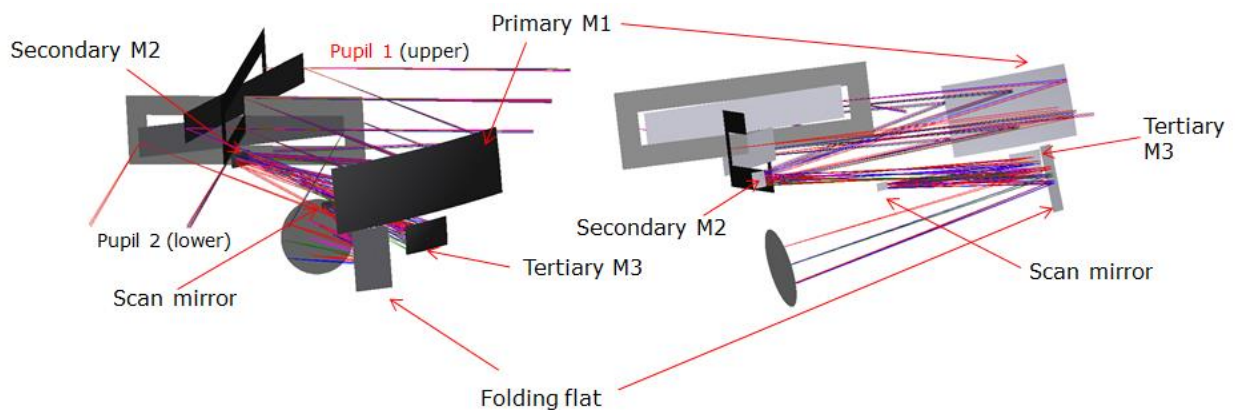
Figure 5-7: Two 3-D views of GaiaNIR baseline telescope

The basic characteristics of the final telescope design are:

- Effective Focal Length = 35.173 mm
- Entrance Pupil 1600 x 250 mm² (each pupil)
- Field of View 0.6º x 0.47º
- Scanning => compensation of sky rotation 0.036º (2.16')
- Design (diffraction limited) wavelength = 900 nm

The flat mirror at the exit pupil can be used as a scanning mirror. De-rotation of the image movement on the detector due to the S/C rotation is then possible to some extent. The limitations of this correction are related to different effects at the image plane. Rotation of the S/C translates into a simple movement (translation of the stars across the FoV) without changing the location of the image plane, whereas a scan mirror at the exit pupil moves the image plane while also introducing a tilt with respect to the

detector and therefore it induces an angle dependent defocus. For a moderate field of view the defocus may be within the performance tolerances, but it remains to be evaluated in detail to what extent. The effect on the PSFs has been assessed here (Figure 5-8, Figure 5-9 and Figure 5-10), but there will also be an effect with respect to location across the field (distortion), which is an important requirement for Gaia- NIR, although no numerical value has yet been specified (Figure 5-11). If the defocus due to image surface tilt or distortion have to be corrected, it will be necessary to add another (re-imaging) telescope behind the exit pupil which would consist of one or more powered mirrors.

An alternative more obvious starting point would be an afocal telescope system with a real and accessible pupil image (e.g. Korsch or Gregorian configurations) yielding a collimated beam at its exit pupil, with a scanning mirror there and another telescope behind that to focus the light onto the detector.

Scan central position
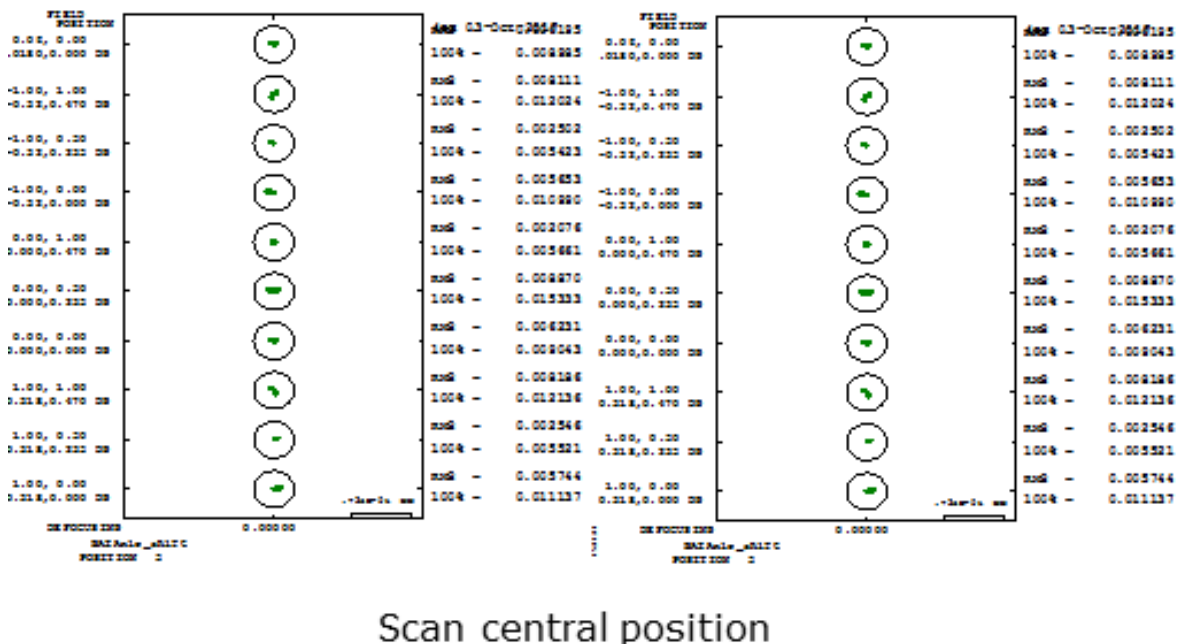
Figure 5-8: Spot diagrams for field objects in two sky directions, each corresponding to one entrance pupil. The small black scale circles are the diffraction limit of a circular aperture of 1.6m for 900nm wavelength. The scanning mirror at the exit pupil is at the centre of its range
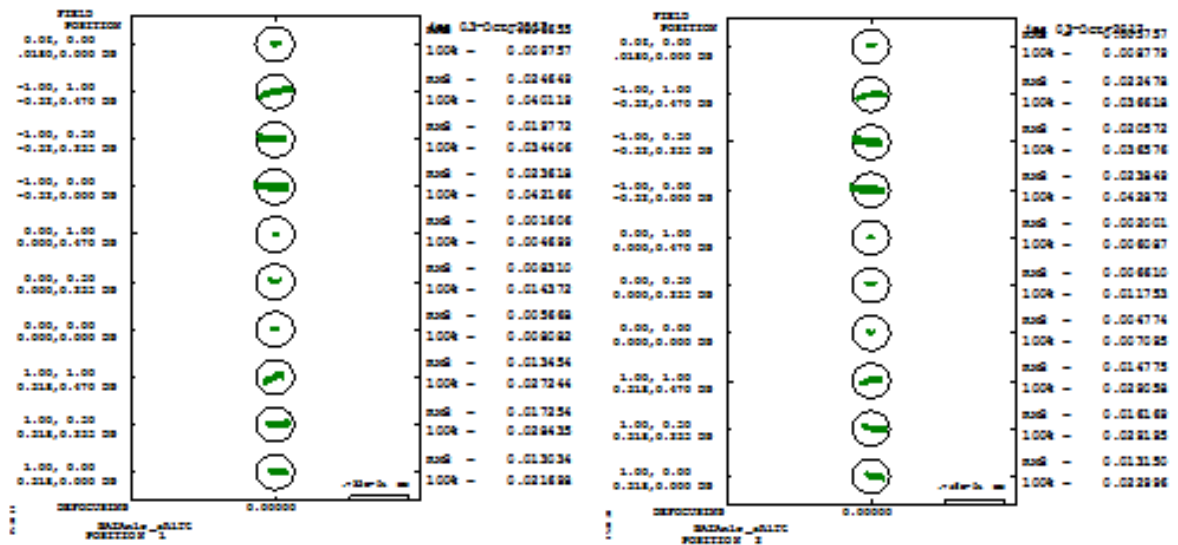
Scan start

Figure 5-9: Spot diagrams for field objects in two sky directions, each corresponding to one entrance pupil. The small black scale circle is the diffraction limit of a circular aperture of 1.6m for 900nm wavelength. The scanning mirror at the exit pupil is at the beginning of its range
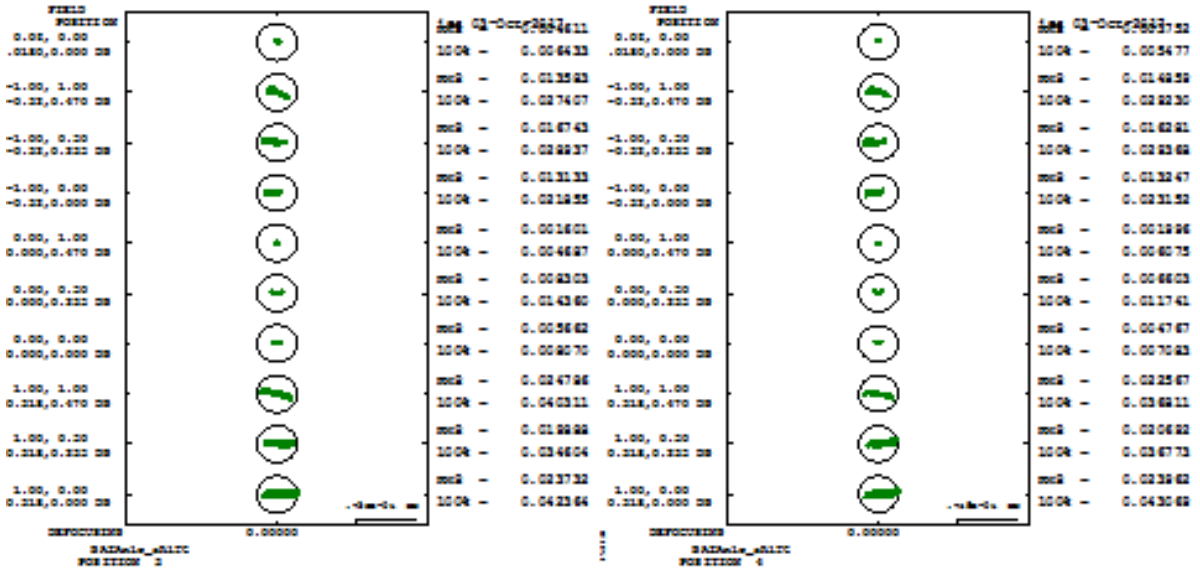
Scan end

Figure 5-10: Spot diagrams for field objects in two sky directions, each corresponding to one entrance pupil. The small black scale circle is the diffraction limit of a circular aperture of 1.6m for 900nm wavelength. The scanning mirror at the exit pupil is at the end of its range
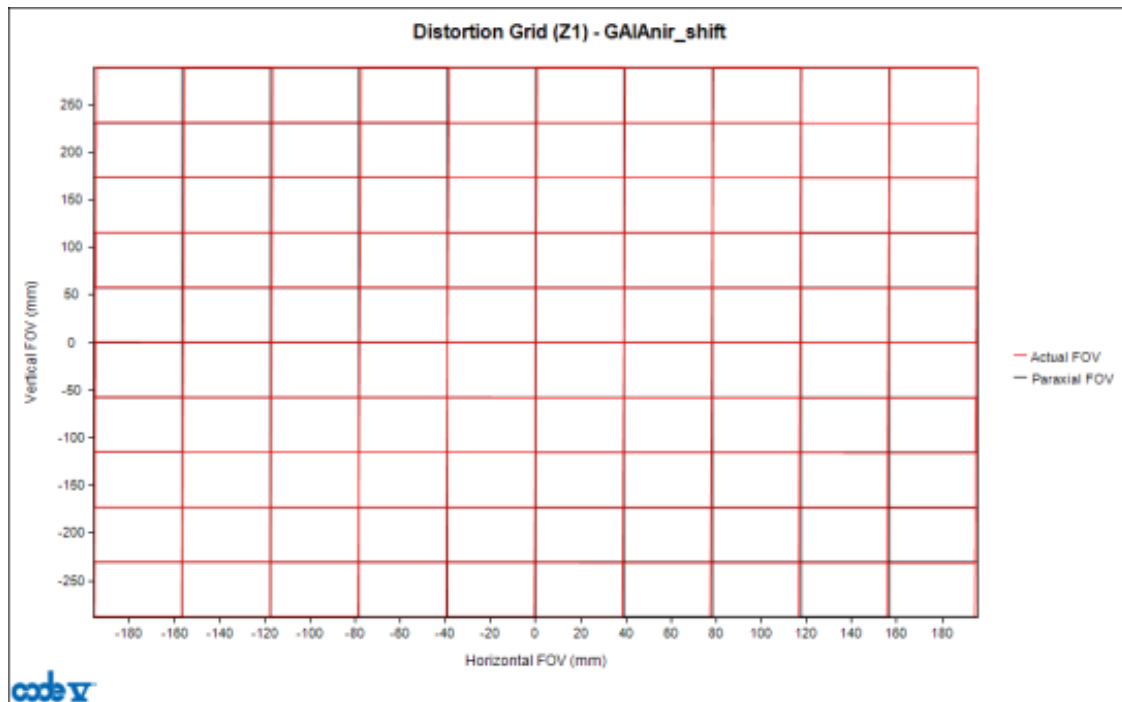
Figure 5-11: Distortion map for GaiaNIR FoV

As mentioned above, the Gaia-NIR baseline telescope optical design does not contain a sky mapper. To include it, the scanning mirror and the flat folding mirror in front of the detector must be split in two. At the exit pupil, the light is deflected in two directions so that the image surfaces are displaced. This introduces a relative tilt between the image surfaces and thus also a defocus, this is illustrated in Figure 5-12. Those tilts can also be corrected by using two additional folding mirrors near the detector, as shown in Figure 5-13. In this way the image surfaces are made coplanar, but are laterally displaced.
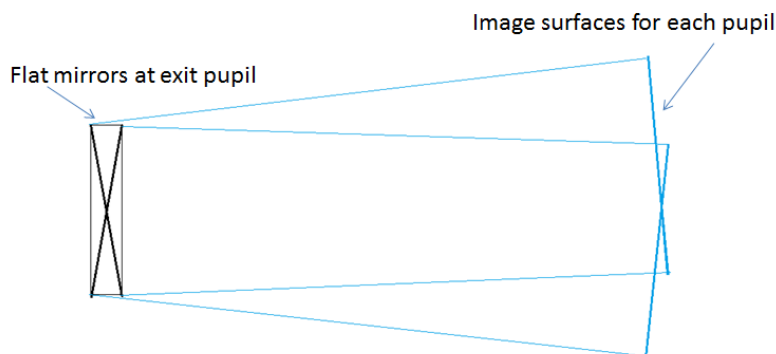
Figure 5-12: Sketch of separation the light beams from each pupil with two mirrors. Only top view is shown. Blue lines represent the envelope of the light paths. Relative tilt of image surfaces is apparent
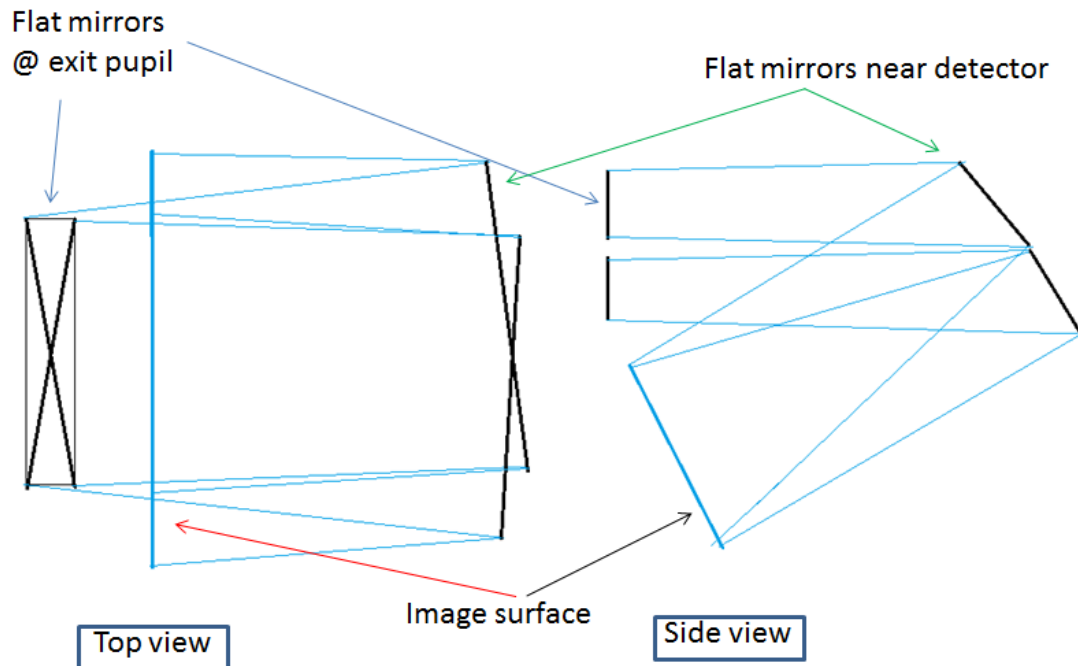
Figure 5-13: Correction of the tilt of the image surface due to the two mirrors at the exit pupil shown in Figure 5-12. Top and side view are shown. Blue lines represent the envelope of the light paths. There is no relative tilt of image surfaces but they are shifted

The final telescope optical design prescription is presented in Appendix C.

5.1.6 Optical Subsystems

There were two additional optical subsystems discussed during the study; a Basic Angle Variability (BAV) monitoring and metrology system – the BAM (SCI-300 310 & 320) RD[20], and an at least 4 band stellar spectral class photometric detection capability (SCI-330 through SCI-510) RD[20]. These are discussed here separately.

5.1.6.1 Basic Angle Monitor

One of the critical instrument parameters for the astrometric solution for the measured stellar positions to be retrieved, is the so called "basic angle" stability. This is the small variation in time of the lines of sights between the two telescope entrance pupils. The top level science requirements SCI-300, 310 and 320 make this requirement mandatory and demand an accuracy of 0.5 micro arc seconds, with a 5 minute sampling period covering the entire full circle scans on the sky.

In Gaia this is measured using an internal optical metrology subsystem called the Basic Angle Monitor (BAM) RD[4]. The Gaia BAM achieves sub micro-arc second resolution in flight which is sufficiently accurate also for GAI-NIR. Another technological concept based on absolute distance measurement, between the two entrance pupil plane mirrors, using a laser frequency comb was discussed and rejected RD[5], & RD[6], as the technology is not yet mature enough, and only relative motion is required.

The GaiaNIR simpler optical system design solution, as compared with Gaia, based around a single telescope with a split entrance pupil, could make the flow down from the Basic Angle scientific requirements to engineering specifications somewhat less demanding. But the shorter total effective optical lever arm between the entrance pupil mirrors (the pointing of which define the two lines of sight) and their projection onto the primary mirror where the beams are combined onto a single common optical element, may reduce both the sensitivity of the system but also the precision with which the BAM variation can be determined. The details of the BAV requirements were not explicitly studied during the CDF, but the need for such a monitoring system is undisputed, given the importance of the Basic Angle parameter and its stability for the astrometric solution, regardless of the specifics of the system design. Therefore, it was concluded that the known flight qualified BAM technology from Gaia be retained as a viable solution for GaiaNIR. While the BAM metrology principles and technique are well known, well understood and flight proven to work, obviously the specific engineering implementation on GaiaNIR will need to be worked out, and most likely will be less complex and therefore easier to implement. The only potentially challenging new requirement is the need to monitor the BAV over the entire astrometric field of view (SCI-320).

5.1.6.2   Photometric

One of the science requirements is to identify the spectral class of the stars being measured. This necessitates the spectral filtering of the stellar images into at least 4 separate photometric bands within the astrometric field, see Figure 7-5. Two methods were evaluated. Using focal plane filters or tuning the spectral response of the detectors with respect to their positions within the focal plane. This second option seemed at the beginning like the logical and most straightforward, and optically preferable, choice. However the maturity of the detector technology and the associated costs with developing and implementing such bespoke tuning of the detector responses was considered prohibitive, and without any guarantee of success. The inclusion of focal plane filters was then the remaining solution. Great care shall nevertheless be needed to be taken in their design, fabrication and testing.

5.2 PLM Detectors

5.2.1 Requirements and Design Drivers

Subsystem Requirements		
Req. ID	Statement	Parent ID
1	Readout noise of <12e- at 300kHz readout frequency for non TID detector	Performance model
2	QE>70 % over 400 nm – 1800nm	Performance model
3	Dark current: <10 e-/pxl/s for a 18*18um pixel pitch	Performance model
4	Pixel size (µm): 20*128	Performance model
6	The staring time is 1.62s	AOCS

5.2.1.1 Requirements explanations:

Req.ID 1: the value indicates a target value for a non TID detector since, without TID the readout noise is summed for all pixel read. The mission GaiaNIR is readout noise limited as shown in the performance chapter. It limits the performances on faint target where the readout noise become limiting.

Req.ID 2: The written value (80%) matches with the value used in the performance chapter. This value is realistic over the range 800-1800nm, not clearly known between 400nm and 800nm.

Req.ID 3: As shown in the performance model chapter, the dark current plays a minor role in the science output and can be relaxed up to 10 e-/pxl/s for a given pixel size of 18*18um.

Req.ID 4: the optimal pixel size is 20*128 pixels but this value does not match with any off-the-shelves detectors pixel size. The performances model chapter shows a sensitivity analysis to the pixel size.

Req.ID 6: the staring time value was computed from the AOCS chapter given the chosen de-spin mirror mechanism options.

5.2.2 Assumptions and Trade-Offs

The trade-offs of the different detectors available is presented in Table 5-1. The colours are chosen in comparison to the requirements. The green, orange and red colours mean respectively, compliant, almost compliant, not compliant to the requirements. The associated astrometric performances can be found in the Performance chapter.

The best astrometric performances with existing detectors performances is achieved using the American Hawaii-2rg or the European ALFA detector. Unfortunately, the pixel size, the buttability and the smaller format of the actual ALFA detector (a new format of 2048*2048 pixels of 15um pitch, 3 side buttable will be available in end 2019) push the choice for baseline to the Hawaii-2rg detector with the current state of the detector performances.

The APD detector, with a sub electron readout noise is very promising technology with the limitation of decreasing the dark current (if we want to operate the detector above 100K), extend the response down to 400nm and increase the detector format. Increase the detector size format is possible as a future technology development. Extend the response down to 400nm is managed by removing a part of the detector substrate allowing visible light to be detected. It is possible for some manufacturer (CEA/LETI) but incompatible for other (Leonardo). Decreasing the dark current needs an intense technology material development as the trap assisted tunnelling is the actual limiting effect.

Parameters	Requirements	Teledyne, US: Hawaii	Sofradir, FR: ALFA	Sofradir, FR: NGP	AIM, GE, SWIR	Leonardo, GB: Saphira, APD used as gain of 1	Rapide, Sofradir,FR APD
Readout noise	<12e- CDS at 300Khz	Slow (<300KHz) <18e- Fast (>500Khz)≈ 80 e-CDS	Slow ≤ 18 e-CDS Fast :unknown	Slow :<170 e-rms (141e-measured in average) @ 170K Fast :unknown	Slow: 120 e-	Fast: 2 e-(TBC)	Slow: 1.5 e-at gain 30
QE Over wavelength range	>80% over 400 nm – 1800nm	>70% over 400 nm – 1800nm	≈75% over 800nm - 2um	>85% 400-2400 nm	>60% from 400 to 2400 nm	≈ 70% between 900-2300um	70% , 400nm-3um
Dark current	1 0e-/pxl/s (for 18*18um pixel size)	0.3 e-/pxl/s at 140K for 1.9um cut-off. This value is extrapolated not measured	3 e-/pxl/s at 140K (glow and hot pixels)	225 e-/pxl/s 130K	$3\ 10^4$ e-/pxl/s at 170K	10 e/pxl/s at 100K	100 e-/s (data limited) at 100K
Power consumption		Slow Detector: ≤ 2mW at 100KHz FEE: ≤ 300mW at 100KHz Fast: Detector: 300mW FEE: 1W	Slow: Detector: <50mW (TBC)	typical 140mW	Not known	30mW	122mW
Operating temperature range		30-300 K	30K-300K	150-170K	150K-250K	30-150K	55-80K

Parameters	Requirements	Teledyne, US: Hawaii	Sofradir, FR: ALFA	Sofradir, FR: NGP	AIM, GE, SWIR	Leonardo, GB: Saphira, APD used as gain of 1	Rapide, Sofradir,FR APD
Format	20*128um	18um*18um 1K by 1K or 2k by 2k or 4K by 4K	15um*15um 640*512 and 2K by 2K available in 2019	1024*1024 with 15 mm pitch	1024*256	320*256 um 24um pixel	30um 320*255 pixel,
Full well		≥ 80 00 e-	≥ 80 00 e-	690ke-	$5 \cdot 10^5$ e-	2.10^5 e-	
Buttable		Yes, 4 side	Yes, 3 side in 2019	No but new version will be buttable 2*2k	no	no	no
TRL level		9	4/5	6/7 plan to fly of Sentinel 5 .	4	4 (wave front sensor)	4 (ground base astronomy)

Table 5-1: Detector trade-offs with European and American detectors

5.2.3 Baseline Design

5.2.3.1 Detector baseline

The baseline design is therefore the Teledyne Hawaii-2rg with the performances listed in Table 5-2 extracted from the Hawaii-2rg data sheet RD[7]. The SIDECAR ASIC will readout and control the Hawaii-2rg detector.

Array format	2048*2048 pixels, 18um pixel pitch square
Frame rate	Slow mode: up to 300 kHz Fast mode: up to 10 MHz
Power dissipation	Slow mode: Detector: ≤ 4mW at 100kHz FEE: ≤ 300mW at 100kHz Fast mode (at 10MHz): Detector: ≤300mW FEE: ≤1W
Cut-off	2.5 um
Mean quantum efficiency	≥70% over 400 nm – 1800nm.
Mean dark current at 140K	10 e-/pxl/s at 140K

Median Readout noise CDS in slow mode	≤18 e-
Full well at 0.25V bias	≥80 000 e-
TRL	9

Table 5-2: Hawaii-2rg detector known or extrapolated performances

To minimise the readout noise and while keeping the longest integration time, the detector readout frequency is chosen to be the highest frequency of the mode call slow mode i.e 300KHz. In that way, the detector readout noise is minimised and the SIDECAR ASIC power dissipation is less than 1W. Detector readout noise and power dissipation have to be verified at this frequency (only data at above or higher frequency are available).

The highest temperature still compliant with the dark current requirement have been chosen. For the detector, a temperature of 140K will generate a dark current of 10 e-/pxl/s. The front end electronic, the SIDECAR ASIC, associated to each detector of the focal plane, can be operated between 50K up to room temperature. It dissipates less than 1W at 300kHz. To limit the area of the radiator on the satellite, the SIDECAR ASIC will be operated at room temperature. More precisions concerning the thermal aspect of GaiaNIR can be found on the thermal chapter.

The Hawaii-4Rg with a pixel pitch of 10um has not been baselined even if it will increase the field of view by 20%. The main reason to reject this detector is the smaller pixel size that would imply a faster readout and therefore a much higher readout noise (<100 e-)

5.2.3.2   Data acquisition and transfer chronogram baseline

According to Req. ID 6, 1.62s are allocated for the staring phase before moving the mirror to the next position. During this time the science information needs to be recorded.

In the current baseline, only a Correlated Double Sampling (CDS) is planned. It is the minimum number of frame that can be recorded to be able to remove the kTC noise created by the reset switch. It consists in 2 frames recorded one after the other without reset ting the detector in between. A frame is a non-destructive readout of all pixels of the detector.

Before reading out the pixels of the detector, they need to be reset. The Hawaii-2rg detector allows reset pixel by pixel, line by line or global reset. In order to maximize the integration time per pixel, the global reset has been selected where all pixels are reset at the same time. This reset time is estimated to be 40us.

After this reset time, pixels are read one after the other through the 32 channels. With a readout frequency of 300KHz, the time to readout the whole detector (2048*2048 pixels) using the 32 outputs is 0.44s.

The first pixel of the first frame is read just after the reset and the last pixel of the first frame is read at T0+0.44s.

The first pixel of the second frame start to be read at t0+1.18s and the last pixel of this second frame is read at T0+1.62s.

The integration time or time when the photon are collected for a given pixel is 1.62 -0.44 = 1.18s.

Between T0 +62s and T0+1.81s, the mirror is pointing to the next field of view.

The front end electronic, the SIDECAR ASIC, allows to transfer the value while digitalizing i.e. transfer the pixel value values to the data processing unit while readout the remaining pixel of a given frame.

The chronogram of the data acquisition is presented in Figure 5-14.
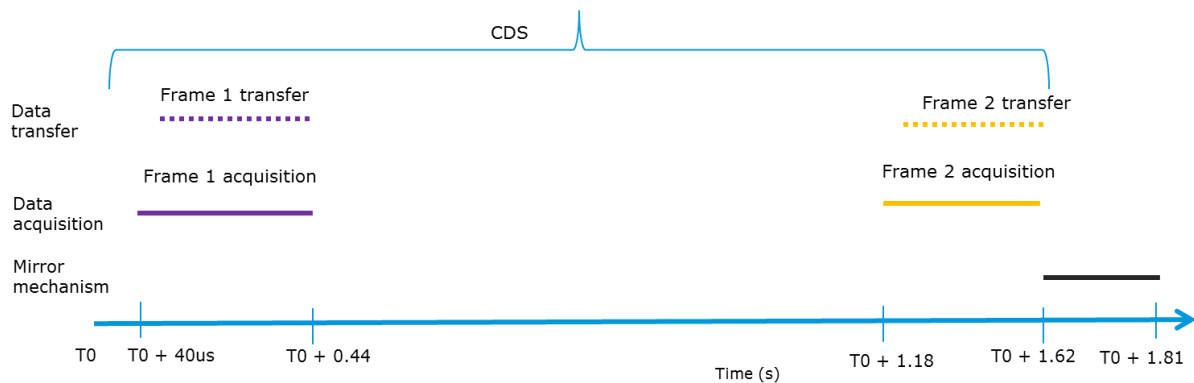
Figure 5-14: Data acquisition chronogram with a CDS

5.2.3.3 Data processing step

Different processing steps are required to be performed on each pixel of the focal plane before downloading the information of the star location. These steps are shown in Figure 5-15 and are the minimum number of steps for a CDS sampling.

The star algorithm detection is based on the Gaia algorithm described in RD[9].

A fraction of the stars need to be telemetered to ground with full 2 dimensional windows (so without AC binning on board) for AC calibrations and attitude reconstruction. For Gaia, this is ~1% of the sources.

Figure 5-15: Data processing step to perform on each pixel of the focal plane.

The time needed to perform theses processing steps is a maximum of 1.81s, corresponding to the starring time of the mirror. A potential improvement is to assess if the actual data handling can support more than 2 CDS frames to be process. This frame increase will allow to decrease the readout noise as shown in section 5.2.5.1.

The details of the processing hardware needed to perform theses operation is described in the data handling chapter.

5.2.3.4   Data budget estimation after processing

To compute the data budget estimation, several assumptions are needed as shown in Table 5-3.

Parameter	Value
Number of star per deg 2	11300
Focal length	35.2
Number of H2rg detectors	8 *7
Number of pixel and pixel size	2040*2040 pixels, 18um square pixel pitch
Detector field of view (deg2)	0.2
PSF pixel size at detector level	26 (AL) * 5 (AC)

Table 5-3: Data budget assumptions

The number of object per day is computed to be 1.2E8 stars/day assuming 2260 stars detected every 1.62s (see section Data acquisition and transfer chronogram 5.2.3.2).We assume as well 16 images per object. The related data generation calculation is described in section 6.7.1 of the Data Handling chapter.

5.2.4   List of Equipment

To operate the Hawaii-2rg detector the front electronic called SIDECAR ASIC RD[8] provided by Teledyne is required. The flex cable linking the detector and the front end electronic is as well part of the deliverable.

	number of items	mass (kg)	total mass (kg)	mass margin (%)	total mass incl. margin (kg)
PLM (Payload Module)			**39.78**	**15.41**	**45.91**
Detector_01 (Detector)	60	0.46	27.60	20.00	33.12
FEE_01 (Front End Electronics)	60	0.14	8.58	5.00	9.01
SCS_01 (Sensor Chip System)	60	0.06	3.60	5.00	3.78

Table 5-4: PLM detectors' list of equipment

5.2.5   Options

5.2.5.1   Options to baseline

If the data processing capabilities allows it (see Data processing chapter) , Fowler(N) or Up the Ramp can be envisaged to decrease the noise. The decreasing of the total noise is given by the formula [RD4]

$$\sigma_{\text{total}}^2 = \frac{12(n-1)}{mn(n+1)}\sigma_{\text{read}}^2 + \frac{6(n^2+1)}{5n(n+1)}(n-1)t_g f - \frac{2(2m-1)(n-1)}{mn(n+1)}(m-1)t_f f.$$

In this expression, σ total is the total noise in units of e rms, σ_{read} is the read noise per frame in units of e- rms, m is the number of frames within a group, n the number of group, tg is the duration time of a group of frames, tf is the time to readout a frame (0.44s) and f is flux in units of e/s/pixel, where f includes photonic current and dark current.

A CDS is considered as 2 groups of 1 frame. In that case, tg=tf=0.44s. The decrease of the readout noise with the number of frame per group is given by the first term of the equation containing the σ_{read} parameter. A value of 12 e- has been considered for the σ_{read} value
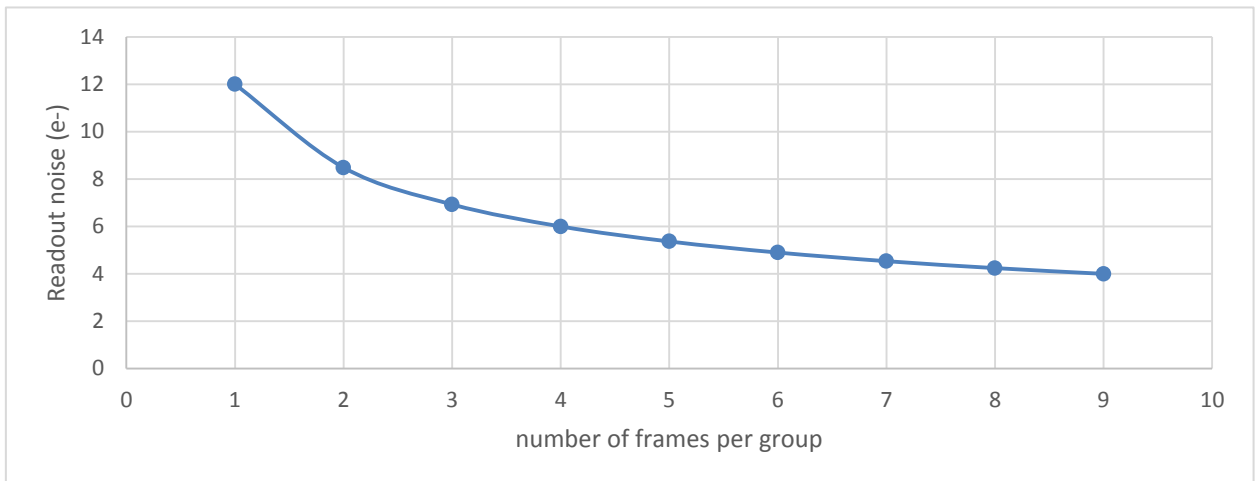
Figure 5-16: Decrease of the readout noise with the number of frames recorded. I assumed a constant number of 2 groups

A second option would be the development of a MCT array with rectangular pixel tuned for the GaiaNIR application as stated in Req.4. This would increase the full-well capacity of the pixels (since they would become larger in volume), would allow to read the pixels at a lower frequency, which would benefit the read-out noise, and would decrease the telemetry volume of the science data. The ideal pixel aspect ratio is the inverse of the entrance aperture aspect ratio.

5.2.5.2 Alternatives detector to baseline

ESA is developing a Technology Development Activity called the `Astronomy Large Format Array' or ALFA program with the goal of creating a Photon-to-SpaceWire detection system comprising of a detector system and the ALFA controller or `ALFA-C'. The timeline of this development activities is shown in Figure 5-17.
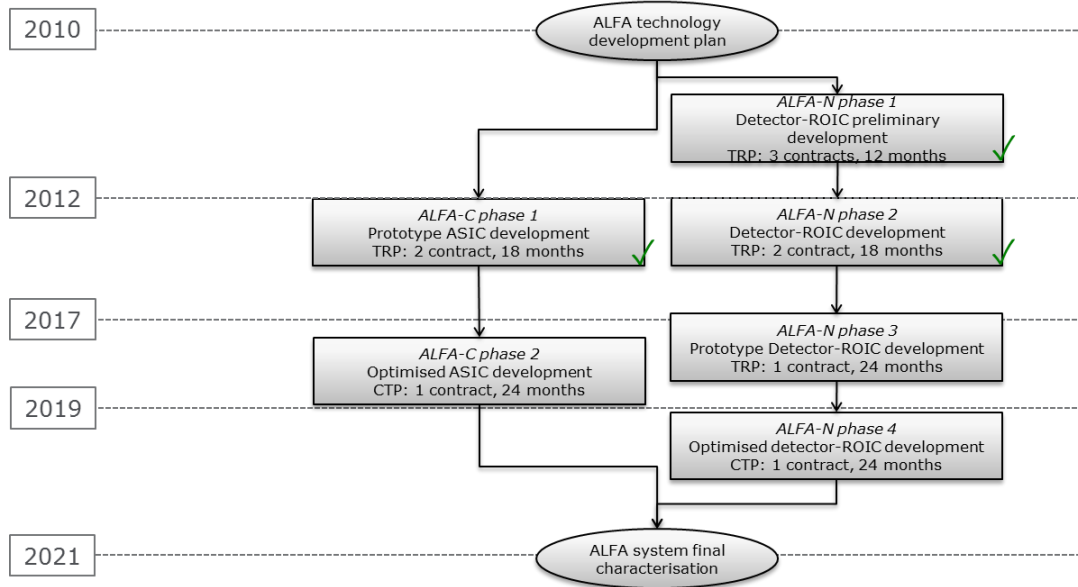
Figure 5-17: ALFA technology development roadmap

Detector hybrid

No. pixels	2048 x 2048
Pixel pitch	15um
Cut-on wavelength	0.8um
Cut-off wavelength	Max QE at 2.1 um
Dark current (100K)	<0.1 e-/pxl/s
QE	>80% over waveband

Control ASIC
Programmable clock sequencer
Bias supplies
16/32 analogue channels including ADC
Cryogenic operation (77K)

Table 5-5: Key detector and readout requirement for the ALFA activity

The European ALFA detector could be considered as an alternative to the baseline. The performances at 300kHz of this detector are not known but this detector has been designed to match the Hawaii-2rg performances. The performances at 100kHz have been measured and shown in Table 5-5. The performances of quantum efficiency in the visible would certainly not match the Req.2. A value higher than 70% has been measured between 800nm till 2um. The actual dark current value is limited by a glow but is still compliant with the GaiaNIR requirements. The detector operability (number of pixels that meet in the same time Req1, Req2 .and Req3) needs to be improved as well to reach the level of the Hawaii-2rg. A warm proton and cold gamma radiation have been performed on prototype from phase 2. The gamma radiation creates an increase of dark current up to 30 times the pre-radiation level. This radiation test campaign was not optimal as the proton radiation was performed at room temperature and unbiased.

The phase 3 of the activity has started and should end with a 2k*2k NIR detector with a cut-off at 2.1um, a glow free detector and higher operability to be able to meet the requirements shown in Figure 5-17. At the end of phase 3, a proper cold proton and gamma radiation would be needed to improve the TRL level.

5.2.6 Technology Requirements

The following technologies are required or would be beneficial to this domain:

Included in this table are:

- Technologies to be (further) developed
- Technologies available within European non-space sector(s)
- Technologies identified as coming from outside ESA member states.

Equipment and Text Reference	Technology	Suppliers and TRL Level	Technology from Non-Space Sectors	Development/modification needed	Feasibility of needed modification
Detector	APS CMOS MCT	Teledyne TRL 9		Development of a MCT array with rectangular pixel (20*128um)	Feasible
Detector	APD MCT detector	Leonardo (UK), TRL 4 Sofradir (FR)	Yes, only ground based astronomy	Decrease the cut-on to 400nm	Difficult
				Increase to 4 side buttable	Feasible
				Change pixel pitch to rectangular (now 24um)	Feasible
				Increase of the dimension (now 320*256 pixel)	Feasible
				Decrease of the dark current	Difficult as need of technology development
Detector	ALFA MCT detector	Sofradir (Fr) TRL?		Decrease the cut-on to 400nm	Difficult
				Increase to 4 side buttable	Feasible
				Change pixel size to 20*128um	Feasible
				Increase the operability	Feasible
Detector	TDI NIR MCT detector	1			

5.3   Calibration

5.3.1   Introduction

Like Gaia, GaiaNIR is envisaged to be a self-calibrating mission. This means that the scientific calibration of the instrument is obtained from the science data itself, without the need to have repeated, dedicated in-flight calibration observations.
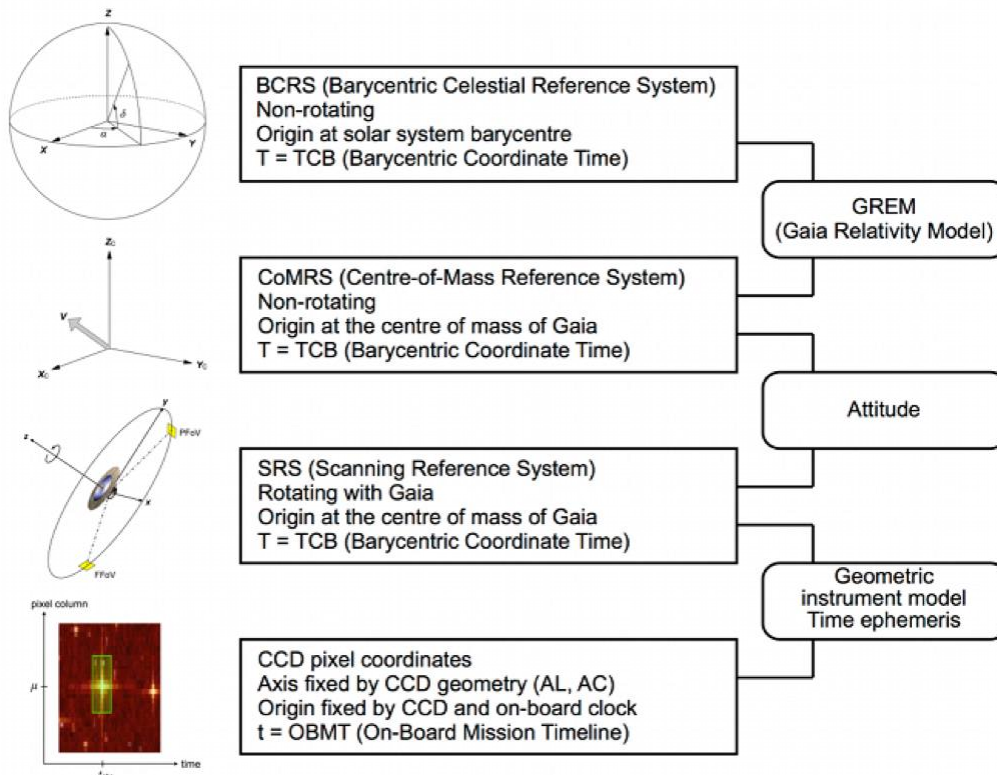
Figure 5-18: Overview of Gaia calibrations. The key goal of the calibration is to refer observations in CCD pixel coordinates made at a certain on-board time (bottom box) to source directions / coordinates in the Barycentric Celestial Reference System at the associated Barycentric Coordinate Time (top box). Figure courtesy Lennart Lindegren (extracted from http://adsabs.harvard.edu/abs/2017gdr1.reptE....V).

The Gaia calibration is described in detail in RD[11] (in particular Appendix A) and summarised in Figure 5-18. The instrument calibration, as well as the astrometric processing of the data (i.e., the derivation of stellar positions, parallaxes, and proper motions, sometimes referred to as source calibration), is done in the Astrometric Global Iterative Processing (AGIS) system. Besides the source calibration, there are two other calibrations in AGIS: the attitude calibration, which links the Scanning Reference System to the S/C Centre-of-Mass Reference System, and the geometric calibration, which links CCD pixel coordinates to observed directions in the Scanning Reference System. It is foreseen that GaiaNIR data will also be calibrated in an AGIS-like system, albeit with several modifications, as discussed below.

5.3.2 Source Calibration

The GaiaNIR source calibration is envisaged to be identical to the Gaia source calibration. Five-parameter source models will be applied as baseline and higher-order (acceleration or orbital) terms will be added as needed for double and multiple stars.

5.3.3 Attitude Calibration

The attitude calibration of the baseline step-and-stare version of GaiaNIR will differ from Gaia not only because of the TDI versus step-and-stare difference but also because systematic, repeatable features of the de-spin mirror mechanism (e.g., undershoot) must be calibrated too since these lead to systematic centroid shifts. Nonetheless, the GaiaNIR attitude calibration is not expected to be(come) prohibitively complex or unfeasible.

5.3.4 Geometric Calibration

Whereas the PSF calibration of GaiaNIR is expected to be similar to that of Gaia, with only smooth variations of the PSF characteristics over the focal plane, the geometric calibration of the detectors will have to be fundamentally different and much more demanding.
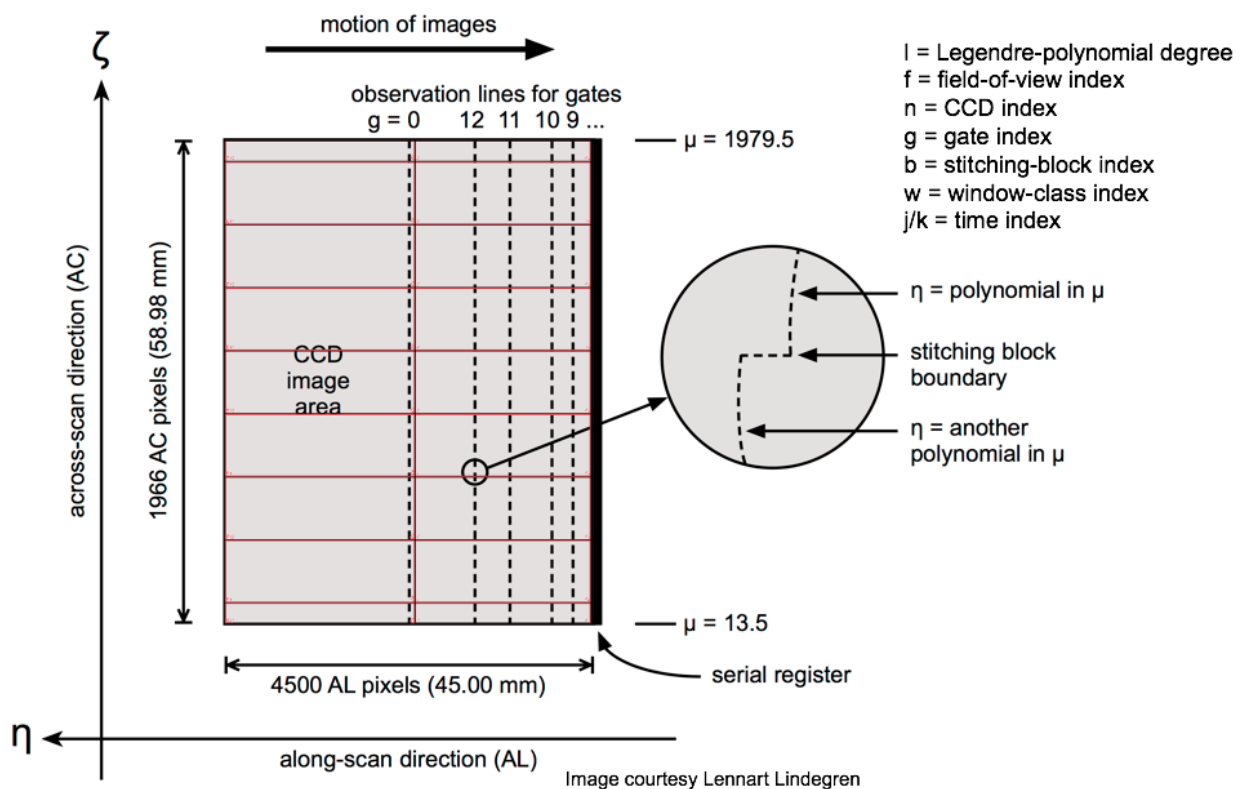
Figure 5-19: Gaia's geometric calibration. Depicted is one CCD detector, with the various fiducial observation lines corresponding to the various TDI gates denoted as dashed vertical lines. The inset shows the effect of stitching-block boundaries. The various labels are explained in the inset (see also Figure 5-20). Figure courtesy Lennart Lindegren.

In the case of Gaia, the geometric calibration greatly benefits from the TDI averaging of the along-scan data over the pixel columns. What is needed for Gaia is just the effective transit time of each image over each detector. The reference for this timing is the so-called fiducial transit line (roughly the midpoint of the CCD). Since Gaia uses 8 TDI gates to reduce the exposure time and limit saturation for bright stars (G < 13 mag), each detector has 9 different fiducial transit lines. For each of the 62 astrometric CCDs, each of these lines need to be characterised as function of the field of view (2 telescopes), the CCD pixel column (1966 columns per CCD, with discrete steps at stitch block boundaries), magnitude (3 magnitude ranges/window classes are used in Gaia), and time (to account for both long-term thermal and radiation effects as well as radiation-, refocus-, and decontamination-induced discontinuities). The Gaia geometric calibration model uses shifted Legendre polynomials per time block (see Figure 5-19). For Gaia DR1, the geometric calibration model uses ~123,000 parameters (see Figure 5-20). For Gaia DR4, it is expected that of order 1,000,000 parameters will be needed. In particular for the short TDI gates, which are applied to bright (and therefore rare) stars, the number of calibration sources in the sky is very limited. This deficit may ultimately limit the final bright-star performance of Gaia.

Kind of parameter	Multiplicity							Total number
	l	f	n	g	b	w	j/k	
$\Delta\eta_{lfnj}^{(0)}$	3	2	62	1	1	1	141	52 452
$\Delta\eta_{lfnj}^{(1)}$	1	2	62	1	1	1	141	17 484
$\Delta\eta_{lfng}^{G}$	3	2	62	9	1	1	1	3 348
$\Delta\eta_{lfnb}^{B}$	2	2	62	1	9	1	1	2 232
$\Delta\eta_{lnw}^{W}$	3	2	62	1	1	3	1	1 116
$\Delta\zeta_{lfnk}^{(0)}$	3	2	62	1	1	1	87	32 364
$\Delta\zeta_{lfnk}^{(1)}$	1	2	62	1	1	1	87	10 788
$\Delta\zeta_{lfng}^{G}$	3	2	62	9	1	1	1	3 348

Figure 5-20: Gaia DR1 geometric calibration (extracted from Appendix A in RD[11]). The columns headed Multiplicity **give the number of distinct values for each dependency: Legendre polynomial degree (l), field-of-view index (f), detector index (n), TDI gate (g), across-scan stitching block (b), magnitude / window class (w), and time interval (j or k). The last column is the product of multiplicities, equal to the number of calibration parameters of the kind. The total number of geometric calibration parameters in Gaia DR1 is ~123,000. In DR4, the total number will be ~1,000,000.**

The TDI averaging effect of Gaia means that the geometric calibration of 4500 TDI lines per detector is collapsed into the calibration of just 9 fiducial transit lines per detector. TDI operation hence allows a simplification of the calibration of a factor 4500/9 ~ 500. This gain is not applicable to the baseline step-and-stare GaiaNIR design which, on the contrary, requires that all along-scan pixel columns are calibrated individually. Taking advantage of the finite PSF size of (say) 2 along-scan pixels, a GaiaNIR detector of 4500 pixels does not require 9 along-scan but 4500/2 = 2250 along-scan calibration points, which explodes the problem by a factor 2250/9 ~ 250. Extrapolating from the ~1 million

geometric calibration parameters ultimately needed for Gaia, this means of order a few hundred million geometric calibration parameters are needed for GaiaNIR. Whether this is reasonable and feasible, even conceptually, requires a dedicated study, which is far beyond the scope of the GaiaNIR CDF. Nonetheless, one consideration can be made already at this stage. A key to the success of self-calibration is the presence of a sufficiently large redundancy ratio between the number of fitted parameters and the number of observations.

- For Gaia's geometric calibration in the final data release (DR4), there are of order 1 million geometric calibration parameters. In AGIS, the number of primary sources, that is those sources that are sufficiently stable – both astrometrically and photometrically – to be used as calibration sources, is around 10% of all sources, so 100 million. With 70 transits each and 9 CCD crossings per transit, these sources generate 100 million $\times$ 70 $\times$ 9 = 63 billion CCD observations. The redundancy factor is hence 63E9 / 1E6 ~ 60E3.

- For GaiaNIR, there are 250 million geometric calibration parameters. Although GaiaNIR will see many more stars compared to Gaia, nearly all of them will be faint and hence contribute calibration sources to the same magnitude range / window class. In particular the bright-end star counts for GaiaNIR will be similar to the (already problematic) Gaia numbers. A potential improvement that is reasonable to assume is to use ~80% of the sources as stable calibration sources (excluding 20% of the sources that are double/multiple and/or variable). This factor 8 gain – which comes at the expense of AGIS processing time – reduces the factor 250 to a factor 250/8 ~ 30 such that the redundancy factor decreases from 60E3 to 60E3/30 ~ 2000.

Whereas it might be the case that a redundancy factor of 2000 is reasonable and workable, this is non-trivial, and far beyond the scope of the GaiaNIR CDF, to either prove or disprove.

5.3.5   Conclusions

For the moment, the feasibility of the two-dimensional geometrical calibration of a step-and-stare version of GaiaNIR – linked to a limited sky density of suitable calibration sources, especially if the calibration includes colour- and magnitude-dependent terms – should be considered as a non-negligible risk.

5.4 Science Performance

In this section, we provide an estimate of the end-of-mission astrometric performance for the GaiaNIR baseline concept as well as for two alternative concepts/variants with the goal to provide guidance in the prioritizing of (detector) technology developments.

In the following, we first give a short description of the model used to estimate the astrometric performance for a given mission concept. We then discuss briefly the model assumptions and limitations and later provide a validation of the model against the Gaia performance and a similar model developed by D. Hobbs – the GaiaNIR lead scientist from Lund (Sweden).

After exposing the different mission concepts studied as well as providing a detailed list of the input parameters used for each case, we present, compare, and discuss the various performance estimates. We also show the impact of several key detector specifications on the mission performance.

5.4.1 Performance Model

5.4.1.1 From centroiding accuracy to end-of-mission parallax error

Astrometry is a generic term used to describe the science of measuring stellar positions, parallaxes, and proper motions. For a given sky scanning law, the sky-averaged position and proper-motion errors can be derived from the parallax error (see RD[12]). Both terms 'astrometric performance' and 'end-of-mission parallax (standard) error' are thus used interchangeably in the following.

We use a bottom up approach to model a given mission concept astrometric performance: going from ultimate one-dimensional centroiding (image location) accuracy as determined by the Cramér-Rao bound theorem to end-of-mission parallax accuracy.

The Cramér-Rao bound is the maximum-achievable performance for a properly sampled signal derived from fundamental principles on information technology. In this work, we assume this bound is achievable not only in theory but also in practice. This assumption is based on Gaia experience. One important caveat is, however, that the Cramér-Rao bound can only be achieved with a proper (Nyquist) sampling of the signal. This condition should always be checked when the Cramér-Rao bound is used.

For a global astrometry scanning mission like Gaia, the 2D astrometric mapping and reconstruction is enabled from combining the various (~70) scans or one-dimensional centroid measurements that are made of each object over the mission lifetime under various, "random" angles. This is explained in Section 3.1 of the Gaia Mission paper (RD[13]).

The end-of-mission parallax standard error relies on the following two critical equations and quantities:

$$\sigma_{det}^2 = \frac{1}{N_e} \left(\int \frac{LSF'(x)^2}{LSF(x) + (\beta + r^2)/N_e} dx \right)^{-1}$$

Equation 1: Cramér-Rao bound in the case of estimating the location of a one-dimensional image as derived in Lindegren 1978

With:

- σ_{det} the ultimate centroiding accuracy (det stands for detector) [pixel]
- N_e the number of collected photo-electrons for the considered cropped image referred to as window in the following [e-]
- LSF the normalised Line Spread Function corresponding to the instrument PSF binned in the across-scan direction [dimensionless]
- x the distance from the LSF centre in the along-scan direction [pixel]
- β the total number of background electrons in the window: i.e. dark current and sky background [e-]
- r the total readout noise within the window [e-]

$$\sigma_{\varpi} = m \times \frac{1.47}{sin(\xi)} \times \sqrt{\frac{\sigma_{det}^2 + \sigma_{cal}^2}{N_{obs}}}$$

Equation 2: End-of-mission parallax error as derived in Gaia-JDB-022 (http://www.rssd.esa.int/doc_fetch.php?id=448635)

- σ_{ϖ} end-of-mission parallax error [as, for arcsecond]
- σ_{cal} (residual) calibration error introduced in the data processing, expressed per elementary observation [as]
- m (= 1.2) margin which accounts for sky complexity, e.g., background inhomogeneity, double stars, crowding [dimensionless]
- ξ =51.5° is the Solar aspect angle for GaiaNIR (compared to 45° for Gaia)
- N_{obs} number of detector observations of a given star, accumulated over the entire mission lifetime (~9 × 70 ~ 630 for Gaia).

For photometry, the baseline focal plane is divided in 4 different wavelength bands [400-800], [400-1100], [400-1500], [400-1800] nm consisting of two detector columns each (also known as detector strip). Because the parallax error is different for each waveband, we compute individual $\sigma_{\varpi,i}$ per detector column and on a per observation basis. We then combine these individual errors into one single error representative of the transit over the entire focal plane as follows:

$$\frac{1}{\sigma_{\varpi}^2} = \sum_i \frac{1}{\sigma_{\varpi,i}^2}$$

Equation 3: Combining individual parallax errors into one

Each star is observed twice per detector (in the CDF baseline, see Table 5-7), hence the total number of individual errors to be computed and subsequently combined is 16. In that case N_{obs} becomes equivalent to the number of times a star transits the focal plane $N_{transits}$. How we compute $N_{transits}$ is described in Section 5.4.1.8. Of relevance in that computation is that the number of detector rows equals 7 in the baseline. The baseline focal plane comprises 8 detector columns (and 7 rows, this relevant only to compute $N_{transits}$), and each star is observed two times per detector, hence i = 16.

5.4.1.2   PSF and LSF modelling

For a given wavelength, the PSF is computed by multiplying the across-scan LSF with the along-scan LSF, which are both modelled as sinc squared – the one-dimensional response function to a rectangular aperture – as follows:

$$LSF(x) = \left(\frac{\sin(\alpha x)}{\alpha x} \right)^2, \text{with } \alpha = \frac{\pi A p}{f \lambda}$$

Equation 4: LSF modelling for one direction (either along- or across-scan)

- A is the aperture dimension: width along-scan, and height across-scan [m]
- p the pixel size: width along-scan, and height across-scan [m]
- *f* the focal length [m]
- λ the wavelength [m]

For each waveband *b*, a polychromatic PSF is computed, as follows:

$$PSF_b = \sum_{\lambda=\lambda_{\text{cut-on}}}^{\lambda_{\text{cut-off}}} n(\lambda) \times PSF_\lambda, \text{with } PSF_\lambda = PSF_{\lambda_{\text{diff}}} \text{ if } \lambda < \lambda_{\text{diff}}$$

Equation 5: Multi-wavelength PSF computation

- PSF_b the PSF for a given waveband defined by [$\lambda_{\text{cut-on}}$, $\lambda_{\text{cut-off}}$] [no dimension]
- PSF_λ the PSF at a given wavelength λ computed using Equation 4 [no dimension]
- λ_{diff} the telescope diffraction limit [m]
- n(λ) the flux at a given wavelength for a given star and detector (see next section). [photons/s/m²/nm].

The resulting PSF is then binned across-scan and normalised to obtain the desired along-scan LSF to be used to compute σ_{det}. Figure 5-21 shows a comparison between monochromatic GaiaNIR binned PSFs (along-scan LSFs) and the polychromatic binned PSF (along-scan LSF) for a G2V type star. Figure 5-22 shows the 2D PSF.

The PSF model is convolved with a Gaussian kernel with a sigma equal to one fourth of the pixel pitch to account for all possible sources of smearing (up to ¼th of a pixel), e.g., de-spin mechanism combined with detector effects such as charge diffusion and charge sharing. Note that the de-spin mechanism error requirement is smaller than ¼th of a pixel (see Mechanism section 5.7 in this report).The ¼th value comes from Gaia and the smearing introduced by the minimum TDI step which corresponds to a CCD pixel electrode.

Last, we include the broadening of the PSF due to the detector response function (effects mentioned above excluded) by convolving the PSF with a rectangular kernel with the pixel dimensions.
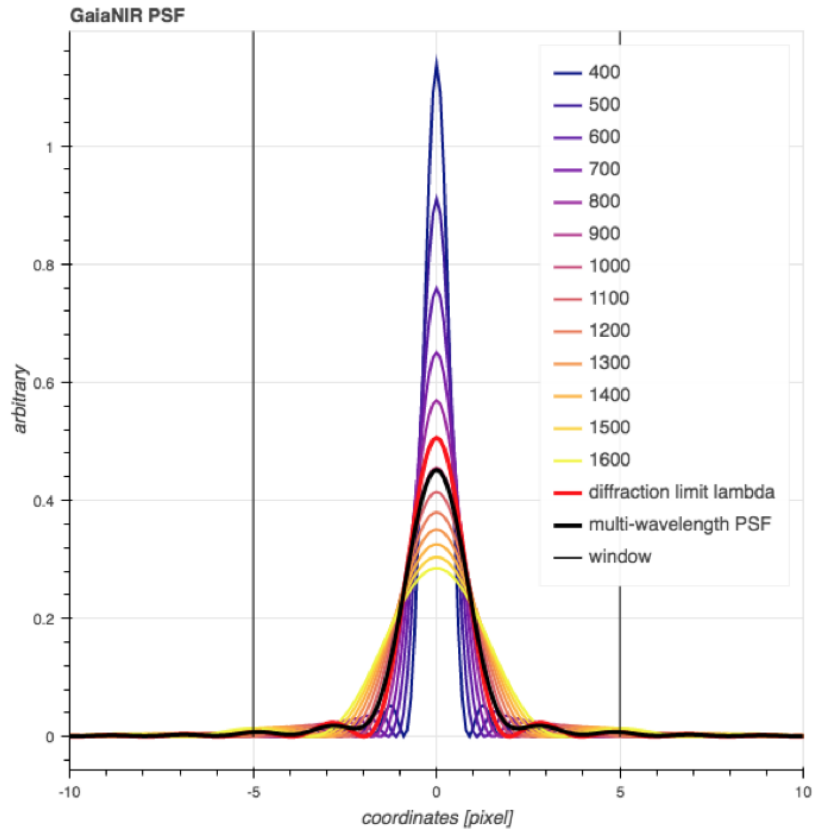
Figure 5-21: Comparison between monochromatic GaiaNIR binned PSF (along-scan LSF) at different wavelengths (indicated in nm) and the multi-wavelength binned PSF (in black), excluding de-spin mechanism smearing and detector response broadening
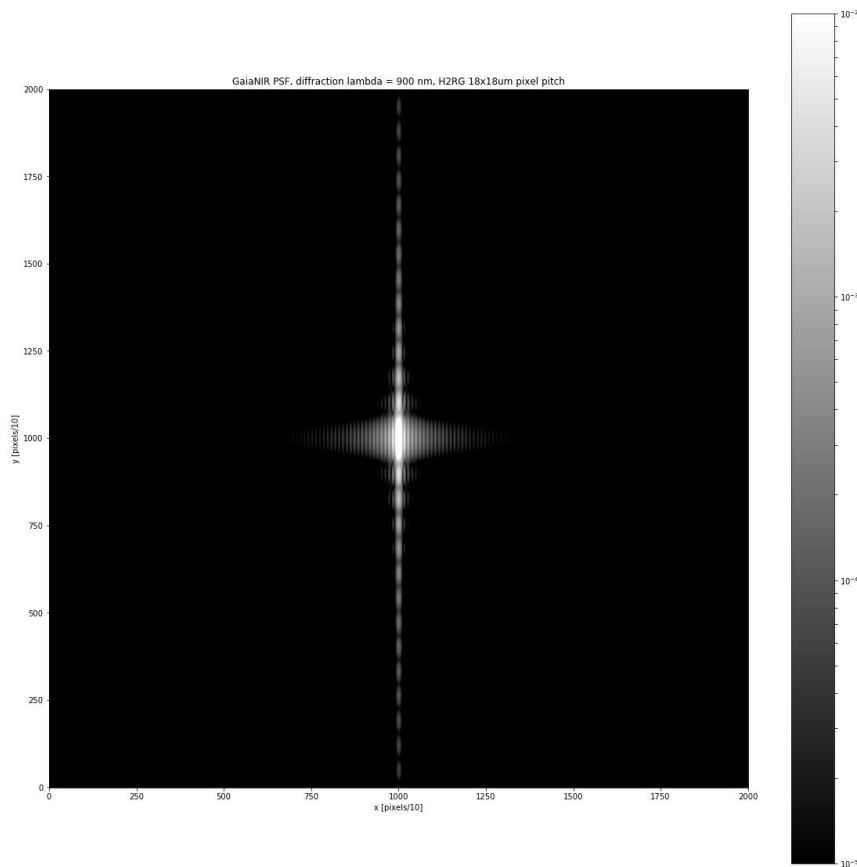
Figure 5-22: Polychromatic GaiaNIR 2D PSF with diffraction limit of 900 nm and excluding de-spin mechanism smearing and detector response broadening

5.4.1.3   Considered star types (SEDs)

Figure 5-23 shows the spectral energy distributions (SEDs) of the seven star types provided by Carme Jordi et al. (Barcelona University) and that we have considered here:

- B1V, G2V, and M0V are standard Gaia spectral types representative of non-evolved, main-sequence hot, solar-like, and cool stars, respectively. Hot, blue B1V stars are very rare and constitute ~0.1% of all stars. Yellow solar-type stars represent ~8% of all stars. The vast majority (75%) of stars in the universe are red M-type stars.
- NextGen_Av0_Teff3000_logg4 represents an even redder (M6V) dwarf, also very common. None of these stars is reddened by interstellar dust (A_V = 0 mag).
- The remaining three objects (B1V, K5III, and M3III) are severely reddened and extinct by interstellar dust (A_V = 5 mag), representative of large distances (in the galactic plane, the typical extinction is around 1 mag per kpc, so 5 mag extinction in the V band would correspond to a distance of ~5 kpc). The K5III and M3III stars are evolved, late-type giants (luminosity class III), which are intrinsically bright and very common. They would be prime targets for GaiaNIR.

All 7 spectral types considered here do emit visible light (see Figure 5-23) and, as such, can be observed by Gaia (provided they are brighter than the survey limit of G = 20.7 mag). GaiaNIR-only objects can be obtained by applying more reddening.

5.4.1.4   From star SEDs to number of photo-electrons

To compute σ_{det}, we need to compute the total number of electrons N_e. This is performed as follows:

- First, we select the spectral energy distribution (SED) of a particular star type.
- The SED is then multiplied by the QE of the selected detector (after interpolation of the QE at the SED wavelengths). Figure 5-24 shows a comparison between the Gaia CCD QE and the QE of two hybrid MCT detectors measured in the ESA SciLab (including our baseline, the H2RG). Note that by removing the substrate on which the MCT is grown, one can make the hybrid MCT detectors sensitive in the visible. This option is retained here and we assume a conservative, flat 70% QE over the range: $400 < \lambda < 800$ nm.
- We then integrate over the given wavelength band, multiply by the telescope throughput, multiply by the integration duration, and scale to any desired magnitude.
- Last, we apply a window-cropping factor to account for electrons falling outside the considered window (typically about 10% of the photo-electrons are lost in this way).
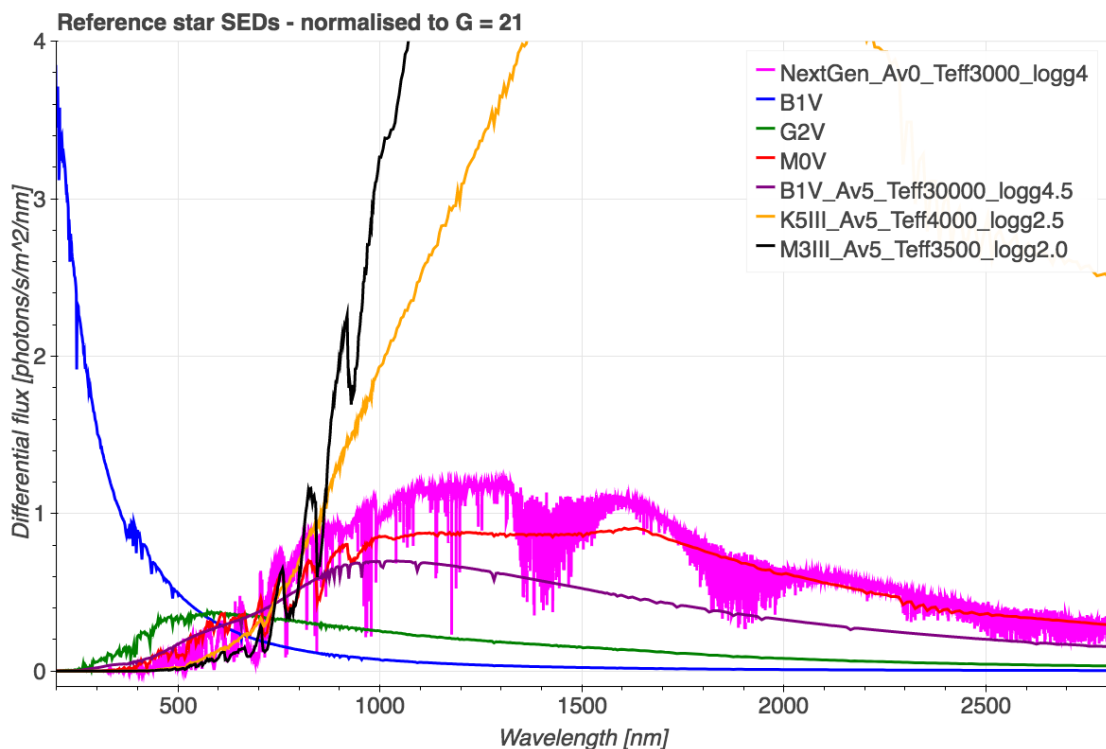
Figure 5-23: Spectral energy distributions for different star types

Detector quantum efficiency

Figure 5-24: Comparison between different, measured detector quantum efficiencies: in blue the Gaia CCDs to show the enlargement of the considered wavelength range, in red the baseline H2RG US detector with a cut-off at 2.5 μm, and in green the ALFA-N detector developed by the CEA Leti in France in the context of an ESA technology development activity. Note that below 800 nm, an average QE of 70% or more can be obtained for the two MCT devices (by removing the substrate on which the MCT photosensitive layer is grown)

5.4.1.5 Background modelling

The background is composed of electrons generated by the detector dark current and collected from the sky background during the exposure.

The number of electrons due to the sky background depends on the considered waveband, detector QE, and integration duration. It is computed in a similar fashion as for the total number of signal electrons (see section 5.4.1.3), using a G2V SED (the Sun) and a sky surface brightness of V = 22.5 mag/arcsec².

On top of temperature, the realistic dark current depends on the selected detector, cut-off wavelength, pixel pitch, and integration duration.

5.4.1.6 Readout noise computation

The readout noise computation depends on the type of detector used and the detector output signal sampling method. It is computed as follows:

$$r = \sigma_{\text{read}} \times \sqrt{N_{\text{pix}}}$$

Equation 6: Readout noise computation for one observation

- r the total readout noise for a given window used in Equation 1 [e-]

- σ_{read} the readout noise per pixel for a given readout frequency and for a post-processed image using a given sampling method e.g., CDS, Fowler, up-the-ramp. CDS is baseline here (see Detector section 5.2 in this report) [e-]
- N_{pix} the number of actual readouts per window: i.e. the total number of pixels in the window for existing standard MCT hybrid detectors (and 'step-stare' mode), but only the number of along-scan pixels for CCD-like detector readout in TDI mode (as on-chip binning across-scan is possible) [dimensionless].

5.4.1.7 Integration duration computation

The integration duration depends on the observation mode (TDI or step-stare) through the de-spin mirror mechanism. In the TDI case, the integration duration is equivalent to the time it takes for a star to cross a detector, and thus only depends on scan rate, plate-scale, and detector size. In the de-spin case, the integration duration depends also on the step duration (baseline half a detector i.e. two observations per detector) from which we also remove (i) the duration of the de-spin mirror mechanism reset (10% of the step time), (ii) the duration of a full frame readout (see Detector section 5.2 of this document).

5.4.1.8 Total number of focal plane stellar transits

There is no simple, parameterisation for the total number of focal plane transits. Estimates of this number require simulations of the scanning law, i.e., the spacecraft pointing as a function of time. The principles behind the scanning law are summarised in Section 5.2 of Gaia Collaboration et al. (2016; http://dx.doi.org/10.1051/0004-6361/201629272). The scanning law follows from solving the differential equations (1) and (2) in that document and require five input parameters:

1. Spin rate;
2. Solar aspect angle;
3. Precession period;
4. Initial spin phase;
5. Initial precession phase.

To determine the number of focal-plane passages, one furthermore needs:

6. The size of the field of view in the across-scan dimension;
7. The number of telescopes / fields of view;
8. The mission length;
9. The observing efficiency, i.e., the mission dead time.

Such simulations have been done in the past for Gaia, resulting in 70 transits for a 5-year mission, 20% dead time, 7 CCD rows across scan with 1966 30-micron pixels each, two telescopes, a 60 arcsec/s spin rate, a 45° solar aspect angle, and a 63-day precession period. In practice, the initial spin and precession phases (items 4 and 5) are irrelevant for the number of focal-plane transits.

In this study, we ignore the dependence of the solar aspect angle and assume that the other parameters remain unchanged for GaiaNIR compared to Gaia. Therefore, the only dependence we include is that of the across-scan size of the field of view, which is a simple, linear scaling.

The end-of-mission number of transits for the GaiaNIR baseline (with 7 H2RG detectors across scan with 2048 18-micron pixels each) equals 43.50. For the GaiaNIR H4RG variant (with 4096 10-micron pixels), the number is 48.34.

5.4.2   Model Assumptions

In the following table, we give a summary of the model assumptions and limitations:

Assumptions	Possible impact
1 Close and beyond full well detector effects	See discussion below.
2 Detection limit of faint stars	See discussion below.
3 All smearing effects on the PSF are smaller than $1/4^{th}$ of the pixel size	This is a conservative assumption; possible 10% level under-estimate of performance for 8 < G < 16.
4 The de-spin mechanism stepping duration is 10% of the total (step + stare) time.	This is a conservative assumption; possible overall % level under-estimate of performance.
6 The QE of the near-infrared detector in the visible [400, 800] nm is flat and has a value of 70%.	This is a conservative assumption; possible overall % level under-estimate of performance.
7 The achievable centroiding performance is equal to the Cramér-Rao bound.	The impact is an over-estimated performance by at most 5%.

Table 5-6: List of the performance model assumptions and limitations

5.4.2.1   Close and beyond full well effects

Considering a charge handling capacity (CHC) of 100 ke-, the widest waveband [400-1800] nm, and a red star (M0V) (i.e., a worst case), we measure that saturation in the LSF core occurs at around G = 12 mag and that saturation in the wings occurs around G = 7 mag. Since Gaia performs centroid measurements for saturated stars with unsaturated wings, un-modelled detector effects occurring close and beyond the detector full well are taken into account by discarding results for stars brighter than G = 7 mag. This implies the assumption that saturation related effects occurring at fainter magnitude (i.e., for 7 < G < 12 mag) such as blooming and persistency can be calibrated out (by special mode of operation or in the data processing).

5.4.2.2   Detection limit

Detection or measurement issues occurring at the faint end of the magnitude range are taken into account by discarding end-of-mission parallax errors for stars for which the centroid measurement error averaged over the four wavebands is greater than 1 pixel (i.e., not meaningful anymore). This gives a rather realistic (not the most conservative) estimate of the faint-end limit for a particular mission concept.

5.4.3   Model Inputs and Studied Case

In the following, we study and compare the end-of-mission performance of a number of GaiaNIR mission cases. The CDF baseline – simply referred to as "baseline" in the following – is used as a reference. Table 5-7 summarises the model input parameters for each considered case:

- "baseline": GaiaNIR including a de-spin mechanism which enables the use of existing H2RG detectors.

- "H4RG": the baseline but using the existing H4RG detectors (larger device with smaller pixel pitch).
- "TDI": this concept uses NIR detectors that can be operated in Time-Delayed Integration (TDI) in the charge domain (see RD3 for a detailed explanation). This technology does not yet exist, however it would have several advantages including enabling a mission concept without a de-spin mechanism and a much improved science return with reduced risk of complex calibrations.

Note that the performance model was validated against the original Gaia mission; the model reproduces the Gaia performance numbers using the Gaia parameters as input (also shown for completeness in Table 5-7).

Model input parameters	Baseline	H4RG	TDI	Gaia
Mission concept				
	Spinning spacecraft with de-spin mechanism allowing for existing detectors	Spinning spacecraft with de-spin mechanism allowing for existing detectors	Spinning spacecraft with NIR TDI detectors	Spinning spacecraft with CCDs operated in TDI mode
Detector parameters				
Detector type	MCT CMOS hybrid		NIR TDI detector	CCD
Detector reference	Teledyne H2RG	Teledyne H4RG	Non-existing	E2v CCD91-72
Readout noise per pixel [e-]	12	70	12	4.5
Readout frequency	300 kHz	5 MHz	N/A	N/A (93 kHz)
Readout channels per detector	32		1	1
Dark current [e-/pixel/s/ μm²]	1e-1/(18*18) at 80 K for 2.5 μm cut-off or at 130 K for 1.9 μm cut-off (non-standard)	-	-	1e-6/(10e-6*30e-6)
Pixel size AC [μm]	18	10	-	30
Pixel size AL [μm]	18	10	-	10
Detector size AC	2048 pixels, 3.7 cm	4096 pixels, 4.1 cm	-	1966 pixels, 5.9 cm
Detector size AL	2048 pixels, 3.7 cm	4096 pixels, 4.1 cm	-	4500 (4496 light sensitive) pixels, 4.5 cm
Cut-on	Define by waveband	-	-	300

wavelength [nm]				
Cut-off wavelength(s) [nm]	Define by waveband	-	-	1000
Diffraction wavelength [nm]	900	-	-	665
Window size [AL x AC pixels]	5 x 28	10 x 64	-	12 x 12
Readout noise computation	All pixels in a window contribute to readout noise	-	Noise-less AC-binning i.e. only AL pixels in a window contribute to readout noise	Noise-less AC-binning i.e. only AL pixels in a window contribute to readout noise
Quantum efficiency	H2RG red curve in Figure 5-24 and for the interval 400 < λ <800 nm, a flat QE of 70%	-	-	Gaia blue curve in Figure 5-24
PSF smearing due to de-spin mechanism plus detector charge diffusion and sharing	¼ of pixel size	-	-	¼ of pixel size
Telescope				
Telescope throughput	0.9	-	-	.73 (also includes detector QE)
Aperture AC [m]	0.25	-	-	0.50
Aperture AL [m]	1.6	-	-	1.45
Focal length [m]	35.2	-	-	35
Mirror mechanism reset duration allocation	10% of total (step + stare) duration	-	N/A	N/A
Computed integration duration [s] (see 5.4.1.7)	1.18 (x2 per detector)	1.70 (x2 per detector)	3.60	4.42
Astrometric focal plane parameters				
Detector columns / strips [AL]	8	-	-	9
Detector rows [AC]	7	-	-	7

FoV AC	0.26 m, 0.42 deg	0.29 m, 0.47 deg	-	0.41 m, 0.68 deg
FoV AL	0.29 m, 0.48 deg	0.33 m, 0.53 deg	-	0.40 m, 0.66 deg
Column per waveband(s): [cut-on, cut-off] [nm]	2x [400-800], 2x [400-1100], 2x [400-1500], 2x [400-1800]			9x [300-1000]

Mission parameters

Number of observations per detector (related to step size)	2	-	1	1
Sky-average number of star transits for a 5-year mission, assuming 20% dead time	43.50	48.34	-	70
Sun aspect angle [degree]	51.5	-	-	45
Scan rate [arcsec/s]	60	-	-	60

Astrometric accuracy computation

Sky complexity margin, m	1.2	-	-	1.2
Residual calibration error per detector σ_{cal} [µas]	100	-	100/√2 (*)	60

Table 5-7: Summary of the model input parameters for all considered cases. "-" indicates that the baseline value is used

(*) The lower σ_{cal} for the TDI case is required to compensate for a simulation artefact that would artificially degrade the bright star performance compared to the baseline due to a lower total number of observations (only one observation per detector in TDI versus two for the baseline), despite the same actual observation time.

Stellar type	'NextGen' M6V	B1V	G2V	M0V	B1V A_V=5	K5III A_V=5	M3III A_V=5
Magnitude [G-band]	End-of-mission parallax error [µas]						
Baseline							
7 (bright)	9	9	9	9	9	9	9
15	77	234	165	81	97	38	27
21	15531	56412*	38660*	16843	21002	5421	2919
H4RG							

7	9	9	9	9	9	9	9
15	417	1509	1036	453	564	144	80
21	104526*	378869*	259912*	113373*	141310*	36377*	19486*
TDI							
7	9	9	9	9	9	9	9
15	34	57	48	34	37	23	19
21	1750	5910	4129	1881	2309	694	426

Table 5-8: Summary of the end-of-mission parallax error estimates for the different GaiaNIR mission concepts. "*" indicates that the detection limit has already been reached. Av=5 refers to a reddened star with A_V=5 mag extinction

5.4.4   End-of-Mission GaiaNIR Performance Estimates

This section shows the results of our performance prediction exercise:

- We first provide a comparison between the three GaiaNIR concepts mentioned above, and this is done for the 7 stellar types and as a function of G magnitude.
- Second, we study the impact of critical detector characteristics by varying pixel pitch, readout noise, and dark current for the baseline case.
- Last, we present validation results where the model predictions are compared to the Gaia performance and to a similar performance model developed by D. Hobbs – the GaiaNIR lead scientist.

5.4.4.1   Performance estimate comparison between the different mission concepts

Figure 5-25 shows the performance estimates for the baseline case for all stars studied: as anticipated, the redder the star, the better the performance gets; for the reddest star studied (M3III Av5), the baseline achieves better than 30 μas parallax errors at G=15 mag. From the figure, we distinguish between two regimes:

- The bright star regime (for G < 10 mag, the flat part of the curves), where the signal to noise ratio is very favourable and where the calibration errors dominate (see Equation 2).
- The "photon-starved" regime (for G > 10 mag), where the detector error contribution dominates, and where all measurement errors gradually increase with magnitude as the signal to noise ratio becomes less and less favourable (a SNR of about 1 is reached at the detection limit).
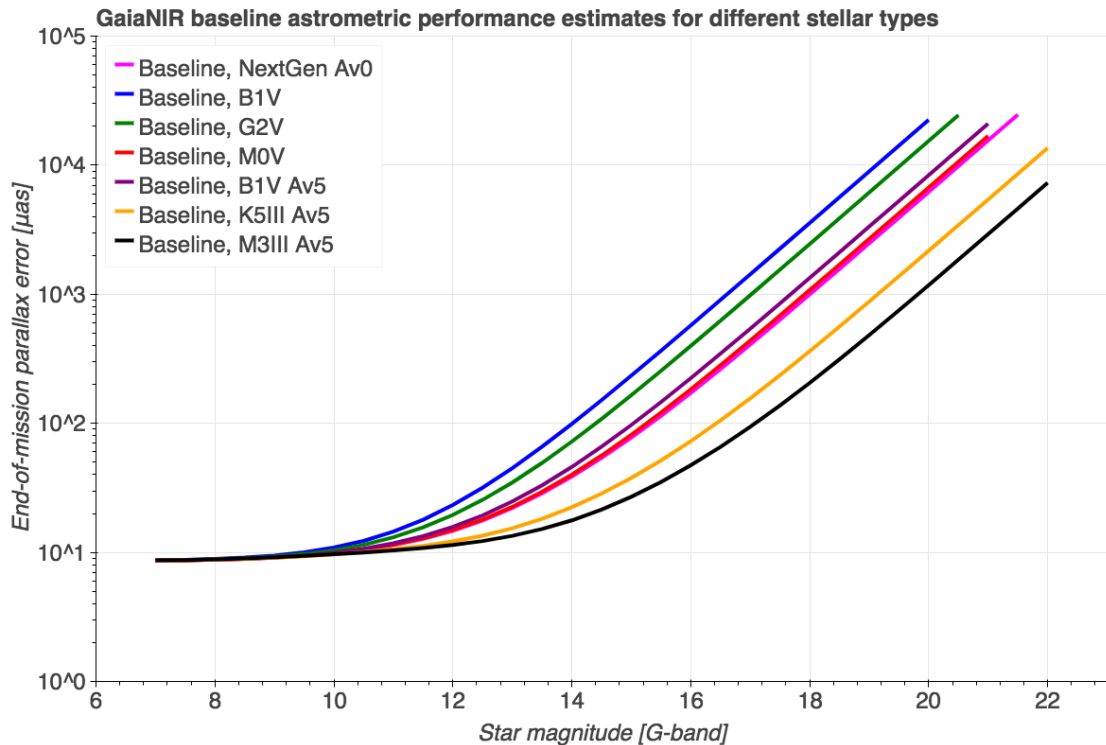
Figure 5-25: Baseline concept performance comparison for different spectral types

The exact boundary between the two regimes varies with the star spectral type; the photon-starved regime is reached at fainter G magnitudes for redder stars. The same goes for the detection limit; we notice that for the bluest stars the limit is reached as early as magnitude 20 (for the baseline case).

Table 5-8 summarises the performance estimates for all concepts and all stellar types at three different magnitudes (G = 7, 15, and 21 mag):

- Despite a slightly larger focal plane, the H4RG option provides no performance improvement; it actually exhibits an order of magnitude worse performance at the faintest end compared to the baseline. This is mainly due to a drastic increase in readout noise implied by the H4RG smaller pixel pitch and slightly larger format; the total number of pixels read out per frame is far larger than for the baseline and decreases the available time for integrating light to such an extent that the detector has to be operated in fast mode (5 MHz). In this mode, the readout noise per pixel increases from 12 e- to 70 e-. The smaller pixel pitch also means that the number of pixels within a window increases, and therefore also the readout noise contributors for a given measurement.

- On the other hand, the TDI option provides a significant improvement compared to the baseline; an order of magnitude in parallax errors at the faintest end and also an extended detection limit especially for the bluer stars (see Table 5-8) of at least one magnitude. These improvements are due to an increase in integration duration (no dead time induced by the de-spin mechanism reset or the detector full-frame readout) but mostly due to a sharp decrease in readout noise (a factor 5) provided by the noise-less binning in the across-scan direction (i.e. only along-

scan pixels in the window contribute to the total readout noise for a given measurement).

- Provided that detector effects do not dominate the PSF smearing (but that PSF blurring caused by the de-spin mechanism dominates), one can expect further improvements at intermediate magnitudes (10 < G < 16 mag). This is not shown here, since the same PSF smearing has been used for both the TDI and baseline cases.

In Figure 5-26, we show parallax errors for the reddest stellar type studied (M3III Av5) for the three GaiaNIR mission concepts (black lines) and compare them to Gaia (blue line); it shows that for red stars as such the baseline concept provides no improvement compared to Gaia but only the TDI concept with a significant improvement as a potential for new science. Figure 5-27 shows a similar comparison for a solar-type star i.e. with most of its flux within the visible band; for this type of stars, the GaiaNIR concepts cannot compete with Gaia. The lack of performance improvement compared to Gaia for red stars, despite a greater sensitivity in the NIR band, is due to:

- A reduced aperture implying less signal per observation
- A reduced focal plane implying fewer observations per object
- And an increase in readout noise introducing more noise per observation.

But it is also due to the fact that for photometry purposes the astrometric focal plane is divided in four wavebands, which means that actually only one fourth of the focal plane benefits from the widest band [400-1900] nm. A different focal plane arrangement may provide better performance with a minimum impact on photometry: e.g., four columns with the widest band and only one column for all other bands and/or a longer cut-off wavelength.
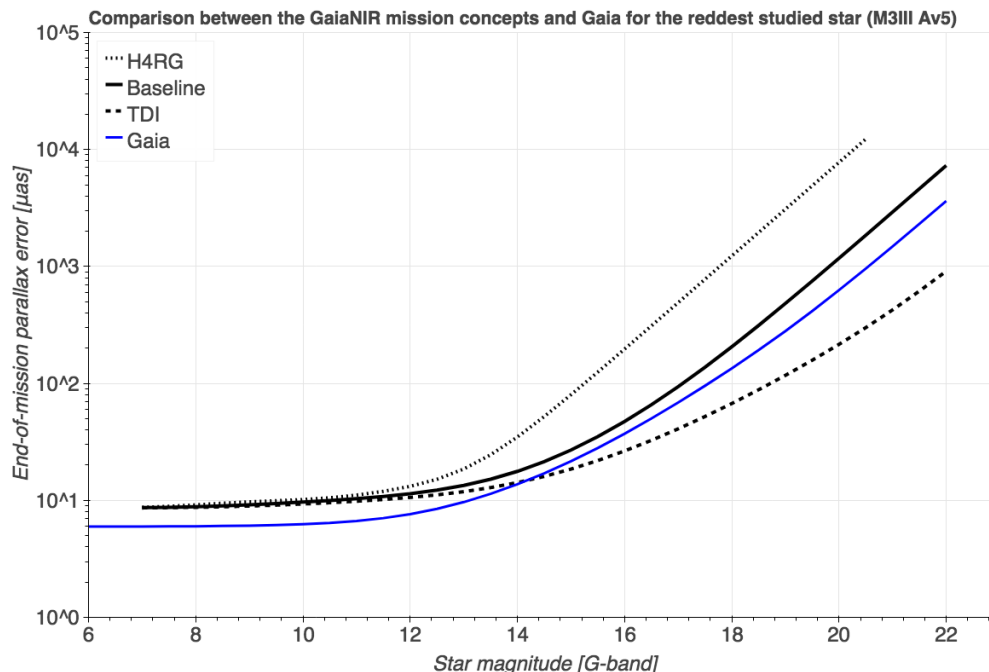
Figure 5-26: Performance comparison between the different GaiaNIR concepts (black lines) and Gaia (blue) for the reddest star studied
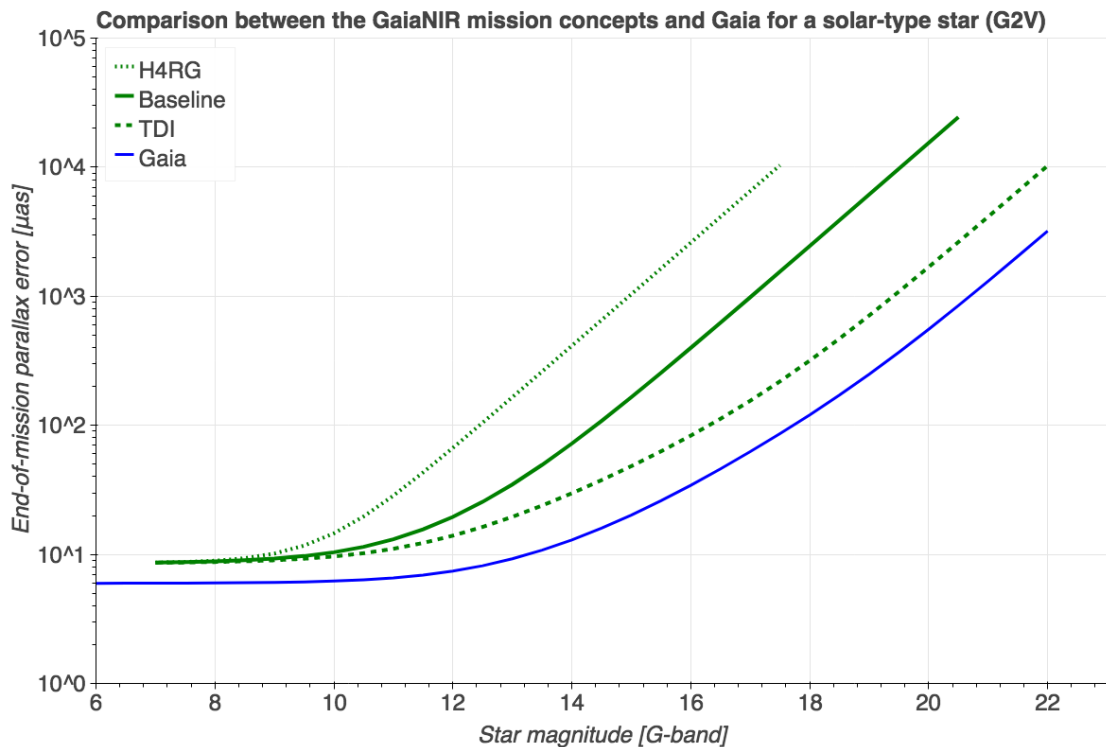
Figure 5-27: Performance comparison between the different GaiaNIR concepts (green lines) and Gaia (blue) for a solar-type star

5.4.4.2 Impact of detector performance on final astrometric accuracy

For a red star spectral type (MoV)), we now investigate the impact of some of the most critical detector specs, namely: readout noise (see Figure 5-28), dark current (see Figure 5-29), and pixel pitch (see Figure 5-30 and Figure 5-31). Only one parameter at a time is varied and all the others are fixed to the baseline case if not mentioned otherwise. The figures show the change in parallax error compared to the baseline as a function of the stellar magnitude: smaller-than-one values mean an improvement in performance, and greater-than-one values degradation.

Figure 5-28 clearly shows that the measurement is readout noise limited especially for fainter targets; hence the lower the readout noise, the better the end-of-mission performance. Only for readout noise values lower or equal than 1 e- (not changing any other detector specs), the baseline performance can reach the TDI performance (dashed line). This points at the potential of MCT APD technology, which provides sub-electron readout noise (see Detector section 5.2). Note that the readout noise per observation can also be decreased:

- by using more advanced sampling methods (see Detector section 5.2),
- possibly by summing up only the pixels containing signal during the on-board processing,
- and more efficiently by modifying the pixel dimensions (see the following).
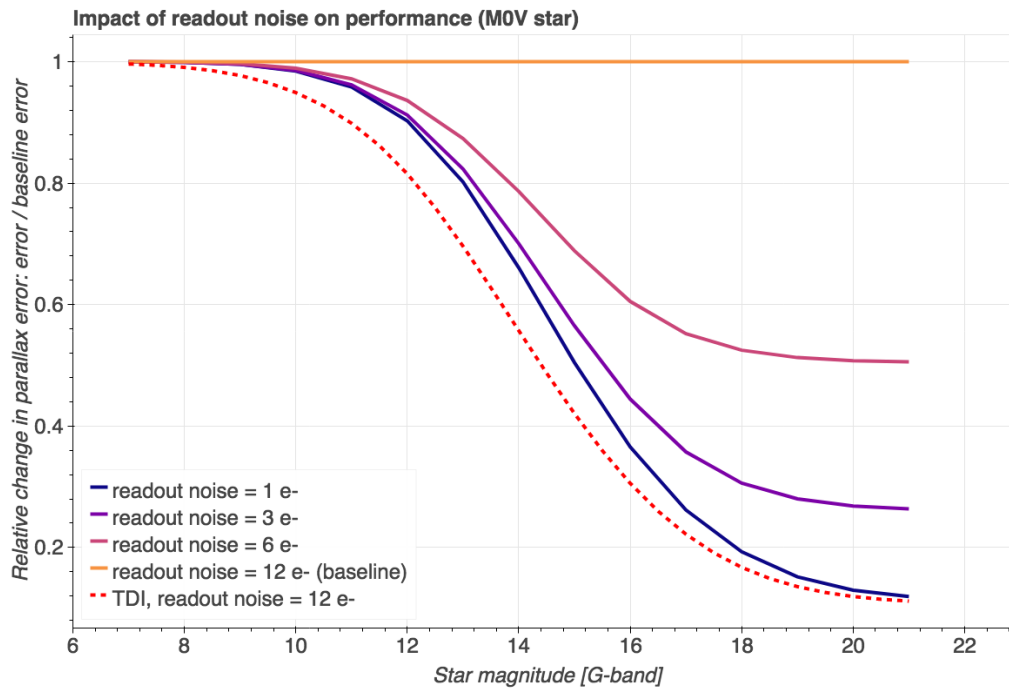
Figure 5-28: Change in astrometric error compared to the baseline (solid lines) for different readout noise values and for the TDI option (dashed line): the baseline requires sub-electron readout noise to catch-up with the TDI performance
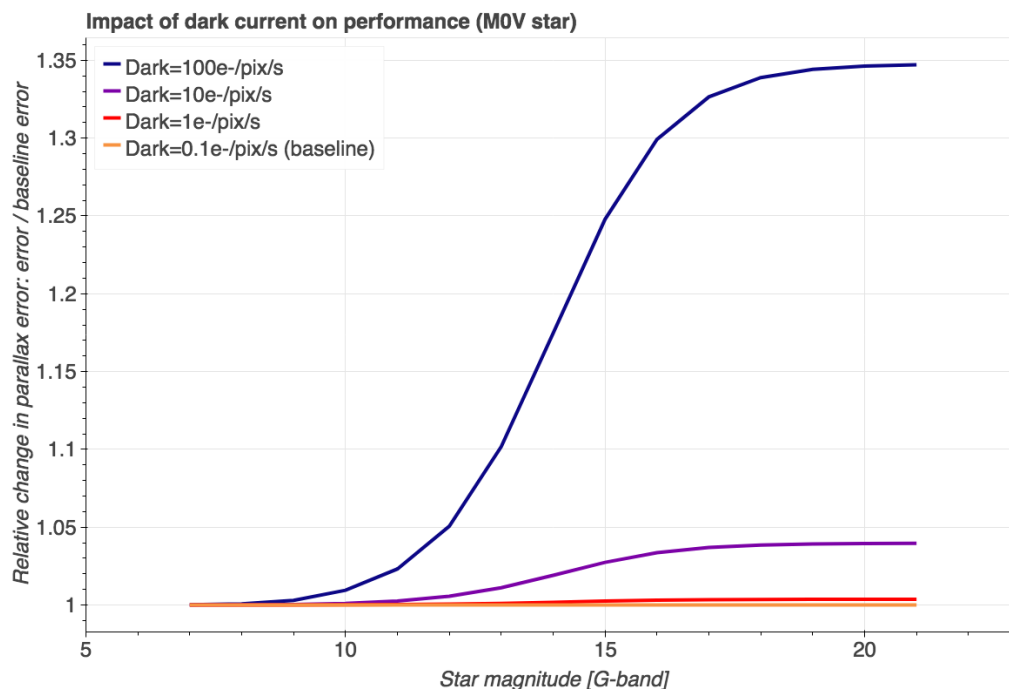
Figure 5-29: Change in astrometric error compared to the baseline for different dark current values; the performance starts to degrade noticeably only for a factor 100 increase in dark current

On the contrary, Figure 5-29 shows that dark current is not a limiting detector spec here, and this remains true even when halving the readout noise (not shown here). This shows that depending on the dark current performance of the detector, the detector operating temperature may be increased with only a small penalty in performance. Furthermore, one should note that we computed the sky background for the widest waveband to be about 0.5 e-/pix/s; dark current values smaller than this number will not provide a performance improvement.

As previously discussed, by increasing the size of pixels the integration duration increases (less pixels in a full frame to read out) and the total readout noise per observation decreases (same area but less pixels within a window). There is some limit to the pixel size increase nevertheless:

- Across-scan one needs to be able to accommodate for on-board measurement of the motion of stars from one detector column to the other.

- And, more importantly, along-scan the sampling of the LSF affects the centroiding accuracy.

We distinguish between across-scan and along-scan pixel size. Figure 5-30 shows that increasing the size of pixels across-scan brings significant improvement in performance, while Figure 5-31 shows that for a M0V star there is an optimum in along-scan pixel size close to 25 μm. (note that this optimum may be different for other stellar types, bluer in particular). For a 30 μm pixel along-scan, we notice first a degradation in performance for intermediate magnitudes (12 < G < 17 mag) followed by an improvement for fainter magnitude; this confirms that, while at the faint end the measurement is dominated only by readout noise, for intermediate magnitudes the shape and sampling of the PSF is critical.
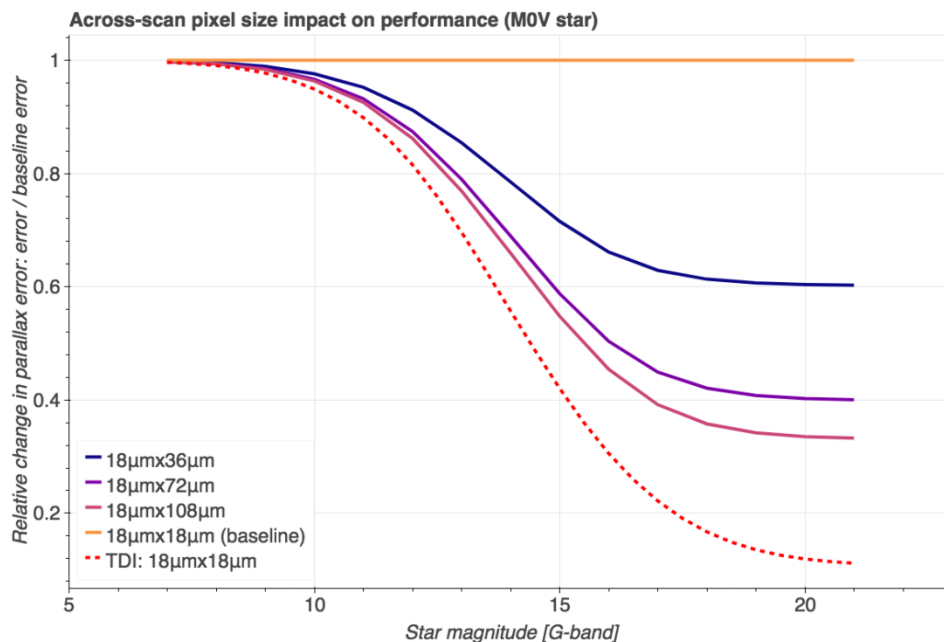
Figure 5-30: Relative change in astrometric performance for different across-scan (AC) pixel sizes: the baseline performance benefit greatly from a significant increase in across-scan pixel size
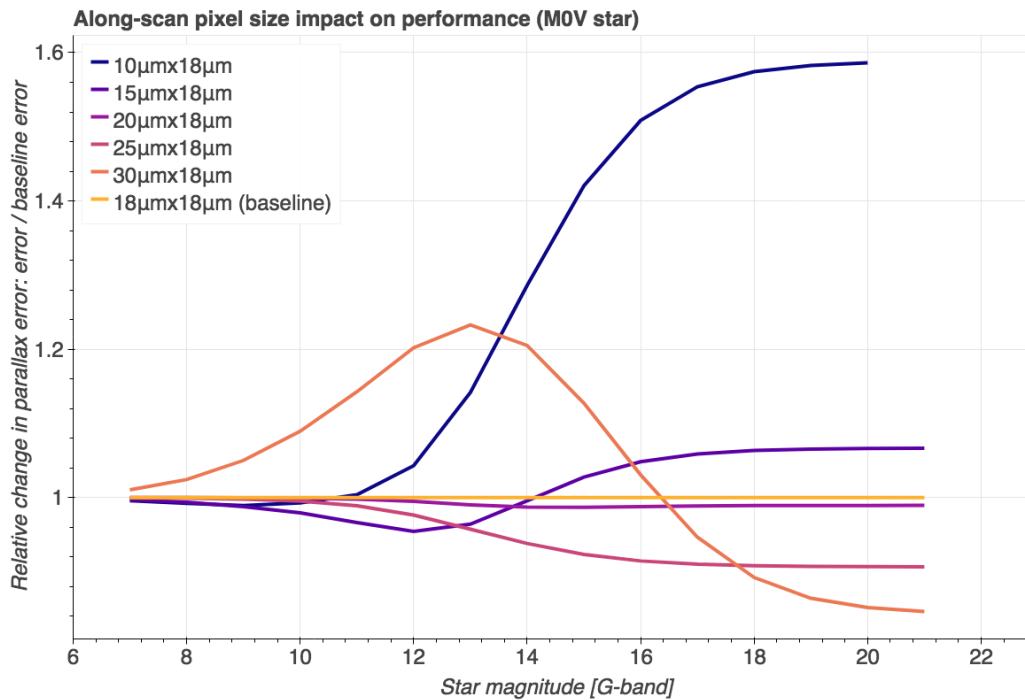
Figure 5-31: Relative change in astrometric performance for different along-scan (AL) pixel sizes: performance improvement for the entire magnitude range occurs only for 20 and 25 μm.

5.4.4.3   Model validation

5.4.4.3.1   *Validation against Gaia's performance*

To validate the end-of-mission performance model presented herein (referred to as CDF model in the following), we compute performance estimates using the original Gaia mission parameters as input (cf. Table 5-7) and compare the obtained results to the actual Gaia performance prediction as published in RD[12].

As can be seen from Table 5-9 and by comparing the green dots (actual Gaia numbers) and green solid line (CDF model) in Figure 5-32, our model estimates for Gaia closely match the Gaia numbers.

Stellar type	G2V	
Model	**CDF**	**Gaia**
Magnitude [G-band]	**End-of-mission parallax error [μas]**	
7 (bright)	6	5-16
14.76 (*)	20	24
19.76 (*)	553	540

Table 5-9: Validation of the presented model against the original Gaia mission end-of-mission parallax errors. (*) The V to G passband conversion introduces the decimals
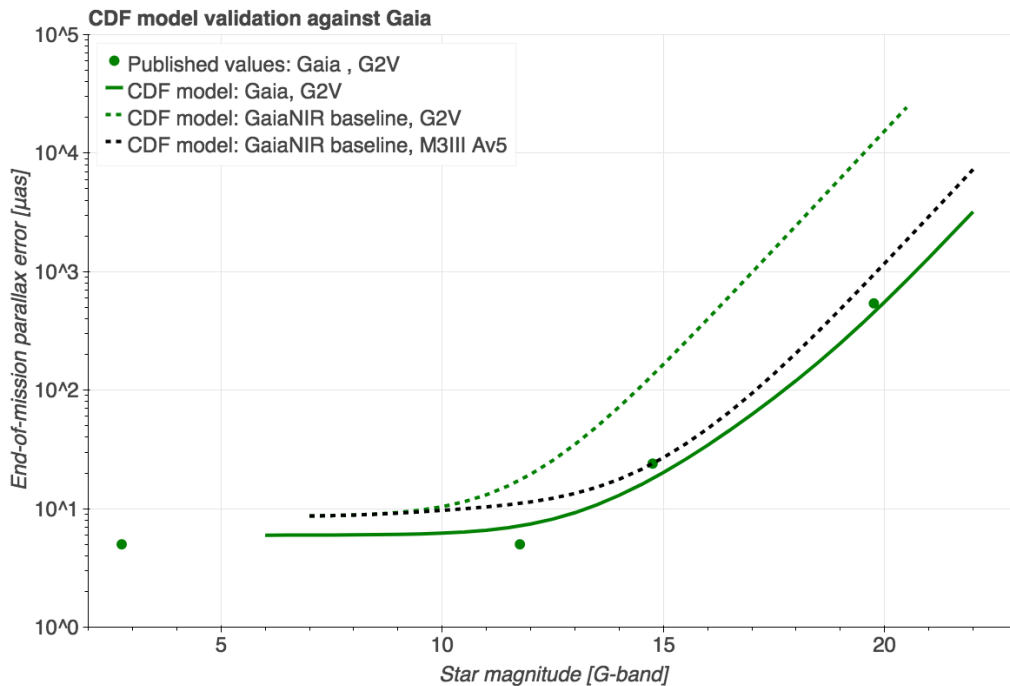
Figure 5-32: Validation of the CDF astrometric performance model using the original Gaia mission as input (green solid line) against the published Gaia performance estimates (green dots) for a G2V star. And for comparison we also show the GaiaNIR baseline parallax errors for a G2V (green dashed) and the reddest star studied (black dashed line). See Figure 5-26 and Figure 5-27 for a more complete comparison including the TDI concept

5.4.4.3.2   *Comparison with Hobbs' model*

In parallel to the CDF model, a similar GaiaNIR model for performance prediction has been developed independently by D. Hobbs – the GaiaNIR lead scientist. Hobbs' model strictly implements the Gaia 'White Paper' performance model as described in RD[13], with modifications to take into account the specificities of the GaiaNIR missions (e.g. the different wavebands). Table 5-10 compares Hobbs' results with the CDF results and shows that:

- The CDF model gives systematically a more conservative estimate.
- However, considering the different approaches of the two models, as well as several differences in input parameters and assumptions, the results match reasonably well (same order of magnitude) with the strongest deviation at the faint end.

Magnitude [G-band]	End-of-mission parallax error [μas]					
Stellar type	G2V		M0V		K5III Av5	
Model	CDF	**Hobbs**	CDF	**Hobbs**	CDF	**Hobbs**
Case	Baseline					
7 (bright)	9	**9**	9	**9**	9	**9**

15	165	**99**	81	**55**	38	**27**
21	38660*	**22533**	16843	**11024**	5421	**3584**
Case	H4RG					
7	9	**8**	9	**8**	9	-
15	1036	**680**	453	**365**	144	-
21	259912*	**170694**	113373*	**91496**	36377*	-
Case	TDI					
7	9	**9**	9	**9**	9	**9**
15	48	**33**	34	**26**	23	**18**
21	4129	**1318**	1881	**714**	694	**312**

Table 5-10: Comparison between the CDF and Hobbs' astrometric performance model estimates for three different stellar types and the three different GaiaNIR mission concepts studied

5.4.5 Conclusion

We have compared three different mission concepts. Both the baseline and the H4RG options rely on existing detectors but a to-be-developed de-spin mechanism (see Mechanism section 5.7). This de-spin mechanism is not needed in the third option, called TDI, but this option relies on the development of a completely new detector technology (see Detector section 5.2).

The TDI option provides an order of magnitude better performance at fainter magnitude as well as a fainter detection limit compared to the baseline, while the H4RG option provides no improvement. We also show that as such only the TDI option provides a potential for new science by bringing an improvement in astrometric performance for redder stars compared to the original Gaia mission.

The baseline concept however provides no improvement compared to Gaia (even for redder stars) due to reasons listed here above and among which the focal plane size and arrangement: minimum number of detector rows and columns and merging of astrometric and photometric fields to minimise cost (due to higher MCT detector cost compared to CCDs, and M-class cost goal).

The limiting detector spec is by far the readout noise. Significant improvement can be reached by altering the pixel pitch of standard detectors (baseline concept), i.e. significantly elongating the pixel dimension across-scan to match the telescope aperture ratio. More advanced sampling methods (e.g., Fowler sampling) and clever on-board processing could further reduce the readout noise such that the baseline option performance can be improved towards the TDI one. Nevertheless, concepts relying on a de-spin mechanism potentially present a greater challenge (and risk) in terms of scientific calibration (see Calibration section 5.3).

Possibly a different arrangement of the focal plane wavebands, maximising the overall flux received in the NIR wavebands while conserving the possibility to perform photometry measurements, would benefit all GaiaNIR mission concepts. This was not

studied here and would require the photometry measurement performance to be also estimated and taken into account.

5.5   PLM Configuration

5.5.1   Requirements and Design Drivers

- Provide the telescope and FPA with a very stable environment. To minimise any mechanical and thermal perturbation.

- Provide the CCD with sufficient shielding

- Support the telescope and FPA during all phases

- Minimise the mass

- Provide sufficient radiator area to meet the thermal requirement. Surface area of 6m^2 and 0.4m^2 for radiator for cold and warm region respectively

- Provide support structure to the optical instrument and radiator

- Optical light path should not be obstructed by the support structure

- Provide set of 3 identical bipods subsystem which include each:
  - o An In-orbit bipod made of glass fibre composite which provides a low thermal conductivity
  - o A Launch bipod made of CFRP that is deployed after launch, then locked in deployed configuration. The launch bipod should be stiff enough to withstand the launch phase.

5.5.2   Assumptions and Trade-Offs

There were no assumptions or trade-offs associated with the payload module configuration.

5.5.3   Baseline Design

The Payload Module of the GaiaNIR Spacecraft includes the common optical bench that facilitates the three instruments and the interface equipment that attaches the PLM to the SVM. The Thermal Tent of the Payload Module is attached to the Service Module to avoid a physical connection to the optical bench.

The optical bench consists of a toroidal structure using silicon carbide material because of its optical, mechanical and thermal properties. The most important aspect for Gaia to meet its science objectives is a thermally stable mounting platform. This is accomplished by using silicon carbide which is known not to expand and contract as a function of temperature.

The torus is about 3.6 meters in diameter being quasi-octagonal in structure consisting of individual Silicon Carbide segments. The optical bench supports the GaiaNIR telescopes and the focal plane assembly.

The PLM Instrument interfaces with the SVM mechanically, at lower interface level of the Bipods and Release Mechanism subsystems. The Bipods and Release Mechanism is a set of 3 identical Bipods subsystems, which include each:

- A Launch bipod with its two Hold-down release mechanisms at its upper end and its hinge-type connection at its bottom end. This bipod is "deployed" after launch, then locked in deployed configuration.

- An In-orbit bipod that is fixed.

Each bipods subsystem is a coherent and integrated subsystem, interfacing on one side on the Service Module (SVM) top floor thru one interface bracket, and on the other side on the PLM Instrument (payload optical bench) thru two identical brackets, at the level of the tore.

The Launch bipods are arranged to support the PLM Instrument during all its lifetime, i.e, including AIT, launch & in-orbit phases. After release of the Launch bipods, while in-orbit, the In-orbit bipods ensure the mechanical connection between the SVM and the PLM Instrument and support the routing of the harness between SVM and PLM Instrument, while minimising thermal exchange between the 2 modules.
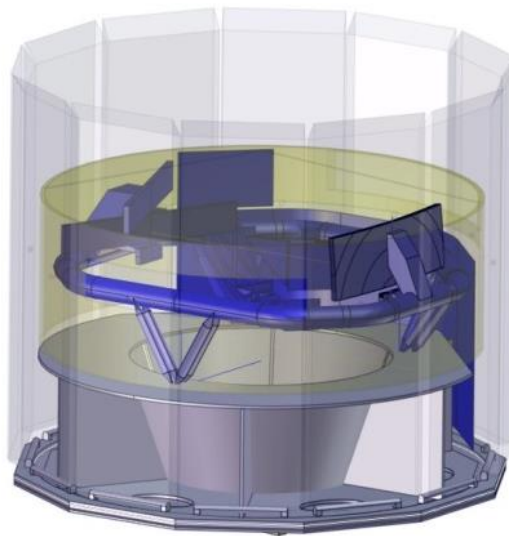
Figure 5-33: GaiaNIR PLM in the launch configuration

The optical path of the telescope is composed of:
- Primary mirror
- Secondary mirror
- Tertiary mirror
- 3x Flat mirrors:
  - At the entrance pupil
  - At the exit pupil
  - Folding mirror after the exit pupil.

Figure 5-34 and Figure 5-35 show the GaiaNIR optical surfaces and light path. Support structures of all optical instruments are directly connected to the torus structure to avoid obstructions of the light path except for the rotating mirror that is located in the middle of the torus structure. Finally, the support structure of the rotating mirror is

designed to be parallel to the light path from the rotating mirror to the FPA see Figure 5-44.
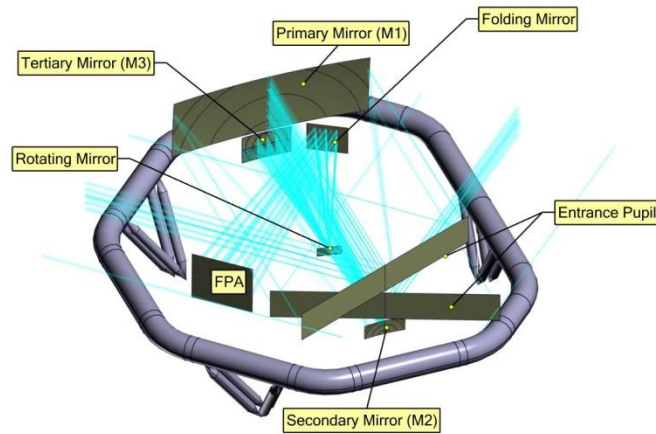
Figure 5-34: GaiaNIR optical surfaces and the light path
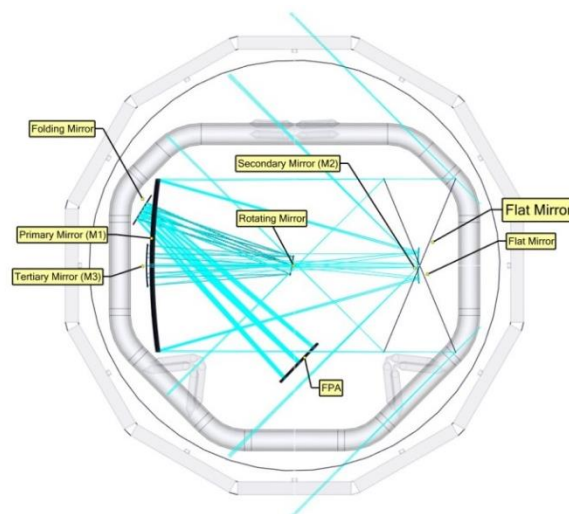
Figure 5-35: Top view of the GaiaNIR Light path

The support structure of the GaiaNIR optical instrument is shown in blue colour in Figure 5-36.
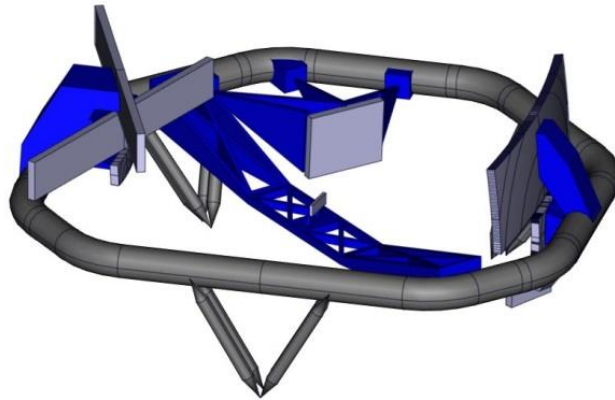
Figure 5-36: Optical support structure
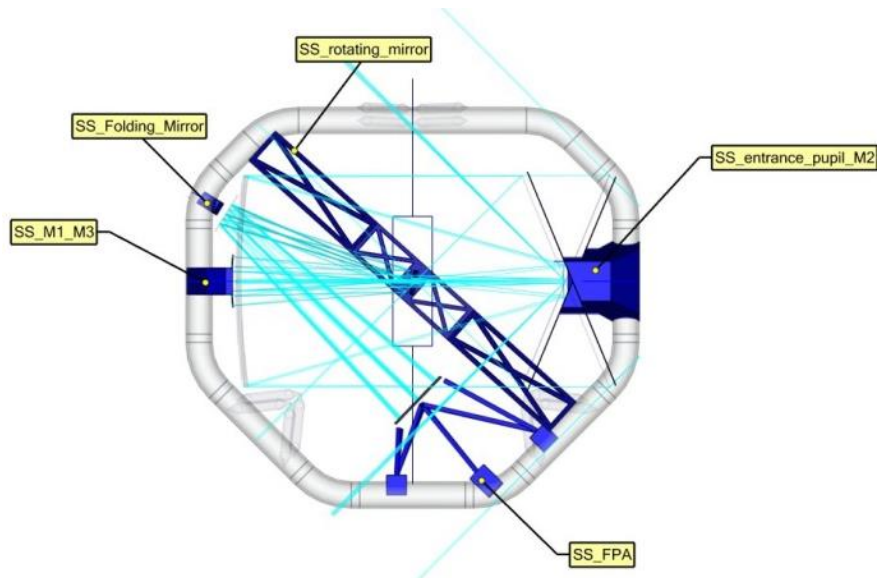
Figure 5-37: Top view of the support structure

Following figures show that the GaiaNIR optical light path is not obstructed by the support structure.
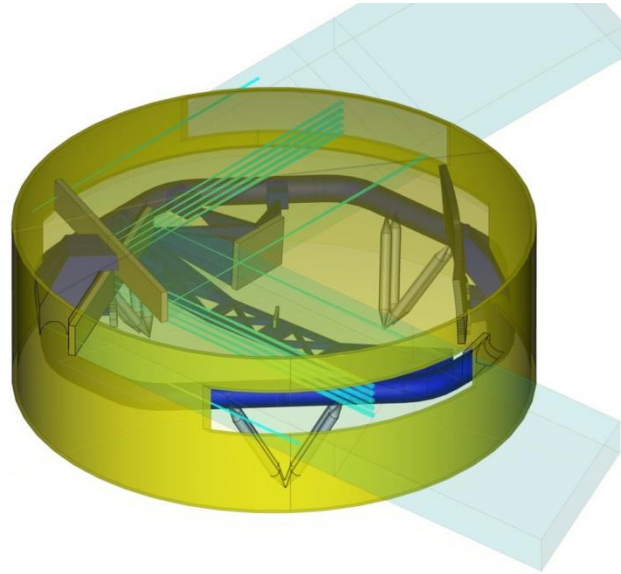
Figure 5-38: Light path at the entrance pupil
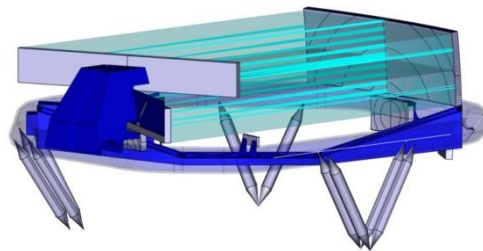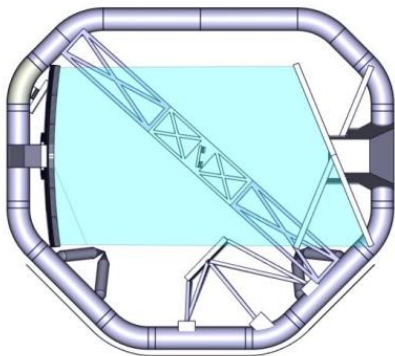
Figure 5-39: Light path on M1
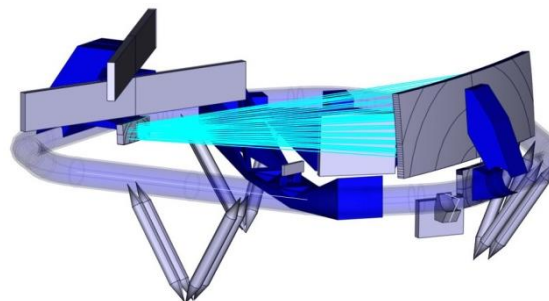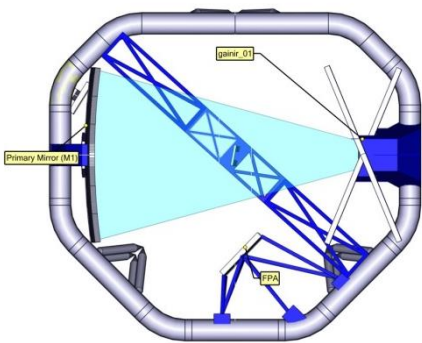
Figure 5-40: Light path on M2
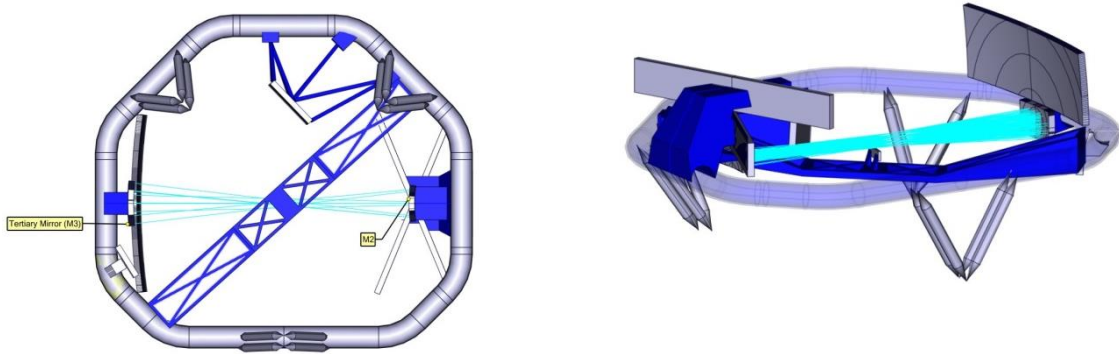
Figure 5-41: Light path on M3
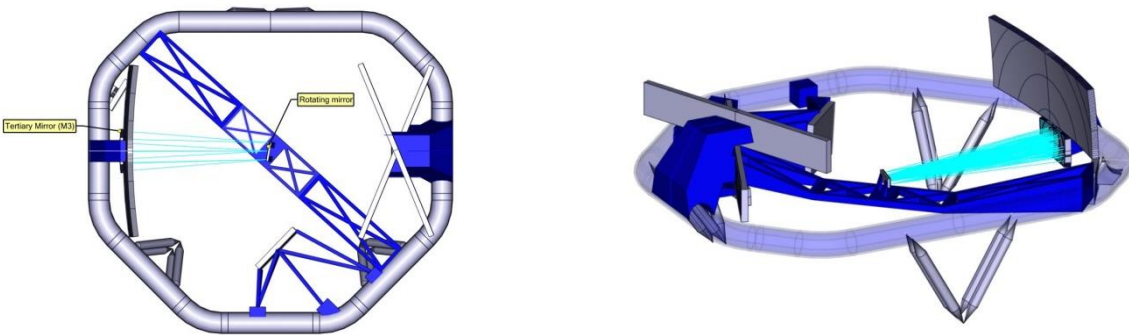
Figure 5-42: Light path on Rotating Mirror
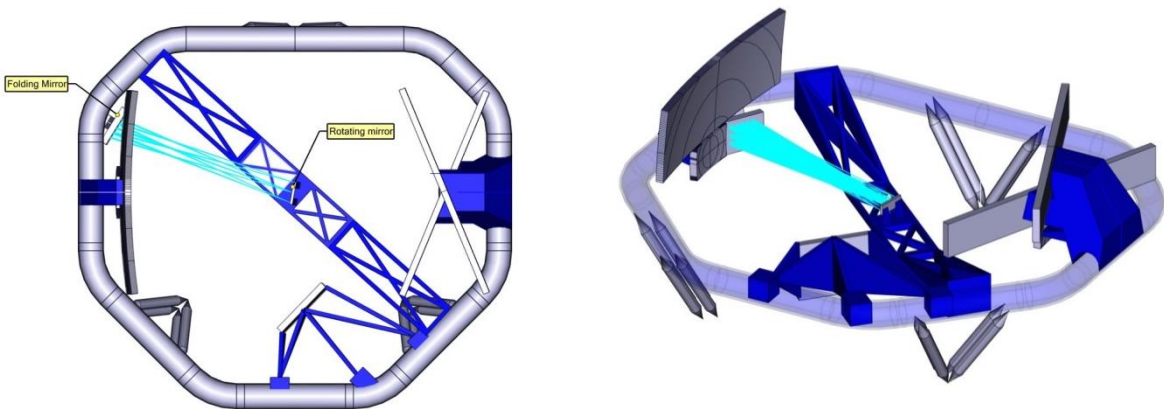
Figure 5-43: Light path on Folding mirror
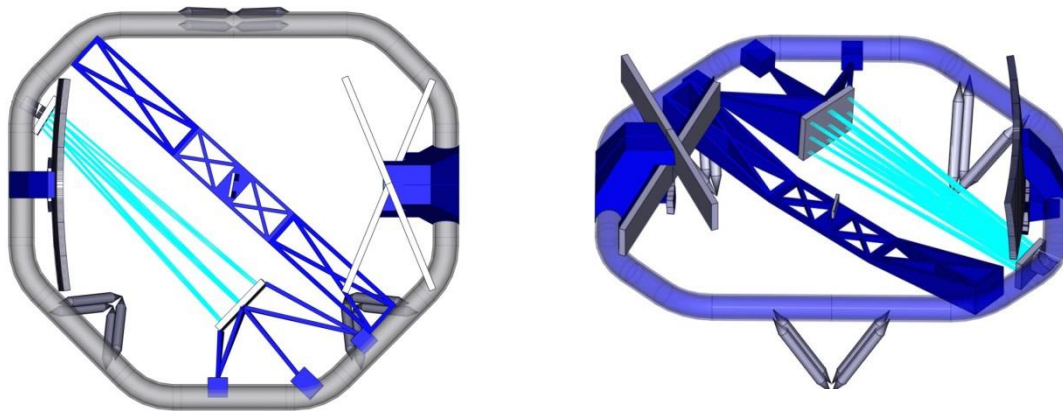
Figure 5-44: Light path to FPA

Figure 5-45 shows the radiator area allocated around the torus structure. There is no detailed study of how the radiator interfaces with the PLM. This should be further investigated in later phase.
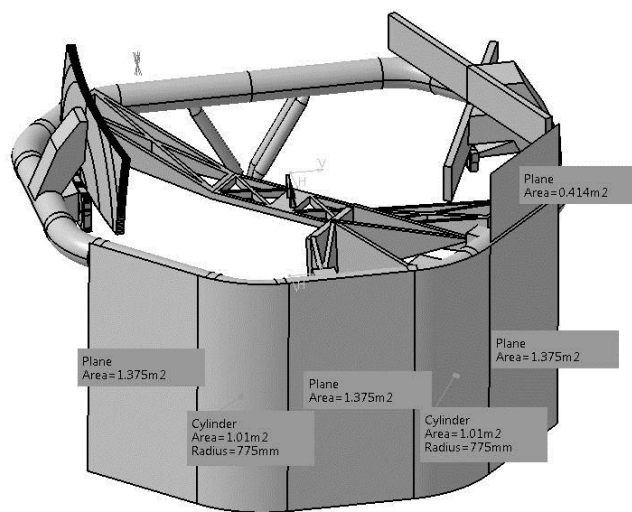
Figure 5-45: PLM Radiator area

5.5.4 Overall Dimensions

Following figures show the overall dimension of the PLM. Dimensions are shown in mm.
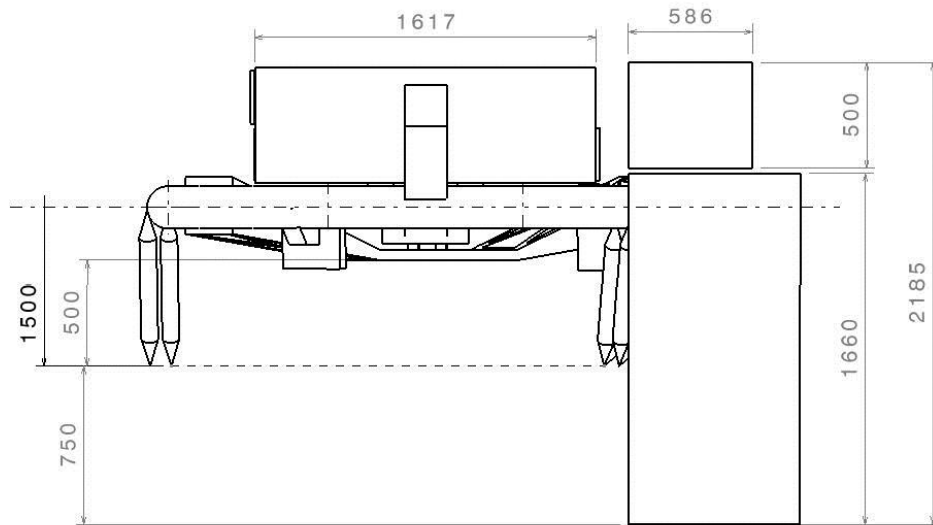
Figure 5-46: Overall PLM dimension (side view)
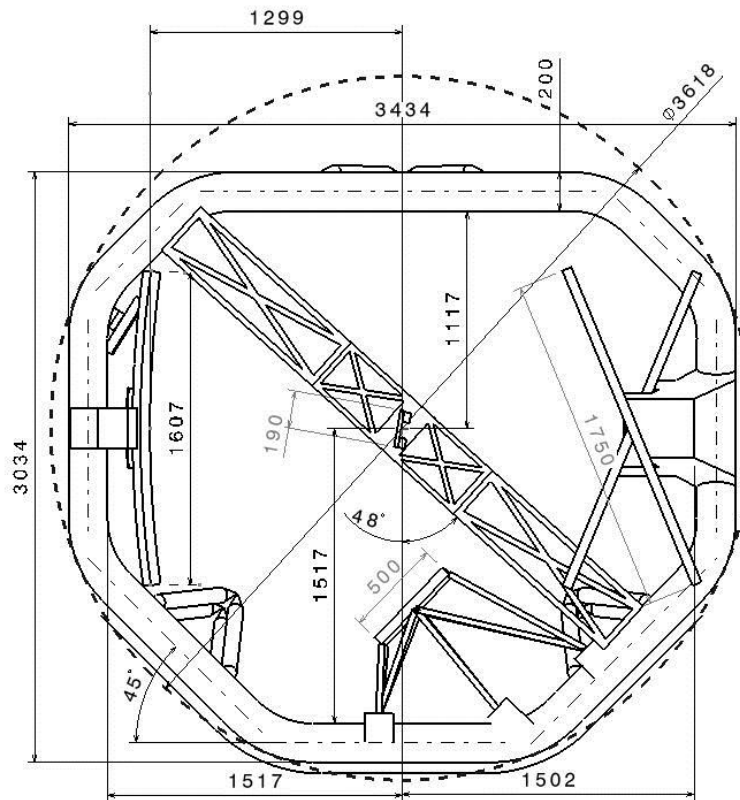
Figure 5-47: Overall PLM dimension (top view)

5.6 PLM Structures

5.6.1 Requirements and Design Drivers

SubSystem Requirements		
Req. ID	**Statement**	**Parent ID**
STR-010	The GaiaNIR PLM structure shall exploit commonalities with the Gaia spacecraft as much as possible.	MIS-050

STR-010: Mission requirement MIS-050 states that the cost to ESA shall not exceed 550M€[2017]. The flow down of this requirement onto the structures domain means that the Gaia design heritage shall be reused as much as possible. Obviously, the optical design is quite different from that of Gaia, even the overall dimensions of the spacecraft – while similar – are sufficiently different that a direct reuse of structural components can be ruled out. However, it is worth to carry-over the overall design principle and therewith the lessons learned during qualification and operation of the Gaia spacecraft.

The number of direct requirements regarding the structural subsystem is thus limited, but several assumptions will be made deriving from that one requirement and the thermal environment requirement TCS-050.

5.6.2 Assumptions and Trade-Offs

Assumptions	
1	The optical bench shall be attached to the SVM by three pairs of quasi-isostatic bipods, one of which is built for launch loads and the other for low thermal conductance and low stiffness. The former can be separated from the PLM and securely folded away. (Same design as Gaia S/C).
2	The optical bench is made of silicon carbide (same design as Gaia S/C).
3	The thermal tent structure is closely derived from the Gaia S/C design.

Assumption 1: The concept of the bipods attaching the optical bench to the SVM is carried over from Gaia. This contains three pairs of quasi-isostatic struts which are dimensioned to sustain launch loads and can be separated and securely folded away. The PLM is also supported by six struts that are optimised for low gravity environment and low thermal conductivity. One strut of each type is basically paired up in a common subassembly that allows the former to do its job until LEOP phase, when its separation is executed and the latter to perform after that.

The secure folding away of the strong strut is required to achieve the best possible steady rotation motion required for science operation, if the struts weren't clamped down after separation from the PLM the quality of the rotation movement could be diminished by shifts in the position of the struts.

Assumption 2: The optical bench are made of silicon carbide (same material as Gaia S/C).

Assumption 3: It is assumed that basically copying the thermal barrier between SVM and PLM from Gaia is sufficient to achieve thermal requirement TCS-050, this pertains to the application of multi-layer insulation between the PLM and SVM.

5.6.3   Baseline Design

The diameter of the optical system is slightly larger than for Gaia, the distance between primary mirror (M1) and the centre point of the flat split mirror (M0) at the entrance pupil is 2459 mm, edge-to-edge the distance between these two is 3176 mm, see Figure 5-48.
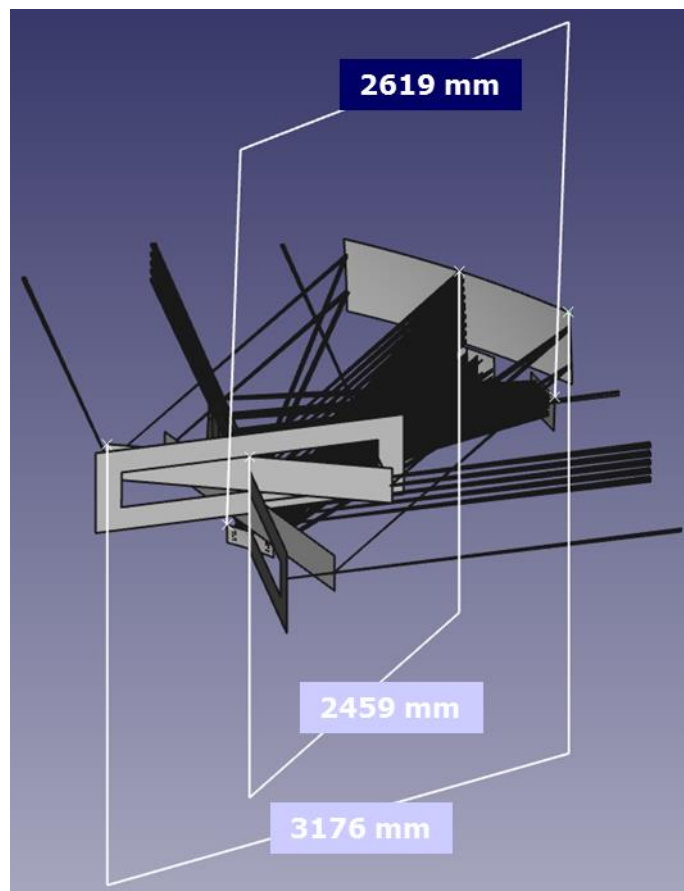
Figure 5-48: GaiaNIR telescope size

However, the torus structure to which all the mirrors are attached does not have to encircle the primary mirror elements M0 and M1, but rather the smaller mirror elements below these. The largest distance between two elements in the lower part of the optics is 2619 mm between the secondary mirror (M2) and the folding mirror (M5). The toroid has to allow for these elements to be placed within it. Accounting for a minimum of 100 mm distance between the torus and each mirror for holding and adjustment brackets this leads to 2820 mm torus minimum diameter. With a torus cross-section of 200 mm the minimum outer diameter of the torus thus is 3220 mm, which is about the same max distance (3176 mm) between flat mirror (M0) and primary mirror (M1). The configuration studies arranging the torus with the mirrors, allowing

for sufficient mounting space for the mirrors and adding the thermal tent around it showed that the GaiaNIR spacecraft body (i.e. the diameter of the thermal tent) will realistically have a diameter of 3.8 m. A size comparison of Gaia and GaiaNIR tori can be seen in Figure 5-49.
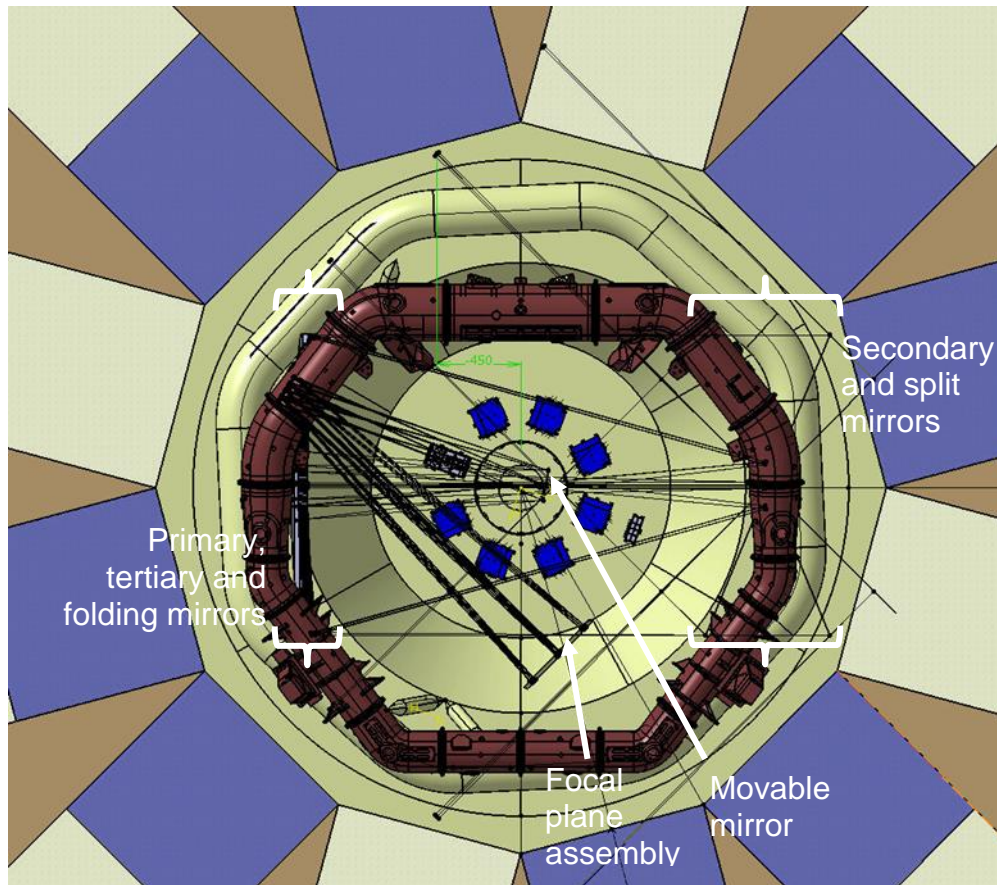
Figure 5-49: Size comparison between Gaia (dark red) and GaiaNIR tori

Figure 5-49 shows that a part of toroid (at the top in the image) carries no optical elements. Accordingly, the torus will be shortened in this region, very much like the overlaid Gaia torus (in dark red) in the image. The size reduction may not only serve a moderate cost reduction but also allow the area to be used for equipments which may be mounted to the top deck of the SVM (of course assuming proper thermal insulation towards the optical assembly). Allocation of equipments in this area may serve counterbalancing the mass of the optical assembly and radiators (more on the radiators below).

The thermal analysis as presented in section 5.8.3.3 shows that to cool the focal plane assembly down to the required 140 K (and bearing in mind that only passive thermal hardware shall be used, requirements TCS-010 and TCS-020) a radiative surface of 6 m² is needed (cold radiator). This is a significantly large proportion of the spacecraft body's surface area. Furthermore, the Front End Electronics (FEE) and Data Processing

Unit (DPU) need to be placed close to the focal plane assembly, according to the thermal analysis these require another 0.4 m² of radiative surface (hot radiator). Figure 5-50 shows the two radiators attached to the PLM.
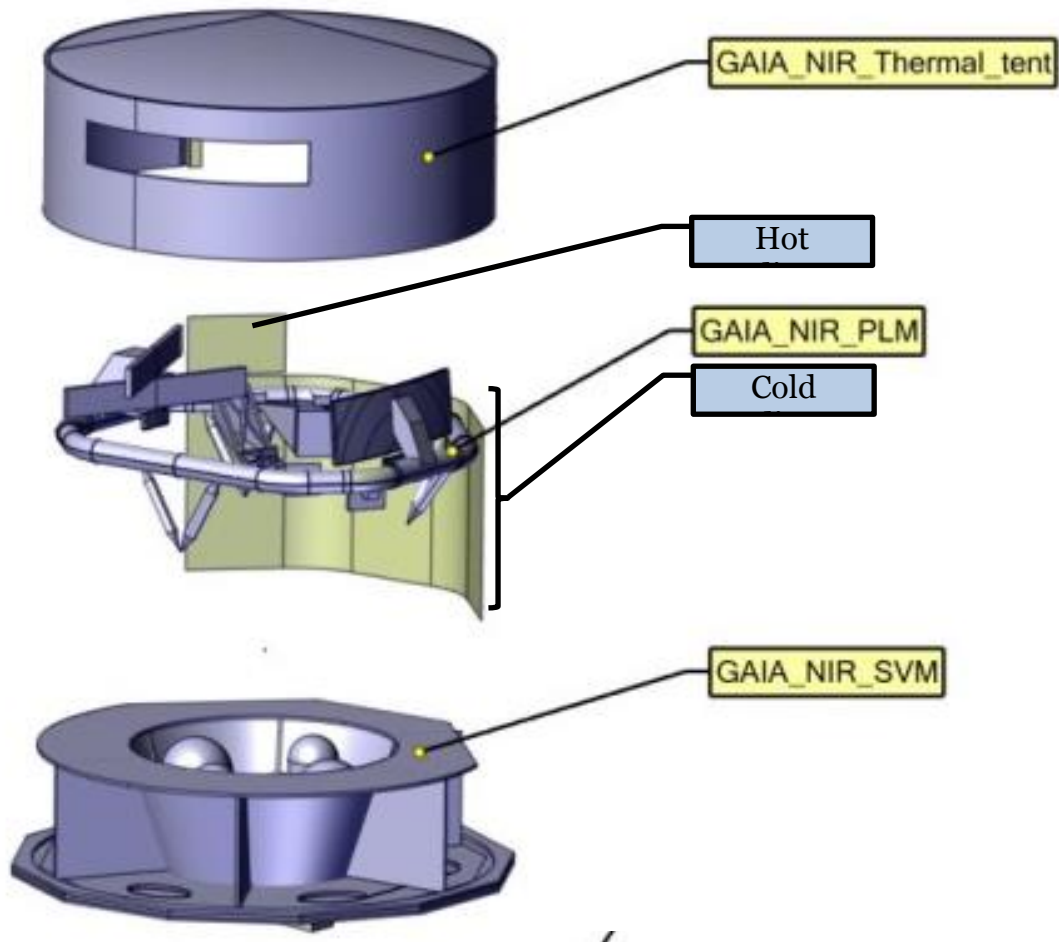
Figure 5-50: Service module (SVM), payload module (PLM) with hot and cold radiators and thermal tent

Due to the size required for the cold radiator, the folding mirror and FPA were allocated such that the focal plane assembly would be on the side of the upper flat (M0) mirror, allowing a radiator height of up to 2 m under the window in the thermal tent. The hot radiator is located to the right of the window on the thermal tent. Figure 5-51 shows the two radiators covering one whole side of the spacecraft body, except the window of the upper flat mirror (M0).

**Figure 5-51: Focal plane assembly radiator (orange) with 6 m² size,
FEE and DPU radiator (red) with 0.4 m² size**

The distances between the detectors, the FEE, the DPU and their respective radiators is of concern. Figure 5-52 shows a distance of the focal plane assembly FPA to the "cold" radiator of about 1 m. The FEE has a distance of about 1.3 m to the "hot" radiator and the DPU can be placed behind the FPA such that it has 0.9 m to the "hot" radiator, for improved clarity, Figure 5-53 shows the conductive distances within the thermal concept sketch (taken from Figure 5-64).
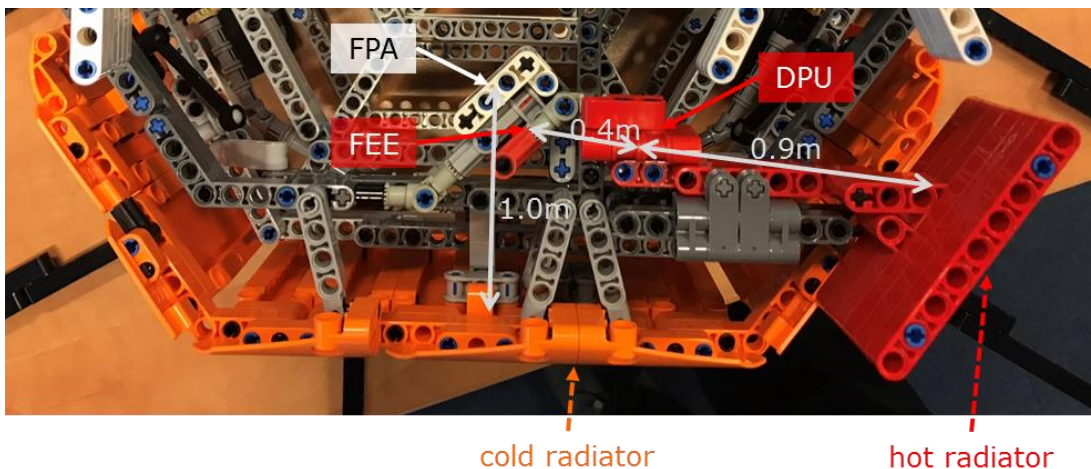
Figure 5-52: Assessment of distances between radiators and FPA, FEE and DPU
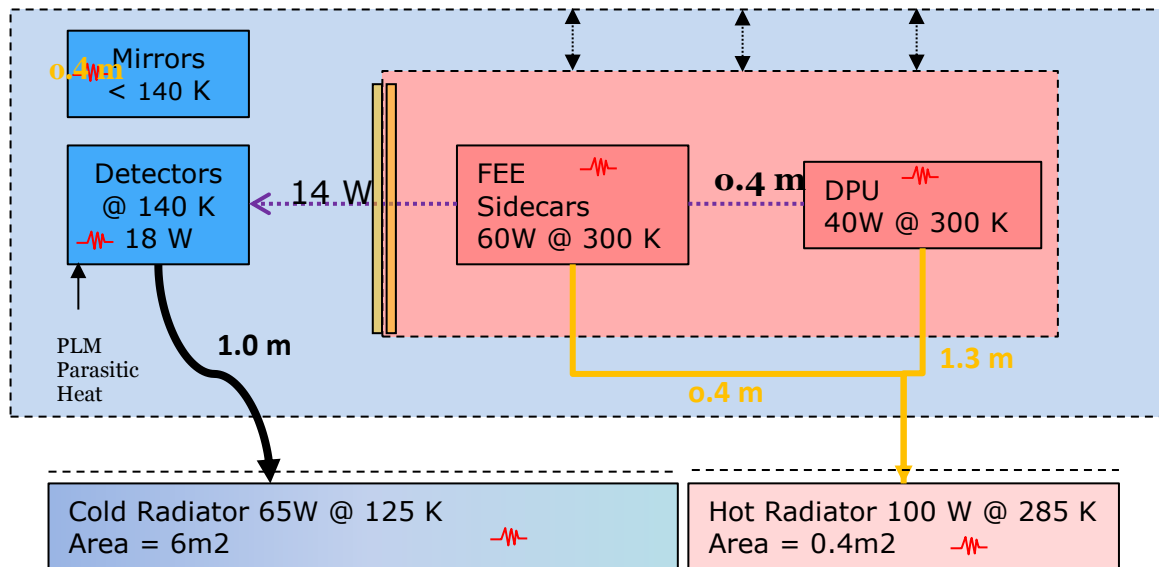
Figure 5-53: Thermal concept sketch (taken from Figure 5-64) with conductive distance lengths

As mentioned above, the concentration of radiators, FPA, FEE and DPU on one side of the PLM means quite a mass imbalance which has to be compensated, ideally not only within the SVM. The torus radius is reduced in the area opposite of the FPA, allowing to place equipments to counterbalance the radiator mass (assuming thermal shielding in between SVM and PLM)

The mass estimate for the PLM structure is closely based on the Gaia PLM masses. The mass of the bipods carrying the PLM remains unchanged, the Periscope/M4 support structure mass of Gaia is kept, representing on GaiaNIR the structure needed to hold the movable mirror M4. The torus mass is increased by 5% wrt. Gaia, representing the size increase. Table 5-11 shows the full PLM structures mass calculation.

Product Tree Item	No. of Items	Gaia Item Mass [kg]	Scaling Factor [%]	GaiaNIR Item Mass [kg]
Mirror Support Structures				**260.74**
Tore	1	192.14	5%	201.75
Tore	1	6.91	5%	7.26
Tore	1	8.28	5%	8.70
Tore	1	2.67	5%	2.80
Main Bipods (fixed + launch struts)	0	12.07	0%	0.00
Periscope/M4 support structure (FOS)	1	33.02	0%	33.02
FOS Invar Shims	1	2.85	0%	2.85
PLM/SVM IF Shims	3	1.46	0%	4.37

Telescope MLI and Thermal Hardware	0	17.35	0%	0.00
Telescope MLI and Thermal Hardware	0	3.40	0%	0.00
Telescope MLI and Thermal Hardware	0	0.50	0%	0.00
Telescope MLI and Thermal Hardware	0	0.60	0%	0.00
Telescope MLI and Thermal Hardware	0	11.00	0%	0.00
Telescope MLI and Thermal Hardware	0	0.38	0%	0.00

Table 5-11: GaiaNIR PLM structure mass estimation

5.6.4 Technology Requirements

No technology developments for structural subsystems required.

5.7 PLM Mechanisms

5.7.1 Requirements and Design Drivers

SubSystem Requirements		
Req. ID	**Statement**	**Parent ID**
MECH-010	The M4 mirror mechanism shall allow step&stare observations on the focal plane every 1.81seconds while the S/C spins at 60 as/s.	
MECH -020	The M4 mirror mechanism shall perform a linear movement over a total stroke of 488.8 arcsec in 1.629 seconds, to de-spin the image at the focal plane (stare phase) .	
MECH -030	The M4 mirror mechanism shall be able to move back (step phase) to the starting position in 0.181 seconds (10% allocation).	
MECH -035	The M4 mirror mechanism shall have a resolution of 5×10^{-4} of the total stroke during the stare phase.	
MECH -040	The absolute position knowledge of the M4 Mirror shall be better then 10^{-5} of the total stroke.	
MECH -050	The M4 mirror mechanism shall have a lifetime of 5 years continuous operation	
MECH-060	The M4 mirror mechanism shall function under cryogenic temperatures of 140k.	
MECH-070	The M4 mirror mechanism shall have a constant dissipation of no more than 1 W and constant heat generation.	
MECH-080	The M2 Mirror shall have a 5DoF refocusing mechanism	

5.7.2 Baseline Design

The baseline design described in the following section contains two mechanisms for the payload module. First the required de-spin mechanism for the 4th mirror is explained, then the 5 degree of freedom refocusing mechanism for the 2nd mirror is shortly discussed. The mechanisms required for the deployable sunshield are covered in the service module section.

5.7.2.1 Mirror Mechanism M4

The mechanism for the 4th mirror (M4M) has the main task to de-spin the optical image on the focal plane so that the spacecraft can continue a steady rotation, but the detectors on the focal plane receive a steady image for ~1.629 seconds.

The M4M is located in the middle of the optical bench and very close (or on) the rotational axis of the spacecraft. This is positive for the exported torques of the mechanism into the spacecraft, but the total build-volume available for the M4M is limited as shown in Figure 5-54 below.
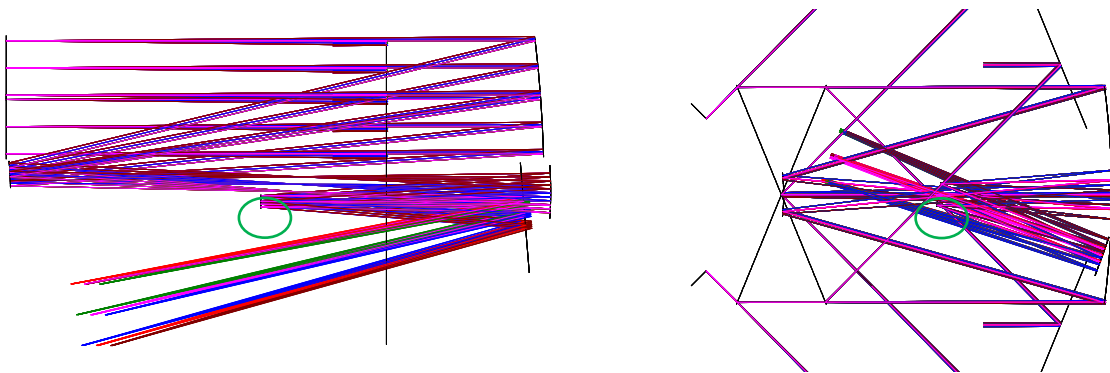
Figure 5-54: GaiaNIR Optics Design

The M4M is located directly on the optical bench and has a mirror attached to it. Therefore the M4M has to work in the same cryogenic temperature ranges as the M4 (140K). Furthermore the exported heat of the M4M has to be very low and constant over time. Same as for Gaia, the thermal requirements for the optical bench and all components located on the bench are very stringent. Temperature impacts from the M4M onto other components will have to be reduced to a minimum (in the range of mK).

The step size (during which the image has to be kept still on the focal plane) is defined by the detector size of the infrared detector. As science requires two images per detector, one step is half the detector size, equal to 18 mm (1024pixels of 18micrometer). Witha focal length of 35m, this corresponds to a 108.625 arcsec angle on the sky. This results in a step& stare time of 1.81seconds with the 60 arcsec/s S/C angular rate. As an initial budgeting, 10% of this time is reserved to move the de-spin mirror mechanism back to the start position, leading to 1.63s for starring (mechanism linear motion to counter the S/C spin) and 0.18s for stepping (mechanism return to original position)Due to the position of the M4M in the optical path, the telescope magnification factor is 10, so the angle at mechanism level is x5 the angle on the sky (reflection accounting for the missing factor x2).

	Stare	Step
Duration	1.63 s	0.18 s
Angle on sky	60 x 1.63 = 97.8 as	
Angle on mechanism	488.8 as (0.136 deg)	
Mechanism speed	300 as/s (0.08 deg/s)	2715 as/s (0.75 deg/s)

These values are the baseline for the mirror mechanism and help define the possible actuation methods for the M4MM. As the total rotation of the mirror is small (0,136°) and the rotation speeds are low (<1°/s), several options are available. The movement profile of the mirror is shown below.

Mirror Movement Profile
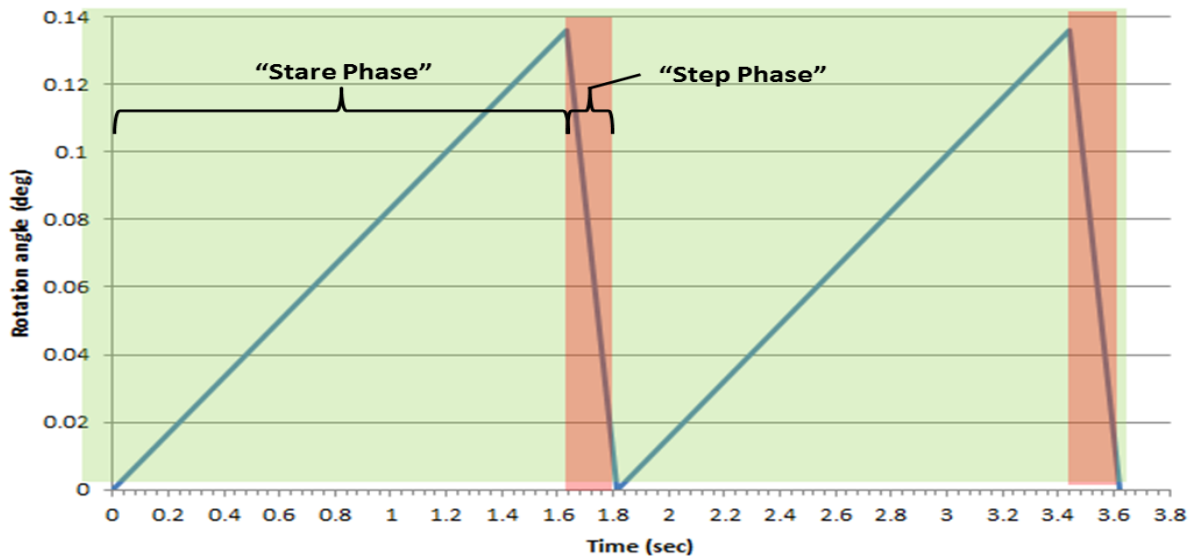
Figure 5-55: Mirror movement profile for M4 mirror

5.7.2.2 Actuator trade-off

Although the rotation of the mirror is back and forth, this movement can still be achieved using a constant rotation actuator. An eccenter mounted to the rotor shaft and amplified using a compliant mechanism can achieve the required stroke.

The working principle is similar to that of a piston in a piston engine and depicted in Figure 5-56. The blue circle represents the rotor, rotating about its rotation axis (grey) with a rod eccentrically fixed to it (black). The rod moves a carriage, which is situated in a rail assembly, thus resulting in a translational motion, indicated by the orange arrow. The range of the translational motion is then exactly the distance between the rotation axis and the point of fixation of the rod. Considering the relatively small motion range (175 µm), a compliant mechanism will presumably be necessary to reduce (!) the stroke to this level, since a distance of 87.5 µm from the rotation axis is hardly implementable.
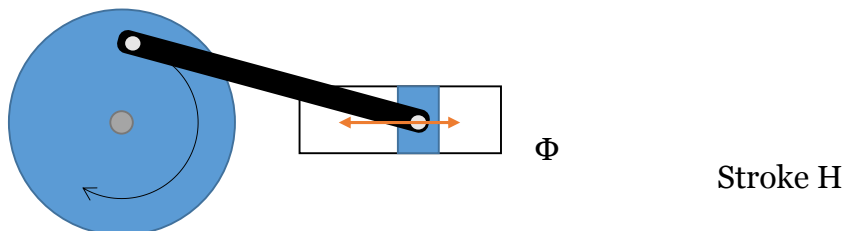
Figure 5-56: Illustration of the working principle of a rotary motor achieving a translation

The linear motion of the carriage in dependence of the rotary angle is depicted in Figure 5-57. A portion of the stroke is unusable to achieve a significant translation, since around the 180 and 0/360 degree position, the rotation results in almost no translational movement. This is why the stare phase starts at 1/12 pi and ends at 11/12

pi. As a result, the maximum and minimum position slightly over-, respectively undershoot, the 0 and 175 μm positions, indicated by the red lines.
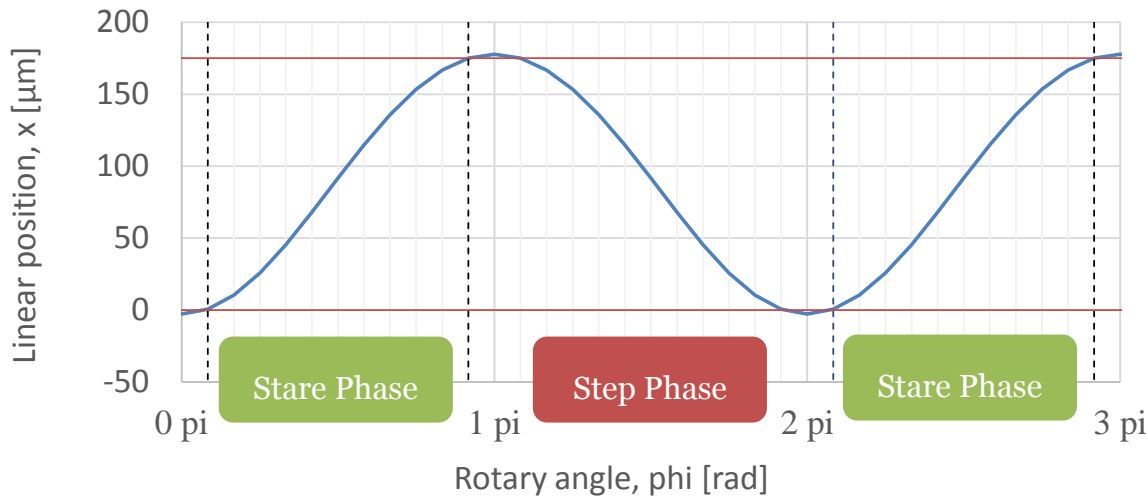
Figure 5-57: Rotation transformed into translation

Figure 5-58 shows the required speed profile and the resulting carriage movement (=> mirror movement) over time, where H is the stroke on mirror-level in micrometres and omega the motor velocity in radians per second. During the stare phase, the rotational speed needs to be constantly adjusted, as to achieve a constant velocity of the carriage. When restoring the position for the next phase, a constant speed can be commanded, resulting in a sinusoidal movement of the carriage.
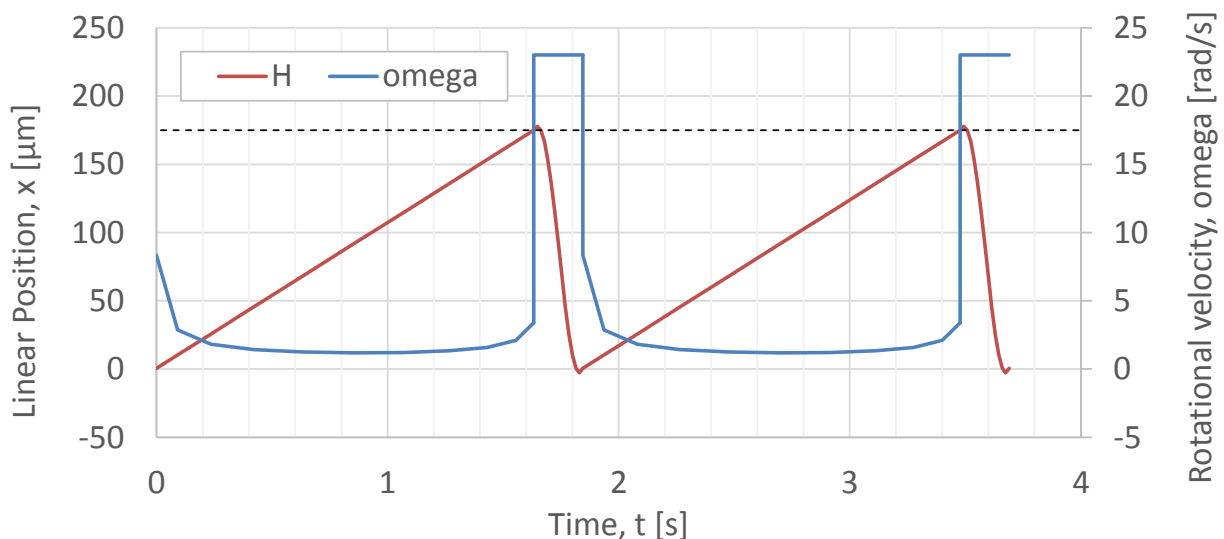
Figure 5-58: Mirror movement and corresponding rotary speed

Altogether, a mechanism like this is inherently complex. It involves a number of components that all present friction interfaces and problematic developments in themselves: a highly accurate and precise rotary motor, two rotary joints, to fix the

transmission rod to the rotor and the carriage, a low friction rail to guide the movement of the carriage and on top of this a compliant mechanism, to reduce the stroke to the required range.

Possible actuators usable for this application could be based on stepper or brushless motors in combination with single or multistage gearboxes. Although the TRL is very high on systems like these, the generated heat from these motors, especially during non-stop operation is severe (several watts depending on motor sizing). The heat generation in combination with mechanical issues such as backlash and exported vibrations caused by bearings and gears, the usage of a rotating actuator was ruled out.

To achieve a linear motion of the mirror, a linear motor could be used. Linear motors are available in two configurations: magnetic or piezo. Magnetic linear actuators such as voice coil actuators are not further considered for this study as similar to the rotating magnetic actuators, the heat generation is in the order of several watts.

Therefore only piezo actuators are a feasible solution for the application.

OTS piezo-actuators come in three configurations:

Parallel prestressed piezo actuator (PPA)

Amplified piezo actuator (APA)

Walking actuators (WA)

Parallel prestressed piezo actuators rely on the elongation & retraction of the piezo crystalline structure to execute a stroke and force. These actuators can produce a very high blocked force (>500N) but only a limited stroke (<100μm).

Amplified piezo actuators rely on a compliant mechanism that amplifies the executed stroke. Although the stroke can be increased by large factors, the blocked force is reduced by the same factor. This decrease is also applicable to the achievable step resolution of an APA.
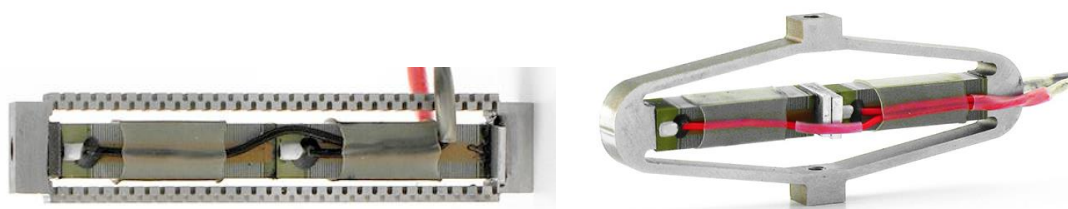
Figure 5-59: Parallel Prestressed actuator (left), Amplified Piezo Actuator (right)

Walking piezo systems rely on friction between several actuated "legs" and the moving part. Usually the movable part is clamped on both sides between these legs and by alternating actuating the legs, the part is moved. The main advantage of this system is that there is no connection between the total achievable stroke and the single step size.

In the baseline design the M4 mirror has a width of 190 mm, the optimal positioning of the actuator should be around 2/3 of the mirror halfwidth. With this leverage arm and the calculated actuation range of 0,136° the total stroke required can be calculated:

$$L_{Leverage} = \frac{2}{3} * \frac{190}{2} mm \sim 60mm$$

$$L_{stroke} = L_{Leverage} * \sin(0.136°) = 142\mu m$$

As important as the required stroke is the lifetime requirement of the chosen actuator. With a stroke of 175μm every cycle, the total travelled distance is:

$$2 * \frac{60 * 60 * 24}{1.63} sec * 175\mu m = 15.1 \frac{m}{day}$$

With an expected spacecraft lifetime of ~5years, this results in:

$16.7 * 365 * 5 \sim 30 km$

It has to be noticed that there is no heritage not test evidence that the walking piezo actuator is able to srvive such a life duration. Actually, all the tests performed so far, especially in vacuum, have demonstrated limitation in the achievable number of cycles these types of actuators could reach. In this sense, it seems that the solution with walking piezo device should not be considered as a viable solution. At the contrary, a mechanism with prestressed piezo actuators shows compliance with this request of life and should be preferred.

A further requirement on the actuator is the smallest achievable and repeatable step size. As piezo actuators require a dedicated piezo drive unit, therefore in the first instance, the drive unit has to be able to provide the required voltages with the specified accuracy. During the CDF study the ratio between stroke and step-size has been defined with $5*10^4$ (0,002%) of the total stroke. This results in a maximum step size of 3.49nm and a 16bit resolution from the piezo drive unit.

The heat generation and dissipation of the M4MM will have a strong impact on the whole optical setup and must therefore be kept as small and stable as possible. Piezo actuators produce heat in the range of milliwatts and the output will be constant during the whole operation. The heat generation by the electronics of the piezo drive unit will be dissipated within the service module.

With the previously described values, a trade-off table (Figure 5-60) has been presented during the CDF. The trade-off shows that pre-stressed or amplified piezo actuator types could both be used for the mechanism. The exact selection between these 2 options should be left for when the requirements (stroke and resolution) will be consolidated.

Requirement (det. value) Actuator	Stroke [µm] (175)	Stepsize [% of stroke] (0.002)	Stepsize [nm] (3.49)	Force [N] (>1)	Repeatability	Heat generation	Lifetime (ambient)	Lifetime (120K, 0bar)	Vibrations	Heritage	TRL
Stepper motor with GB & eccenter	>1000	-	~4	scalable	+	--	++	++	--	++	>6
Brushless DC with GB & eccenter	>1000	-	~4	scalable	+	--	++	++	--	++	>6
Linear coil actuator	>1000	-	>100	scalable	o	--	++	++	o	?	?
Prestressed Piezo	<100 (scalable)	0.001	0.45	>1000	++	++	++	++	++	+	>6
Amplified Piezo	<500	0.001	2-8	<100	++	++	++	++	++	+	>6
Walking Piezo	>1000	-	0.3	<100	++	++	o	--	?	+ (*)	<5 *

Figure 5-60: Actuator trade-off table

As for the design of the M4MM itself, several options are possible, either a 1 degree of freedom system in which the mirror is rotated around a flexible pivot point or a 2 degrees of freedom mechanism which provide tip/tilt movements. As can be seen in Figure 7, the 1DoF mirror setup could be realised with only one actuator but requires increased stroke which implies increased difficulty to achieve the required accuracies and thermal restrictions. Furthermore the optical centre of the mirror is shifted when the mirror is rotated.
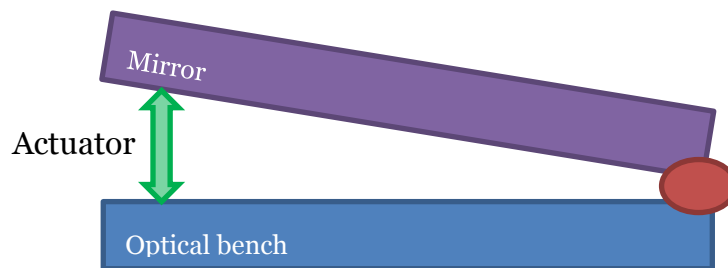
Figure 5-61: 1DOF Mirror Setup

A second option would be to have the mirror actuated in 2 (3) degrees of freedom. Therefore a Tip/Tilt movement is possible which could eliminate further disturbances within the spacecraft rotation (or to ensure no parasitic motion is induced between tip and tilt). While this option adds complexity, it is considered to be feasible.
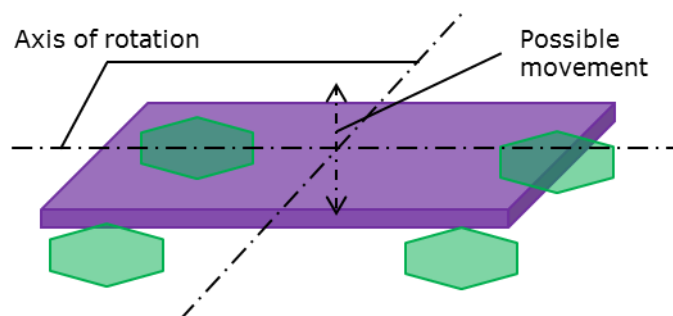
Figure 5-62: 3 DoF tip/tilt mechanism

Heritage on such mechanisms, including piezo in cryogenic conditions, exists (e.g. TDA on cryogenic fine steering tip/tilt mechanism for EChO/ARIEL with Cedrat Technologies).

5.7.2.3   M2 - 5DoF and 3DoF

Similar to the original Gaia mission, a refocusing mechanism for the second optical mirror is required. For this CDF-study, the part was reused as flown on Gaia (see Figure 5-63) as the requirements for the mechanism are similar. Currently a new mechanism is under development from RUAG (3DoF Tripod configuration). The activity is at the moment in the detailed design phase. Both these designs use stepper motors and gearboxes as actuators.
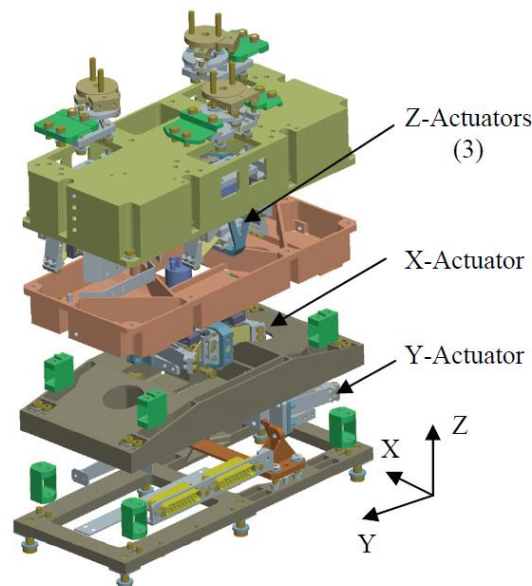
Figure 5-63: Gaia M2 Mirror Mechanism (Sener)

5.7.3   List of Equipment

	mass (kg)	mass margin (%)	mass incl. margin (kg)
PLM (Payload Module)	**10.00**	**15.00**	**11.50**
DeScan_mech (DeScan Mechanism)	5.00	20.00	6.00
M2_RFM (M2 Refocussing Mechanism)	5.00	10.00	5.50

Table 5-12: PLM Mechanism's list of equipment

5.7.4   Options

No further option has been identified at this stage of the project.

5.7.5   Technology Requirements

The following technologies are required or would be beneficial to this domain:

Included in this table are:

Technologies to be (further) developed

Technologies available within European non-space sector(s)

Technologies identified as coming from outside ESA member states.

Equipment and Text Reference	Technology	Suppliers and TRL Level	Technology from Non-Space Sectors	Additional Information
Cryogenic Fine Steering Mirror	Piezo actuated, cryogenic 2-DoF.	CEDRAT Technologies – TRL 4	-	R&D activity in test phase.
Mirror 2 Moving Mechanism, 5 DoF	Stepper motor plus planetary gearbox	Sener – TLR 9	-	Flight heritage in Gaia A 3-DoF version is being implemented in Euclid.

5.8   PLM Thermal

5.8.1   Requirements and Design Drivers

SubSystem Requirements		
Req. ID	Statement	Parent ID
TCS-010	The TCS shall be composed of only passive thermal hardware (MLI, thermal links, heaters and heat pipes)	
TCS-020	The TCS shall not produce any mechanical vibrations (e.g. no mechanical coolers)	
TCS-030	The FPA shall have a temperature stability of +/- 5 mK during a TBD period	
TCS-040	The decontamination temperature of the PLM shall be set as 193 K (-80 ℃), based on Gaia	
TCS-050	The SVM shall be thermally decoupled from the PLM in such a way that temperature fluctuations in the SVM do not carry over an influence on the thermal and mechanical stability of the PLM	

5.8.2   Assumptions and Trade-Offs

Assumptions	
1	The FPA is composed of 7*8 + 6 detector arrays (60 in total) of Teledyne HgCdTe HAWAII type detectors, with a working temperature of 140 K and a dissipation of 300 mW per detector array
2	The FPA's Front End Electronics or SIDECAR ASIC, has a dissipation of 1 W per readout chain (60 in total) and is operating at room temperature. NOTE: This value has evolved to 0.5W per readout chain, however this change does not significantly impact the design. This baseline design is now more conservative.
3	The detector harness linking the SIDECAR to the FPA has a maximum length of 100 mm and has a thermal conductance of 1.5 mW/K per readout chain (60).
4	The data processing unit has to be within 0.4 m of the SIDECAR and has a dissipation of 40 W, and will be operating at room temperature
5	A beginning-of-life value for the infrared emissivity of 1.0 for the black paint on the radiator is considered for the decontamination power estimate. An end-of-life value of 0.8 is considered for the radiator sizing.
6	A temperature gradient of 15 K between FPA and radiator is considered for the radiator sizing, to take into account contact resistances, thermal link conductance and radiator efficiency losses due to gradients on radiator (non-uniform temperature across radiator)
7	The mirror de-spinning mechanism has a constant dissipation of 1 W and will be operating at a temperature of 140 K

Assumptions	
8	Cryogenic Radiator sizing with 100% margin on cryogenic heat loads, given the current CDF-level design status and additional parasitic heat loads

5.8.3 Baseline Design

- Two distinct thermal regions with dedicated radiators:
  - One cold region at about 140 K for most of the PLM, detectors, mirrors and mechanism;
  - One Hot region at about 293 K for the SIDECAR and Data Processing Units. The FPA is thermally coupled via 6 flexible aluminium thermal straps to the cryogenic radiator at 6 m² and at 125 K. Thermal straps are employed instead of heat pipes thanks to the relatively low heat flux to reject, of 32 W.
- The Warm region of the PLM is thermally coupled to the warm radiator of 0.4 m² with a regular ammonia heat pipe, given the high heat flux of 100 W considered.
- The Warm region is thermally insulated from the remaining cold PLM, via MLI shielding and via mechanical stand-offs providing thermal decoupling (use of glass-fibre reinforced plastic such as G10 or S-Glass)
- The high temperature stability required for the FPA will be better achieved by employing an enclosed thermal tent coated black on the inside, as for Gaia, in order to reach a high temperature uniformity in the PLM cold region
- The PLM shall have open loop heater control applied on the FPA and SIDECAR and DPU, in order to compensate for dissipation variations high enough to induce significant temperature oscillations on the FPA
- Mirror de-spinning mechanism passively cooled by the PLM cavity, which at a thermal tent temperature of 125 K, requires 0.15 m² of radiating surface at 0.8 emissivity
- Detector temperature 130-140 K, as it cannot be guaranteed that the PLM offers a radiative sink temperature of sub-140K for the FPA (FPA 20-30K colder than Gaia with comparable dissipation), the baseline design considers a large external radiator with view factor to deep space.

5.8.3.1 Temperature Requirements

The temperature requirements for the PLM are shown in Table 5-13. The table shows the subsystem requirements with a 15K margin to size the radiators and heater powers. The decontamination temperature is 193 K (the same as for Gaia) for the detectors and mirrors of the PLM and is used to size the decontamination heater power.

Note that non-operating temperature limits have not been defined for the detector and de-spin mirror mechanism. To be conservative the operating range is used to size the heater power.

In addition, the detectors have a temperature stability requirement of +/-5mK.

Case	Requirement				Margin	Radiator and Heater Sizing				Heater Sizing
	Operating		Non-Operating			Operating		Non-Operating		Decontamination
Subsystem	Max [K]	Min [K]	Max [K]	Min [K]	+/- [K]	Max [K]	Min [K]	Max [K]	Min [K]	Max [K]
Detectors	140	130	140	130	15	125	115	125	115	193
FEE + DPU	293	283	303	273	15	278	268	288	258	N/A
Mirror Mechanism	140	130	140	130	15	125	115	125	115	193

Table 5-13: Temperature requirements for the PLM subsystems

5.8.3.2   Dissipation Requirements

The summary in Table 5-14 shows the dissipation of the PLM during each mode of S/C operation. Red and blue indicate dissipation at the hot and cold regions of the PLM respectively. The detectors dissipation has a 100% margin included to account for parasitic heat loads and modelling uncertainty.

Case / Subsystem	LM [W]	SAM [W]	SM [W]	DM [W]	OCM [W]	STM [W]
Detectors	0	0	0	0	65.7	65.7
FEE	0	0	0	0	60.0	60.0
DPU	0	0	0	0	40.0	40.0
Mirror Mechanism	0	0.5	0	0	0	1.02

Table 5-14: Dissipation for each subsystem in each S/C mode

5.8.3.3   PLM Thermal Concept

The thermal concept for the PLM is outlined in Figure 5-64 showing the main sources of heat and the main heat rejection paths via radiators to deep space.
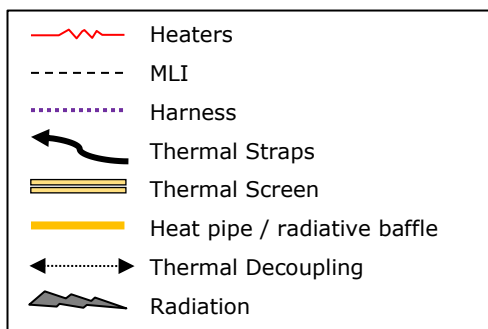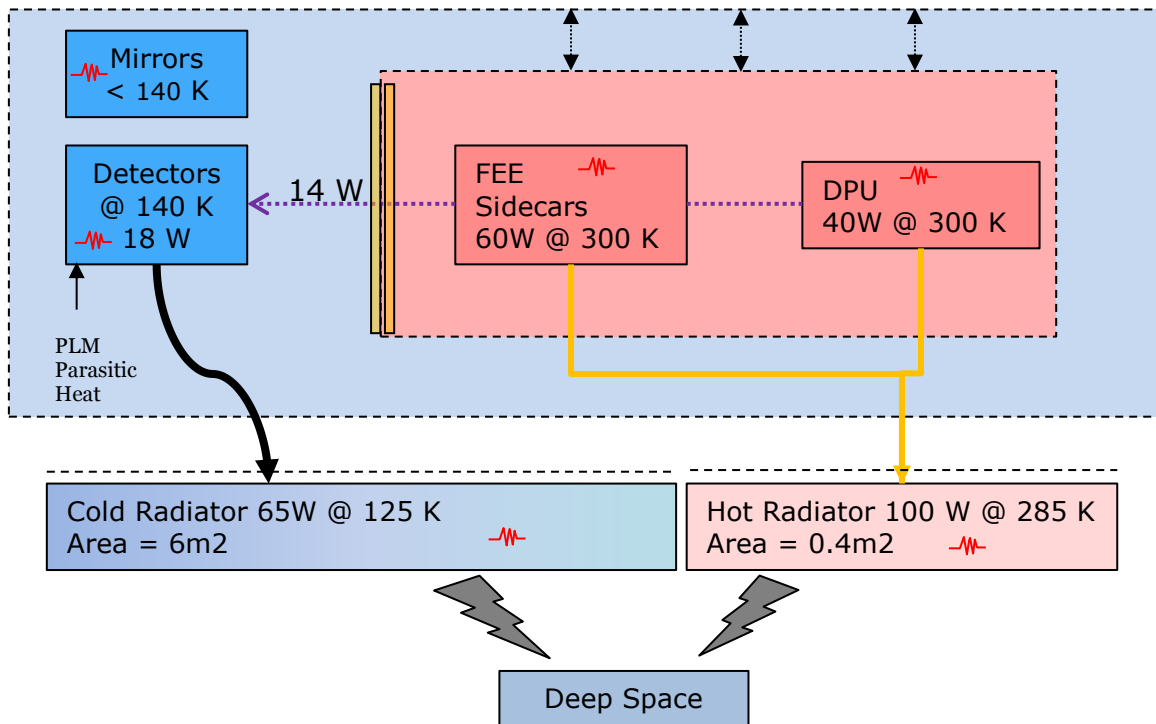
Figure 5-64: PLM Thermal Concept representing main dissipations and heat paths

5.8.3.3.1   Cold Region

The cold radiator area has been sized at: **6.0 m²**
Radiator emissivity considered as: **0.8**

The PLM will be mostly cold at around 140 K to accommodate the operating temperature requirement of the detectors. The main heat path connects the detectors directly to the large cold radiator via thermal straps. A gradient of 15 K is considered between the detectors and radiator. The main quantifiable heat loads to be rejected on the detectors are:

- Internal dissipation of the detectors (300mW per detector = 18W)
- Conductive heat through the electrical harness to FEE
  (1.5mW/K per detector considering a dT of 155 K gives 14 W)

In addition, the main parasitic sources of heat should be evaluated by thermal analyses:

- Multi-reflections and radiative heat sources in the PLM environment
- Conductive heat loads through structural couplings
- Losses through MLI and thermal screens
- Reduction of radiator radiative exchange factor to deep space due to the proximity of the rear of the Sun shield.

As a result, the radiator is sized with a 100% margin on the quantifiable cryogenic heat load, typically considered at early study phases RD[15] RD[16].

The cold end is thermally insulated from the hot end with the use of a thermal screen with small gaps for the detector harnesses. This screen may consist of two parallel aluminium plates separated by a perforated SLI for the FPA harness.

5.8.3.3.2   Hot Region

The hot radiator area has been sized at: **0.4 m²**
Radiator emissivity considered as: **0.8**

Note: Radiator sizing has been performed for 1W per FEE read out channel, this value has since evolved to 0.5W giving a total FEE+DPU dissipation of 70W instead of 100W (baseline). The current baseline design will now be more conservative.

The hot region of the PLM will house the Front End Electronics (FEE) and Data Processing Unit (DPU) which must be placed in close proximity to the detectors. These electronic units are chosen to operate in the same temperature range from 20-30 °C due to the following constraints:

1. A higher radiator temperature results in a better heat rejection capacity (100 W required) of the hot radiator. This will result in a small radiative area compared to a lower operating temperature.
2. The minimum qualification temperature limit of the DPU electronics is -40 °C.

5.8.3.3.3   Radiators

The cryogenic radiator of 6 m² is currently considered to consist of a 3 mm thick Aluminium series 6 (improved thermal conductivity) plate with a reinforcing rib structure, either directly milled from a thicker plate or welded on the plate. A hold-down release mechanism is taken into account in the baseline design given the size of the radiator. This simple solution is chosen given the relatively low heat flux on the FPA of 32 W.

In case a significantly larger heat flux would occur, the radiator panel would probably require either brazed heat pipes on it, or consist of a honeycomb panel with embedded heat pipes, to improve its in-plane thermal conductance and decrease the temperature gradient over the radiator. However, honeycomb panels with embedded heat pipes at such low temperatures are not currently qualified.

The warm radiator has been designed similar to the cold radiator, however with an ammonia heat pipe brazed on it. Its smaller size of 0.4 m² favours a simple configuration, even if the heat flux is higher, of 100 W. In case a larger warm radiator would be required a lighter solution would be to use a honeycomb panel with embedded heat pipes, which is readily available for the ambient temperature range.

5.8.3.3.4   Heat transport

Due to the high heat rejection 100W and long distance to the hot radiator, thermal straps are not considered the baseline heat transport method. Instead, either a radiative baffle design or the use of ammonia heat pipes is considered. The radiative baffle would provide a heat path to a sink with a view factor to deep space. This would be a simpler solution without the need of heat pipes and their AIT constraints, but might be difficult to accommodate in the PLM structure.

Alternatively, the use of the ammonia heat pipes will allow the removal of the heat to a radiator over a longer distance with a relatively small thermal gradient. The Ammonia Heat Pipe will likely have to be redundant and has a minimum operating temperature of -40 °C, and a minimum non-operating temperature of -50 °C, to stay clear off the ammonia's freezing point at -77 °C. The heat pipe should be integrated in a horizontal position to allow proper functioning on ground for AIT purposes. Otherwise, the condenser's lowest point will have to be higher than the evaporator in order for it to work in re-flux mode.

On the cold region, thermal straps are considered, given the low heat flux of 32 W which is distributed by 6 thermal straps, made of Aluminium foil in series 1000x with 5N of purity. This configuration has a higher thermal conductance at the given temperature range than copper straps. A common value of 0.5 W/K is considered for each thermal strap's overall thermal conductance. A higher performance (thermal conductance / mass) could be attained by employing Pyrolitic-Oriented Graphite straps (POG), however they have a lower TRL in Europe and may pose contamination issues.

5.8.3.3.5 *Insulation Warm Region*

The Warm region, containing the FEE and DPU is thermally insulated from the remaining cold PLM, via MLI shielding and via mechanical stand-offs providing thermal decoupling (use of glass-fibre reinforced plastic such as G10 or S-Glass). The part that faces the FPA, given its low clearance of only 100 mm and all the harness in the middle may pose a challenge for MLI installation. In case MLI is not possible to install on both sides, a thermal screen consisting of a perforated aluminium sheet (providing passage for the harness) and a low emissivity coating on both sides together with SLI on each side may be used. However this is subject to a more detailed design.

5.8.3.4 Heaters

Fluctuations on FPA, FEE and DPU dissipations will be compensated by the use of open loop control heaters to remain in a steady state case and mitigate temperature fluctuations. All the heaters on the PLM, namely the ones on the cold radiator and FPA, will also be used for decontamination, which is the sizing case for the heater installation. A summary of the PLM's heaters usage is presented in Table 5-15.

Location	Operation	Decontamination	Remarks
Detectors	Yes, Open loop*	Yes	*Compensation heater power
Mirrors		Yes	
FEE + DPU	Yes, Open loop*	No	*Compensation heater power
Mirror Mechanism	Yes	Yes	
Hot and Cold Radiators	No	Yes	
PLM structure and thermal tent	No	Yes*	*feedback from Gaia decontamination team

Table 5-15: PLM heaters operation and decontamination use

5.8.3.5 Thermometry

For most parts of the PLM, regular thermistors with a precision of +/- 0.1 K may be used. However, given the high temperature stability required of +/- 5 mK, a high precision of about 0.1 mK will be required. Solutions employing an AC bridge with a Platinum RTD (PT100 or PT1000) can have drifts as low as of 10 ppm/C, which is one order of magnitude lower than the 0.1 mK considered above.

An additional issue will be regarding the option of having either absolute or relative measurement precision. For absolute precision, the thermistors will require the calibration and the internal standard resistors to remain stable over the spacecraft's lifetime, which might be difficult. A relative precision however, should prove sufficient to verify temperature stability.

5.8.3.6 Mirror Mechanism Thermal Control Concept

The rotating mirror mechanism is estimated to dissipate up to 1W into a critical region of the PLM. The mirror must also be kept a temperature sub 140 K. This dissipation must be carefully considered as it could degrade the thermal stability of the mirror and have a secondary effect as a heat load seen on the detectors. The baseline design is to radiate the generated heat towards the top deck of the SVM thermal tent with a fixed radiative surface. The top of the SVM tent will be at a lower temperature with a view factor to deep space. The top of the SVM tent external surface should have a higher emissivity coating to improve its heat rejection capability and lower its temperature.

5.8.3.7 Heater Power Sizing

The summary in Table 5-16 shows the heater powers required to keep the individual subsystems above there minimum temperatures in each S/C mode. The heater powers presented include a 20% design maturity margin. The sizing case is the decontamination mode with a total of 438 W required to heat up the PLM to the decontamination temperature.

In case the decontamination temperature requirement evolves to a higher temperature, the power system may become unbearably large in order to keep the cryogenic radiators at these higher temperatures.

A solution in the TCS could be to use a thermal cut-off provided by a methane heat pipe linking the FPA to the cryogenic radiator, which would reach its critical point at 191 K and above that would stop its circulation.

Case / Subsystem	LM [W]	SAM [W]	SM [W]	DM [W]	OCM [W]	STM [W]
Detectors	71	71	71	407	5	5
FEE	67	67	67	15	6	6
DPU	45	45	45	10	4	4
Mirror Mechanism	1	1	1	6	1	0
Total	**183**	**183**	**183**	**438**	**16**	**15**

Table 5-16: PLM Heater Power Sizing per S/C mode

5.8.3.7.1   Mass budget

The mass budget breakdown is summarised in with the margin applied to each item. The margin philosophy has been iterated with the system engineering team.

Item	Mass [kg]	Margin	Estimated Mass including margin [kg]
Radiator (HOT = 0.4m² + COLD = 6.0m²)	51.7	20 %	62
Heaters / Thermistors + harness	0.95	5 %	1.0
Paints and coatings	1.0	5 %	1.1
Thermal straps / links	1.1	20 %	1.3
Ammonia heat pipe to hot radiator	7.2		8.6
MLI on Torus (Gaia assumption)	4.3	5 %	4.5
MLI + SLI on FPA (Gaia assumption)	3.0		3.1
Thermal Screens (Gaia assumption)	34.6		36.3
Miscellaneous (doublers / fillers / tapes / grounding)	8.6	5 %	9.0
Total	**112.5**		**126.9**

Table 5-17: PLM Thermal Mass budget

5.8.4   List of Equipment

The following is a list of equipment associated with the PLM thermal subsystem:

- 6 m² Cryogenic Radiator – Aluminium Plate with reinforcing ribs
- 0.4 m² Warm Radiator – Aluminium Plate with reinforcing ribs, or radiative baffle
- 6x Flexible Thermal Straps – Aluminium foil series 1000x 5N's of purity
- MLI – On inside of radiators, on all PLM thermal tent and also on warm region FEE+DPU
- Ammonia Heat Pipe – From Warm region to warm radiator
- Heaters: 438 W installed
- Thermistors: Regular ones and high precision ones for the FPA

All proposed Thermal Control System hardware is of TRL 9 and of passive nature.

5.8.5   Options

Heat transport method:

- Warm region (FEE+DPU) mounted directly on radiator
- Radiative baffle.

Decontamination

- Gaia thermal design requirement 300 K RD[17]
  Note: That during Gaia flight, decontamination campaigns of up to 193 K were performed.
- Baseline decontamination at 193 K –> 440 W

If higher decontamination T required (> 193 K):

- Point radiator towards Sun
- Methane heat pipe for detector to cold radiator link
  Conduction reduced due to fluid at critical point (191 K) – results in less heater power.(example on Sentinel 5p).

5.8.6   Technology Requirements

The following technologies are required or would be beneficial to this domain:

Included in this table are:

- Technologies to be (further) developed
- Technologies available within European non-space sector(s)
- Technologies identified as coming from outside ESA member states.

Equipment and Text Reference	Technology	Suppliers and TRL Level	Technology from Non-Space Sectors	Additional Information
Thermal Strap	POG Graphite Thermal Strap	CASA, Absolut System, Thermacore (US) TRL 3		Not baselined, would bring improvement
Cryogenic Radiator	Cryogenic Honeycomb panel with Embedded Ethane Heat Pipe	Eurocomposite, EHP, TRL2		Not baselined, could be required if cryogenic heat load rises dramatically
Thermistor	High Precision Thermometry		MicroK Precision Thermometry Bridge, by ISOTECH	0.03 ppm/C

6   SERVICE MODULE

6.1   SVM Configuration

The GaiaNIR spacecraft consists of a Payload Module (PLM), a Service Module (SVM), a thermal tent and a Deployable Sunshield Assembly (DSA), which enables to protect the satellite from the thermal variations due to the in-orbit Sun environment.
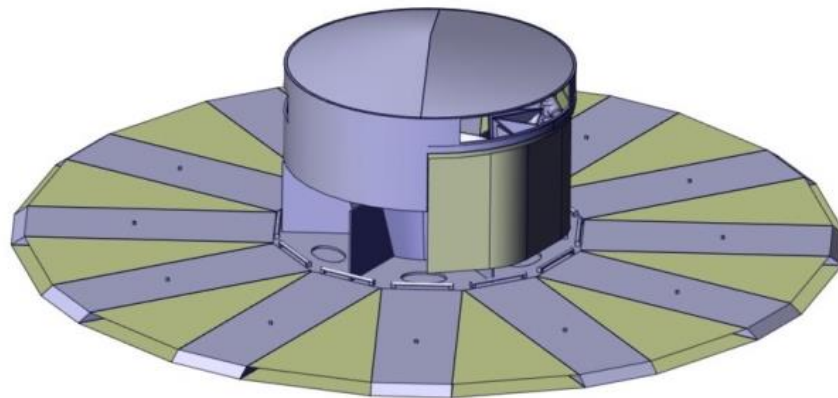
Figure 6-1: Gaia-NIR spacecraft orbital configuration
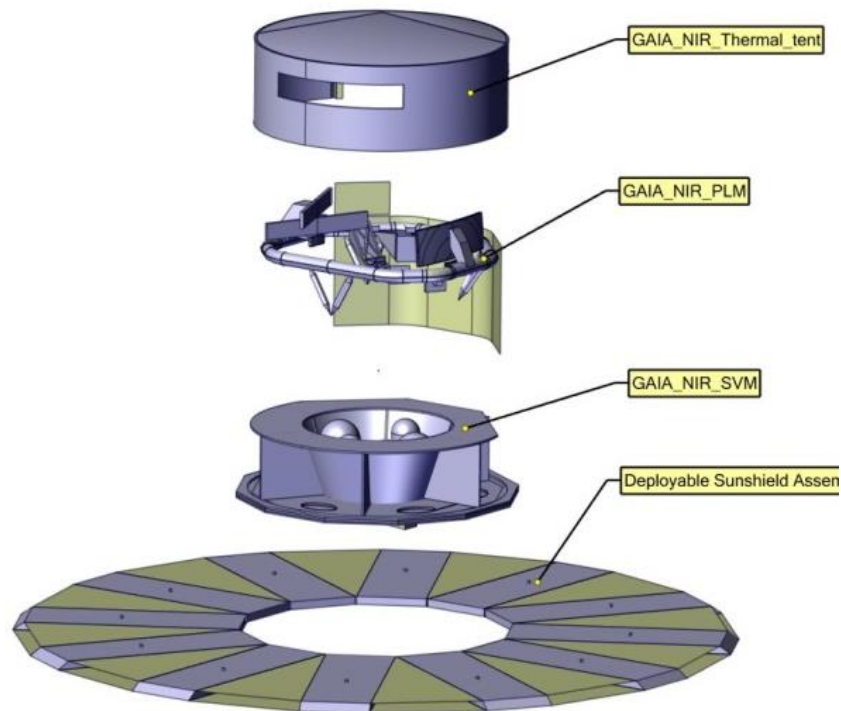
Figure 6-2: Gaia-NIR Spacecraft main elements

The configuration of the Service Module and the Deployable Sunshield Assembly are explained in this chapter.

6.1.1 Requirements and Design Drivers

6.1.1.1 SVM Requirement

SubSystem Requirements		
Req. ID	Statement	Parent ID
CFG-010	The SVM design is derived from the Gaia SVM design	
CFG-020	Optimise the mass with respect to stiffness, strength, radiation, and functional requirements	
CFG-030	Interface to the launcher vehicle adapter with a standard I/F ring of 1666mm diameter	
CFG-040	Interface with the PLM optical bench by means of two parallel sets of bipods to carry the launch loads and in-orbit loads on 3 points I/F	
CFG-050	Interface with the PLM tent structure	
CFG-060	Provide integration of DSA	
CFG-070	Provide spacecraft power through solar array. The fixed solar array is placed around LVA interface and if needed, the deployable solar panels shall be fitted to the deployable sunshield assembly	
CFG-080	Provide support to the chemical- and micro-propulsion subsystem	
CFG-090	Provide all spacecraft equipment with all required mechanical thermal and harness interfaces and resources	
CFG-100	It shall guarantee an adequate mechanical and thermal environment throughout their operating life and ensure that its thermos-elastic distortion is kept within acceptable limits for the PLM instrument to meet its scientific requirement	
CFG-110	Comply with launcher frequency requirement	
CFG-120	Accommodation and access to equipment	

6.1.2 Assumptions and Trade-Offs

The SVM of Gaia is used as a reference to design SVM of GaiaNIR. Due to a larger overall dimension of the Gaia-NIR optical layout, outer dimension of the SVM of Gaia-NIR becomes larger than the one from Gaia.

6.1.3 Baseline Design

The SVM design is a generic spin-stabilised spacecraft with a central cone. The central cone has 1100mm height. It contains the lower I/F ring providing the interface to the 1666 SF launch vehicle adapter.
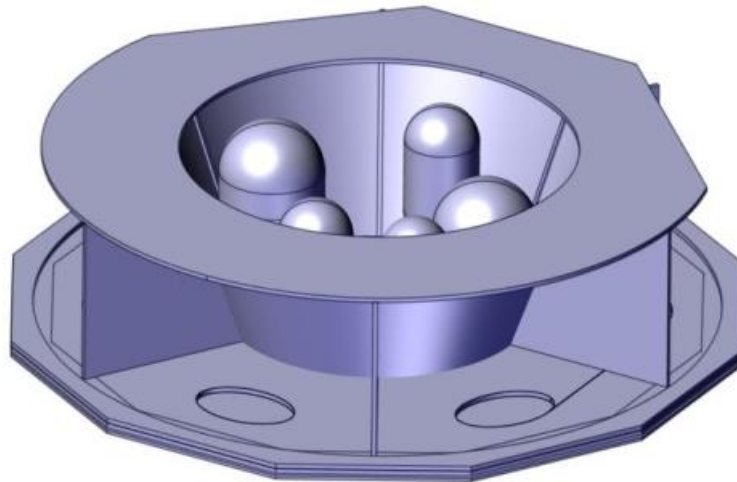
Figure 6-3: Service Module

Central Cone:

The Central Cone connects the PLM interfaces at the upper rim to the Launch Vehicle Adapter (LVA) at its lower interface. Its lower interface requires a rigid ring to comply with LV requirements. Special attention has to been paid also to the upper cone interfaces. where all brackets and cleats have been made out of titanium to minimise thermal distortions close to the PLM interface.

Six panels are radially attached to the Central Cone and serve as equipment support and as stiffener for the Top and Bottom Floor. They carry the electronic units and three of them carry additional load from the PLM three interfaces at their inner area.

Top panel:

The top panel serves mainly as a stiffener for the radial panels and the cone upper rim and supports also the lateral load of the PLM. It interfaces to the Thermal Tent structure covering the Payload Module on its outer rim at the connection points to the radial panels.

Bottom panel:

The Bottom panel is a dodecagonal shaped panel to comply with the 12 frames of the Deployable Sunshield Assembly (DSA). The DSA is not part of the SVM structure however it supports as a minimum 8 segments of the Deployable Solar Panels. The bottom panel carries the Solar Array on its lower sun-side surface and the DSA on its outer upper rim. It must be noticed that the DSA axial loads are fully taken by the Bottom Panel since the DSA upper attachment to the Thermal Tent structure supports only the radial and tangential load component. The inner rim of the Bottom Panel is attached to the Central Cone. It contains 6 man holes to get access to the units after individual removal of the SAP's.

Secondary Structure:

The Phased Array Antenna (PAA) Plate is located inside the Central Cone close to the LVA interface ring.

The CPS and Cold Gas Tanks are mounted inside the Central Cone. Other CPS and MPS equipment is located on Support Panels attached tangentially to the outer face of the Central Cone. Those CPS and MPS panels are dismountable.

DSA Ring:

The DSA ring increases the Bottom Panel outer rim axial stiffness and serves mainly as functional structure of the DSA, when dismounted from the Bottom Panel.

PAA Plate:

The PAA Plate is a secondary structural element that carries the PAA and its electronic units. It is attached to the Central Cone by Brackets or by a flange of the LVA interface ring. Four cut-outs on its outer rim are needed for the CPS thrusters.

Support Panels (on cone attached):

Those panels are attached to the cone and support light weight CPS and MPS components and the Battery. 3 half panels for PCA, MPS and battery and a full panel for PIA are foreseen.

Tank Support structure:

A polar mounting interface has to be considered for all tanks. All tanks except the He-Tank are oriented with the polar axis in upright position. The required tank support structure can be attached to the upper or lower cone interface ring. A principle design of the support structure is shown below.
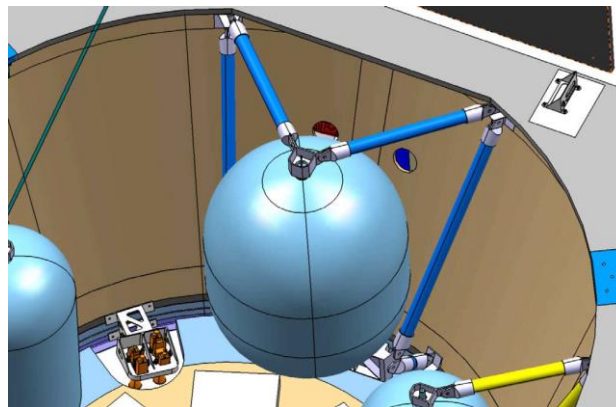
Figure 6-4: Tank support structure
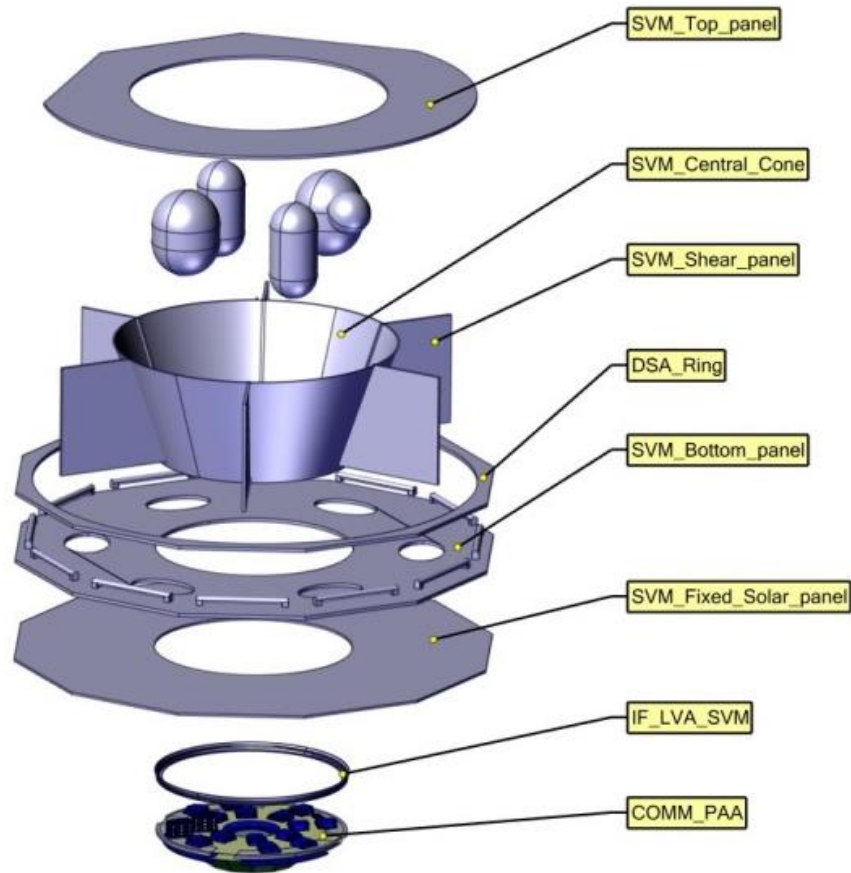
Figure 6-5: SVM elements

The thermal tent structure has several functions: it protects the optical bench from stray light and contamination. It provides the thermal environment of the focal planes & the stability of the optical bench from sunshield remaining thermal variations. Its structure supports the stowed sunshield during launch and enables handling of the complete spacecraft.
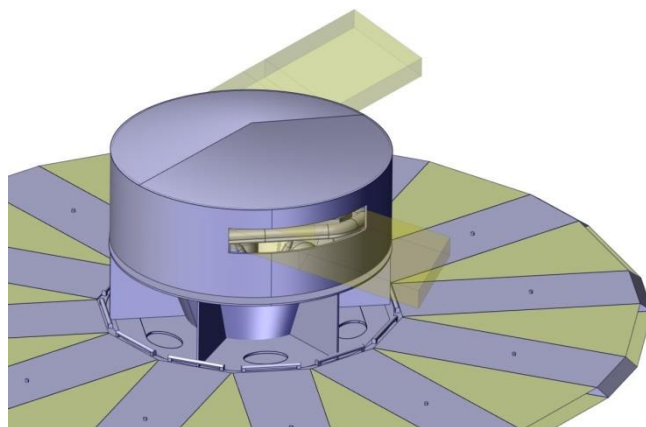
Figure 6-6: Thermal tent protection

6.1.3.1 GaiaNIR S/C Dimensioning
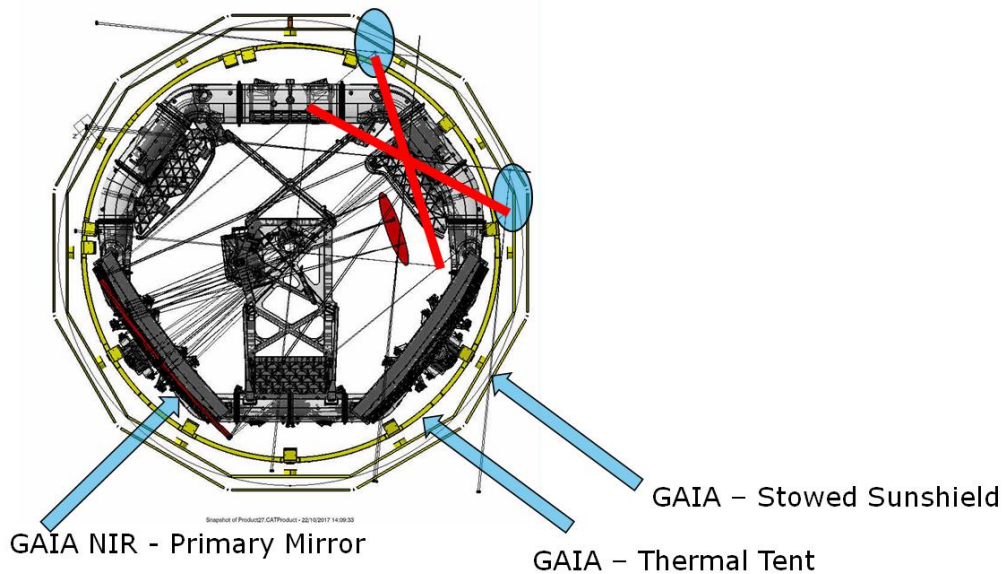
Figure 6-7: Gaia-NIR optical layout

GaiaNIR has a different optical layout then the one on Gaia. The Gaia spacecraft overall design need to be adapted to accommodate Gaia-NIR payload as follow:

- Larger Optical bench torus outer dimension
- Larger diameter of the thermal tent namely d = 3800mm instead of 3240mm
- Larger diameter of stowed Sunshield namely d= 4330mm instead of 3800mm
  - keep the same distance between outer diameter of Gaia thermal tent and inner surface of the sunshield in stowed configuration = 102mm
- Larger diameter of the SVM top plate namely 3810mm instead of 3250mm
- Larger diameter of the SVM bottom plate.

6.1.3.2 Sun Angle Calculation
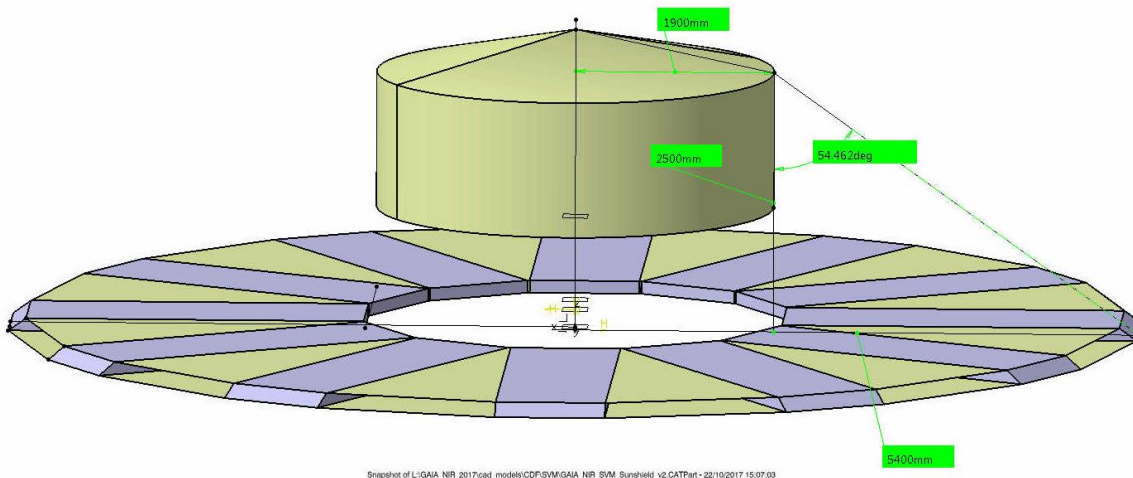
Figure 6-8: Gaia-NIR DSA - Sun angle

GaiaNIR Sun aspect angle is calculated using following parameters:

- Thermal tent diameter of 3.8m
- S/C total height of 2.5m
- DSA deployed diameter of 10.8m (same as Gaia)
- increase the spin axis w.r.t. the Sun (Sun aspect angle) from 45° (Gaia) to 55° (improve science - astrometric performance)
- accounting for a ~3° AOCS margin
- 0.53° Sun width to mitigate straylight issues

This results in a Sun aspect angle of ~51°

Table 6-1 summarises the main dimension difference between Gaia and Gaia-NIR:

	Gaia	Gaia-NIR
Sunshield stowed diameter	3.8m	4.33m
Sunshield surface area (one segment)	2.054m²	3.568m²
Thermal tent diameter	3.24m	3.8m
Thermal tent surface area	10.861m²	10.885m²
SVM top plate diameter	3.25m	3.81m
SVM surface area at the bottom	7.2m²	11.292m²

Table 6-1: Gaia and Gaia-NIR comparison table

6.1.4 Overall Dimensions
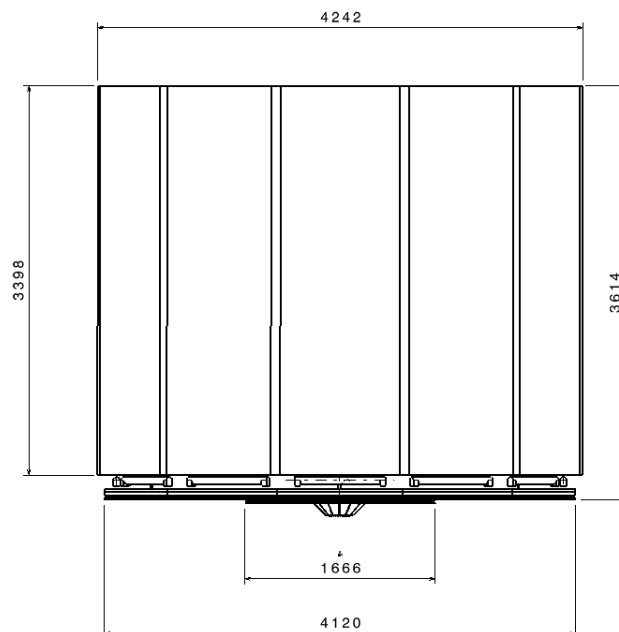
Figure 6-9: Side view - Gaia-NIR Overall dimension of stowed configuration
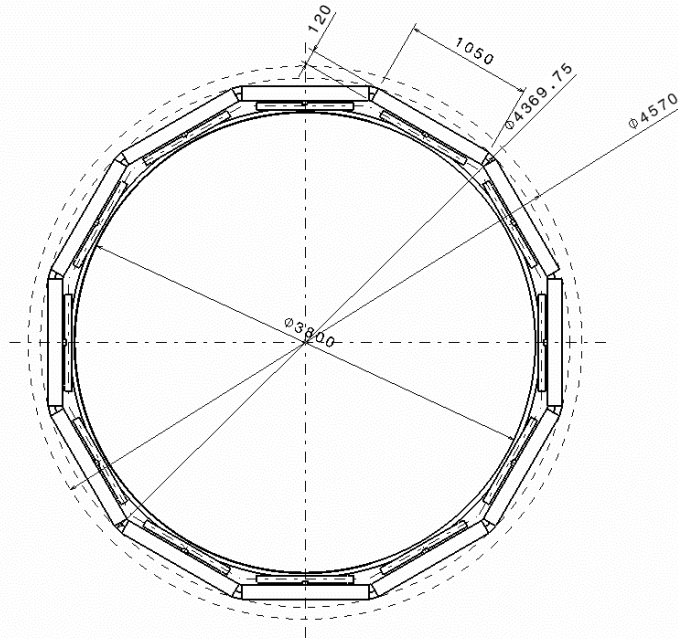
Figure 6-10: Top view - Gaia-NIR Overall dimension of stowed configuration
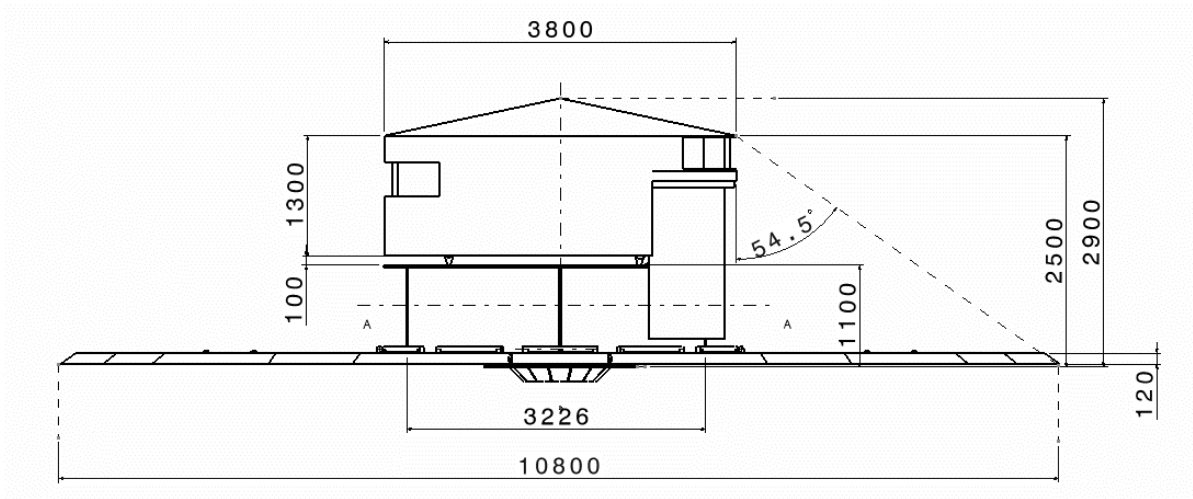
Figure 6-11: Side view - Gaia-NIR Overall dimension of deployed configuration
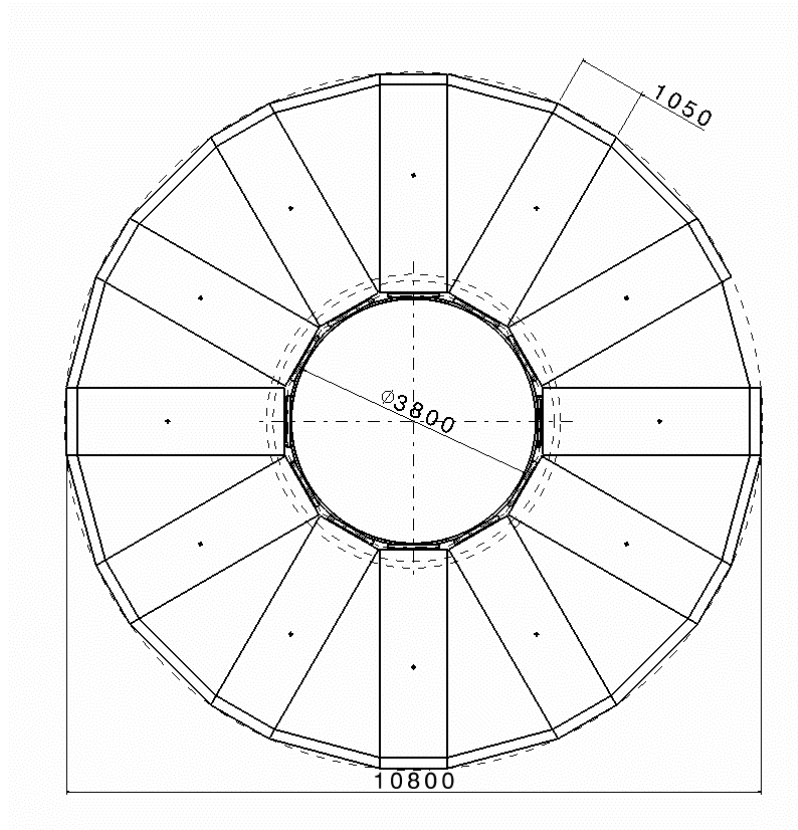
Figure 6-12: Top view - Gaia-NIR Overall dimension of deployed configuration

6.2 SVM Structures

6.2.1 Requirements and Design Drivers

SubSystem Requirements		
Req. ID	**Statement**	**Parent ID**
STR-010	The GaiaNIR PLM structure shall exploit commonalities with the Gaia spacecraft as much as possible.	MIS-050

STR-010: Mission requirement MIS-050 states that the cost to ESA shall not exceed 550M€[2017]. The flow down of this requirement onto the structures domain means that the Gaia design heritage shall be reused as much as possible, which obviously is limited to carrying-over the overall design principle and therewith the lessons learned during qualification and operation of the Gaia spacecraft.

6.2.2 Baseline Design

The design of the GaiaNIR service module (SVM) is closely derived from the Gaia SVM, maintaining the top plate, the bottom plate connecting cone and six shear panels. As shown in section 5.6 (PLM Structures) the GaiaNIR spacecraft body diameter is 3.8 m. This applies to the SVMs top plate and the thermal tent, the bottom plate is larger in size than, it has to support the sunshield, which in stowed configuration surrounds the thermal tent with sufficient clearance, see Figure 6-13. While GaiaNIR has a larger diameter than Gaia, the PLM of GaiaNIR has less height than Gaia's PLM, the service module height remains the same, see also Table 6-2.

	GAIA	GAIA NIR	Ratio
SVM & PLM height	2994.6	2500	83.48%
Thermal Tent height	1864.6	1370	73.47%
SVM & tent diameter	3240	3800	117.28%
Baseplate diameter	3800	4265	112.24%

Table 6-2: Gaia and GaiaNIR SVM dimensions
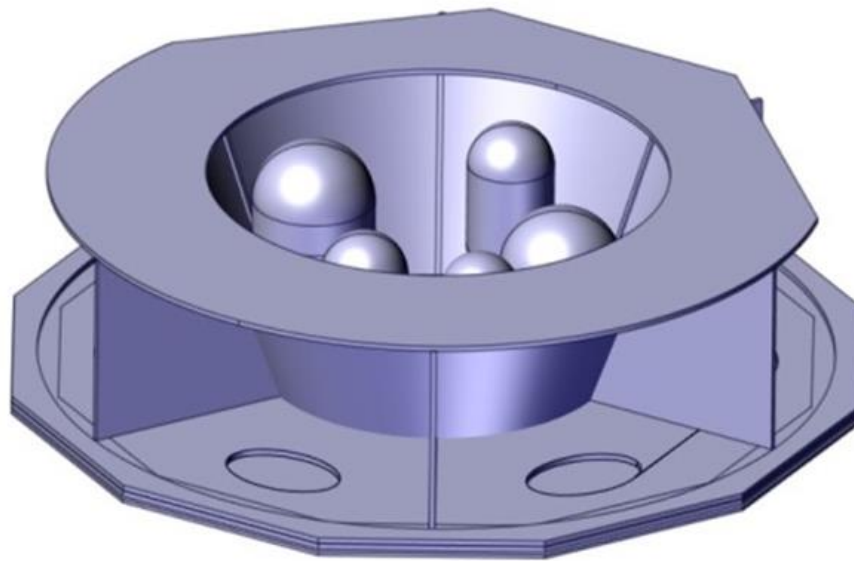
Figure 6-13: Service Module structure with propellant tanks
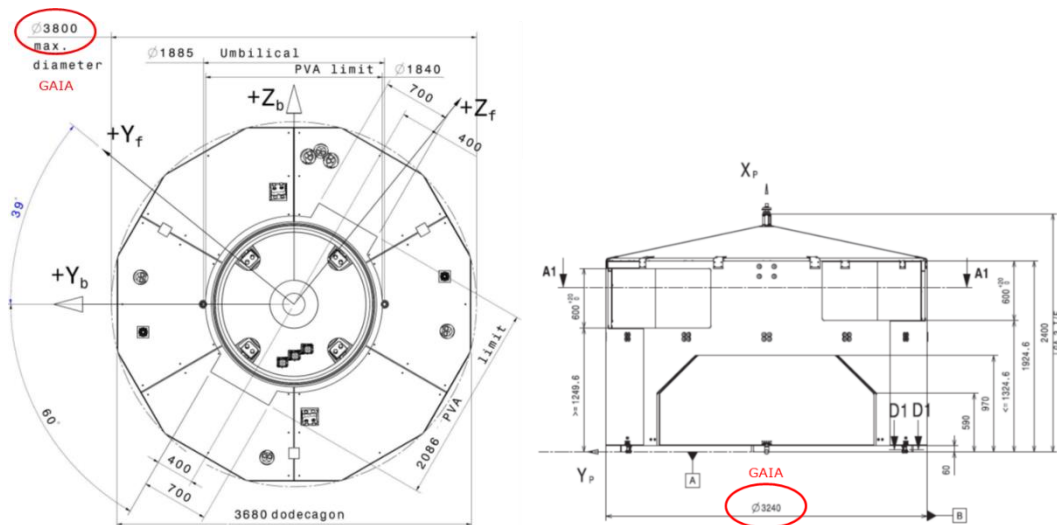
Figure 6-14: Gaia spacecraft body dimensions

The GaiaNIR SVM mass budget is compiled from the Gaia mass budget, scaling the element masses according to the changes in size. This is performed in Table 6-3, while the thermal tent cylindrical surface is reduced due to the shorter spacecraft body, its top surface grows with the square of the radius increase. Similarly, the upper plate ("top floor ring panel" in Table 6-3) and lower plate ("bottom floor ring panel") and six radial equipment panels scale with their respective surface area increases.

Thermal Tent Structure		**83.70**		**79.819**
Primary Structure				77.894
Lateral Panels	1	53	-14%	45.672
- openings	1	9	0%	9.000
Top Plate	1	19.8	17%	23.222
Secondary Structure	1	1.925	0%	1.925
SVM Structure		**349.80**		**339.016**
Primary Structure				236.380
Top floor ring panel	1	27.849	38%	38.308
Bottom floor ring panel	1	42.277	26%	53.257
DSA panel ring	1	10.446	0%	10.446
Stiffening struts	1	8.752	0%	8.752
Antenna panel	1	19.453	0%	19.453
Central cone	1	54.753	0%	54.753
LVA I/F ring	1	15.627	0%	15.627
Radial equipment panel 1	1	2.095	38%	2.882
Radial equipment panel 2	1	4.19	38%	5.764
Radial equipment panel 3	1	4.19	38%	5.764
Radial equipment panel 4	1	4.19	38%	5.764
Radial equipment panel 5	1	4.29	38%	5.901
Radial equipment panel 6	1	4.19	38%	5.764
Support equipment panel 1	1	1.042	0%	1.042
Support equipment panel 2	0	0	0%	0.000
Support equipment panel 3	1	1.741	0%	1.741
Support equipment panel 4	1	1.164	0%	1.164
Support equipment panel 5	0	0	0%	0.000
Support equipment panel 6	0	0	0%	0.000
Secondary structure				92.649
Brackets, hard points, reinforcem., GR etc.	1	55.071	0%	55.071
Tank support	1	37.578	0%	37.578
Miscellaneous				9.987
Micro-Thruster Protection & RCT Plume Shield	1	6.359	0%	6.359
Top Floor MLI Bar & Stand-Offs	1	3.628	0%	3.628

Table 6-3: GaiaNIR SVM structure mass estimation

6.2.3   Technology Requirements

No technology developments for structural subsystems required.

6.3   SVM Mechanisms

6.3.1   Requirements and Design Drivers

SubSystem Requirements		
Req. ID	**Statement**	**Parent ID**
MECH-090	The GaiaNIR Service Module shall have a deployable sunshield	

Requirements and Design Drivers for the service module are inherited from Gaia mission. A sun shield shall be deployed to allow for the instruments to operate.

1. Assumptions and Trade-Offs

Assumptions	
1	The Gaia sunshield deployment mechanism technology is available
2	The Gaia sunshield deployment mechanism technology is suitable for deploying the sunshield required for GaiaNIR

6.3.2   Baseline Design

The baseline design for the GaiaNIR service module contains one mechanism which is used to deploy the sunshield. As the sunshield has a similar size and layout as for the original Gaia mission, and considering the considerable development and test work performed at that time for this item, it is recommended to take advantage of the experience in place and reuse it. Due to that, no further iterations have been done on this mechanism for the CDF-Study.
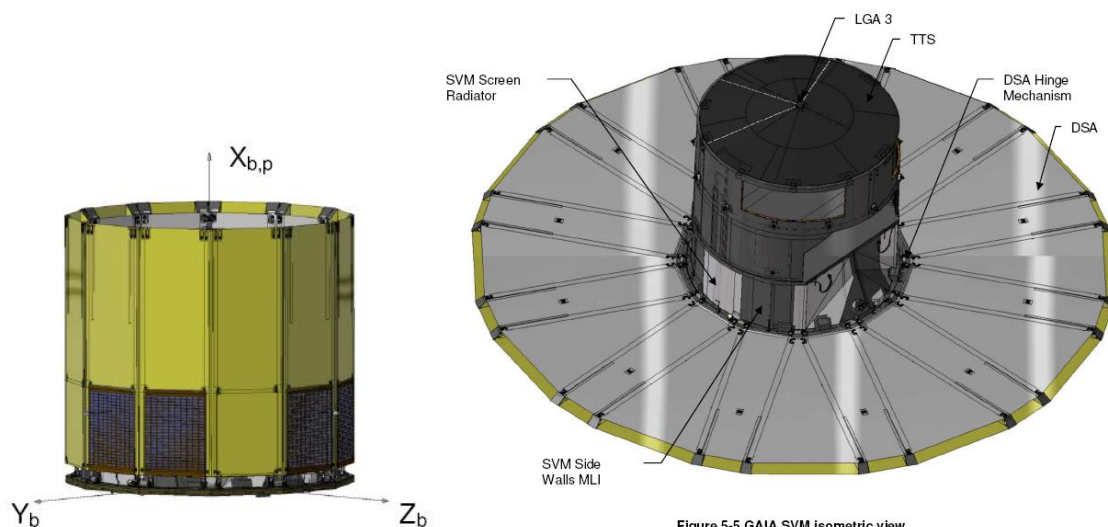
Figure 6-15: Gaia DSA Deployment Mechanics

The Gaia Deployment Sunshield Assembly (DSA), developed by Sener (E), provides a stable and continuous shadow environment to the SVM and PLM of the satellite. The DSA is composed by 12 rectangular petals joined by 12 triangular sectors to form an almost circular plane around the base of the spacecraft. The difference of temperature between the sunside layer and the shadowside layer is around 150º C.

In working configuration the DSA is a flat circle of about 10.200 mm diameter. Due to the geometrical constrains of the rocket fairing, for launch purposes the sunshield was folded into a dodecagonal prism configuration around the thermal tent, to fit into the fairing diameter of 3.800 mm.

Each petal is formed by a structural frame (H shaped) composed by CFRP tubes joined by metallic fittings bonded to the tubes.

The thermal function of the DSA is achieved by two layers of thermal foils: sun side foil and shadow side foil designed to meet the thermal requirements. These foils are kept in place by special tensioning devices which maintain the thermal insulation in a controlled manner once the item is deployed.

In the centre of the H shape's intermediate tube the fitting through which the frame is fixed to the S/C through the Hold down and release mechanism.

The structural frames are hinged at the base (two hinges per frame), attached to a ring assembled over the base of the SVM. The hinges perform the deployment function by means of loaded springs. The 12 frames are joined at the hinges axis via flexible couplings, composing a single shaft loop in order to achieve a synchronous deployment when the deployment is triggered.

The deployment is controlled actively by two DSA actuators. Each of these actuators are based in an actuator and a Four-Bar Linkage Mechanism that brakes or provides actuating torque to ensure the 90 degree deployment of the DSA. In order to control the actuators, a motor driving electronic system per actuator is required to apply the electrical inputs to the motor windings to run proper steps. These electronics apply required inputs to the actuators by means of a specific actuator harness.

Characteristics:

- The sunshield provides thermal insulation from solar radiation of several orders of magnitude. Of a total of 1400 W/m2 of solar radiation, only 5 W/m2 reaches the telescope with a uniformity of 20 milliwatts/m2.
- The total weight, including the electronics, is 125 kg, and it consumes less than 20 W in the course of the 4 minutes of deployment.
- The sunshield's structure secures solar panels, as well as the thermal protection, delivering great dimensional stability with deformations of less than 0.05% in a temperature range of 150°.
- Besides their insulating capacity, the thermal protections, arranged in two layers of multi-layer insulation (MLI), include novel fixation systems. Their design permits in-orbit deployment, from undeployed to deployed configuration, in a unique design that allows their volume to be compacted by a factor of 12.
- The mechanisms include a combination of well-tested elements, such as Sener's actuator HDRA, with other newly design elements, such as the flexible connectors

that synchronize deployment, the thermal protection tensors that reduce deployment resistance, or the actuator's coupling mechanism, which determines the motoring profile throughout deployment.

Another mechanism which is inherited from Gaia is represented by the bipods struts, which connect the payload module and the service module. They are constituted by a structural link which is required to offload the launch loads, and by a thermal link which is needed to minimise the heat transfer from the warm service module to the payload module. After launch the structural link is released via hold down mechanisms, allowing for a reduced heat transfer.
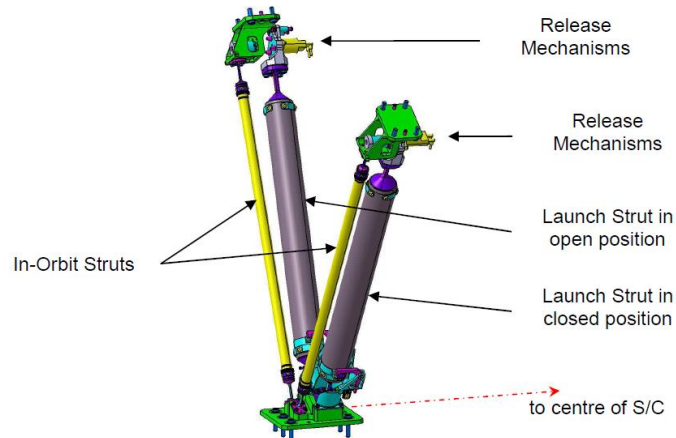
Figure 6-16: Gaia launch and in orbit bipods

In addition to the above mentioned mechanisms, for which Gaia heritage can be heavily taken into account, hold down systems for the 2 baselined radiators shall be addressed for GaiaNIR study. Considering the size of the radiators, it is deemed necessary to allocate 2 HDRMs each to sustain loads during launch. Acknowledging the wide use of these kind of mechanisms and assuming for this application the selection of an NEA device, the allocated mass per mechanism including brackets is 5 kg with 20% margin. This technology is considered well mastered and does not require any preparatory development activity.

6.3.3   List of Equipment

	mass (kg)	mass margin (%)	mass incl. margin (kg)
SVM (Service Module)	**190.00**	**6.58**	**202.5**
Dep_SSH (Deploayble Sunshield)	134.00	5.00	140.70
Rad_HDRM (Radiator Hold Down and Release Mechanism)	20.00	20.00	24.00
L_Bpod (Launch Bipods)	36.00	5.00	37.80

Table 6-4: SVM Mechanism's list of equipment

6.3.4   Options

No option has been identified at this stage of the project.

6.3.5 Technology Requirements

The following technologies are required or would be beneficial to this domain:

Included in this table are:

Technologies to be (further) developed

Technologies available within European non-space sector(s)

Technologies identified as coming from outside ESA member states.

Equipment and Text Reference	Technology	Suppliers and TRL Level	Technology from Non-Space Sectors	Additional Information
Sun shield deployment mechanism	Active deployment system	SENER (E), 7	-	Delta qualification might be needed due to resizing (TBC)

6.4 SVM Propulsion

6.4.1 Requirements and Design Drivers

There were no specific requirements or design drivers identified for the propulsion system.

6.4.2 Assumptions and Trade-Offs

6.4.2.1 Assumptions

The table below lists the assumptions:

Assumptions	
1	Similar design as for Gaia, where possible; (architecture: two tank bipropellant system, two tank cold gas system for accommodation reasons).
2	Gaia components where possible.
3	Thruster pointing and therefore geometrical efficiency as for Gaia.
4	Bipropellant thruster Isp = 291 s (S10-18).
5	Cold gas propellant thruster Isp as in Gaia and defined by the AO GNC domain.

Table 6-5: Propulsion assumptions

6.4.2.2 Trade offs

The following trade-offs were carried out during the course of the study.

6.4.2.2.1 *Monopropellant vs Bipropellant System*

During the study, several mission options have been addressed, each with their own set of velocity increments. Therefore initially a monopropellant system seemed feasible and was most mass efficient. However, the larger orbit insertion velocity increment that was confirmed for the baseline design option, indicated that a Bipropellant system would be the most mass efficient.

The trade-off results are listed below in a simplified way for a dry mass reference mass Gaia-like. Since the dry mass only increased, the result (selected bi-prop system) remained valid.

Simple trade off results:

- 361 kg for a MON MMH bi-prop system
- 435 kg for a Hydrazine mono-prop system.

Accommodation of the bi-propellant system, as well as the cold gas system, drove the configuration towards a 2-tank architecture (normally a 4 tank system is selected to keep the Centre of Mass (CoM) on the centre line of the S/C). This is in line with the Gaia approach.

6.4.2.2.2 *Exact geometrical efficiency or average geometrical efficiency*

Due to the thruster arrangement and pointing on the S/C, a 100% geometrical efficiency can not be achieved during thrusting.

As a first conservative approach, the average geometrical thruster-efficiency of the Gaia mission was used to calculate the propellant required for each manoeuvre, which gives acceptable results for a pre phase A study. The thruster geometrical efficiencies were taken from RD (1) and can be found in Table 6-6.

Manoeuvre	Δv [m/s]	Geometrical Efficiency [%]	Applied v for propellant calculations [m/s]
Lau_disp_corr	30.9	63	49.05
Per_vel_corr	13.1	63	20.79
TCM1_corr	2.2	63	3.49
Orbit_ins	165.0	63	261.90
Orbit_main	36.8	63	58.41
Eclipse_man	10.0	63	15.87
Disposal_man	10.0	63	15.87
Contingency	10.0	63	15.87
	Total: 278	Average: 63 %	Total: 441

Table 6-6: Propellant load when using average geometrical efficiency of thrusters

During the study, the thruster pointing was selected to be identical to the Gaia configuration, so the geometrical efficiency is assumed to be the same as for the Gaia mission for each delta-v manoeuvre. The exact geometrical efficiency gave the more accurate results and was therefore used. For delta-v manoeuvres, where no geometrical efficiency from the Gaia mission was available, the average of 63 % geometrical efficiency was used. The propellant load when using average geometrical efficiency of thrusters can be found in Table 6-7.

Manoeuvre	Δv [m/s]	Geometrical Efficiency [%]	Applied v for propellant calculations [m/s]
Lau_disp_corr	30.9	90	49.05
Per_vel_corr	13.1	90	14.5
TCM1_corr	2.2	63	3.5
Orbit_ins	165.0	90	183.3
Orbit_main	36.8	35	105.0
Eclipse_man	10.0	30	33.3
Disposal_man	10.0	63	15.9
Contingency	10.0	45	22.2
	Total: 278	Average: 63 %	Total: 412

Table 6-7: Propellant load when using exact geometrical efficiency of thrusters

6.4.3   Baseline Design

6.4.3.1   Chemical Bipropellant System

The architecture of the MON MMH propulsion system is identical to that of Gaia.

The baseline design of the chemical (MON/MMH) propulsion system makes use of 8 primary +8 redundant (total 16) 10N thrusters (S10-18 thruster shown in Figure 6-17 below) with an Isp = 291 s. The thruster characteristics are listed in Table 6-8 and Table 6-9 below:
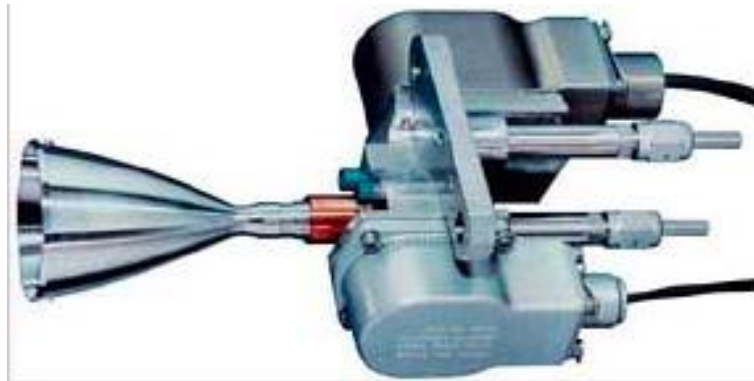
Figure 6-17: S-10-18 thruster

Property	Value
Oxidiser	MON-1/MON-3
Fuel	MMH
Nom. Thrust (Range min/max)	10.0 (7.0 - 11.7) N
Nom. Specific impulse (Range min/max)	291 (287 -) s
Nom. Mixture Ratio (Range min/max)	1.65 (1.20 - 1.90)
Nom. Inlet Pressure (Range min/max)	16.0 (10.0 - 23.0) bar
Nom. Mass flow (Range min/max)	3.5 g/s
Mass (Thruster with Valve)	0.65 kg

Table 6-8: S-10-18 thruster characteristics (1)

Components	Value
Valve	Upstream, bistable 51-215 (Moog) 25-43 V DC, Power: 8W max W
Valve 2	Downstream, monostable 51-215 (Moog) 25-43 V DC, Power: 8W max W
Chamber Material	Pt/Rh, Nimonic75
Injector Type	Double Cone Vortex
Cooling System	film & radiative

Table 6-9: S-10-18 thruster characteristics (2)

Propellant is stored in two (2) Eurostar 2000 tanks, of which the cylindrical section is adapted to the propellant needs.

Pressurant gas is stored in a single pressurant tank. Via a number of pyro-and latch-valves and a mechanical pressure regulator, the pressurant enters the tanks, thereby forcing the propellant to the thrusters. A set of redundant non return valves prevents propellant vapours from entering into the inlet manifold.

Propellant isolation valves make sure that the propellant is isolated from the surroundings and in combination with thruster valves guarantee the 3 barriers against leakage on ground when personnel could be present.

The image below shows a CAD image of the chemical propulsion system.
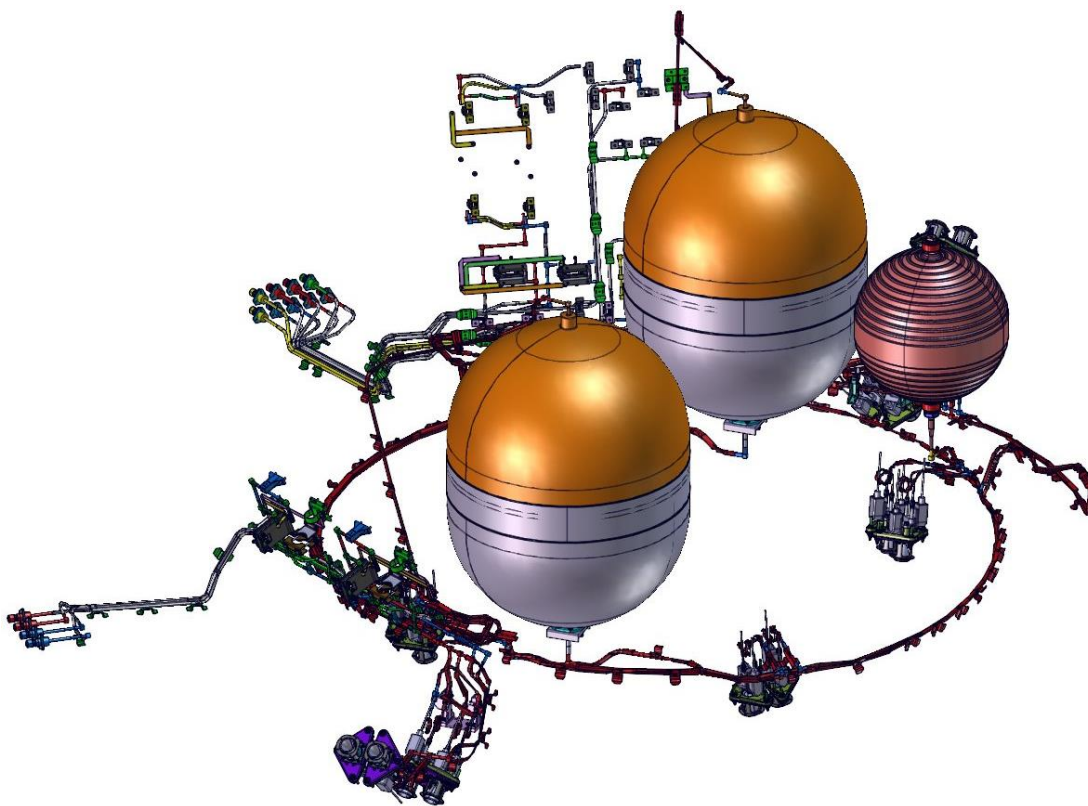
Figure 6-18: Chemical bipropellant propulsion system

The baseline design for GaiaNIR includes propellant tanks derived from the Eurostar 2000 line propellant tanks, by incorporating a dedicated cylindrical section. Figure 6-19 shows the complete Eurostar 2000 tank line option.
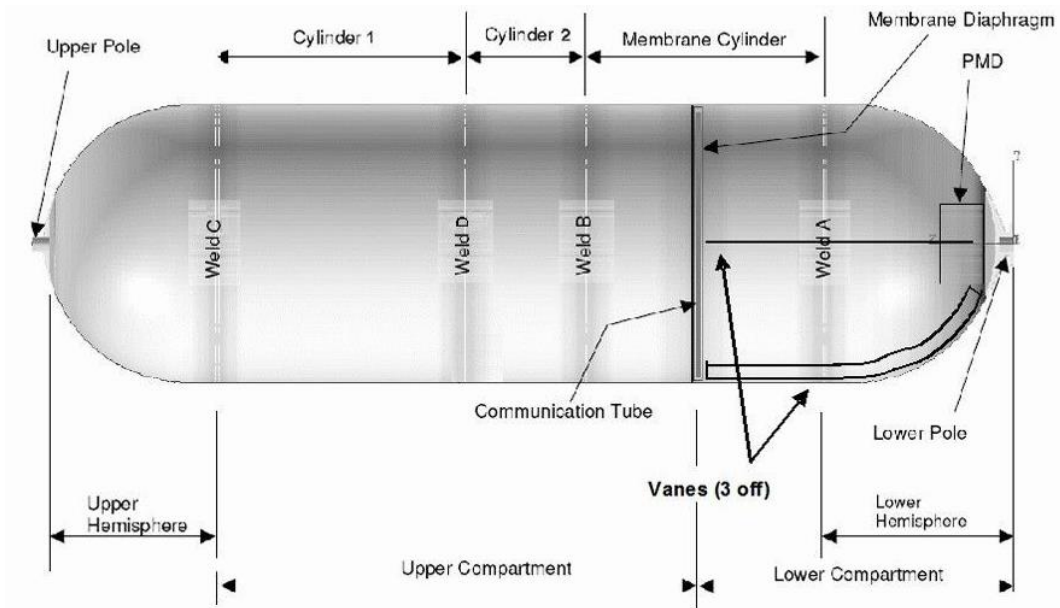
Figure 6-19: Eurostar 2000 propellant tank

The image below shows the area of change with respect to the original Gaia propellant tank. Such an adaptation to the section has already been conducted for many projects for example in Gaia, Mars Express, Venus Express, Nilesat and in a large variety of different sized telecommunication satellites in GEO.

Propellant demand requires changing the length of the cylindrical section of the tank
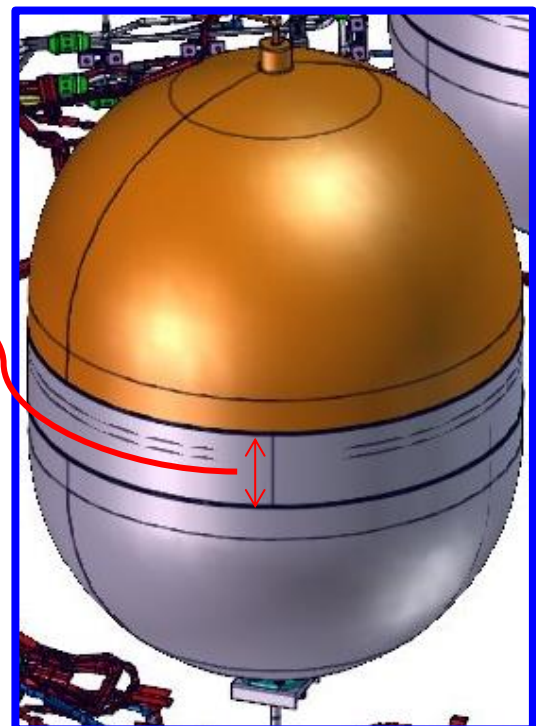
Figure 6-20: Eurostar 2000 propellant tank area of change when comparing to Gaia

Table 6-10 provides the propellant mass and pressurant mass for the chemical propulsion system for the GaiaNIR S/C.

Current Dry Mass	1838 kg
Propellant mass (exact geometrical efficiency)	303 kg (includes residuals)
MMH	114 kg
MON	189 kg
Helium (Pressurant)	1.6 kg
Lifetime	5.5 years

Table 6-10: Propellant and Pressurant masses for chemical bipropellant system

6.4.3.2 Sensitivity Analysis with respect to Changes of Dry Mass

Table 6-11 shows a sensitivity analysis with respect to changes of dry mass. When dry mass increases with respect to a set point of 1838 kg, the required propellant mass is shown as well as the impact on tank mass, length of cylindrical section of the tanks and total tank height.

Spacecraft mass [kg]	Propellant mass [kg]	L cylindrical section [mm]	M tank [kg]	L tank [mm]
1838+0	291	164	10.6	764
1838+50	299	180	10.7	780
1838+100	307	195	10.8	795
1838+150	315	211	10,9	810
1838+200	322	226	11.0	825

Table 6-11: Sensitivity analysis of propellant tanks dimensions and mass wrt. GaiaNIR S/C dry mass

The baseline design for GaiaNIR led to a S/C dry mass of 1887 kg. In order to accommodate the required propellant load of 362.23 kg (including residuals) and taking into account that 15% of additional propellant could be added to the tank (e.g. in order to be able to extend the mission lifetime if needed), the tanks are estimated to require a length of 785 mm and a mass of 10.7 kg each.

6.4.3.3   Cold Gas Mono -propellant Propulsion System

The baseline design of the cold gas propulsion system, used for fine attitude control, makes use of 6 primary + 6 redundant (total 12) cold gas thrusters. Nitrogen propellant is stored in two (2) high pressure tanks from the US identical to those in Gaia. The thrusters are organized in two branches, each branch with its own pressure regulator. Via a system of valves and pressure sensors, the exact total impulse can be tuned for each thruster firing.

The sizing of the tanks is based on AO GNC needs. Detailed information regarding fine tuning attitude control is given in GNC Chapter 6.5.

The architecture for the Cold Gas Mono-propulsion System for GaiaNIR S/C is shown in Figure 6-21 below:
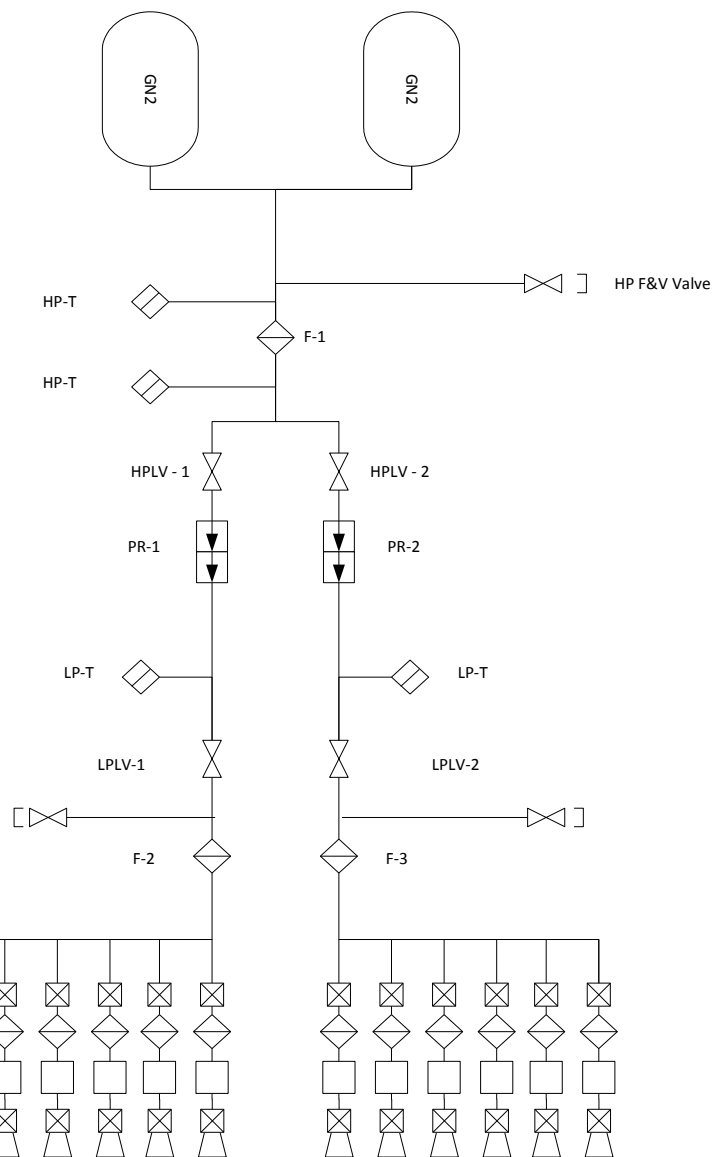
Figure 6-21: Cold gas monopropellant propulsion system

The mass and characteristics for the Cold Gas Mono-propulsion System for GaiaNIR S/C are shown in Table 6-12 below:

Current Assumptions	
Coldgas	Nitrogen
Number of thrusters	6 + 6 = 12
2 Tank configuration	~ 90 l per tank Current requirement of 60 kg propellant
Propellant Mass	60 kg (incl. margin) derived from Gaia
Coldgas System Dry Mass	39 kg (incl. margin)

Table 6-12: Propellant mass and characteristics of Cold Gas Monopropellant System

Figure 6-22 shows a CAD image of the cold gas monopropellant system.
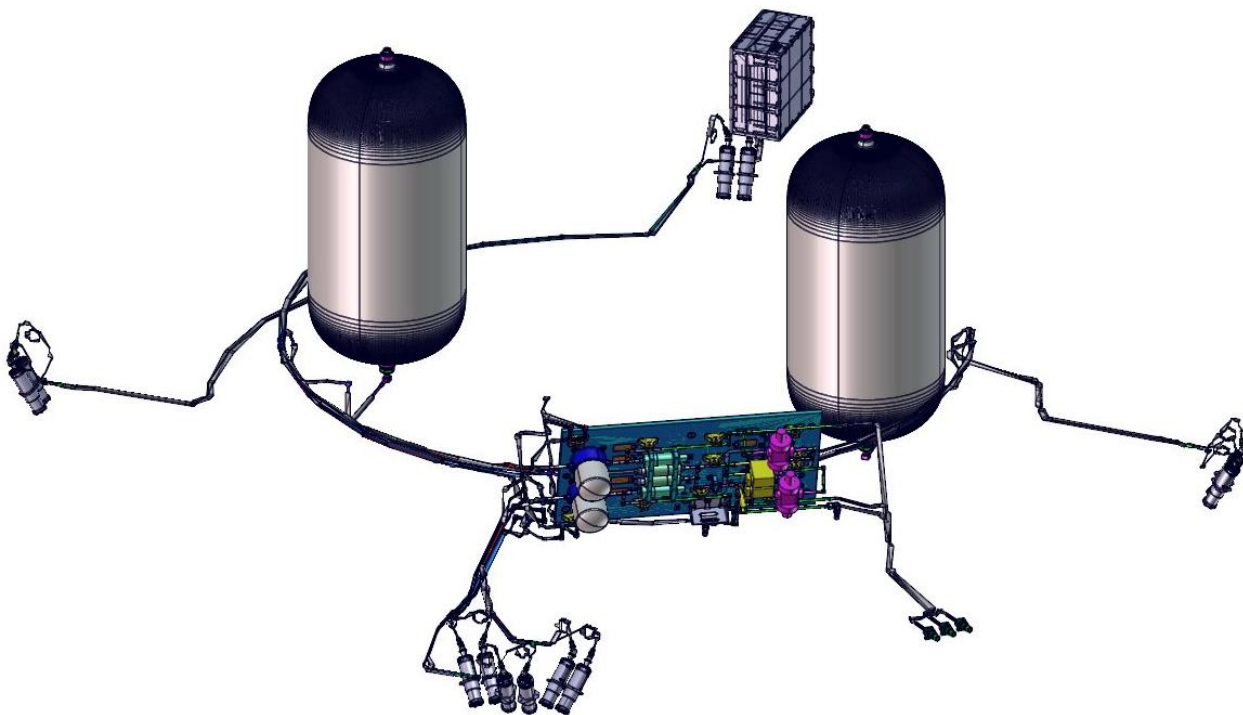
Figure 6-22: Cold gas (N2) mono propellant propulsion system

The selected cold gas tank (N_2) is the ATK-80475-1.

Table 6-13 shows the specs of two cold gas thrusters that could be used for GaiaNIR S/C.

Thruster	Thrust Range	Specific Impulse	Thruster Mass	Response Time	Other mission
Leonardo Micro Cold Gas Thruster	1 – 500 µN	45 – 60	< 0.4 kg	Response Time: 40 ms For Thrust=0: > 300 ms (in Gaia)	Gaia, Euclid
Bradford Micro Proportional Thruster (option)	1 – 2000 µN	>45 s	< 0.4 kg		PROBA-3, developed for Gaia

Table 6-13: Cold Gas thrusters characteristics

Leonardo micro cold gas thruster

Based on heritage, the same thruster used for Gaia S/C (see Figure 6-24) was selected for GaiaNIR. The main characteristics of the thruster are described in Table 6-14 below.

Figure 6-23: Cold thruster selected used on Gaia

Thrust Range	1 – 500 µN
Thrust Resolution	> 1 µN
Isp	> 45 s
Noise Level	< 1µN/√Hz
Provided Lifetime	60000 h (6.8 Years)

TRL	9
For Thrust=0:	> 300 ms in Gaia

Table 6-14: Characteristics of selected (Gaia) thruster

6.4.4   List of Equipment

Table 6-15 and Table 6-16 show the list of equipment for the baseline for GaiaNIR chemical propulsion subsystem.

Equipment	Number of items	Mass (single)	Margin	Overall mass incl. margin
Fill&Drain Valve	13	0.07	5.00	0.96
Filter	3	0.07	5.00	0.22
High Pressure Transducer	1	0.22	5.00	0.23
Low Pressure Transducer	2	0.25	5.00	0.53
Latch Valve	4	0.55	5.00	2.31
Non Return Valve	4	0.10	5.00	0.42
Pipes	-	5.00	20.00	6.00
Pressure Regulator	1	1.20	5.00	1.26
Pressurant Tank	1	8.20	5.00	8.61
Pyro Valve	11	0.16	5.00	1.85
Eurostar 2000 Tank	2	10.70	10.00	23.54
Bipropellant Thruster	16	0.65	5.00	10.92
Total: Bipropulsion System				**56.85**

Table 6-15: Bi-propulsion System List of Equipment

Equipment	Number of items	Mass (single)	Margin	Overall mass incl. margin
Coldflow Sensor	12	0.43	5.00	5.42
High Pressure Filter	1	0.08	5.00	0.08
High Pressure Transducer	2	0.22	5.00	0.46
High Pressure Fill&Vent Valve	1	0.21	5.00	0.22
High Pressure Latch Valve	2	0.80	5.00	1.68
Low Pressure Filter	2	0.02	5.00	0.04
Low Pressure Fill&Vent Valve	2	0.07	5.00	0.15
Low Pressure Transducer	2	0.25	5.00	0.53
Low Pressure Latch Valve	2	0.34	5.00	0.71
Pipes	-	3.00	20.00	3.60
Pressure Regulator	2	1.2	5.00	2.52
Coldgas Tank	2	22.7	5.00	47.67

Equipment	Number of items	Mass (single)	Margin	Overall mass incl. margin
Coldgas Thruster	12	0.18	5.00	2.27
Total: Coldgas System				65.35

Table 6-16: Cold Gas System List of Equipment

6.4.5   Options

The only option identified is the use of an alternative cold gas thruster, the Proportional Micro Thruster from Bradford Engineering (Figure 6-24)
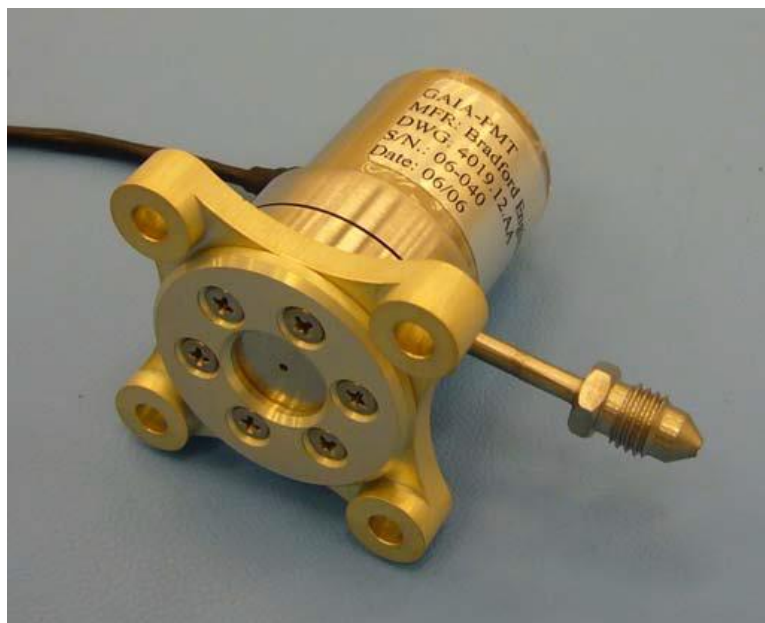
Figure 6-24: Proportional Micro Thruster (Bradford Engineering)

Table 6-17 lists the characteristics of the Proportional Micro Thruster from Bradford Engineering. The thruster has been developed for Gaia and has been tested in EPL (ESA Propulsion Laboratory).

Thrust Range	$0 - 2000$ µN
Thrust Resolution	1 µN
Isp	> 45 s
TRL	7

Table 6-17: Characteristics of Proportional Cold Gas thruster

6.4.6 Technology Requirements

No new technologies are required specifically for GaiaNIR mission for the propulsion subsystem, since the design is based on Gaia.

The propellant tank shall be modified by changing the cylindrical section. This is often done already in the past for the specific selected tank. A moderate requalification effort would be required.

6.5   SVM GNC

6.5.1   Requirements and Design Drivers

The main AOCS requirements are presented below:

SubSystem Requirements		
Req. ID	**Statement**	**Parent ID**
AOCS-010	The component of the rotation vector about the satellite XS axis shall be kept constant, with a nominal value 60"/s (the associated nominal spin period equals 6.0 hours).	SCI-0020
AOCS-020	The satellite spin axis shall have a forced precession motion (mean value over the year equals 0.173"/s) about the Sun to Earth direction at controlled speed.	SCI-0050
AOCS-030	The GaiaNIR spacecraft design shall comply with the pointing and rate error requirements on both astrometric fields-of-view as reported in the following table. *(see table below)* 99.73% per AL/AC axis confidence level, temporal statistics. τ = 1.629s. $\Delta\tau$ = 8s (TBC)[1]. The above requirements have been relaxed with respect to those included in RD[20], considering the larger AL pixel size (106 mas) and PSF size with respect to the Gaia case. It has been agreed to relax original Gaia requirements by a factor 2.	SCI-0640 SCI-0650
AOCS-040	The Astro telescope line of sight jitter along scan with respect to the inertial frame shall be such that its Power Spectral Density $PSD_{APE}^{AL}(f)$ satisfies the following inequality (RMS):	SCI-0660

Parameter	Requirement
Attitude Measurement Error (AME)	< 20"
Rate Measurement Error (RME) (AL direction)	1.8 mas/s
Rate Measurement Error (RME) (AC direction)	5.4 mas/s
Absolute Pointing Error (APE)	60"
Relative Pointing Error (RPE) (AL) over τ	10 mas
Relative Pointing Error (RPE) (AC) over τ	20 mas
Mean Rate Error (MRE) (AL)) over $\Delta\tau$	4 mas/s
Mean Rate Error (MRE) (AC)) over $\Delta\tau$	20 mas/s

---

[1] τ is the image integration time. $\Delta\tau$ in Gaia was defined as the time for an object to cross the focal plane from SM1 to AF1 readout (see also RD[25]). With similarity, in GaiaNIR it becomes 4*1.81=7.24 => 8s.

$$\Delta\theta_{AHFD}(f) = \left(\int_{1/(10T)}^{\infty} PSD_{APE}^{AL}(f) K_{AL} sinc^2(\pi f T) df \right)^{1/2}$$

$$< 6.8 \text{ μas}$$

where $K_{AL} = 1/(1+1/(2 f dt)^{1/2})$ where $dt = 0.5 \pi \tau$ and T is the time for an object to cross the Astro focal plane (i.e. from the 1st to the last AF read-out). [2]

T has been considered equals to 32.58 s[3].

---

[2] The value has been derived considering an allocation to the on-ground attitude reconstitution error to final parallax accuracy equals to 2 μas.

From the following equation (see page. 2 in LL's paper, and also David's presentation RD[21], RD[22])

$$\sigma_\pi = g_\pi \frac{\sqrt{\sigma_\xi^2 + \sigma_{cal}^2}}{\sqrt{N_{transit}}}$$

σ_π : parallax accuracy at the end of the mission

g_π : mean geometrical factor for the parallax (1.93 in Gaia)

σ_ξ : accuracy in the AL star coordinate in an individual FoV transit

σ_{cal} : accuracy in the AL for the calibration (focal plane, on-ground attitude determination, etc.) in an individual FoV transit.

$N_{transit}$: mean number of AL transits per star in the mission (83 in Gaia)

The above statement in the LL's paper asks that the contribution of the OGAD error on the final parallax accuracy shall be lower than 1 μas.

$$\sigma_{\xi\_cal} = \sigma_{\xi\_OGAD} = \frac{\sqrt{N_{transit}}}{g_\pi} \sigma_\pi = \frac{\sqrt{83}}{1.93} 2 \text{ μas} = 9.4 \text{ μas}$$

Considering (as for LL's paper pag. 3, formula 5 RD[21])

$$\sigma_{\xi\_OGAD}^2 = \sigma_{\xi\_OGAD\_o}^2 + \sigma_{\xi\_OGAD\_m}^2$$

$\sigma_{\xi\_OGAD\_o}$: low-frequency error: it is dominated by observational noise

$\sigma_{\xi\_OGAD\_m}$: high-frequency error: it is due to model errors (limited number of degrees of freedom in the reconstitution base)

Preliminary allocation considered in the reference LL's paper

$$\sigma_{\xi\_OGAD\_o} = \sigma_{\xi\_OGAD\_m} = 6.8 \text{ μas}$$

[3] The time T for an object to cross the Astro focal plane has been considered equal to $T = 2 \tau 9 = 32.58s$ (2 is due to the number of observations to be performed by each detector, 9 is the number of detectors in the AL direction for the GaiaNIR Astro focal plane.

AOCS-050	The Astro telescope line of sight jitter across scan with respect to the inertial frame shall be such that its Power Spectral Density $PSD_{APE}^{AC}(f)$ satisfies the following inequality (RMS): $$\Delta\theta_{AHFD}(f) = \left(\int_{1/(10T)}^{\infty} PSD_{APE}^{AC}(f)K_{AC}sinc^2(\pi fT)df \right)^{1/2}$$ $$< 200 \text{ μas}$$	SCI-0670

Figure 6-25 shows the weighting functions involved in the AHFD computations. The sinc weighting function (green line) can be approximate as for dark line (sinc function as 1/f, no transmission zeros, conservative approach).
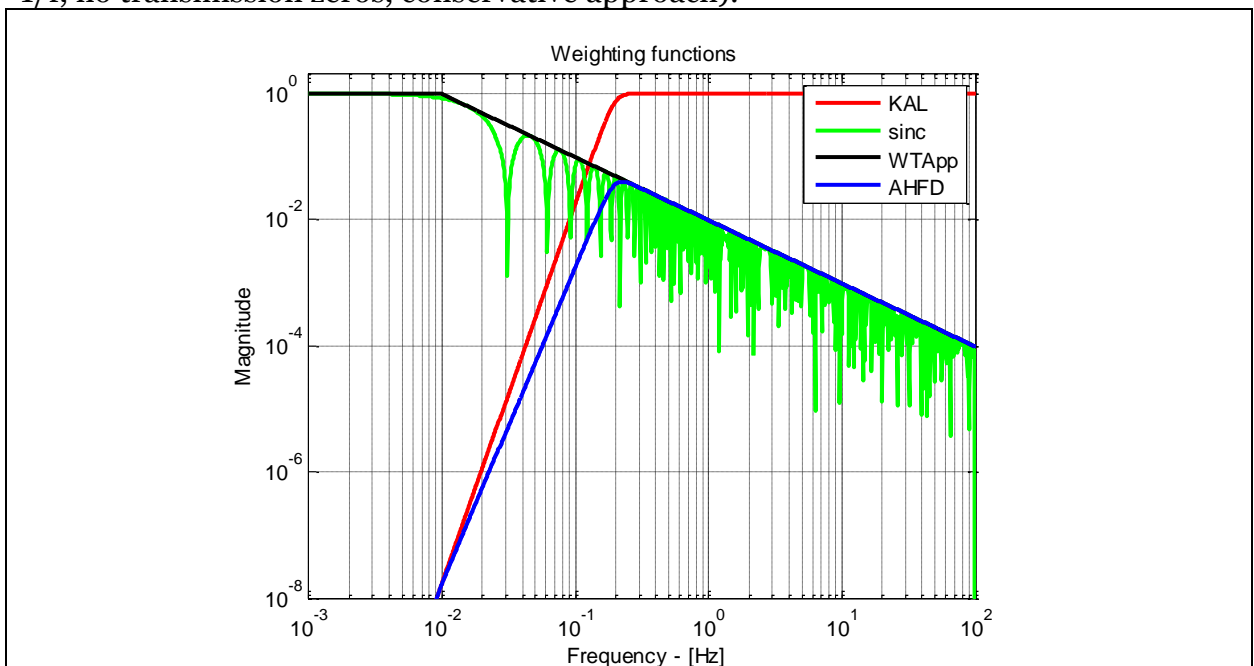
Figure 6-25: AHFD weighting functions (the blue curve has been derived considering the sinc approximation)

Before entering in the presentation of the performed analyses and sub-system description, it is considered worthwhile to spend a few words on the requirement AOCS-030 (linked to SCI-0640, RPE and MRE) constraining the image quality (see also chapter 6.5.2.3). It has been analysed considering the Modulation Transfer Function (MTF) approach.

Figure 6-26 shows the MTF in the AL direction due to: a) telescope/optics (at the diffraction limit); b) detector pixel; c) RPE requirement (jitter, 99.73% confidence level); d) MRE requirement (drift, 99.73% confidence level).

It is possible to observe that:

- The impact on the overall MTF (system) due to AOCS is quite limited if compared with the diffraction and detector ones. It will be still more relevant taking into

account that both the telescope and detector MTFs are indeed optimistic (Strehl ratio <1, detector MTF at Nyquist limit < 0.64);

- The effect of the drift is very low compared to the jitter one.
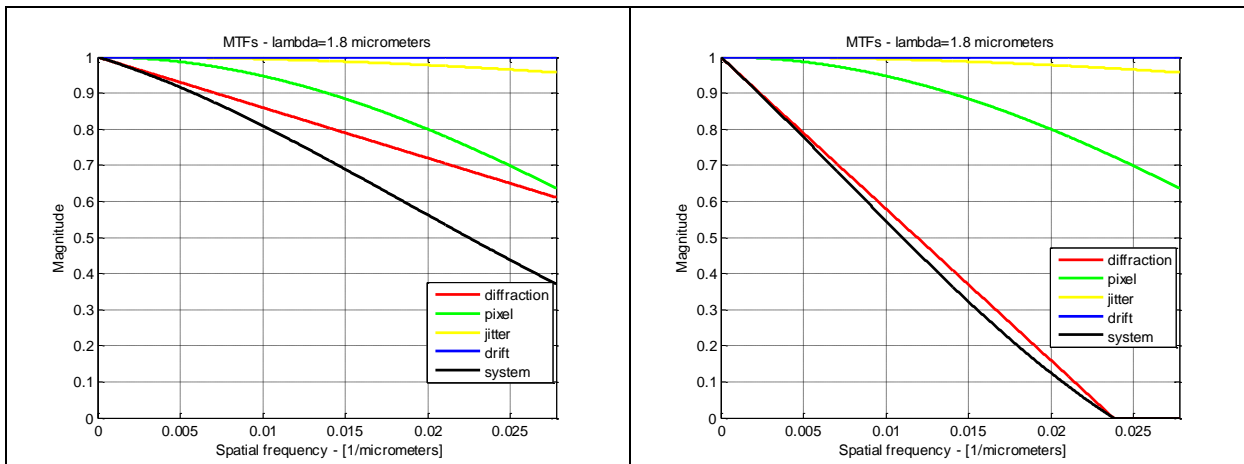
Figure 6-26:   System MTF and contributors (detector Nyquist limit: 0.05 μm⁻¹) at 0.6μm (left) and at 1.8 μm (right) wavelength

In Gaia, there was the need to limit the rate error due to TDI, that is itself responsible of an additional MTF reduction. In the case that GaiaNIR will be implemented considering the de-scan mechanism (see later in the chapter), a more balanced apportionment could be considered relaxing RPE and MRE.

The RPE and MRE value have an impact on the PSF shape stability between acquisitions. For example, increasing the allowed RPE/MRE, the PSF calibration accuracy reduces and the AL star-coordinate accuracy as well. In that case, the requirements need to be revisited in agreement with the science team.

6.5.1.1   Design Drivers

The AOCS design is driven by the image quality requirements and AHFD (see also chapters 6.5.1 and 6.5.2.2.2): their analysis and design implications have been addressed in the frame of the CDF activities.

In addition, step&stare solution has been considered as a system option and it has been analysed at sub-system level as well.

6.5.2   Assumptions and Trade-Offs

Assumptions	
1	For the case of step & stare solution, the step size in the along scan direction is equal to half detector, i.e. 0.0301 deg. 11960 is the number of steps per revolution.
2	In the case of step & stare solution, the S/C slew has been computed considering the bang-bang acceleration profile, that provides the minimum slew time, requesting the maximum power or fuel consumption.
3	The mass properties considered to trade/access the step & stare solution have been Ixx=3300 kgm², Iyy=Izz=3000 kgm² (about 10% lower than the Gaia ones (see

RD[22])).

4	The Micro-Propulsion System (MPS) maximum force has been considered equal to [0.5, 1.0, 2.0] mN.
5	In the case of MPS based on cold-gas (nitrogen), the considered Isp value has been 60s (see RD[22]).
6	The lever arm of the MPS thrusters (effective length with respect to the S/C COM) has been 2m (in line with Gaia solution).
7	In the case of slew performed with reaction wheels (hybrid solution like for Euclid, or pure reaction wheel), the considered available torque were 0.1-0.2 Nm.
8	In case of reaction wheels solution, an additional stabilisation time of 20-30s has been considered (it can be reduced using a smart slew profile, but this requires a longer slew time)
9	The time T for an object to cross the Astro focal plane is equal to 2 times for the step time multiplied for the number of detectors in the same direction.

The AOCS trade-offs are closely related to the main system options investigated during the GaiaNIR CDF Study and presented in the Systems Chapter 7. The major AOCS contributors are details in the following sections.

6.5.2.1   Step&stare versus spinning solution

Considering the MPS solution, the following results have been derived without any margin (in the computation of the equivalent sky scan-rate, the image integration time has been fixed to 0s):

- Max thrust = 0.5 mN   => Slew time = 80.7s, 0.832 kg/rev and 27.2 kg/year. Equivalent sky scan-rate < 1.34 "/s (<32.7 rev/year)

- Max thrust = 1.0 mN   => Slew time = 57.1s, 1.18 kg/rev and 54.4 kg/year. Equivalent sky scan-rate < 1.90 "/s (<46.2 rev/year)

- Max thrust = 2.0 mN   => Slew time = 40.4s, 1.66 kg/rev and 109 kg/year. Equivalent sky scan-rate < 2.69 "/s (< 65.4 rev/year)

In the case of electric MPS, the propellant mass reduces by a factor 50-100, but the allowed equivalent sky scan-rate will not change.

In the MPS solution, the equivalent sky scan-rate is about 20-40 times lower than the required one (60"/s).

In the case of reaction wheel solution (ball bearing or magnetic bearing reaction wheel), the step time reads 5.7s (0.1 Nm) and 4.04 s (0.2 Nm). On top of this, it is necessary to take into account the tranquilization time to cope with sloshing and other possible flexible modes (Gaia sunshield first mode is about 1Hz). From that, the equivalent sky scan-rate <= 3.2 "/s (30s tranquilization time) and <= 4.5 "/s (20s tranquilization time).

In the end, whatever the actuators are, the S/C step&stare solution with the current baselined step (0.0301 deg) induces an equivalent spin rate not greater than 5"/s.

The specified sky spin rate can be considered compatible with a step of about 0.18 deg (0.1Nm torque), that is about 3 times the detector angular size.

Considering the above results, at system level it has been decided to consider a spinning S/C Gaia-like.

6.5.2.2   Spinning S/C (Gaia-like) with De-scan mechanism

6.5.2.2.1   De-scan-mirror mechanism

The de-scan mechanism is based on a rectangular mirror as shown in Table 6-18. From that, the following preliminary mass properties have been derived:

- SiliconCarbide: $m_{SiC} = 0.811\ kg,$ $I_{mirrSiC} = 2.547 \times 10^{-3}\ kgm^2$

- Zerodur: $m_{Zero} = 0.639\ kg,\ I_{mirrZero} = 1.745 \times 10^{-3} kgm^2$

	Mirror main properties

	• dimensions:
	    ○ $L = 0.19\ m$
	    ○ $W = 0.07\ m$
	    ○ $T = 0.019\ m$
	• materials (two options)
	    ○ Silicon Carbide: $\rho_{SiC} = 3210\ kg/m^3$
	    ○ Zerodur: $\rho_{Zero} = 2530\ kg/m^3$

Table 6-18: Mirror drawing, considered dimensions and materials

The rotation profile of the mirror is shown in Figure 6-27: the time for each step T_{step} lasts 1.81 s. It has been considered 0.181s (10% reduction in the star observation time, to be considered in updating the scientific performance) for the movement of the mirror back to its initial position to start the initial acquisition. From that, the allowed integration time plus the readout time is 1.629s.

According to the optical design, the magnification factor M of the de-scan mirror is equal to 5 (the magnitude of the mirror rotation that is requested to compensate a unitary S/C rotation around a parallel axis; e.g. 1" S/C de-pointing is recovered by 5" mirror rotation => M=5).
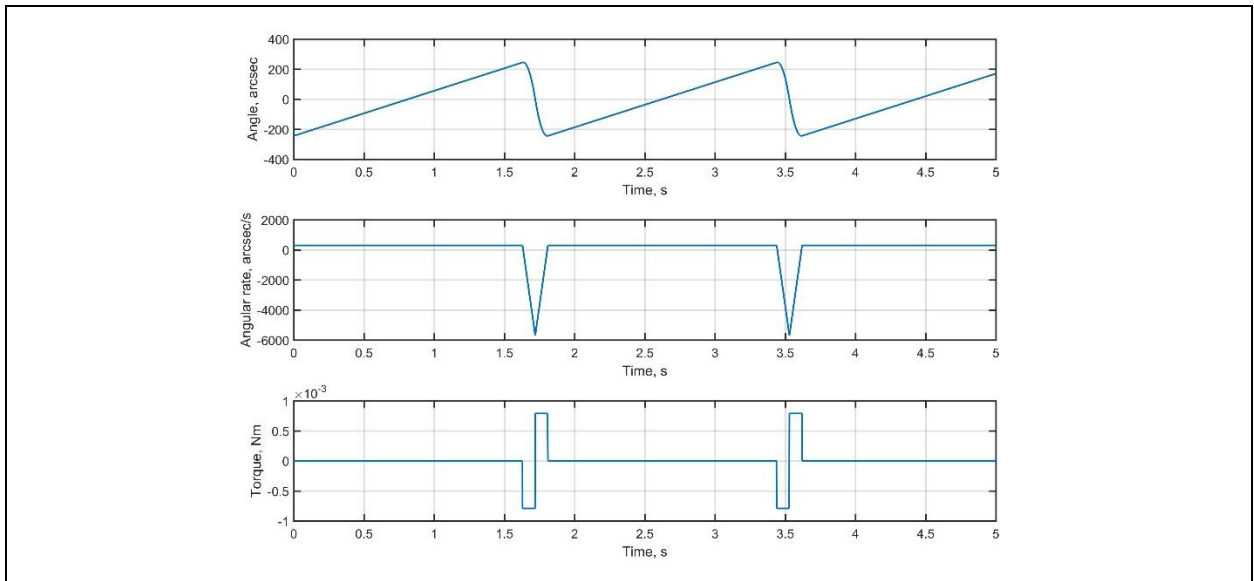
Figure 6-27: Mirror rotation profile and torque (SiC mirror)

The mirror is moving to compensate the S/C spin rate with respect to the sky in 1.629s, and the rotation angle is $\theta_{mirr} = \pm244.35''$.

Furthermore, the speed of the mirror becomes:

- During the sky observation: $\omega_{mirr} = M \cdot \omega_{sc} = 300''/s$
- When the mirror comes back to start a new observation: $\omega_{mirrMAX} = 5700\ ''/s$

In the case of SiC based mirror, the magnitude of the torque is equal to $7.92 \times 10^{-4} Nm$. According to theory, the magnitude of the frequency spectrum of the mirror movement is:

$$\theta(kf_o) = \frac{2\Delta T f_o\, T_{mirr}}{\left(2\pi(kf_o)\right)^2 I_{mirr}} \frac{\left(sin(\pi(kf_o)\Delta T)\right)^2}{(\pi(kf_o)\Delta T)}$$

where:

ΔT 　: 0.09s (half the time interval required to comes back to start a new observation)

f_o 　: 0.5525Hz.

k 　: index of the harmonic.

Figure 6-28 shows the magnitude of the mirror torque frequency spectrum (left) and of the attitude rotation frequency spectrum (right) (SiC mirror). However, it shall be taken into account that any nonlinearities in the mechanism movement will add sub-harmonics and fraction harmonics, or change harmonics magnitude with respect the above derived considering theory.
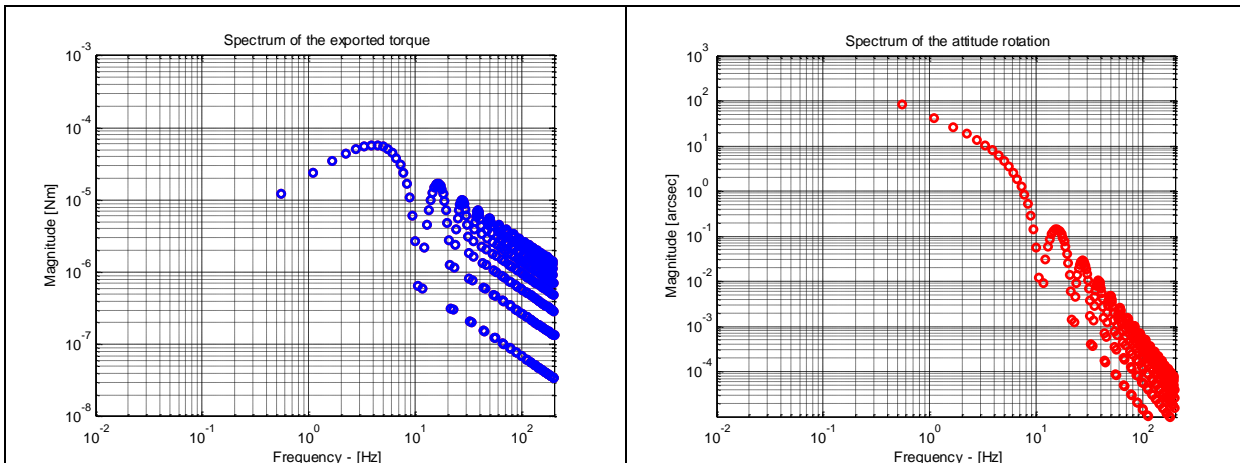
Figure 6-28: Spectrums of the mirror exported torque (left) and attitude rotation (right) - SiC mirror

In the frame of the study, it has been assumed the possibility to use a balancing system for the mechanism (see Mechanism Chapter 6.3). Figure 6-29 (left) shows the disturbance torque attenuation considered at S/C level (@0.5525Hz torque/force exported toward the spacecraft is 1/10 of the actual one requested by the mirror to follow the rotation profile). Figure 6-29 (right) shows the magnitude of the exported torque frequency spectrum.
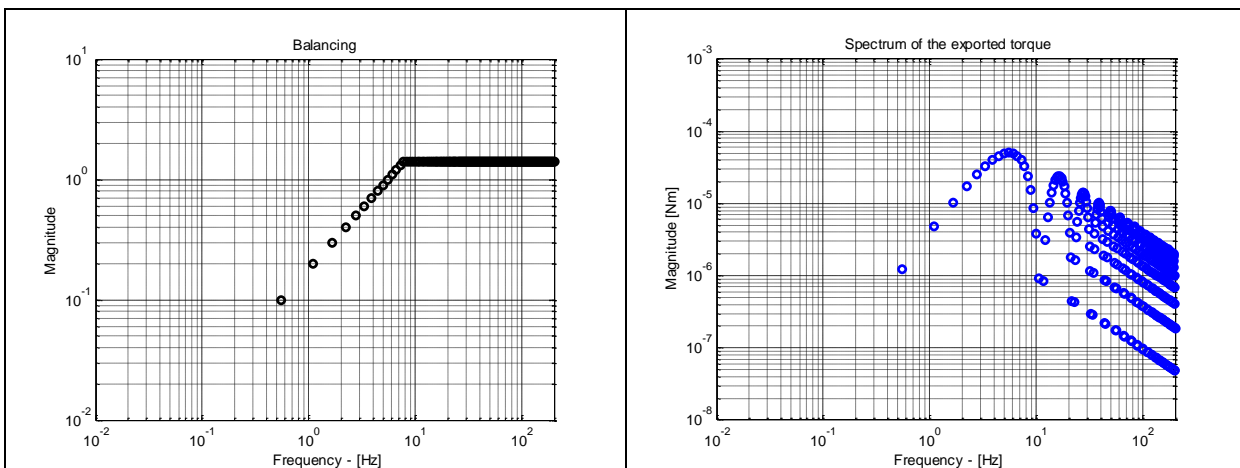
Figure 6-29: Spectrums of the balancing mechanism effectiveness (left) and exported torque (right) - SiC mirror

6.5.2.2.2 *Architecture and requirements allocation*

The requirements included in chapter 6.5.1 respond to three kinds of different objectives:

1) Tracking of the sky scanning low (APE, AME)
2) Image quality (MRE, RPE)

3) Error in the on-ground LoS attitude determination: it is due to "not observable" attitude high-frequency components (AHFD).

In the Gaia concept, all above requirements affect the AOCS design. In the de-scan-mechanism based GaiaNIR, the above requirements affect both the AOCS and the de-scan-mechanism itself.

Different architectures have been considered:

- Architecture A

  The S/C rotates, implementing the nominal reference attitude and rate trajectory, and the mirror performs the de-scanning nominal rotation in a coordinated and synchronised way with the Astro focal plane image integration and acquisition/readout operations. The attitude controller forces the spacecraft to follow the nominal reference attitude, and the de-scan mechanism controller forces the mirror to follow the de-scanning nominal rotation: no interactions between these controllers. The scan-mechanism operates using its own measurement provided by transducers like capacitors.

  The de-scan mechanism and focal plane detectors integration and readout phases are synchronised. The AOCS and the payload (focal plane and de-scan mechanism) operate in parallel: just coarse synchronization (or time stamps data) is requested to feed the rate/attitude control by star coordinates measurement.

- Architecture B

  The S/C rotates, implementing the nominal reference attitude and rate trajectory, and the mirror performs the de-scanning nominal rotation in a coordinated and synchronised way with the Astro focal plane image integration and acquisition/readout operations. The attitude controller forces the S/C to follow the nominal reference attitude, and the de-scan mechanism controller forces the mirror to follow the de-scanning nominal rotation: no interactions between the controllers. The scan-mechanism operates using its own measurement and the focal plane star coordinates in order to reduce the impact on image quality of the mirror movement errors.

  The de-scan mechanism and focal plane detectors integration and readout are synchronised. The AOCS (platform) and payload (focal plane and de-scan mechanism) operate in parallel: just coarse synchronization (or time stamps data) is requested to feed the rate/attitude control.

The architecture A was selected since:

- It permits to re-use the successful Gaia architecture that is flight proven (algorithms, s/w, etc).
- The de-scan mechanism needs to be synchronised just with the Astro: the coupling between payload and platform are limited as in line with current Gaia design.

Architecture B would have allowed relaxing the AOCS requirements and/or the scan-mechanism control requirements since image quality would have been recovered by the additional control loop between mirror and focal plane. However, due to the reduced number of focal plane measurements during the integration time (star coordinates available every 30-50ms=> 40-60 measurements each integration time => not enough information) it cannot be effective.

Considering Architecture A, a set of consistent requirements between AOCS and de-scan-mechanism have been derived.

The image quality (MRE, RPE) requirement allocation has been performed assuming uncorrelated the AOCS and the de-scan mechanism errors, and defining an apportionment factor K:

$$\theta_{AOCS} = \frac{K}{\sqrt{1 + K^2}} \theta_{GaiaNIR}$$

$$\theta_{mirror} = \frac{M}{\sqrt{1 + K^2}} \theta_{GaiaNIR}$$

Considering in preliminary way K=2, the allocation shown in Table 6-19 has been obtained.

The apportionment for the requirements constraining the tracking of the sky scanning law errors (APE and AME), has been performed considering the error as correlated (e.g. long-term thermal effects).

The apportionment of AHFD requirement has been done considering uncorrelated the uncertainties on the Astro LoS displacement due the attitude spacecraft and the de-scan mirror rotation; a preliminary allocation for the AL AHFD could be:

- 3.4 μas to spacecraft (AOCS, thrusters noise, mirror movement effect)
- 6*M=30 μas to mirror movement uncertainty and overall mechanism disturbances, in the mirror reference frame ($6.8^2=3.4^2+6^2$).

All the AL and AC requirements are included in Table 6-19.

Scanning law

Parameter	Attitude control requirement	De-scan mirror requirement
Attitude Measurement Error (AME)	< 15"	25" (*)
Rate Measurement Error (RME) (AL direction)	1.6 mas/s	4 mas/s (****)
Rate Measurement Error (RME) (AC direction)	4.8 mas/s	7 mas/s (****)
Absolute Pointing Error (APE)	45"	75" (*)

Image quality

Parameter	Attitude control requirement	De-scan mirror requirement
Relative Pointing Error (RPE) (AL) over $1.629s$	9 mas	22 mas (**)
Relative Pointing Error (RPE) (AC) over $1.629s$	18 mas	44 mas (***)
Mean Rate Error (MRE) (AL) over $8s$	3.6 mas/s	8.8 mas/s (**)
Mean Rate Error (MRE) (AC) over $8s$	18 mas/s	44 mas/s (***)

On-ground attitude reconstitution

Parameter	Attitude control requirement	De-scan mirror requirement
AHFD (AL)	3.4 µas	30 µas
AHFD (AC)	100 µas	870 µas

Table 6-19: Pointing requirements for the attitude control and de-scan mechanism

(*) to be translated in alignment and stability of the mirror alignment. Calibration between STR and ASTRO, mechanism and ASTRO shall be considered with a given periodicity.

(**) These are the driver requirements to design the mirror position and speed controller. The nominal rotation and angular rate trajectories shall be followed with the above errors in low frequency (MRE) and high frequency (RPE). The MRE takes into account drift between calibrations, bias. RPE takes into account the high-frequency effects of the mirror movement filtered by RPE weighting mask.

(***) These requirements constrain the behaviour of the scanning mirror in the AC direction. In the case of one-degree of freedom mechanism, it forces alignment and stability of the alignment. E.g. if the mirror rotation axis is not perfectly normal to the Astro focal plane AL direction, this translates into a rate error in the AC direction (e.g. 1" => 0.3 mas AC).

(****) are relevant to support the mirror trajectory control. As per the AOCS, the requirements on rate shall be considered/reviewed in the frame of overall specific controller design.

The design drivers for both AOCS and mechanism are the RPE, MRE and AHFD.

6.5.2.2.3   *Impact of the de-scan-mirror mechanism on the S/C attitude*

The movement of the mirror induces S/C attitude displacement, that cannot be compensated by the AOCS attitude control (the time response of the MPS is not compatible with the mechanism commanded torque). According to the angular momentum conservation, the S/C attitude and angular rate disturbances become:

$$\theta_{SC\ SiC} = \theta_{mirr} \cdot \frac{I_{mirrSiC}}{I_{scX}} = 244.35'' \cdot \frac{2.547 \times 10^{-3} kgm^2}{3300\ kgm^2} = 0.185\ mas$$

$$\omega_{SC\,SiC} = \omega_{mirr} \cdot \frac{I_{mirrSiC}}{I_{scX}} = 300''/s \cdot \frac{2.547 \times 10^{-3}\ kgm^2}{3300\ kgm^2} = 0.224\ mas/s$$

The perturbations are well inside the MRE and RPE requirements and a specific balancing mechanism is not requested to meet image quality requirements.

A coarse assessment of the impacts on AHFD has been performed considering just the nominal mirror movement: nonlinearities in the mechanism will add sub-harmonics or higher harmonics that are not taken into account in the provided assessment.

Without any balancing mechanism:

- AHFD considering sinc function : 0
- AHFD considering the continuous approximation of the sinc function as 1/f (see previous figure) in high-frequency: 0.82 µas.

With the introduction of a balancing mechanism:

- AHFD considering sinc function : 0
- AHFD considering the continuous approximation of the sinc function as 1/f in high-frequency: 0.095 µas.

The following aspects shall be considered in the implementation of the GaiaNIR based on the de-scan mirror mechanism:

- The coupling between mechanism torque/force and sunshield structural modes. The relevant sunshield structural modes should not couple with the harmonics induced by mirror movement. To this purpose:
  - Sunshield relevant modes below 0.45Hz (but still high enough for attitude control modes needs)
  - Compensation mechanism helps
- The coupling between mechanism torque/force and telescope structural modes. To this purpose:
  - Compensation mechanism helps at low frequency.

6.5.2.2.4 Impact of the de-scan-mirror mechanism on the on-ground attitude determination

The contribution on the AHFD due to de-scan mechanism has been computed starting from the Fourier series as for the above description.

It has been computed:

- AHFD considering the full sinc function : 0 µas
- AHFD considering the continuous approximation of the sinc function as 1/f in high-frequency: 1.08 10^6 µas.

To assess the required repeatability, the following computations have been performed:

a) τ = 1.629 s , T = 32.58 s => AHFD = 0 µas
b) τ = 1.629 s , T = 32.58 * (1+10^{-7}) s => AHFD= 7.2 µas

c) $\tau = 1.629 s$, $T = 32.58* (1+10^{-6}) s => AHFD= 72 \mu as$

d) $\tau = 1.629 s$, $T = 32.58* (1+10^{-5}) s => AHFD= 720 \mu as$

Any nonlinearities in the mechanism will add sub-harmonics or higher harmonics that are not taken into account in the above computation. In addition, from the LL's paper (RD[21]), it seems that the average concept (transmission zeros) should be considered not in hard way (by the way, the average FoV transit considered above does not take into account the space between detectors). A more robust approach shall be instead considered.

The solution can be derived coming back to the basic concept: AHFD constraints the uncertainty in the Astro LoS knowledge. On ground, the spacecraft attitude can be reconstructed using stars, and the mirror attitude can be reconstructed using the measurement that feed its control loop.

If the on-ground mirror attitude determination will be able to estimate the mirror instantaneous attitude with a given accuracy, it can be included/merged with OGAD in order to reconstruct the Astro telescope LoS.

A preliminary exercise has been performed on the required accuracy in the on-ground mirror attitude determination. Two weighting functions providing the requested relative knowledge accuracy (including random and calibration residual errors) have been considered (see Figure 6-30). The selection of the weighting functions has been done to meet the AHFD requirement; the following results have been obtained:

A) *weighting function with flat uncertainty equals to 10^{-5} up to 30Hz => AHFD = 13* μas

B) *weighting function with 10^{-6} @0.5525Hz and with 60dB/decade slope => AHFD = 15* μas

From a preliminary assessment, the above accuracy seems to in line with the mechanism real-time control needs (dynamic range 10^5-10^6) (TBC).
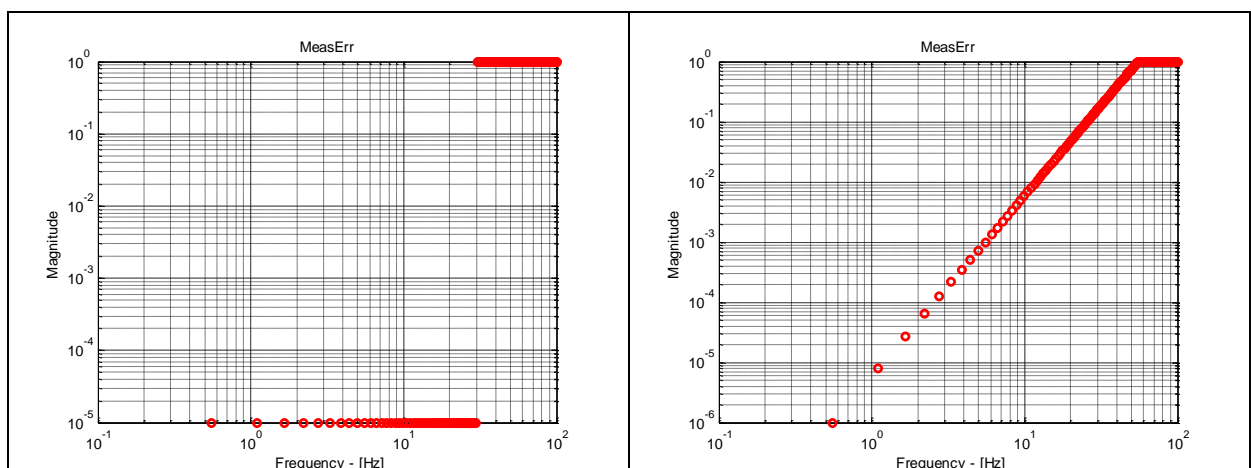
Figure 6-30: On-ground mirror attitude determination error - Weighting function A (left) and weighting function B (right)

6.5.2.2.5 Impact of the thruster noise on the on-ground attitude determination

The thruster noise profile shown in Figure 6-31 has been considered (Gaia Requirement):
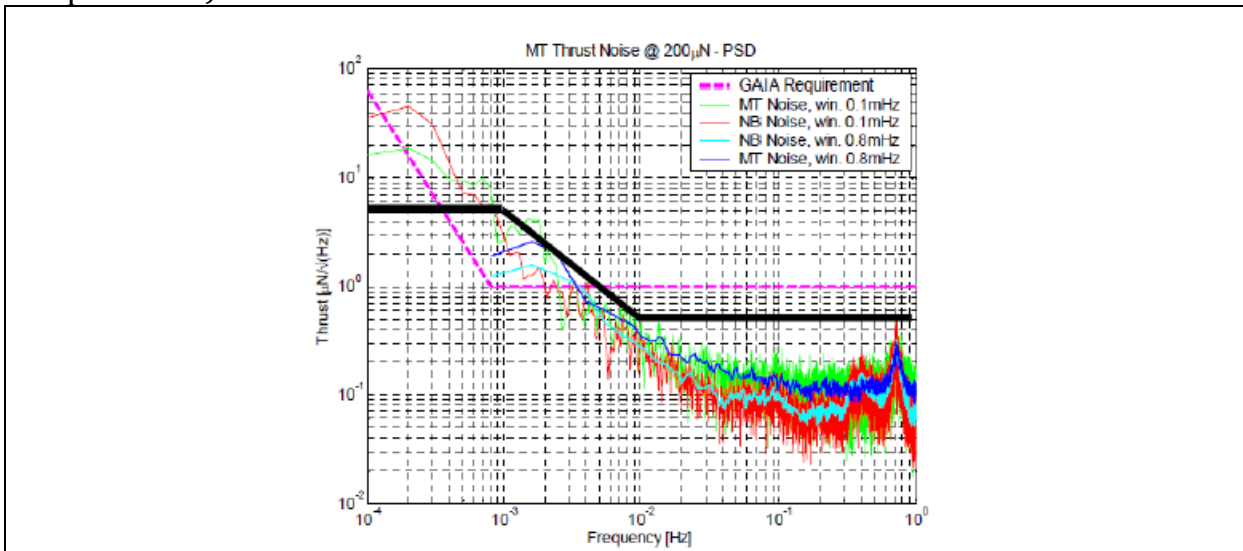
Figure 6-31:   Thruster noise profile (see RD[25])

The computed contribution to the AHFD is equal to:

- AHFD considering the full sinc function : 1.1 µas

- AHFD considering the continuous approximation of the sinc function as 1/f in high-frequency: 1.5 µas.

6.5.2.3   On-board rate and attitude determination

The on-board rate and attitude determination could be based on the data-fusion (e.g. gyro-stellar like estimator) between star-tracker attitude measurement, gyroscope and Astro focal plane (Astro telescope 1 and Astro telescope 2) rate measurement.

The use of a specific set of sensors depends on the AOCS operating mode (see chapter 6.5.3). With particular reference to the scientific mode, the Astro focal plane processing is required to meet the rate control requirement.

Using the positions on the focal plane achieved by a set of reference and bright stars (selected on-board in real time) in the different image acquisition times, it is possible to estimate the focal plane star rate, and then the spacecraft inertial angular rate.

In Gaia, the rate determination was based on the processing of star images on Star Mapper (SM1 and SM2) and AF1 (see RD[25]) to determine the S/C inertial angular rate. The SMs permit to discriminate the FoV by optical design: on SM1 just the star images from Astro telescope 1 (preceding FoV) are focused, and, in the same way, on SM2 only the star images from Astro telescope 2 (following FoV) are focused. Following the movement of the stars on AF1, it was possible to derive the AL and AC rates and then the S/C inertial angular rate.

In order to save GaiaNIR costs, in the frame of the CDF study, the option to not include the SMs has been considered. This option will be analysed in the following.

Let Astro reference frame be the reference frame considered for attitude control (AOCS) (see Figure 6-32):

- X axis: is the spin axis;
- Y axis: is aligned with the telescope line-of-sight;
- Z axis= cross (X,Y).

The Astro1 (Astro telescope 1) reference frame is nominally rotated with respect to the Astro reference frame as for the following rotation matrix:

$$_{AS}R_{A1} = \begin{bmatrix} 1 & 0 & 0 \\ 0 & \cos(\varphi_1) & -\sin(\varphi_1) \\ 0 & \sin(\varphi_1) & \cos(\varphi_1) \end{bmatrix}$$

In similar way, the Astro2 (Astro telescope 2) reference frame is nominally rotated with respect to the Astro reference frame as for the following rotation matrix:

$$_{AS}R_{A2} = \begin{bmatrix} 1 & 0 & 0 \\ 0 & \cos(\varphi_2) & -\sin(\varphi_2) \\ 0 & \sin(\varphi_2) & \cos(\varphi_2) \end{bmatrix}$$

$$\varphi_1 = \frac{\varphi_{BA}}{2}$$

$$\varphi_2 = -\frac{\varphi_{BA}}{2}$$

$\varphi_{BA} = 106.5 \, deg$ GaiaNIR basic angle.
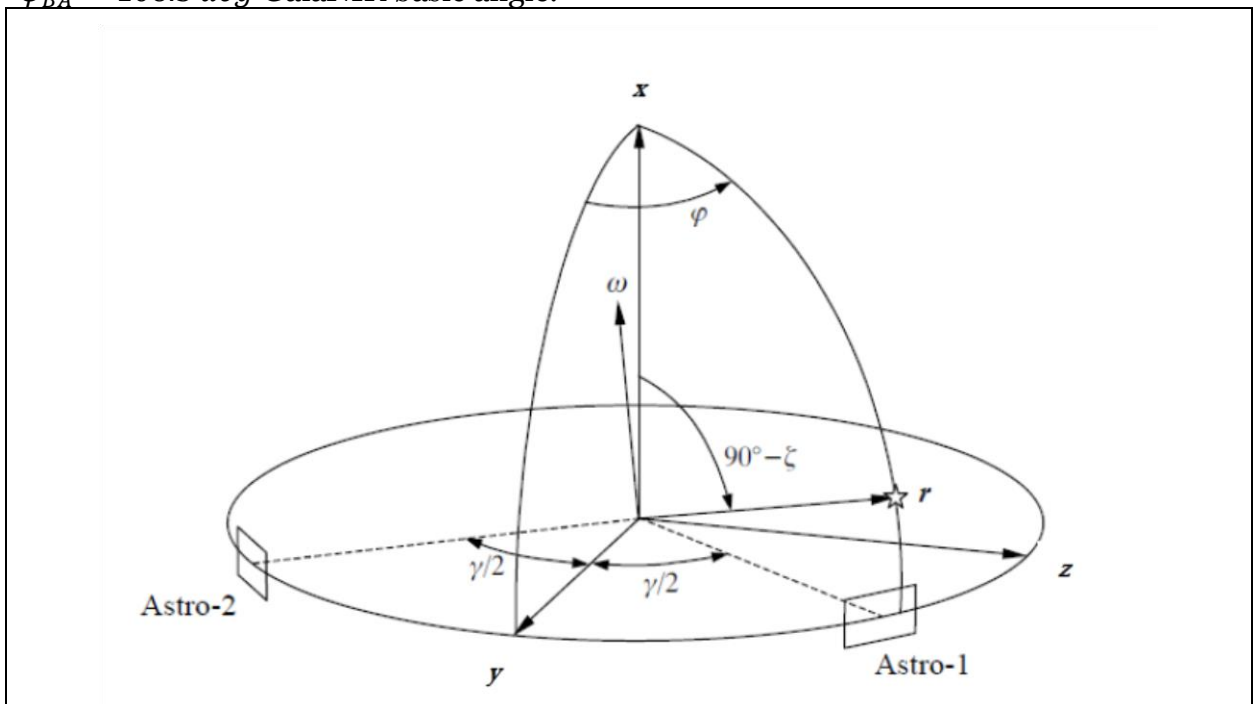
Figure 6-32:   Definition of the considered reference frames

Let $\boldsymbol{\omega}$ be the S/C inertial angular rate in the Astro (attitude control) reference frame

$$\boldsymbol{\omega} = \begin{bmatrix} \omega_X \\ \omega_Y \\ \omega_Z \end{bmatrix}$$

The angular rate in the Astro1 and Astro2 (generic index i) reference frames becomes:

$$\boldsymbol{\omega_i} = \left[{_{AS}R_{Ai}} \right]^T \begin{bmatrix} \omega_X \\ \omega_Y \\ \omega_Z \end{bmatrix} = \begin{bmatrix} 1 & 0 & 0 \\ 0 & \cos(\varphi_i) & \sin(\varphi_i) \\ 0 & -\sin(\varphi_i) & \cos(\varphi_i) \end{bmatrix} \begin{bmatrix} \omega_X \\ \omega_Y \\ \omega_Z \end{bmatrix}$$

$$\begin{bmatrix} \omega_X \\ \omega_Y \\ \omega_Z \end{bmatrix}_i = \begin{bmatrix} \omega_X \\ \cos(\varphi_i)\,\omega_Y + \sin(\varphi_i)\,\omega_Z \\ -\sin(\varphi_i)\omega_Y + \cos(\varphi_i)\,\omega_Z \end{bmatrix}$$

Considering the pinhole camera model, the focal plane coordinates are linked to the field coordinates by the following formula (x: AC, z: AL):

$$\begin{bmatrix} x \\ z \end{bmatrix}_i = -f_i \begin{bmatrix} \frac{n_x}{n_y} \\ \frac{n_z}{n_y} \end{bmatrix}_i \cong -f_i \begin{bmatrix} n_x \\ n_z \end{bmatrix}_i$$

$n_y \cong 1$ due to small FoV.

Unit vector for the given star in Astro i reference frame:

$$\begin{bmatrix} n_x \\ n_y \\ n_z \end{bmatrix}_i = \begin{bmatrix} \sin(\beta_i) \\ \cos(\beta_i)\cos(\alpha_i) \\ \cos(\beta_i)\sin(\alpha_i) \end{bmatrix} \cong \begin{bmatrix} \sin(\beta_i) \\ 1 \\ \sin(\alpha_i) \end{bmatrix}$$

The star velocity measured in the focal plane becomes (x: AC, z:AL):

$$\begin{bmatrix} \dot{x} \\ \dot{z} \end{bmatrix}_i \cong -f_i \begin{bmatrix} \dot{n}_x \\ \dot{n}_z \end{bmatrix}_i$$

and

$$\begin{bmatrix} \dot{n}_x \\ \dot{n}_y \\ \dot{n}_z \end{bmatrix}_i = -\boldsymbol{\omega_i} \times \begin{bmatrix} n_x \\ n_y \\ n_z \end{bmatrix}_i = \begin{bmatrix} (-\sin(\varphi_i)\omega_Y + \cos(\varphi_i)\,\omega_Z) - (\cos(\varphi_i)\,\omega_Y + \sin(\varphi_i)\,\omega_Z)\sin(\alpha_i) \\ -(-\sin(\varphi_i)\,\omega_Y + \cos(\varphi_i)\,\omega_Z)\sin(\beta_i) + \omega_X\sin(\alpha_i) \\ (\cos(\varphi_i)\,\omega_Y + \sin(\varphi_i)\,\omega_Z)\sin(\beta_i) - \omega_X \end{bmatrix}$$

At first order, the velocity measured in focal plane becomes:

$$\begin{bmatrix} \dot{x} \\ \dot{z} \end{bmatrix}_i \cong -f_i \begin{bmatrix} (-\sin(\varphi_i)\omega_Y + \cos(\varphi_i)\,\omega_Z) \\ -\omega_X \end{bmatrix}$$

$$\begin{bmatrix} \dot{\zeta} \\ \dot{\eta} \end{bmatrix}_i = -\frac{1}{f_i} \begin{bmatrix} \dot{x} \\ \dot{z} \end{bmatrix}_i \cong \begin{bmatrix} (-\sin(\varphi_i)\omega_Y + \cos(\varphi_i)\,\omega_Z) \\ -\omega_X \end{bmatrix}$$

The S/C angular rate can be determined considering a set of AC and AL elementary measurement and using a Least Square like approach.

From the above formula, it is clear that, in order to reconstruct properly the angular rate in Astro (AOCS) reference frame, it is necessary to know in any operating conditions from which telescope (1 or 2) the imaged star comes. In particular, the observability of the y-axis angular rate is possible thanks to the different and well separated telescope FoVs (if $\varphi_{BA} = 0$, the y-axis angular rate cannot be observed at first order).

In the nominal case (ω_P magnitude of the precession rate)

$$\begin{bmatrix} \omega_Y \\ \omega_Z \end{bmatrix} = \omega_P \begin{bmatrix} \cos(\omega_S t) \\ \sin(\omega_S t) \end{bmatrix}$$

and then

$$\dot{x}_i \cong -f_i \omega_P \cos(\omega_S t + \varphi_i)$$

$$\dot{\eta}_i \cong \omega_P \cos(\omega_S t + \varphi_i)$$

Figure 6-33 shows the 6h time evolution of the nominal AC rate $\dot{\eta}_i$ for Astro1 and Astro2. From that, it is possible to observe that a criteria to discriminate if the star comes from Astro1 or Astro2 telescope could be based on the different AC displacement of the star during the FoV transit. There are however two time instants every 6h period (at 0 and 11800s in Figure 6-33, hereafter named "critical points"), in which the AC rate is the same for both the telescopes. The Astro discrimination can be still be performed in quite easy way on ground having the benefit from more accurate star coordinates estimate, and longer observation time (the discrimination can take place just considering the last column detectors in the focal plane).
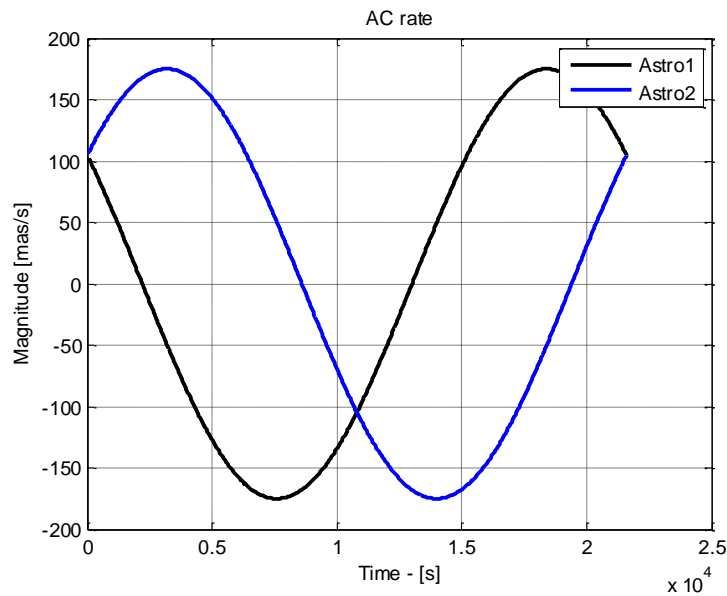
Figure 6-33: Nominal evolution of the AC rate for Astro1 and Astro2

On board, for attitude control purpose, the angular rate shall be properly know at each AOCS sampling time with a maximum allowed delay to cope with stability requirements. From that, the point has been analysed with mode details.

For t close to 0h (and similarly at 3h),

$$\dot{\eta}_1(t) \cong \omega_P co\, s\left(\frac{\varphi_{BA}}{2}\right) - \left(\omega_S\, \omega_P sin(\frac{\varphi_{BA}}{2})\right) t$$

$$\dot{\eta}_2(t) \cong \omega_P co\, s\left(\frac{\varphi_{BA}}{2}\right) + \left(\omega_S\, \omega_P sin(\frac{\varphi_{BA}}{2})\right) t$$

In order to discriminate between Astro 1 and Astro2 stars, the separation after $\frac{\Delta t}{2}$ from the critical points shall be greater than a given quantity. This quantity is related to the requested k-confidence level (e.g. under assumptions on Guassian distribution, $k=3$ sigma means for confidence level equals to 99.8%, i.e. the risk of mismatch between Astro1 and Astro2) ($\sigma_{ACpixel}$ is the accuracy in the AC star coordinate in pixel units):

$$|\dot{\eta}_1(0) - \dot{\eta}_2(0)|\, \frac{\Delta t}{2} \cong 2\left(\omega_S\, \omega_P \sin\left(\frac{\varphi_{BA}}{2}\right)\right) \frac{\Delta t}{2} > k\sigma_{AC}$$

$$\Delta t > k\, \frac{\sigma_{AC}}{\left(\omega_S\, \omega_P \sin\left(\frac{\varphi_{BA}}{2}\right)\right)} \cong 2630\, k\, \sigma_{ACpixel}$$

In the time intervals $\left(-\frac{\Delta t}{2}, \frac{\Delta t}{2}\right)$ (around 0h and 3h), the separation between Astro1 and Astro2 cannot be performed at a specified risk. The following table shows some results.

Accuracy [AC pixel]	k=2 (about 97.8% c.l.)	k=3 (about 99.8% c.l.)
$\sigma_{ACpixel} = 0.01\, ACpixel$ (1.06 mas)	52.6s	78.8s
$\sigma_{ACpixel} = 0.05\, ACpixel$ (5.3 mas)	263s	394s
$\sigma_{ACpixel} = 0.1\, ACpixel$ (10.6 mas)	526s	788s

Table 6-20: Duration of the time intervals across 0h and 3h without discrimination with the given confidence levels

In the case of $\sigma_{ACpixel} = 0.01$, $\sigma_{AC} = 1.06 mas$ and with a required discrimination capability equal to 99.8%, the time in which we are not able to meet the discrimination requirement lasts about 80s.

It is possible to withstand such an interval considering the ASTRIX 200 gyroscope measurement. Hereafter the foreseen approach:

- The gyroscope shall be put in a quite stable environment, and the overall rotation between gyro measurement reference frame and Astro1&Astro2 focal plane reference frames shall be "enough" stable during the observation (allowed misalignment drift < 1 arcsec in 200-300s).

- During nominal operation condition, it is possible to calibrate on-board the relative misalignment between the gyroscope and Astro1 and Astro2. The

accuracy should be proved with respect to the actual misalignment (misalignment shall be known with accuracy better than 1/60000).

- Around those critical points, it is possible to use the gyro rate measurement and couples of Astro 1 and Astro 2 star images with longer time distance (e.g. 1st column with last column, etc.).

The second order moment of the rate estimate $\sigma_{\dot{\eta}}$ based on Astro measurement reads:

$$\sigma_{\dot{\eta}} \cong \frac{\sqrt{2}\,\sigma_{AC}}{T_{step}}$$

where

σ_{AC} : accuracy in the AC star coordinate;

T_{step} : time separation between two consecutive measurement (1.81s).

6.5.3 AOCS Modes and Equipment

To cope with all the mission phases, the following AOCS modes have been considered. They are in line with the Gaia heritage, with the exception of a specific SRM (as proposed in Euclid).

The following modes have been considered:

- Stand-By Mode (SBM)
  - o This mode is used during the Launch Mode
  - o No sensors or actuators are active during this mode
- Sun Acquisition Mode (SAM)
  - o This mode is used during Sun Acquisition System Mode. It is the first active AOCS mode after the launch or Survival Mode. The purpose of this mode is to acquire the Sun and achieve a stable Sun-pointing attitude.
  - o Sensors used: Fine Sun Sensor, Gyroscope and a Coarse Rate Sensor
  - o Actuators used: Reaction Control Thrusters
- Inertial Guidance Mode (IGM)
  - o This mode is used to slew and maintain inertially fixed attitudes, to initiate the scan law, and as an intermediate step in transitioning from RCT modes to MPS nodes.
  - o Sensors used: Gyroscope, Star Tracker
  - o Actuators used: Reaction Control Thrusters
- Orbit Control Mode (OCM)
  - o This mode is used to perform orbit corrections and station-keeping maneuvers. A decision was made to include an accelerometer to GaiaNIR design especially for this mode (Euclid heritage).
  - o Sensors used: Gyroscope, Star Tracker, Accelerometer
  - o Actuators used: Reaction Control Thrusters
- Normal (NM)

o   This mode is the fine pointing mode and is used when science data is collected.

o   Sensors used: Astro, Gyro and Star Tracker

o   Actuators used: MPS

- Transition Mode (TSM)

o   This mode is used for the transition between RCT and MPS-based attitude control, and for convergence to dynamical conditions needed for Normal mode.

o   Sensors used: Astro, Gyro and Star Tracker

o   Actuators used: MPS

- Survival Mode (SRM)

o   This mode is used for any level 4 FDIR triggered events. It can be entered from any AOCS mode.

The allowed transitions between different modes are depicted in Figure 6-34. Transitions can be performed by telecommands or can be autonomous (e.g. FDIR).
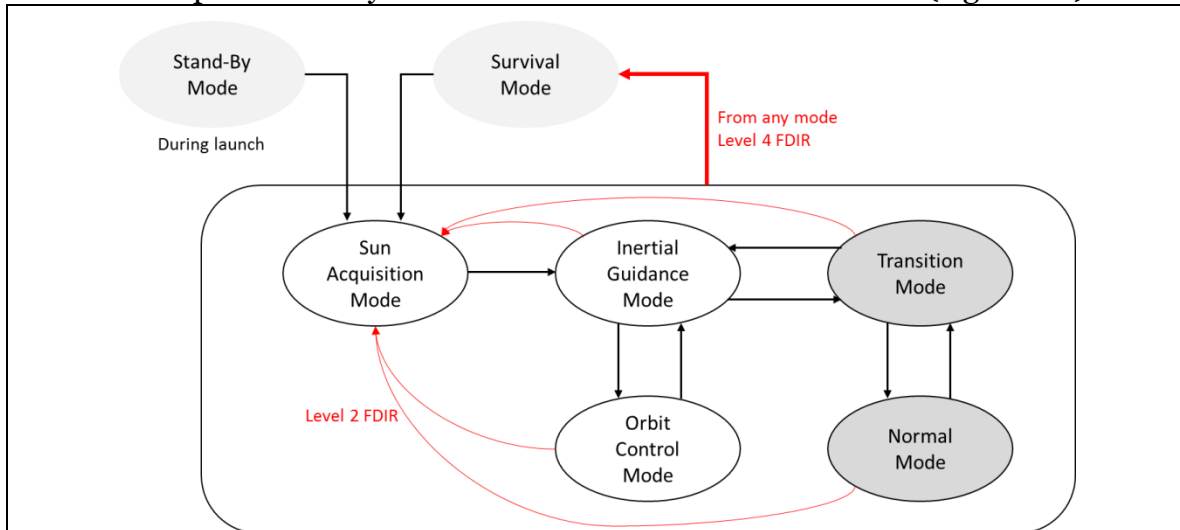
Figure 6-34: AOCS mode organisation and transitions

The correspondence between AOCS modes and System modes (REF to SYS modes) is shown in Table 6-21. Table 6-22 shows the used equipment for each AOCS mode.

AOCS mode/Mode	LM	SAM	SM	DM	OCM	STM
SBM	X					
SAM		X				
IGM				X		
OCM					X	
NM						X
TSM						X

AOCS mode/Mode	LM	SAM	SM	DM	OCM	STM
SRM			X			

Table 6-21: AOCS and System modes correspondence.

Mode	SBM	SAM	SRM	IGM	OCM	TSM	NM
Sun sensor		X	X	X(FDIR)	X(FDIR)	X(FDIR)	
Gyroscope		X	X	X	X	X	X
Astro						X	X
Star tracker				X	X	X	
Coarse rate sensor		X	X	X(FDIR)	X(FDIR)	X(FDIR)	
Accelerometer					X		
MPS					X	X	X
RCT		X	X	X	X		

Table 6-22: Equipment used during the different AOCS modes

6.5.3.1 Cold-gas mass

The assessment of external disturbance is relevant for actuator sizing and fuel budget computation.

Since the GaiaNIR S/C is very similar in terms of size, shape, material to the Gaia one, it has been considered more effective and representative to start directly from the available Gaia analysis reports and budget (the uncertainty on detailed accommodation, etc. are bigger in this phase).

The GaiaNIR RCT thrusters and the MPS will have the same maximum force as for Gaia spacecraft: 10N (RCT) and 0.5 mN (Gaia heritage) or 1mN (Euclid heritage). The same MPS thruster accommodation can be considered as well. (RCT assembly shall take into account the different SAA).

From RD[24], the required cold gas for 6 years reads 41,4 kg (Isp=60s) and 46 kg (Isp=53.9s). A scaling rule has been derived considering:

- The GaiaNIR sunshield diameter equals to 10.8m (10.2m in Gaia) (RD[24]);
- The SAA equal to 55deg (45 deg in Gaia) (RD[24]);
- The distance between the separation plane and the COM for GaiaNIR is assumed to be the same as for Gaia.

From the above assumptions, the following cold-gas mass estimate is derived:

- 60s Isp: the cold gas mass required for 6 year missions reads 43.6+0.5=44.1 kg.
- 53.9s Isp: the cold gas mass required for 6 year missions reads 48.5+0.5=49.0 kg.

6.5.3.2 List of Equipment

The equipment required by AOCS are described in Table 6-23.

Equipment	Picture
Fine Sun Sensor (FSS): **Model: TNO & Bradford** 3 units Performance: <1 deg (on-axis), <2 deg (off-axis)	
Star Tracker (STR) **Model: Leonardo AA-STR (and possible evolutions)** 2 units Bias = 8.25"(pitch/yaw), 11.1"(roll), FoV spatial error = 3.3"(pitch/yaw), 15.6"(roll) Acquisition in less than 9s, Update rate up to 10Hz, Acquisition and tracking up to 2deg/s Mass = 2.6 kg for each Power = 5.6W @ 20°C, Power bus = 60V to 110V, 20V to 52V	
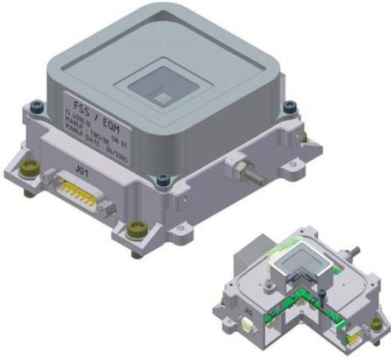
Equipment	Picture
Gyroscope (GYR) Model: Astrix 200 Airbus 1 unit internally redundant: 4 channels used nominally, 3 in case of failure. ARW = 0.1 mdeg/sqrt(hr) (1 sigma), Bias = 0.5mdeg/h (3 sigma), Scale factor stability over 1 month = 30 ppm Full performance up to +/- 5deg/s, turn-on in <3s Mass = 12.7kg Power = 7.5W per channel, hence 30W in total, power bus = 22 to 50V . This Inertial Measurement Unit features 4 independent inertial rotation sensors based on FOG technology, and mounted in skewed configuration.	
Coarse Rate Sensor (CRS) **Model: Arietis-1, Innalabs**	
Accelerometer (ACC)	The accelerometer is included in the EU of the Astrix 200 gyroscope channel.
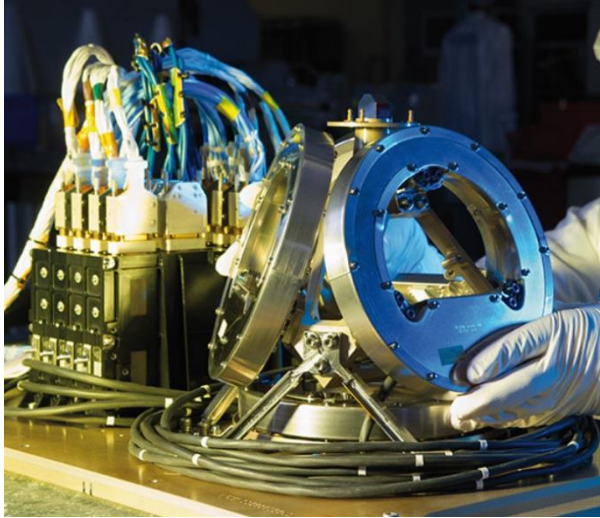
Table 6-23: AOCS equipment list

6.5.4   Options

The sub-system architecture does not change if a TDI or a de-scan mechanism with spinning Gaia-like S/C are selected. As for previous chapters, in the case of TDI solution, the requirements for the NM mode are a little bit less demanding.

6.5.5   Technology Requirements

The proposed AOCS design does not need additional technology developments. The sub-system will take benefits from natural technology evolution and already planned developments like CRS and GYRO.

6.6 SVM Power

6.6.1 Requirements and Design Drivers

The main function of the Electrical Power Subsystem (EPS) is to provide sufficient electrical energy to power all loads, during all mission phases. To perform this function the EPS has to fulfil the requirements presented in the following table.

The design of the EPS for the GaiaNIR satellite is subject to several mission specific factors. The main sizing parameters include the average and peak power demands, mission duration and flight profile. These inputs drive the selection of the energy source, energy storage and power management and distribution equipment. Since GaiaNIR is a science mission, its payload consists of equipment sensitive to temperature variations, mechanical vibrations and EMC disturbances. This has to be taken into consideration for the EPS design.

SubSystem Requirements		
Req. ID	Statement	Parent ID
POW-1	The Electrical Power System (EPS) shall provide electrical power to satisfy all power supply load requirements during all mission phases.	
POW-2	The EPS shall be sized to meet all requirements EoL, for all operation modes, under Worst Case conditions.	

6.6.2 Baseline Design

6.6.2.1 Electrical Power Subsystem Architecture

The EPS architecture provides an overview of the power system components (and their interfaces with respect to each other). These power system components include the Solar Arrays (SA) for primary power generation and a battery as secondary power source for the case that power from the SAs is unavailable during the normal mission profile. A Power Conditioning and Distribution Unit (PCDU) is implemented to autonomously condition and manage the power supply and to distribute power to the different subsystems and payload. Because GaiaNIR is a science mission, with sensitive equipment, the baseline EPS architecture will be based on a 28V regulated bus, as is schematically represented in Figure 6-35.

The choice for a 28V regulated bus results in a stable bus voltage, which will be further distributed to the different subsystem equipment and payload. This will come at the expense of some additional mass and dissipation compared to an unregulated EPS architecture, because of the need for additional Battery Charge and Discharge Regulators (BCDR).

Another EPS architecture related trade off that needs to be considered has to do with the Solar Array Regulator (SAR) converter type, which can be either a Maximum Power Point Tracker (MPPT) or a Sequential Switching Shunt Regulator (S3R). The first is heavier and less efficient, but able to extract all the available power from the solar arrays under a large range of conditions (BoL, EoL, Temperature, etc.). The latter is simpler, lighter, cheaper and more efficient, but is very rigid in the way it extracts power. Under

varying conditions, the S3R is unable to extract all available power, which negatively influences the SA sizing. Therefore, the S3R provides an advantage over MPPT in combination with a regulated bus in an environment with a stable incoming solar flux. Based on the EPS equipment sizing results for both converter types (Section 6.6.2.3), the S3R is considered the most suitable SAR converter for GaiaNIR.
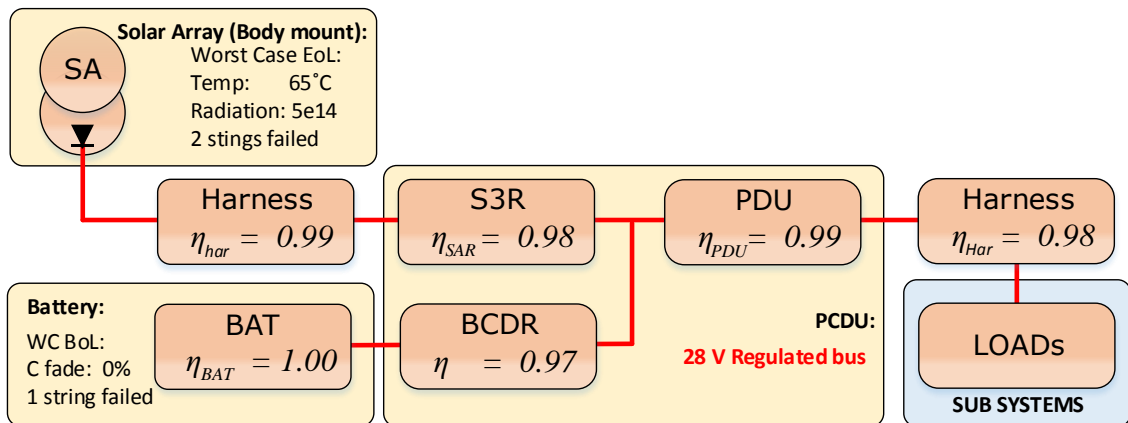
Figure 6-35: Electrical Power System Architecture

6.6.2.2 Power and Energy Budgets

This section presents the power budget and the resulting energy budget that are used as input for the sizing of the power system components. The power budget for GaiaNIR is presented in Table 6-24. This table provides an overview of the on power P_{on}, standby power P_{stby} and duty cycles of all system equipment, during each mission phase. Based on these data the average power consumption P_{avg} is calculated.

A simple power and efficiency flowchart as presented in Figure 6-35 is used to calculate the losses related to the conversion and distribution of power from the source to the loads. The total power loss from source to load is considered 6%, whether the power is coming from the Solar Arrays or the Battery. The battery will normally only be used Beginning of Live during the Launch (LM) and Sun Acquisition (SAM) mission phases, when the power from the Solar Arrays is still unavailable. For all other mission phases, power from the solar arrays is utilized. Therefore, battery recharging is not considered in the power budget.

A power system margin of 20% is applied on top of the average calculated power consumption, including the total conversion losses.

Table 6-24 provides an additional energy budget that is used as input for sizing the batteries. The energy budget presents the required energy from the batteries when the solar arrays are unable to provide power. This is during the Launch (LM) and Sun Acquisition (SAM) mission modes, when the Solar Arrays are not yet deployed and their pointing angle to the sun is uncertain. The total time until sun acquisition and deployment can take up to 192 minutes.

Power Budget: GAIA_nir Power (W)	Qty	Pon	Pstby	Launch (LM) P_avg	Duty	(SAM) P_avg	Duty	Safe (SM) P_avg	Duty	(DM) P_avg	Duty	(OCM) P_avg	Duty	Transmitting (STM) P_avg	Duty
AOGNC				0.0		40.1		35.6		40.1		40.1		40.1	
Cold Rate Sensor (CRS) (x2)	1	5	0	0.0	-1%	5.0	100%	5.0	100%	5.0	100%	5.0	100%	5.0	100%
Gyro_Astrix_200	1	30	0	0.0	-1%	30.0	100%	30.0	100%	30.0	100%	30.0	100%	30.0	100%
Star Tracker (STR_AASTR) (x2)	1	4.5	0	0.0	-1%	4.5	100%	0.0	-1%	4.5	100%	4.5	100%	4.5	100%
Sun Sensor (SUN_BradTNO_FSS)	3	0.2	0	0.0	-1%	0.6	100%	0.6	100%	0.6	100%	0.6	100%	0.6	100%
COMS				0.0		11.7		11.7		11.7		393.6		393.6	
X_XPND (x2)	1	27.34	10	0.0	-1%	11.7	10%	11.7	10%	11.7	10%	27.3	100%	27.3	100%
PAA_DCDC	1	33	0	0.0	-1%	0.0	-1%	0.0	-1%	0.0	-1%	33.0	100%	33.0	100%
PAA_BFN_MODULE (x8)	8	41.7	0	0.0	-1%	0.0	-1%	0.0	-1%	0.0	-1%	333.2	100%	333.2	100%
Data Handling (DHS)				29.0		29.0		29.0		29.0		29.0		79.0	
OSCAR (OBC)	1	15	10.0	15.0	100%	15.0	100%	15.0	100%	15.0	100%	15.0	100%	15.0	100%
Solid State Maa Memory (SSMM)	1	10	10.0	0.0	-1%	0.0	-1%	0.0	-1%	0.0	-1%	0.0	-1%	10.0	100%
Data Processing Unit (DPU)	1	40	24.0	0.0	-1%	0.0	-1%	0.0	-1%	0.0	-1%	0.0	-1%	40.0	100%
Generic Remote Terminal (RTU)	1	14.0	14.0	14.0	100%	14.0	100%	14.0	100%	14.0	100%	14.0	100%	14.0	100%
CPROP				0.0		15.2		15.2		15.2		79.5		44.6	
Biprop_HP_Trans	1	0.3	0.3	0.0	-1%	0.3	5%	0.3	5%	0.3	5%	0.3	70%	0.0	-1%
Biprop_LP_Trans (x2)	1	0.8	0	0.0	-1%	0.0	5%	0.0	5%	0.0	5%	0.6	70%	0.0	-1%
Biprop_LV (x4)	2	30	0	0.0	-1%	3.0	5%	3.0	5%	3.0	5%	42.0	70%	0.0	-1%
Biprop_PR	1	15	5	0.0	-1%	5.5	5%	5.5	5%	5.5	5%	12.0	70%	0.0	-1%
Biprop_Thruster (x16)	8	3.5	0	0.0	-1%	1.4	5%	1.4	5%	1.4	5%	19.6	70%	0.0	-1%
Cold_Flow_Sensor (x12)	6	0.15	0	0.0	-1%	0.0	-1%	0.0	-1%	0.0	-1%	0.0	-1%	0.9	100%
Cold_HPLV (x2)	1	29	0	0.0	-1%	0.0	-1%	0.0	-1%	0.0	-1%	0.0	-1%	0.3	1%
Cold_HP_T (x2)	1	0.3	0	0.0	-1%	0.0	-1%	0.0	-1%	0.0	-1%	0.0	-1%	0.3	100%
Cold_LPLV (x2)	1	29	0	0.0	-1%	0.0	-1%	0.0	-1%	0.0	-1%	0.0	-1%	0.3	1%
Cold_LP_T (x2)	1	0.8	0	0.0	-1%	0.0	-1%	0.0	-1%	0.0	-1%	0.0	-1%	0.8	100%
Cold_PR	1	15	5	0.0	-1%	5.0	0%	5.0	0%	5.0	0%	5.0	0%	15.0	100%
Cold_Thruster (x12)	6	4.5	0	0.0	-1%	0.0	-1%	0.0	-1%	0.0	-1%	0.0	-1%	27.0	100%
MECH				0.0		0.0		0.0		0.0		0.0		0.0	
Deployable Sunshield (Dep_SSH)	1	0	0	0.0	0%	0.0	-1%	0.0	-1%	0.0	0%	0.0	0%	0.0	0%
THES				378.8		306.8		306.8		231.1		0.0		0.0	
Heater lines (HTR)	1	378.8	0	378.8	100%	306.8	81%	306.8	81%	231.1	61%	0.0	-1%	0.0	-1%
PAYLOAD (PLM)				124.9		125.4		124.9		438.1		187.2		227.4	
Heater (HTR_PLM) (x2)	1	438.1	0	124.9	29%	124.9	29%	124.9	29%	438.1	100%	0.9	0%	0.0	-1%
Instrument Control Unit (ICU)	1	40.0	15	0.0	-1%	0.0	-1%	0.0	-1%	0.0	-1%	0.0	-1%	40.0	100%
DeScan_mech	1	0.02	0	0.0	-1%	0.0	-1%	0.0	-1%	0.0	-1%	0.0	-1%	0.0	100%
Astro Focal Plane (AFP)	1	156.37	0	0.0	-1%	0.0	-1%	0.0	-1%	0.0	-1%	156.4	100%	156.4	100%
Detector (x60)	60	0.3	0	0.0	-1%	0.0	-1%	0.0	-1%	0.0	-1%	18.0	100%	18.0	100%
FEE (x60)	60	0.2	0	0.0	-1%	0.0	-1%	0.0	-1%	0.0	-1%	12.0	100%	12.0	100%
M2 Refocussing Mech. (M2_RFM)	1	1	0	0.0	-1%	0.5	50%	0.0	-1%	0.0	-1%	0.0	-1%	1.0	100%
PWR				30.0		30.0		30.0		30.0		30.0		30.0	
PCDU	1	30	0	30.0	100%	30.0	100%	30.0	100%	30.0	100%	30.0	100%	30.0	100%
PCDU															
Total consumption P(W)		1393.9		562.7		558.3		553.3		795.3		759.4		814.7	
Losses (SAR/BCDR, PDU, Harness)		6%		34		33		33		48		46		49	
TOTAL S/C				596		592		586		843		805		864	
Power Budget incl. Margin P(W)		20%		716		710		704		1012		966		1036	
Energy Budgett: Energy (Wh)															
Duration (min):				42		150									
Battery Energy Requirement (Wh)				501.0		1775									

Table 6-24: Power and Energy Budget

6.6.2.3 Power System Sizing

The Electrical Power Subsystem equipment consists of Solar Arrays, a battery and a PCDU, as were schematically presented in Figure 6-35. The sizing of these components is discussed in the next subsections and a power equipment overview, including a final mass budget is presented afterwards.

6.6.2.3.1 Battery Sizing

The battery is used as secondary power supply on board of the spacecraft. It supplies the power when the power from the SAs is unavailable, or to provide additional power during peak demand. For GaiaNIR the Launch (LM) and Sun Acquisition (SAM) operation modes are identified as design drivers for the battery sizing. These two consecutive operation modes occur only at the beginning of the mission. The required energy during these modes can be determined from the energy budget as presented in Table 6-24. The sizing of the battery is based on BoL Worst-Case conditions, where the following assumptions do apply:

- Maximum DoD for occasional occurrences ≤ 70%
- One battery string failure.
- BoL: 0% capacity fade and 100% SoC at the beginning of the mission.
- 30% additional construction mass on top of the total cell mass.

For battery sizing a model that is based on steady-state calculations is applied. The energy requirements from the energy budget are used as input for the model.

The battery sizing inputs and the calculated performance results have been summarised in Table 6-25. All efficiency drops are already taken into consideration in the power budget of Figure 6-35.The use of two different battery cell types have been compared. The first is the Saft VES 16, which has been widely used in the space industry. The second is the ABSL 18650NL. The ABSL cell has a higher energy density compared to the Saft cell, however it also has a higher capacity fade over time. The calculation results show that the ABSL 18650NL provides the lightest solution and is therefore used as baseline in the current design. The resulting battery consists of 26 strings of 8 cells in parallel, having a capacity of 144 Ah, reaching a Worst-Case DoD of 67% until Sun acquisition is achieved and having a mass of 29.3 kg. The resulting battery has approximately double the mass of the 72 Ah, 14.8 kg battery used on Gaia. The difference in capacity and mass are primarily caused by the higher power consumption of the Thermal Subsystem equipment during Launch and Sun Acquisition modes.

Battery sizing: GAIA nir		
Requirement input:	**LM+SAM**	**LM+SAM**
Energy (Wh)	2276.3	2276.3
Battery Selection:		
Type:	**VES16**	**18650 NL**
Vnom (V)	3.6	3.6
V_EoC (V)	4.1	4.2
Capacity (Ah)	4.5	2.4
Ebat(Wh/cell)	16	7.2
Operating Temp. (gradC)	-20 to +60	-20 to +60
Weight (kg/cell)	0.16	0.05
Maximum discharge (in C	2	2
Battery sizing input:		
Battery efficiency (%)	100	100
BDR efficieny (%)	100	100
Capacity fade EOL (%)	0	0
WC strings down	1	1
Ns	8	8
Np	28	60
Battery Performance:		
Vbat (V)	28.8	28.8
Vbat (V) EoC	32.8	33.6
Ibat (A) (max)	252.0	288.0
Ebat (Wh)	3584.0	3456.0
Ebat (Wh) WC	3456.0	3398.4
Capacity (Ah)	126.0	144.0
DOD EOL WC	**66%**	**67%**
Battery:		
height (mm)		143
length (mm)		173
width (mm)		648
Weight (kg)	**45.14**	**29.33**

Table 6-25: Battery sizing results

6.6.2.3.2   *Solar Array Sizing*

The solar arrays are sized for both the case that MPPT converters and the case that S3R converters are used for solar array regulation. The results of both calculations are used as trade-off for selecting the most suitable SAR converter type.

The sizing of the solar arrays is based on a worst case scenario, where the following assumptions do apply:

- A distance to the Sun of 1.01 AU.
- A Solar Aspect Angle (SAA) of 53°
- A radiation impact of 5E14.
- 2 strings of SA cells failed.
- A SA diode voltage drop of 0.8V.
- A SA to spacecraft harness efficiency of 99%.

- A SAR efficiency of 94% in case of a MPPT converter.
- A SAR efficiency of 97% in case of a S3R converter.

The sizing is based on a model that takes into account all the assumptions stated before, as well as the cells and panels electrical and thermal properties, in order to derive the relevant operating temperatures and efficiencies. The model is based on steady-state calculations, which is suitable for the purpose of this study.

The driving mode for the solar array sizing is the Science and Transmitting mode (STM). During this mode the average power requirement is 1036 W, as can be derived from Table 6-24.

The 30% efficient GaAs triple junction cell from Azur Space (Type: TJ GaAs 3G30C) is currently the most efficient solar cell with flight heritage and is therefore selected as baseline for this study. The solar array cells will be body mounted to the sun facing side of the spacecraft, with a packing factor $k_{packing}$ of 85%. If necessary, additional solar cells can be mounted on the space craft heat shield. The total mass m_{SA} of the SA including mounting structure is approximated by taking 2 times the mass of the bare cells alone.

The sizing and modelling results are presented in Table 6-26, for both the cases that a MPPT converter and a S3R converter is used, including their performance Beginning of Life (BoL) and during the Worst Case (WC) End of Life (EoL) conditions. The resulting Solar Array VI-characteristic clearly demonstrates the difference between BoL and the WC EoL scenario. Because the voltage is fixed when using an S3R (dashed line at 28V), it is clear that not all power can be extracted from the panels during WC and therefore their area is increased accordingly. The result is that the total SA panel area and weight is smaller for the MPPT option. However, this advantage is mitigated due to the increased mass of the PCDU when applying the MPPT option. Therefore, the S3R option is selected as baseline for this study.

The Solar Array area and mass of the Gaia space craft is also provided as reference in the presented table. For Gaia the power requirement was 2300W during normal operation, which is roughly double the required power of GaiaNIR during STM. Further, the Gaia EPS employed MPPT SA regulators, reducing the overall size of the SA compared to an EPS based on S3R SA regulators. To conclude: GaiaNIR SA is roughly 35% smaller in size and mass compared to the Gaia SA.

Solar Array Sizing: GAIA nir				
Requirement input:				
Power (W)	**1036**	Science and Transmitting Mode (STM)		
Environmental cond.:	**BOL MPPT**	**BOL S3R**	**EOL MPPT**	**EOL S3R**
Radiation	0	0	5.00E+14	5.00E+14
Distance (AU)	1.01	1.01	1.01	1.01
Solar Aspect Angle (SAA)	53	53	53	53
Flux Correction Factor	0.58	0.58	0.58	0.58
Cell information:			**BoL**	**EoL (RAD)**
Type:	TJ GaAs 3G30C	Cell Voc (V)	2.70	2.56
Area (m2)	0.003018	dVoc/ΔT (V/°C)	-0.0062	-0.0066
Packing factor	0.85	Cell Isc (A)	0.52	0.51
Specific weight (kg/m2)	0.86	dIsc/ΔT (A/°C)	0.0004	0.0004
Qualification flux (W/m²)	1367	Cell Vmp (V)	2.41	2.29
cell absorbtivity α	0.915	dVmp/ΔT (V/°C)	-0.0067	-0.0071
Cell front ε	0.76	Cell Imp (A)	0.50	0.50
Cell back ε (effective)	0.03	dImp/ΔT (A/°C)	0.0002	0.0002
SA sizing input:	**MPPT**	**S3R**		
Bus voltage (V)	28	28		
SAR efficiency (%)	97	100	(Included in Powerbudget)	
Voltage drop SA diode (V)	0.8	0.8	(Buck MPPT)	
SA harness efficieny (%)	99	99		
WC string failure	2	2	**Check MPPT:**	**Check S3R:**
Ns	20	18	**OK**	**OK**
Np	100	132	**OK**	**OK**
SA Performance:	**BOL MPPT**	**BOL S3R**	**WC MPPT**	**WC S3R**
Solar flux (W/m²)	797.3	797.3	797.3	797.3
SA Voc (V)	49.4	43.7	46.0	40.9
SA Isc (A)	31.0	41.1	30.0	40.0
SA Vmp (V)	42.1	37.0	39.0	34.5
SA Imp (A)	29.8	39.5	29.1	38.6
efficiency (%)	26.4	20.1	23.8	19.6
SA Temp. (°C)	57.8	64.6	60.6	65.1
SA Power to bus (W)	1217.9	1135.9	**1100.6**	**1111.8**
SA:	**MPPT:**	**S3R:**	**Gaia reference:**	
Area bare cells (m²)	6.0	7.2		
Weight bare cells (kg)	5.2	6.2		
Area SA (m²)	**7.1**	**8.4**	**12.6**	
Weight SA (kg)	**10.4**	**12.4**	**18.7**	

Solar arrays VI-char. BOL and EOL
— MPPT Converter
— S3R Converter
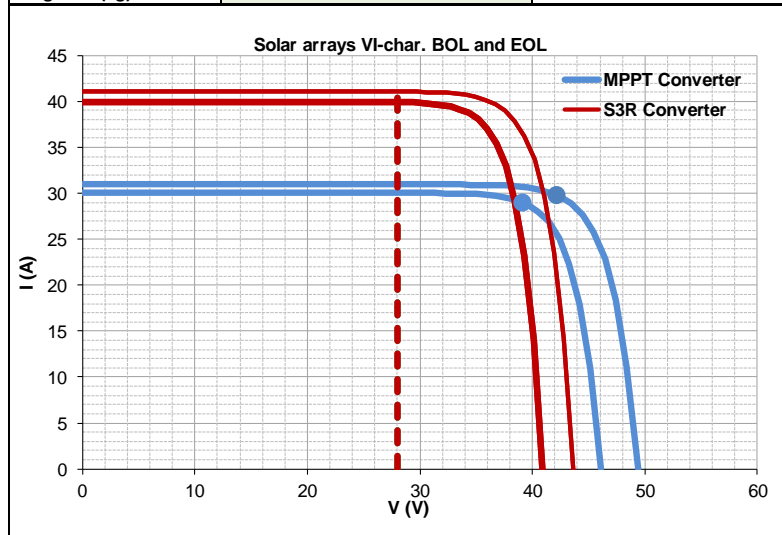
Table 6-26: Solar Array sizing results

6.6.2.3.3   PCDU Sizing

The Power Conditioning and Distribution Unit (PCDU) is responsible for conditioning the voltage and currents according pre-determined specifications and to distribute it to the payloads from the different subsystems.

The PCDU is sized based on the Modular Medium Power Unit (MMPU) from Terma, using Off-The-Shelf (OTS) modular boards that have flight heritage. These modular PCDUs can contain up to 21 modules.

An overview of the required modules and the resulting mass estimation is presented in Table 6-27. Other suppliers' PCDUs could also be applicable, but it should be noted that mass can vary greatly from one manufacturer to another.

Option MPPT:

Function:	Capbility	Mass [kg]	Modules	Total Mass [kg]
(CM) Command and Monitoring (MIL1553)		0.458	2	0.92
(SAR) MPPT module	250 W	0.500	6	3.00
(PDU) Power Distribution module	16 LCL	0.570	2	1.14
(BCDR) Battery Charge Discharge	250W	0.550	4	2.20
(HPD) Heater Power Distribution	400W	0.477	2	0.95
(PPD) Propulsion Power Distribution	350W	0.530	1	0.53
(PF) Pyro Firing	25	0.476	1	0.48
(BM) Backplane module		0.500	1	0.50
		Mass of all modules		9.72
		Total mass of PCDU		**14.85**

Option S3R:

Function:	Capbility	Mass [kg]	Modules	Total Mass [kg]
(CM) Command and Monitoring (MIL1553)		0.458	2	0.92
(S3R) S3R module	1000 W	0.480	2	0.96
(PDU) Power Distribution module	16 LCL	0.570	2	1.14
(BCDR) Battery Charge Discharge	250W	0.550	4	2.20
(HPD) Heater Power Distribution	400W	0.477	2	0.95
(PPD) Propulsion Power Distribution	350W	0.530	1	0.53
(PF) Pyro Firing	25	0.476	1	0.48
(BM) Backplane module		0.500	1	0.50
		Mass of all modules		7.68
		Total mass of PCDU		**11.73**

Table 6-27: PCDU Sizing results

For the GaiaNIR study the PCDU with S3R SARs is selected as baseline, this results in the least complex PCDU with the lowest mass. For the Gaia mission A PCDU with MPPT based SAR, a power capability of 2300W and a mass of 26.2 kg was developed.

6.6.3   List of Equipment

A complete list of the necessary power system components is presented in Table 6-28, together with their redundancy concept, maturity level, mass and mass margin. A mass margin of 10% has been applied to all equipment.

List of Components: S3R option			MASS [kg]				
Unit	Equipment Name	Qty:	Unit mass excl. margin	Redundancy:	Maturity Level:	Margin [%]	Total Mass incl. margin
1	PCDU	1	11.7	No	Modified	10	12.90
2	Battery	1	29.3	1 string fail	Modified	10	32.26
3	Solar Array (Body mount)	1	12.4	2 strings fail	Modified	10	13.63
	Subsystem total:	3	53.45				58.79

Table 6-28: Power System Final Mass Budget

6.6.4 Options

6.6.4.1 Solar cells with improved performance

The 30% efficient GaAs triple junction cell from Azur Space (Type: TJ GaAs 3G30C) is currently the most efficient solar cell with flight heritage and is therefore used as baseline for this study. However, the TJ GaAs 3G32C solar cell, which has an efficiency of 32% is currently under development and is expected to have flight heritage as of 2020. By applying this newly developed solar cell, the total mass and area required for the Solar Array can be reduced by approximately 5%.

6.6.4.2 MPPT Solar Array regulator

Selecting MPPT based Solar Array Regulators for the PCDU, instead of the S3R based SAR will result in an increase of PCDU mass and a decrease of SA mass. The resulting EPS mass will increase by approximately 1.2 kg.

For the Gaia mission MPPT based SARs were selected because their possible ability to reduce conducted emission to the Solar Arrays and therefore radiated emission from the Solar Arrays.

6.7 SVM Data Handling

6.7.1 Design Drivers

6.7.1.1 Expected Star Count

One of the main design drivers for the needed data processing on-board is the star count expected during the mission. Full-sky star-count estimates in the infrared are highly uncertain, possibly up to a factor of two (or more). The estimations used in this study can be summarised as follow:

- 3.5 billion stars in total with |b| < 10° (so distributed over ~7000 deg² in the galactic plane)
- 1.5 billion stars in total with |b| > 10° (so distributed over the remaining ~34000 deg² on the sky).

Where 'b' is the galactic latitude (altitude above the galactic plane, in which stars are concentrated on the sky), running from -90 deg at the south galactic pole to +90 deg at the north galactic pole. These estimates represent our current best knowledge and are not conservative and do not carry margin: the real counts may possibly be higher, possibly by up to a factor 2.

Following these estimations, the average densities are then:

- In the galactic plane region: 0.5 million stars per deg² (over the ~7000 deg²)
- Towards the galactic polar caps: 0.05 million stars per deg² (over ~34000 deg²)
- The density ratio is ~10.

The AC FoV for the GaiaNIR H2RG focal plane is 0.42 deg (7 detectors with 2048 pixels of 18 micron with 35.2 m focal length). When scanning at 60 arcsec/s in the AL direction, one 360-deg scan takes 6 hours so there are 4 scans of in total 4 x 360 = 1440 deg length per day. With two telescopes superimposing the light into the common focal plane, this means that GaiaNIR scans $2 \times 605 = 1210$ deg² per day (both telescopes combined).

With an assumed constant density of $2 \times 0.5E6 = 1E6$ stars/deg² (which is representative of the galactic plane region observed by both telescopes at the same time), this means 6E8 objects per day (and 4E9 objects per week). This would represent the worst case situation in which GaiaNIR scans along the galactic plane for 7 days in a row. Note that such situations do naturally appear a few times per year as a result of the scanning law. Note that the only uncertainty in this calculation is in the star counts.

For clarification, the aforementioned figures refer to the worst case in which the scan is along the galactic plane all the time, during one week.

A more representative, typical 6-hour scan of the sky (covering 360 deg AL) encounters:

- 2 x 20=40 deg AL of Milky-Way conditions when crossing the galactic plane
- 360 − 2 x 20 = 320 deg AL of galactic-cap conditions for the rest of the time.

This typical case gives, for the two telescopes combined, 1.2E8 objects per day (and 8.5E8 objects per week). Each object will generate 16 images (8 detector columns, two images on each detector; see 5.4.1.1).

Gaia is commonly referred to as the billion star surveyor. This, however, only reflects the ESA marketing term and links to the mission requirement that the Gaia Catalogue should contain at least 1 billion objects. Pre-launch expectations, based on ground-based sky models only calibrated with space-based data using a few pencil beams, suggested ~1.2 billion objects could be observed with a limiting magnitude of G = 20.0 mag. The uncertainty on this number was deemed to be around 20%. After launch, the faint limit of Gaia was lowered from 20.0 to 20.7 mag, leading to more stars. In Gaia DR2, more than 1.5 billion objects are included and around 2 billion objects can be expected in the final, Gaia DR4 Catalogue. With an estimated star count of 3.5 + 1.5 = 5 billion stars, in this respect GaiaNIR would thus represent a factor 2.5 improvement compared to Gaia.

6.7.1.2   On-Board Data Storage

Given the star count described above, the Data Handling Subsystem (DHS) is required to store four days of data without any downlink pass. On the typical case:

- 0.12 billion objects per day
- 16 images per object
- 99% of the objects can be binned (16 bits/pixel * 5 pixels/object = 80 bits/object/image)
- 1% of the objects require full storage (16 bits/pixel * (5*26) pixels/object = 2080 bits/object/image).

The required typical data storage capacity per day without margin is 192 Gbit.

To be noted that the final binned or windowed star location information, denoted above as objects, is formatted in standard int-16, which binary size is 16 bits. Considering:

- Compression algorithm of 2:1 ratio (as Gaia)
- File system overhead of 5% (typical)
- Error correcting code overhead 20% (worst case)

The total on-board generated data for a typical day is 120.26 Gbit. To size the mass memory, though, the no-contact and free-space requirements need to be taken into consideration:

- 4 days no contact downlink
- 50% free space (general science requirement).

The minimum required data storage for a typical day is then **967.68 Gbit**.

Instead, if the system needs to be dimensioned for the data generation worst case (galactic-plane pass during a week), it is expected to see 0.6 billion objects per day (instead of 0.12 billion). With the same characteristics described above, the resulting required data storage for worst-case scenario is 4.94 Tbit. To be noted that this figure is for information only, as represents a worst-case of the already worst-case of no ground contact in 4 days.

6.7.1.3   On-Board Data Processing Algorithm

Due to the data volume generation and the downlink X-band limitations there is the need to process part of the data on-board:

- 60 detectors
- 2048x2048 pixels per detector
- 12 bits per pixel (resolution selected on the SIDECAR converters)
- 2 samples every 1.81 seconds.

This results is a data generation rate of 3.34 Gbits/s, not realistic to download it on real time (the ground contact rates are usually in the order of few dozens of Megabits per second in X-band). Therefore, and following Gaia's example, it is proposed to execute a preliminary star detection algorithm on-board and download only binned stars data and large stars windows. The algorithm consists on the following steps:

- CDS
- Reference pixel correction
- Lateral pixel correction
- Saturated pixel flagging
- Star detection
- Binning/windowing.

The total calculated complexity of such algorithm is 1160 million of operations per detector.

6.7.2   Assumptions and Trade-Offs

6.7.2.1   Assumptions

Assumptions	
1	Fully recurrent platform (computer, mass memory and S/C house-keeping acquisition).
2	Power dissipation in the PLM needs to be as low as possible to facilitate thermal control close to the detectors.
3	The on-board data processing needs to be based on existing EEE components.
4	Baseline design including TRL 5 units reachable in 5 years timeframe.

6.7.2.2   On-Board Data Processing Trade-off

Starting from the approach followed in Gaia and trying to make use of the same solution (but using the new Maxwell SCS750 board), it can be easily realised that the nature of the processing algorithm is so radically different that makes the approach not viable:

- One Maxwell processing board can perform 1700 MIPs maximum
- One Maxwell processing board dissipates 30 W
- Total processing algorithm complexity per detector: 1160 million of operations.

The processing unit would need to be composed of 60 Maxwell SCS750 boards, one per detector, consuming 1.8 kW total. This value considers only the boards without any coordination device (a best-case estimate).

Synthesising the analysis to that simple calculation, the immediate implication is that the approach is forced to change: more operations need to be done in parallel, not sequentially as the Maxwell board does. Looking at the currently available programmable devices, FPGAs seem the most feasible solution, and the Xilinx Zynq

Ultrascale+ the most powerful component in the space portfolio of all the FPGA vendors. For this reason, the data processing unit is based on this device.

To be noted that the possibility to design a new ASIC with the necessary functions has been taken into account. As the characteristics of the processing algorithm are so specific using a programmable device (as FPGAs) would be recommended . A dedicated technology development for an new ASIC would be specifically required for GaiaNIR with a development time of around 5 years.

6.7.3   Baseline Design

6.7.3.1   Overview

The Command and Data Handling subsystem is composed of:

- A standard computer from Airbus DS capable of receiving telecommands, forwarding telemetry to ground, distributing commands within the S/C via CAN bus, distribute the on-board time and issue reconfiguration actions.

- A standard modular remote terminal unit from Airbus DS capable of acquiring housekeeping telemetry, issue high-power commands and control the AOCS subsystem.

- A mass memory unit able to store in a file based system and ECC protected the necessary payload data.

- An instrument control unit located in the PLM able to control and collect the data of sixty H2RG detectors, and forward it to the SVM.

- A data processing unit able to apply the required algorithm to the incoming burst, and forward to the mass memory the packets containing detected stars that need to be downloaded, discarding background information.

In Figure 6-36 and Figure 6-37 diagrams of the general architecture have been depicted.
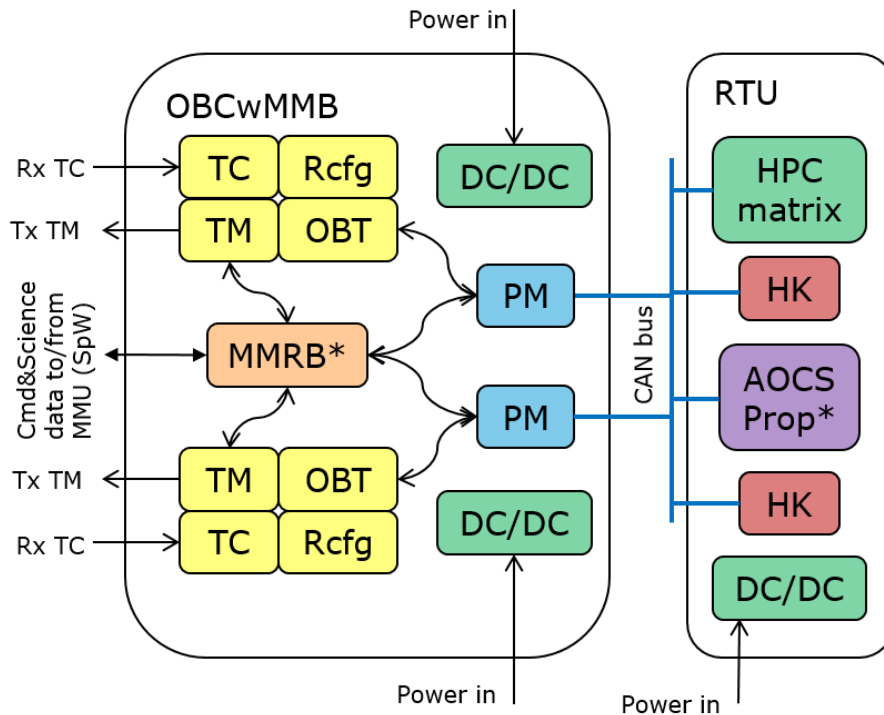
Figure 6-36: On-board computer and remote terminal unit function diagram
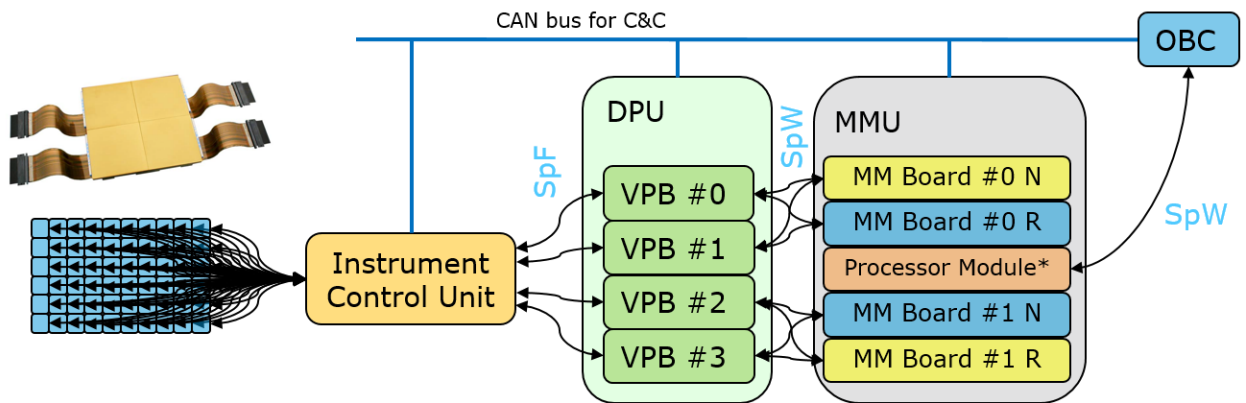
Figure 6-37: Data Processing architecture; to be highlighted that the ICU is placed in the PLM and the DPU, MMU and OBC in the SVM

6.7.3.2 On-Board Computer (OBC)

For the GaiaNIR mission, the OSCAR on-board computer from Airbus Defence&Space has been selected as it complies with the GaiaNIR requirements. To be noted that this is a standard product that is likely to be improved in terms of features, mass, power consumption and size in the next 5 years.

This unit has been designed with the aim of providing an avionic product suitable for a wide range of missions. It has been selected in 15 LEO missions so far, and this particular configuration, explained here, has been developed on the frame of SEOSAT

project. Airbus D&S offers the same performances for different class quality programs, with adapted EEE components selection and manufacturing quality level.

This OBC, usually referred as Command and Data Management Unit (CDMU) due to its enhanced capabilities, is composed of two identical boards in selectable hot or cold redundancy with interlink between CPUs, as it is depicted in Figure 6-38.
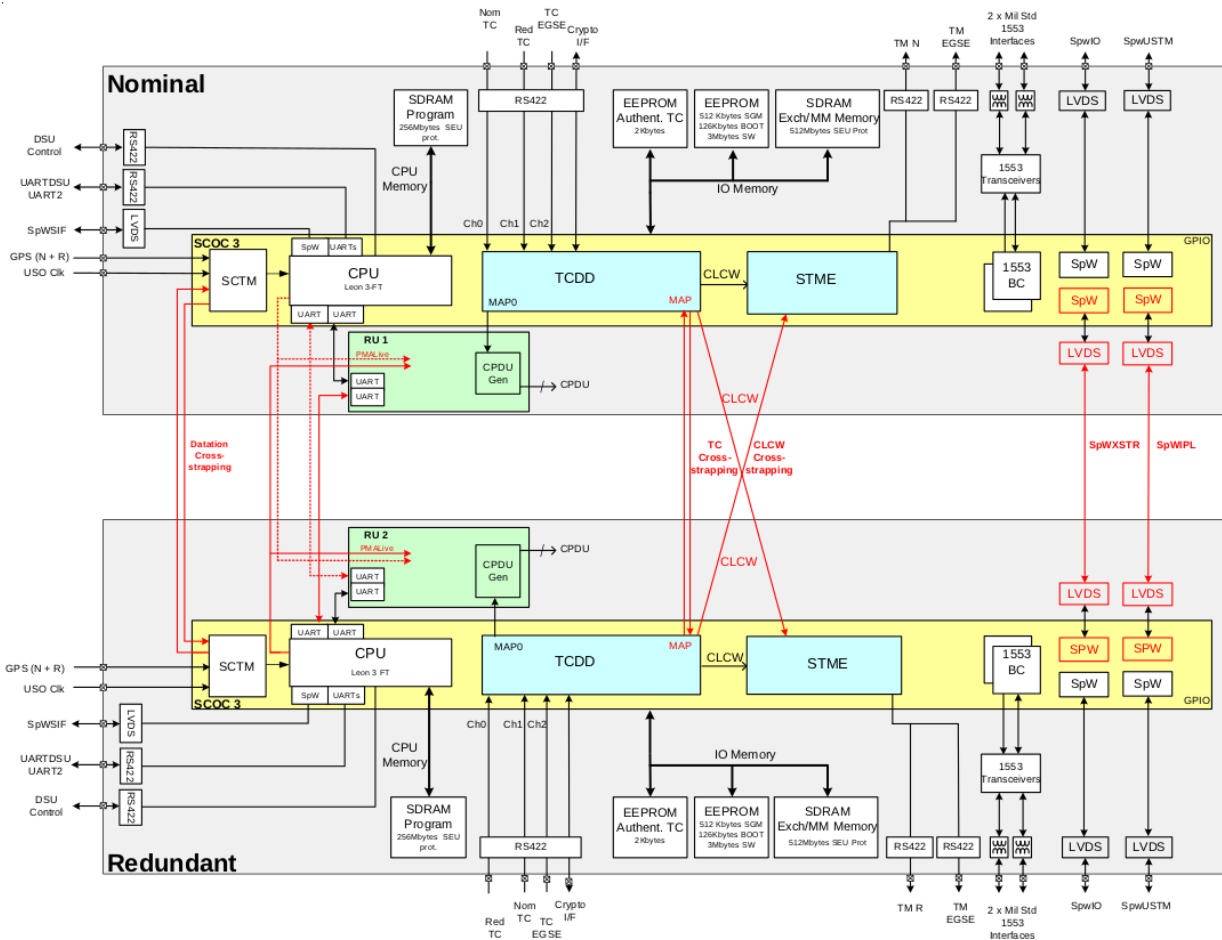
Figure 6-38: OBC Redundancy Scheme and Architecture

The core of the unit is a complex System on a Chip ASIC (SCOC3) gathering all the main digital functions of the OBC and Data Management system. Its small size allows it to integrate the whole computer on one board, and its implementation on 180 nm rad-hard technology provides the necessary reliability. At architectural level, it integrates in a single chip a LEON3 processor with caches, Memory Management Unit and Floating Point Unit. The Telemetry/Telecommand logic and all the standard peripherals controllers (SpaceWire, CAN bus, Mil-1553, UART) are also integrated along with the processor in the same die. The performances are up to 68 MIPS@80MHz with 256 MiBytes of dedicated CPU memory, which is estimated to have enough performance to cope with any standard ESA science mission. The reconfiguration function and 2.5 GiBytes SDRAM On-Board Memory are hosted in the same board.

Cross-strap links are implemented to connect the processor of each board to the TC Decoders, the Reconfigurations Units, the Safeguard Memories and the Mass Memories of both boards.

The available interfaces include:

- 7 SpaceWire links: 4 are allocated internally to TM/TC channels and for cross-strapping, the others are available for the platform usage.
- CAN or Mil-Std-1553 busses as S/C bus
- UARTs.

Figure 6-39: OSCAR Computer by Airbus D&S

6.7.3.3 Remote Terminal Unit (RTU)

To complement the interfaces of the OBC, the Modular RTU from CRISA (Airbus Defence and Space España) has been selected:

- Propulsion submodule is able to deal with 4-8 thrusters, 4-8 heater lines, separation status acquisition, etc.
- Housekeeping module is able to acquire 300 thermistor, 16 bi-level signals, 30 analogue interfaces, 4 UARTs, etc.
- AOCS submodule can interact with the Sun sensor and the reaction wheels (pulse, speed & voltages).
- High-power command matrix is programmable to have up to 40 HPCs with different level and duration characteristics.
- Several digital interfaces as CAN bus, MIL-1553-bus and SPI are also available.

To be noted also on this unit that its modularity and standard interfaces makes its susceptible to be improved in the following years is terms of features, mass, power consumption and size, but it already fulfils the requirements for GaiaNIR. Furthermore, if any of the GaiaNIR requirements change, its modularity gives it the flexibility to include new or different board modules to cope with the situation.

6.7.3.4   Mass Memory Unit (MMU)

To cope with the high data storage requirement (1 Tbit approximately) an external mass memory has been chosen to be part of the baseline. Given the large amount of data to be stored and the high data throughput needed, and even if the solid state mass memory technology evolves as fast as it has been doing during the past 20 years, it is not likely that the MMU equipment can be merged with that of the OBC. A separate MMU unit has therefore assumed to be necessary.

The selected equipment is the MMU from Steel Electronique (FR); the equipment is qualified for Merlin new generation of S/C (CNES) currently at TRL 7. Currently the largest option of mass memory modules inside the unit is 8 Tbit (also available in 4Tbit and 2 Tbit sizes), which is sufficient not only for the baseline design, but also to cope with the worst-worst case presented in 6.7.1.2. An architectural diagram of the unit is depicted in Figure 6-40.
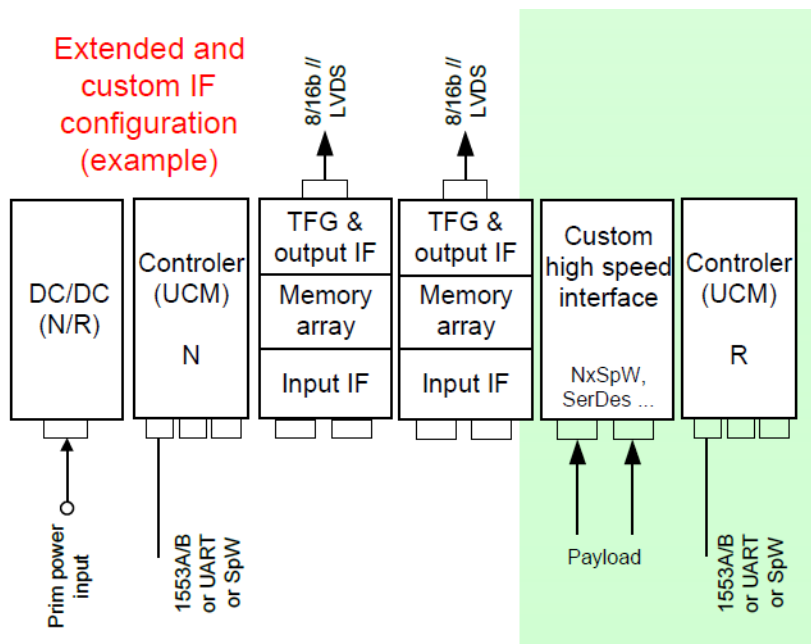
Figure 6-40: Steel Electronique Mass Memory Unit

The unit counts with dedicated SpaceWire links running up to 400 Mbps, and also the provision to place a custom high speed link to specific payloads. The commanding and control can be done also via CAN bus, even if it is not depicted in the figure (UCM board is based on GR712 running RTEMS and it supports that option at both HW and SW level).

6.7.3.5   Data Processing Unit (DPU)

As was presented previously, the approach to process the data from the detectors needs to change with respect to Gaia. In this case, a brand new Data Processing Unit needs to be developed. It will be composed of four identical boards, each of them with its own rad-hard controller and a state of the art processing FPGA:

- Xilinx Ultrascale+ ZU19EG Radiation Tolerant SoC FPGA (see Figure 6-42) with the following internal components:
  - Large programmable array (1.143 million logic cells)
  - Quad-core ARM® Cortex™-A53 MPCore™ up to 1.5GHz
  - Dual-core ARM® Cortex™-R5 MPCore™ up to 600MHz
  - Mali™-400 MP2 GPU up to 667MHz
  - 1,968 DSP slices for parallel mathematical operation (see Figure 6-41:)
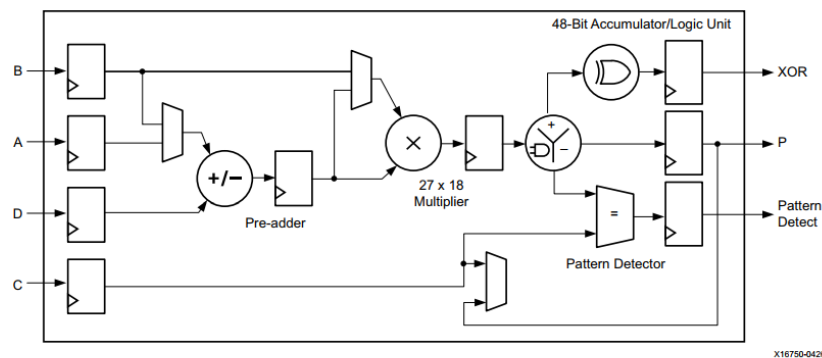
Figure 1-1:   **Basic DSP48E2 Functionality**

Figure 6-41: Xilinx Zynq Ultrascale+ FPGA DSP Slices

- Incoming high-speed SpaceFibre links from the ICU.
- Outgoing 400 Mbps SpaceWire links to the MMU.
- 16 DDR 1 Gbit memory modules at 333MHz 16-bit interface.
- LUCA latch-up protection devices for the FPGA power rails.
- GR740 Radiation Hardened LEON-4 Quad-core Processor with CAN interface with the OBC.

The GR740 rad-hard multi-processor core would be able to program and control the FPGA, as well as to connect to the OBC, execute commands and packetize telemetry. It provides the necessary reliability to cope with the SEE that the complex FPGA SoC experiences under radiation. There are currently two GSTP activities that are looking to this FPGA, for a processor for generic reconfigurable avionics and processing systems.

The 16-memory array is used to temporarily store the large incoming data frames for processing, as the processing of each detector can only be done once the whole sample frame is available, and each FPGA board will handle the data from 15 detectors.

Each of these boards are completely independent and the DPU represents only a mechanical housing, making it a perfectly modular system. If more processing power is needed, more boards can be added to the unit.

With this approach the DPU is able to process the minimum requirement of data processing (CDS, two samples per observation) in 0.407 seconds. The calculation is based on the current features of these devices and only with the processing capability of the FPGA part of the Xilinx SoC. This means that there is a large computing power margin provided by the several processors and GPUs inside the SoC.
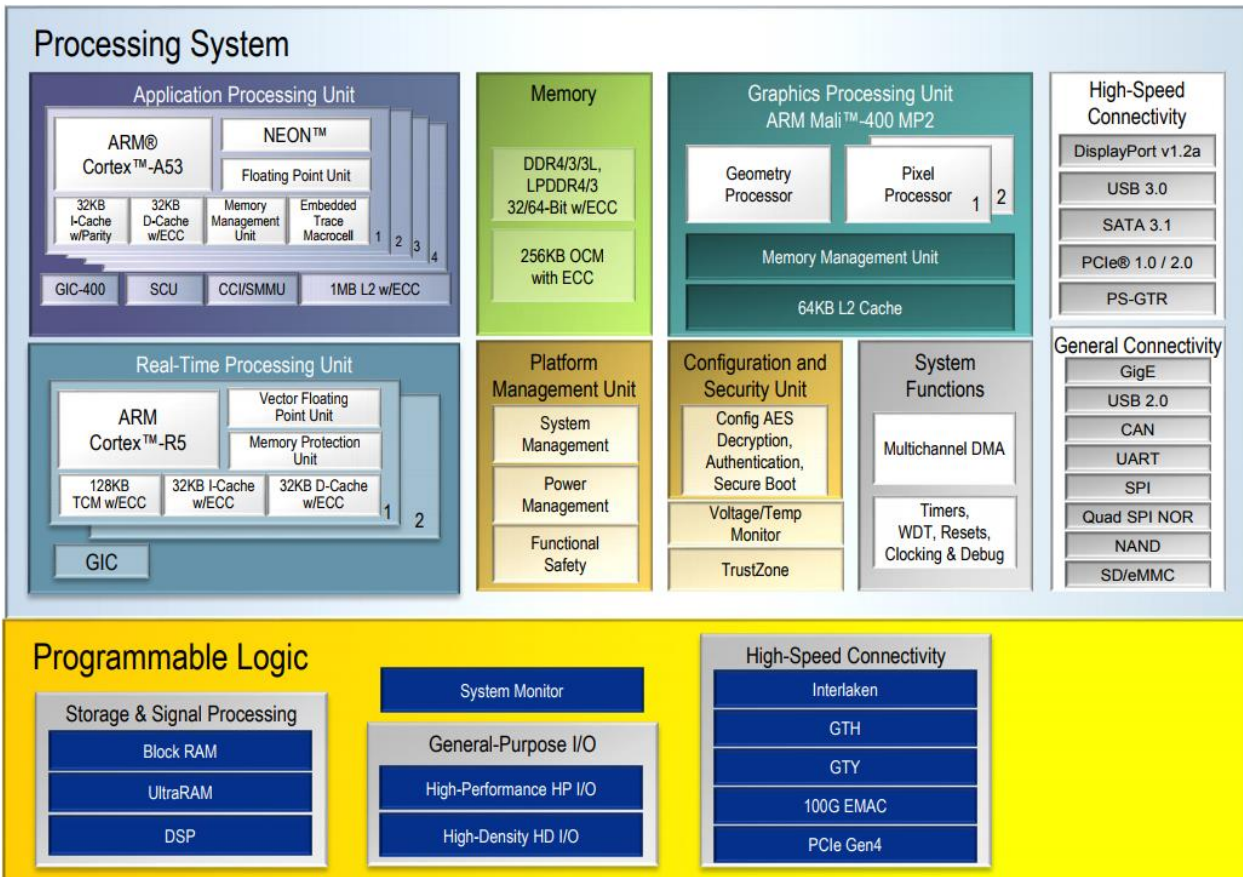
Figure 6-42: Xilinx Zynq Ultrascale+ FPGA internal architecture

6.7.3.6   Instrument Control Unit (ICU)

The distance between SVM and PLM is too long to be able to control the detectors from the DPU directly (clock distribution to the SIDECARs is needed and data is sampled with the outgoing clock; the propagation time limits the length of the link), hence the decision has been made to place an intermediate unit, an Instrument Control Unit (ICU) in the proximity electronics of the PLM. This unit would also require an ad-hoc development as:

1. It needs to be so close to the detectors that it affects the sizing of the cold and hot radiators, therefore it needs to be very efficient in terms of power dissipation.
2. It has to collect 24 LVDS pairs from each of the 60 detectors, plus commanding through another 2 differential lines per detector. This results on the collection of 1560 LVDS pairs to be controlled by the ICU, a number large enough to drive the whole layout of the PCB.
3. The outgoing multi-lane SpaceFibre links towards the DPU require a dedicated high-speed digital design that needs an ad-hoc layout.

Again, the most efficient way to resolve the design is to base it on FPGAs. In this case, the well settled in the market Xilinx Virtex-5QV FPGA is the selected solution, for its reliability and well-established availability of design groups in all the prime contractors.

Four boards will be necessary to fit this large number of interfaces which are connected to the OBC via CAN bus. Each of the FPGA boards is independent and is able to interface with the SIDECAR ASICs from 15 detectors, as well as receiving directly from the OBC the necessary commands to configure them.

Apart from interfacing the SIDECAR ASICs, the FPGA will be able to packetize the data and forward it via SpaceFibre to the DPU in a multi-lane configuration of 15 Gbps.

6.7.4   List of Equipment

	mass (kg)	mass margin (%)	mass incl. margin (kg)
SC (Spacecraft)	**23.20**	**8.88**	**25.26**
PLM (Payload Module)	**4.00**	**20.00**	**4.80**
ICU (Instrument Control Unit)	4.00	20.00	4.80
SVM (Service Module)	**19.20**	**6.56**	**20.46**
OSCAR (On board computer OSCAR)	5.20	5.00	5.46
RTU (Remote Terminal Unit)	7.00	10.00	7.70
SSMM (Solid State Mass Memory)	3.00	10.00	3.30
DPU (Data Processing Unit)	4.00	0.00	4.00
Grand Total	**23.20**	**8.88**	**25.26**

Table 6-29: DHS List of Equipment

Power (W)		
	P_on	P_stby
SC (Spacecraft)	**119.00**	**73.00**
PLM (Payload Module)	**40.00**	**15.00**
ICU (Instrument Control Unit)	40.00	15.00
SVM (Service Module)	**79.00**	**58.00**
OSCAR (On board computer OSCAR)	15.00	10.00
RTU (Remote Terminal Unit)	14.00	14.00
SSMM (Solid State Mass Memory)	10.00	10.00
DPU (Data Processing Unit)	40.00	24.00
Grand Total	**119.00**	**73.00**

Table 6-30: DHS Power Budget

6.7.5   Options

An option to take into consideration to enhance the science performance is the possibility to sample the detectors more than twice per observation. This implies an explosion of the amount of data that the ICU needs to forward to the DPU. Keeping the same processing strategy on the DPU would imply that the detectors data from two consecutive samples are subtracted already in the ICU, and the already computed difference is forwarded to the DPU afterwards. With the current design it is possible to

do such subtraction on-the-fly inside the ICU adding just an extra memory device in each ICU board, but the estimation is without margins. If introducing a 50% margin, the implication is that the ICU will need two more boards to cope with the new data-rates, which inevitably ends up in a significant increase of the power consumption. On the one hand, this option could enable to process up to four samples per observation hence reducing significantly the read-out noise; on the other hand, increasing the power dissipation so close to the instrument will impact the radiators size and again, inevitably, mass and volume budgets.

The processing of 4 samples instead of only 2 per observation (the current CDS baseline) is likely to be possible, with the benefit that the readout noise would decrease from 12 to 12/sqrt(2), corresponding to just over 8 electrons (see Figure 5-16 of the PLM Detectors chapter). From Figure 5-28, depicting a 50% improvement in performance above magnitude 18 for 6 electrons, it can be deduced that this would result in a substantial performance increase (the performance is read out noise limited, and therefore benefits greatly from any improvement in read out noise).

6.7.6 Technology Requirements

The following technologies are required or would be beneficial to this domain:

Included in this table are:

- Technologies to be (further) developed
- Technologies available within European non-space sector(s)
- Technologies identified as coming from outside ESA member states.

Equipment and Text Reference	Technology	Suppliers and TRL Level	Technology from Non-Space Sectors	Additional Information
ICU		TRL2		All components available, an equipment supplier needs to take all the building blocks and make a unit for this purpose.
DPU		TRL2		All components available, an equipment supplier needs to take all the building blocks and make a unit for this purpose.

6.8 SVM Telecommunications

6.8.1 Requirements and Design Drivers

6.8.1.1 Requirements

The requirements for the telecommunication subsystem are the followings:

SubSystem Requirements		
Req. ID	**Statement**	**Parent ID**
COM-010	The telecommunication subsystem shall be able to perform the following functions regardless of the launcher's attitude, throughout all the mission phases: • Receive and demodulate the uplink signal from the ground segment and transmit the telecommands (TC) to the data handling system as defined in RD[26] and RD[27]. • Receive a telemetry (TM) data stream from the data handling system and transmit this data to the ground segment as defined in RD[26] and RD[28], • Receive, transponder, and re-transmit a ranging signal as defined in RD[29].	
COM-020	Active (hot) redundancy shall be provided for telecommand (uplink) and passive (cold) redundancy for telemetry (downlink).	
COM-030	The link budget margins shall be as defined in RD[26] • Nominal > 3 dB • Mean 3*sigma > 0 dB • RSS worst case > 0 dB	ECSS-E-ST-50-05C Req. 8.3.2-i
COM-040	Selected Sun Aspect Angle is 51.47º	

6.8.1.2 Design Drivers

The main design drivers for the communication subsystem are the *data volume to be downloaded and G/S availability*: the total data volume at the input of the encoder (including protocol encapsulation, re-transmission, and compression) together with the G/S availability (hours/day for download) defines the minimum TM bitrate for science data download of the RF link. The bitrate drives the frequency selection, power consumption, and antenna size.

6.8.2 Assumptions and Trade-Offs

For the design of the communication subsystem, four main assumptions have been taken:

- Data Volume: based on the calculation provided in Section 6.7.1.2, the total amount of instrument data has been estimated 120.96 Gbit/day and is shown in Table 6-31.
- Mass memory technology and maximum latency: it has been assumed that those do not drive the bitrate of the communication subsystem, i.e. the TM link bitrate

can be sized on the average data rate generation, instead of its peak. Data not downloaded because of possible missed G/S passes, will be collected during next G/S passes by increasing the contact time.

- S/C separation: the S/C separation is assumed at 960,000 km from Earth for computing the worst case of irradiated power on Earth surface (power flux density, PFD) as required by ITU regulations.

The assumptions are summarised in the following table:

Assumptions	
1	The average instrument data volume is 120.96 Gbit/day. *NB: the amount of data is the average rate.*
2	Mass memory technology and maximum latency (from data generation to data download) do not drive the bitrate of the communication subsystem. *Rationale: the TM link bitrate can be sized on the average data generation, rather than its peak.*
3	S/C separation occurs at 960,000 km from Earth or higher *Rationale: S/C separation is taken into account for checking the worst case of irradiated power on Earth surface (power flux density) as by ITU regulations and Space Frequency Coordination Group (SFCG) recommendations.*
5	The maximum G/S availability is 12 hours/day, possibly to be reduced to 9 hours/day.

6.8.2.1   Bitrate sizing

Following assumptions 1 and 2, the total amount of data to be downloaded through the TM RF link has been estimated as 130.64 Gbit/day as per calculations shown in Table 6-31. Therefore, if a TM bitrate of 9.3 Mbps is adopted with a G/S contact time of 9 hours/day, all data can be download with large margin[4].

---

[4] After the CDF final presentation the data budget was refined, leading to an amount much lower than previously expected. To avoid a new design iteration at system level, it was decided to keep the resulting large margin that will need to be reconsidered during next phases. For instance the margin could be reduced in favour of a lower bitrate, in favour of a lower G/S contact time (e.g. around 5-6 hours/day), or in favour of a higher downloaded data volume.

Parameter	Value	Notes
Data stored in the Memory [Gbit/day]	120.96	
TF CCSDS packet overhead	8%	
Total Data to be Transmitted [Gbit/day]	130.64	At FEC encoder input
G/S [hours]	9.00	Minimum
Data rate [Mbps]	9.30	
Data downloaded per day [Gbit/day]	301.32	
Margin	130.65%	

Table 6-31: Estimation of the total amount of data to be downloaded through the TM RF link

Notice that this choice sets up a TM bitrate higher than Gaia that was instead from 5.00 Mbps to a maximum of 8.75 Mbps, where 8.75 Mbps was achievable only in favourable link conditions, taking full advantage of the 10 MHz bandwidth.

6.8.2.2   Antenna Trade-Offs

Considering requirement SYS-040 (spin rate >60 arcsec/s), and possible Sun-S/C-Earth angle, the antenna shall have a pointing capability of 360 degrees in Azimuth and the SAA of 51.5 degrees +/- 15 degrees in elevation[5]. At the same time, micro vibrations are not considered acceptable during science operations, ruling out the use of a mechanical steerable antenna. Therefore, a Phased Array Antenna (PAA) is considered mandatory and becomes an important driver for the frequency allocation trade-off.

6.8.2.3   Frequency Allocation

The GaiaNIR orbit is around L2, hence it can be considered as Category A (Near Earth) Space Research mission as defined in ECSS RD[26]. For Category A, Space Research missions, the frequency allocation trade-off can be limited to the following options:

- X/X: X-Band is adopted for either TTC and download of the science data (as in Gaia),
- X/X/K: X-Band is adopted for TTC and K-Band 25-27 GHz for science data download.

The main advantages of the X/X option is the re-use of most of the Gaia equipment, in particular transponders, RFDN elements, PAA component technology, etc. On the other hand, X-Band for Space Research Near Earth has a bandwidth limitation of 10 MHz that will impact on the maximum TM bitrate.

Differently, the X/X/K option does not have bandwidth limitations but requires the design and development of a K-Band PAA and the use of a dedicated K-Band transmitter (as external unit or integrated in the transponder), with an impact on cost and mass of the communication subsystem.

---

[5] Azimuth and elevation values are given considering a body frame with the Z-Y plane including the S/C sunshield, and +X axis in opposite direction to the SVM structure.

For the frequency trade-off, a preliminary high-level design of the communication subsystems has been carried out for all cases. The following figures have been considered:

- The maximum bitrate
- The estimated subsystem mass
- The complexity of the PAA (as expected number of active elements per sub-array since it drives the overall subsystem complexity)
- The size of the PAA cone (that drives the overall volume) and
- A qualitative figure on the procurement cost.

These figures have been assessed in Table 6-32 for the following three cases:

1. *X/X conservative (bitrate <10 Mbps):* this option is mostly based on Gaia technology with minor variations like the PAA. However the transponder exploits recent TM technologies (described further later) for high spectral efficiency modulations, i.e. PSK/APSK modulations having up to ~5 Mbps per MHz of available bandwidth. Such modulations and coding profiles allow to overcome the limit that Gaia had of 8.75 Mbps in 10 MHz.
2. *X/X with major re-design of PAA for high bitrate (>10 Mbps):* beyond the transponder improvement as in previous point, this option foresees a major re-design of the PAA in order to increase the equivalent isotropically radiated power (EIRP) and thus achieve a higher TM bitrate.
3. *X/X/K*: this option considers a dedicated K-Band transmitter as standalone unit (Euclid-like) or integrated in the X/X Transponder (X/X/K transponder).

From the table it is clear that the first option represents the best choice and it will be adopted for the baseline design.

However, during the CDF study it has been found that the trade-off is highly driven by Assumption 1 of Section 6.8.2. For instance, if the required TM bitrate increases in the range 10 to 20 Mbps, option 1 becomes unfeasible allowing only option 2 or 3, which selection in turn will be mainly driven by costs for the PAA procurement (Gaia X-Band PAA modified versus K-Band PAA new design and development). If the bit rate increases further (>22.5 Mbps) then option 3 (K-Band) is the only one feasible.

Hence, **for Phase A it is recommended to carry out an early assessment and consolidation of the data rate and, in case option 1 results no longer feasible, also an early assessment of the Gaia PAA required modifications and its cost for procurement**. A preliminary design of option 2 and 3 is better discussed in Section 6.8.5.1 and 6.8.5.2 of this CDF study report.

	Opt.	Frequency	Data rate [Mbps]	Mass [kg]	PAA elems	PAA Cone	Cost
Best							
Good	1	X-Band	9.5	30-35	6	GAIA size	GAIA Heritage
Poor	2	X-Band	22.5	80-90	16	increased	PAA modified
Not Feasible	3	K-Band	57.1	35-40	16	GAIA size	PAA new dev.

Table 6-32: Frequency allocation trade-off

6.8.3   Baseline Design

The baseline design of the X-Band communication subsystem foresees architecture as shown in Figure 6-43 and includes:

- Two X-Band transponders
- A phased array antenna (PAA)
- Two low gain antennas (LGAs)
- The radio frequency distribution network (RFDN) that interconnects all the aforementioned devices.

Of the two transponders, only one is adopted for nominal operation. The second transponder is used for redundancy: its transmitter is operating in cold mode and its receiver in hot mode (see requirement COM-020). The transponder (together with the data handling subsystem) is able to modulate/demodulate the following formats:

- A TC signal SP-L modulated and LDPC (128,64) coded (as specified in CCSDS 231.0-B-3 RD[27]), with symbol rates up to 128 ksps (for decreasing TC sessions – Gaia lesson learnt),
- A low bitrate TM signal NRZ/PSK/PM modulated, Reed-Solomon Convolutional Coded (Concatenated), with interleaver depth I=5, and error correction capability E=16, with symbol rate up to 2 ksps.
- A high bitrate TM signal, QPSK modulated Turbo-coded as by specification for ACM5 in CCSDS 131.2-B-1 RD[26] (spectral efficiency 1.39 bit/chs).

It is pointed out that the use of ACM5 implies (most likely) that the transponder is able to support the full CCSDS 131.2-B-1, although the link adaption (i.e. adaptive coding and modulation function) could even not be used.

The output TM signal from the active transponder can be routed by means of the RFDN to the LGAs (for low bitrate TM) or the PAA (for high bitrate TM). The two LGAs are opposite directions for obtaining an almost omnidirectional coverage, while during next phases it shall be assessed if a third LGA is required as in Gaia.

The RFDN consist of hybrids, switches, and waveguides that interconnect all the equipment. A possible design of the RFDN is provided in Figure 6-44, and with respect to the LGAs provides an estimated G/T of -33.2 dBK and an on-board loss of 5.4 dB from the transmitter to the antenna port. These values will be adopted in next sections for assessing the link budget, but it is pointed out that a more detailed RFDN design shall be performed during next phases by trading off reliability, dimension, mass, and power losses and its optimisation as it is out of the scope of the CDF study.
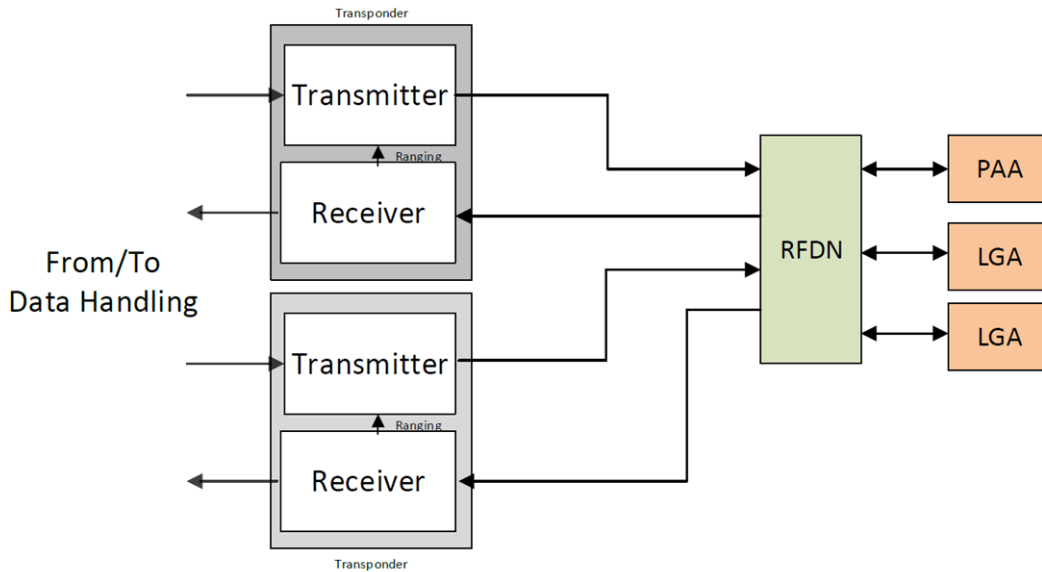
Figure 6-43: Block diagram of the communication subsystem
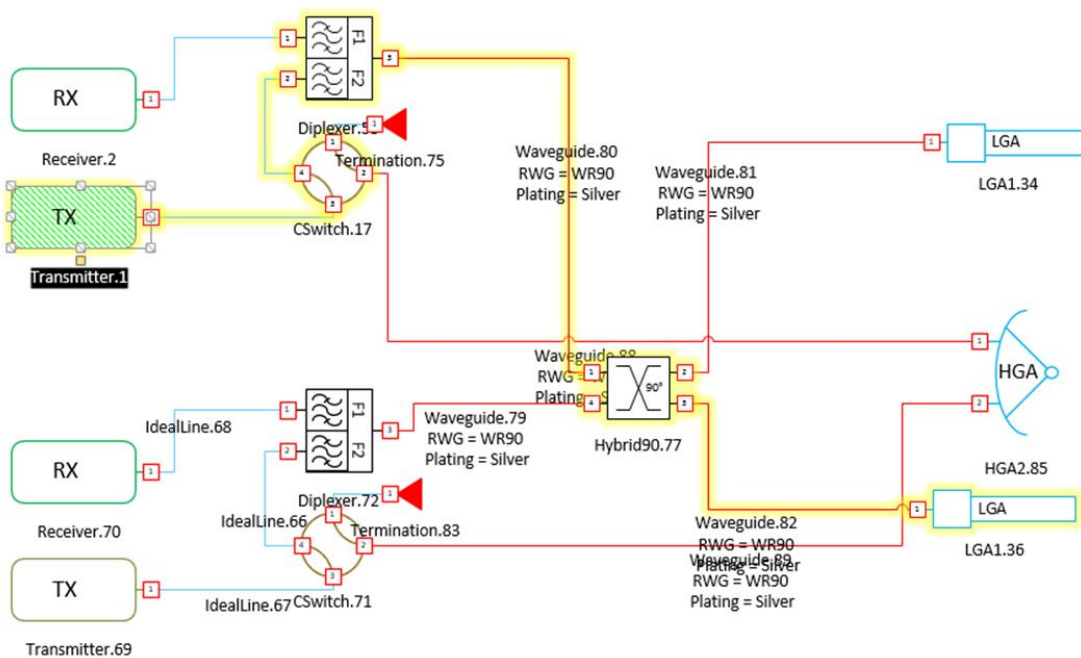
Figure 6-44: possible implementation of the RFDN

6.8.4 List of Equipment

The transponder considered for the baseline design is the X-Band transponder for deep space missions developed by Thales-Italy. The transponder is the same adopted in Gaia, with the following modifications:

- Modifications of the uplink RF/IF section and the digital section for supporting LDPC (128,64) at low signal-to-noise ratio (SNR).

- Integration of a payload transmitter, able to support CCSDS 131-2-B-1.

It is assumed that the modified transponder will have dimension 154 x 204 x 117 mm, mass equal to 3.5 kg, and power consumptions ~17.4 W for the transmitting function and 10 W for the receiving function. Currently the technology has TRL 3, and TRL 5 is expected by 2022.
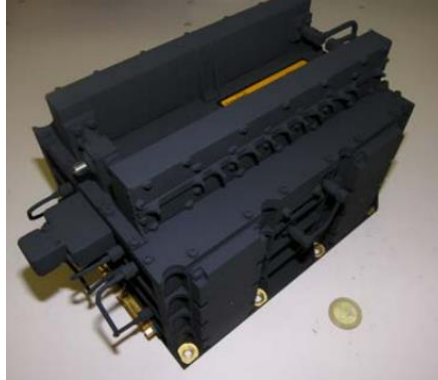
Figure 6-45: X-Band Transponder

A possible solution for the X-Band LGA is manufactured by TRYO and is shown in Figure 6-46. Its mass is 0.4 kg, diameter 90 mm, height 240 mm, and TRL 9.

Figure 6-46: X-Band LGA

The PAA considered instead is the one manufactured by EADS for Gaia having radiating cone and RF stage as shown in Figure 6-47. The PAA cone shall be modified in order to cover an elevation angle = selected SAA of 51.5 degrees +/- 15 degrees (instead of 45 +/- 15 degrees) keeping the 18 dB gain of Gaia, hence a protoflight approach is expected and TRL 5 is assumed. The amplification stage of the beam forming network (BFN) shall be modified/improved in order to achieve 35 dBW (1 dB more than Gaia). For the kind of modifications an EQM or PFM approach is expected and the current TRL is considered 5.
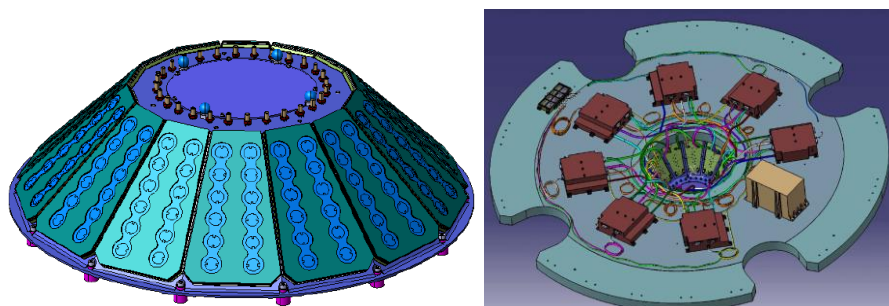
Figure 6-47: PAA antenna cone (left) and RF stage (right)

The RFDN elements are developed by different manufacturers, but typically a common procurement at RF harness or communication assembly level can be done. An example is TRYO procurement for hybrids, coaxial cables, and waveguides. All elements have TRL 9.

6.8.4.1 Technical budgets and performance

A preliminary link budget (worst case) for the TC and TM by means of LGAs is shown Table 6-33. It can be noticed that the use of LDPC coding in uplink allows TC up to 64 kbps (128 ksps) when the G/S EIRP is 108 dBW, i.e. when a 35m G/S uses an X-Band high power amplifier (XHPA). If the G/S adopts instead a low power amplifier (XLPA), the achievable bitrate is 16 kbps (32 ksps). These allow decreasing the TC session down to 16 and 4 times with respect to the Gaia mission. On the downlink side, the achievable bitrate is 1 kbps (worst case), that is lower than 2 kbps of Gaia, but it can be easily improved by modifying the RFDN design.

Uplink SPL/PM

Parameter	Values	Notes
EIRP [dBW]	108.00	XHPA
freq. [MHz]	7235.00	
Path Loss [dB]	234.59	Computed
Atm. Loss [dB]	1.00	
G/T [dB]	-33.20	Estimation with proposed RFDN
Point+Pol Loss [dB]	1.00	
Other Loss [dB]	0.00	
C/N0 [dB]	66.81	Computed
Prc/N0	61.46	Computed
Ptc/N0	65.31	Computed MI=1.0
Prng/N0	-1.55	Computed MI=0.7
Bandwidth RNG [kHz]	550.00	for 220 kHz
SNR_TC	4.90	Computed

Parameter	Values	Notes
Required SNR for Tracking [dB]	17.00	
Carrier Loop Bandwidth [Hz]	400.00	
Implementation Loss [dB]	1.00	
Req. Prc/N0	44.02	Computed
Margin [dB]	22.79	

Tc Recovery

Parameter	Values	Notes
Required EbN0 for decoding [dB]	5.50	LDPC CCSDS (128,64)
Implementation Loss [dB]	2.50	SPL
Bitrate [kbps]	64	128 ksps (4000 * 2^4 as by ECSS)
Req. Ptc/N0	56.06	Computed
Margin [dB]	9.25	>3 dB standard ESA

Downlink NRZ/PSK/PM

Parameter	Values	Notes
mtc_eff	0.001	
mrn_eff	0.000	
alpha	0.000	
RF Power [dBW]	5.40	
TX Gain [dB]	-1.00	
On-Board Loss [dB]	5.40	Estimation with proposed RFDN
EIRP [dBW]	-1.00	Computed
freq. [MHz]	8500.00	
Path Loss [dB]	235.99	Computed
Atm. Loss [dB]	1.00	
G/T [dB]	50.80	
Point+Pol Loss [dB]	1.00	
C/N0 [dB]	40.41	Computed
Prc/N0 [dB]	36.95	Computed
Ptm/N0 [dB]	37.37	Computed MI=1.2

Carrier Recovery

Parameter	Values	Notes
Required SNR for Tracking [dB]	17.00	
Carrier Loop Bandwidth [Hz]	20.00	
Implementation Loss [dB]	1.00	
Req. Prc/N0	31.01	Computed
Margin [dB]	5.94	

TM Recover

Parameter	Values	Notes
Required EbN0 for decoding [dB]	2.50	RS+CC I=5, E=16
Implementation Loss [dB]	0.50	
Bitrate [kbps]	1	
Req. Ptm/N0	33.00	Computed
Margin [dB]	4.37	>3 dB standard ESA

Table 6-33: Preliminary link budget for TC and low data rate TM

For high data rate TM by means of the PAA, a preliminary link-budget for ACM5 is shown in Table 6-34, where it is shown that for EIRP 35 dBW, a bitrate of 9.5 Mbps can be achieved when G/T>50.8 dBK (typical of a 35 m G/S). For checking the occupied bandwidth the QPSK signal at RF output has been simulated and power spectral density computed as shown in Figure 6-48. Its bandwidth resulted 9.3 MHz, and thus it is compliant to the ITU limitation of 10 MHz.

PARAMETER	Value	Notes
RANGE [km]	1770000.0	L2 worst case
FREQUENCY [MHz]	8500	X-Band, SR, Category A
TX EIRP [dBW]	**35.00**	
PATH LOSSES [dB]	**235.99**	**Calculated**
ATMOSPHERE LOSS [dB]	0.20	
POL+POINTING LOSS [dB]	1.00	
RX G/T [dBK]	50.80	35m G/S (Cebreros as REF)
DEMOD. LOSS [dB]	1.00	Estimation
MOD. LOSS [dB]	0.00	QPSK
REQUIRED Eb/No [dB]	2.99	CCSDS 131.2 ACM 5
MINIMUM MARGIN [dB]	3.44	Standard ESA >3 dB
MAX BIT RATE [dBHz]	69.78	
MAX BIT RATE [Mbps]	**9.51**	

Table 6-34: Preliminary link budget for ACM5 at 9.5 Mbps
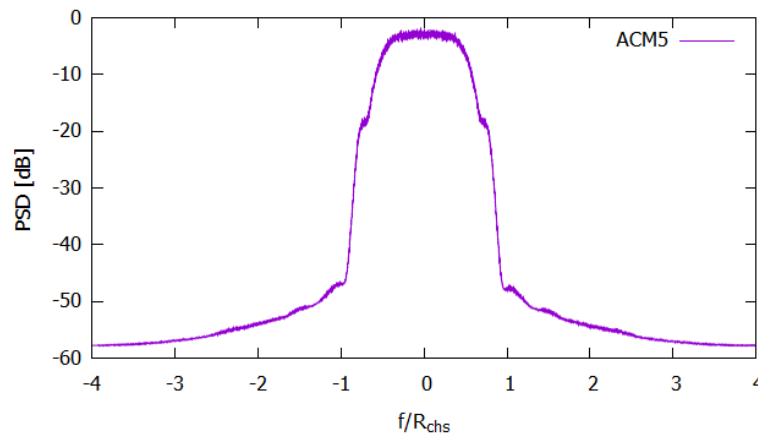
Figure 6-48: ACM5 simulated power spectral density at the RF output

Thanks to the use of CCSDS 131.2-B-1, the data return to G/S can be slightly improved by using the link adaption function. For instance, a preliminary estimation suggests that bitrate can be increased for certain periods up to 13.5 Mbps. Thus, the use of the link adaption function of CCSDS 131.2-B-1 can be a possible option of the baseline design that can be assessed during Phase A (although not mandatory).

The mass and power budget of the communication subsystem are shown in Table 6-35 and Table 6-36, where it can be seen that the overall estimated mass is 32.36 kg (including margins), and the peak power consumption is ~376 W when transmitting with the PAA[6].

---

[6] NB: For the transponders Pon shall be considered as the power consumption when transmitting and receiving, while Pstby shall be considered as the power consumption when receiving only. Hence, the peak power consumption is given by the total shown in the table decreased by the power consumption of one transmitter.

	mass (kg)	mass margin (%)	mass incl. margin (kg)
SC (Spacecraft)	**29.70**	**8.96**	**32.36**
SVM (Service Module)	**29.70**	**8.96**	**32.36**
PAA (Phased Array Antenna)	6.00	10.00	6.60
PAA_BFN_1 (PAA BFN Module 1)	1.50	10.00	1.65
PAA_BFN_2 (PAA BFN Module 2)	1.50	10.00	1.65
PAA_BFN_3 (PAA BFN Module 3)	1.50	10.00	1.65
PAA_BFN_5 (PAA BFN Module 5)	1.50	10.00	1.65
PAA_BFN_6 (PAA BFN Module 6)	1.50	10.00	1.65
PAA_BFN_7 (PAA BFN Module 7)	1.50	10.00	1.65
PAA_BFN_8 (PAA BFN Module 8)	1.50	10.00	1.65
PAA_DCDC_Converter (Phased Array Antenna DCDC Converter)	3.50	5.00	3.68
PAA_RF_Splitter (Phased Array Antenna RF Splitter)	0.20	5.00	0.21
X_Band_RFDN (X Band Radio Frequency Distribution Network)	2.00	5.00	2.10
X_LGA_1 (X Band Low Gain Antenna #1)	0.25	5.00	0.26
X_LGA_2 (X Band Low Gain Antenna #2)	0.25	5.00	0.26
X_XPND_1 (X Band Transponder #1)	3.50	10.00	3.85
X_XPND_2 (X Band Transponder #2)	3.50	10.00	3.85
Grand Total	**29.70**	**8.96**	**32.36**

Table 6-35: Mass budget for the communication subsystem

Power (W)	P_on	P_stby
SC (Spacecraft)	**393.19**	**20.00**
SVM (Service Module)	**393.19**	**20.00**
PAA (Phased Array Antenna)	0.00	0.00
PAA_BFN_1 (PAA BFN Module 1)	43.65	0.00
PAA_BFN_2 (PAA BFN Module 2)	43.65	0.00
PAA_BFN_3 (PAA BFN Module 3)	43.65	0.00
PAA_BFN_5 (PAA BFN Module 5)	43.65	0.00
PAA_BFN_6 (PAA BFN Module 6)	43.65	0.00
PAA_BFN_7 (PAA BFN Module 7)	43.65	0.00
PAA_BFN_8 (PAA BFN Module 8)	43.65	0.00
PAA_DCDC_Converter (Phased Array Antenna DCDC Converter)	33.00	0.00
PAA_RF_Splitter (Phased Array Antenna RF Splitter)	0.00	0.00
X_Band_RFDN (X Band Radio Frequency Distribution Network)	0.00	0.00
X_LGA_1 (X Band Low Gain Antenna #1)	0.00	0.00
X_LGA_2 (X Band Low Gain Antenna #2)	0.00	0.00
X_XPND_1 (X Band Transponder #1)	27.34	10.00
X_XPND_2 (X Band Transponder #2)	27.34	10.00
Grand Total	**393.19**	**20.00**

Table 6-36: Power budget for the communication subsystem

Finally, the power flux density has been computed at 960,000 km (see Assumption 4), and it has been found that margins are above 30 dB w.r.t. the -150 dBW/m2/4 kHz at 0 degrees, and -140 dBW/m2/4 kHz at 90 degrees, hence once again compliant with ITU regulations.

6.8.5 Options

If the amount of data to be downloaded increases with respect to the one shown in Section 6.8.2.1, the current baseline design will not allow increasing further the TM bitrate unless a major redesign is done. In particular, during the CDF study two options have been found relevant:

- X-Band with major redesign of the PAA: suitable for TM bitrate between 10-20 Mbps.

- K-Band with new design of the PAA: of interest for TM bitrate >20 Mbps.

These two options are described in the two following subsections. Finally, the last subsection reports some options that were excluded during the CDF study, but are reported for the reader information.

6.8.5.1 X-Band with major redesign of the PAA

By increasing the EIRP it is possible to resort to CCSDS 131.2-B-1 ACMs with higher spectral efficiency, i.e. TM bitrate can be increased by still meeting the X-Band 10 MHz requirement. However, because of the band limitation, it shall be kept in mind that the TM bitrate will increase as a logarithmic function of the power instead of a linear function as usually happens.

Hence, during the CDF study a preliminary design that fully exploits the X-band has been carried out. This design still foresees the same block diagram shown in Figure 6-43, (same transponders, LGAs, and RFDN) but the PAA requires a major redesign. Figure 6-49 shows the new X-Band PAA where the following modifications have been done:

- Cone upper diameter increased to 1.3 m, inner diameter to 0.875 m, and height 0.33 m.

- Number of sub-arrays increased to 97, each with 16 elements of 8 dBi gain (same kind of elements as in Gaia).

- The BFN network is low-level (amplification and phase actuator per radiating element) instead of hybrid as done in Gaia.

The overall estimated mass for the modified PAA is around 60 kg. All these modifications allow to achieve an antenna Gain >30.1 dB and thus EIRP of >46.9 dBW. Consequently, it can be shown that using ACM16 (16APSK Turbo-coded) GaiaNIR can achieve 22.6 Mbps, with symbol rate ~28.5 Msps, and channel symbol rate of ~7 Mchs/sec. Again, a simulation of the waveform has been done, and it has been found that the occupied bandwidth is 9.3 MHz, thus meeting the ITU requirement.
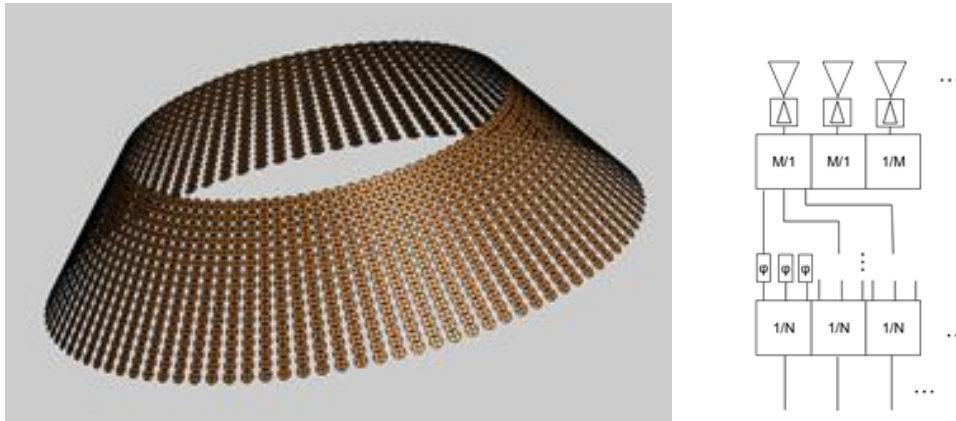
Figure 6-49: PAA cone (left) and low-level BFN (right) that guarantee Gain >30.1 dB

It is pointed out that this solution represents an extreme case and, depending on the data rate, smaller and simpler PAA designs can be adopted. A high-level estimation of what can be expected for different TM bitrate is shown in Figure 6-50, where it can be seen how few Mbps less can decrease the PAA mass noticeably.
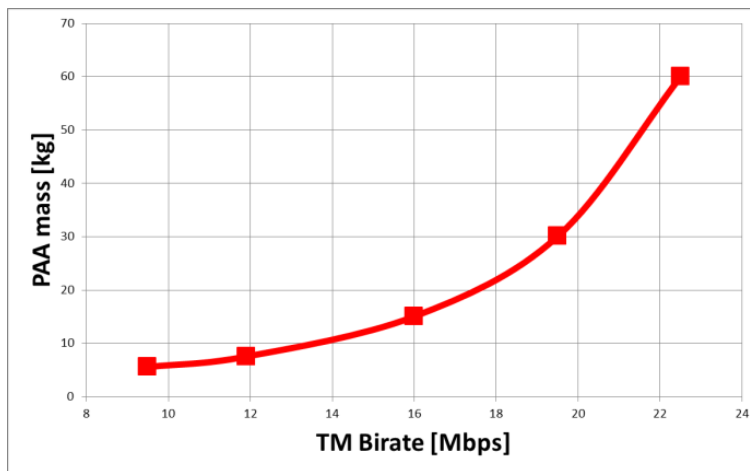
Figure 6-50: Rule-of-thumb for PAA mass versus TM bitrate in X-Band

6.8.5.2 K-Band with new design of the PAA

As shown in the previous section, the PAA EIRP and mass increases as exponential function of the TM bitrate. Hence, for bitrates higher than 20 Mbps, X-Band becomes unfeasible. However, if K-Band (25-27 GHz) is adopted the PAA dimensions decrease. However the use of K-Band implies the followings:

- A dedicated K-Band transmitter, as the Euclid K-Band modulator (TRL 9 by 2020), shall be used. Alternatively, an X/X/K-Band transponder shall be developed and qualified (currently TRL 3, with GSTP proposal in ESA for reaching TRL 5 by 2021).

- A K-Band PAA shall be design and developed.

If the same PAA design described in Section 6.8.5.1 is considered (97 subarrays with 16 elements), the antenna size has upper diameter ~0.45 m, height ~0.1 m, and expected mass ~7 kg. Such antenna is still able to provide EIRP >46.9 dBW and it can be shown by means of link budget, that such EIRP allows a bitrate >55 Mbps by using classical suppressed modulations (e.g. GMSK or OQPSK) and ECSS Turbo Coding 1/4, with codeword length 7136.

6.8.5.3 Options excluded during the CDF study

An option quickly investigated and immediately excluded was the use of Ka-Band (33 GHz) instead of the K-Band (26 GHz). An X/X/Ka-Band option would allow using the X/X/Ka-Band transponder of BepiColombo that can have a lower price of procurement than a dedicated K-Band transmitter (or than developing a X/X/K transponder). Hence, during the CDF study it was questioned if Ka-Band can be adopted in case the Gaia GaiaNIR orbit around L2 increases such that the distance from Earth is slightly above 2 million km (and thus classified as Deep Space). However, adopting such strategy would put GaiaNIR in the worst condition for satisfying all ITU Deep Space requirements, with a clear risk for the mission during next phases.

A second option investigated was to increase the PAA coverage in elevation to +/-27 degrees instead of +/- 15 degrees, because it would allow a larger orbit around L2 with a decrease in DeltaV. However, during the CDF study trade-offs showed that such an orbit would increase the sunshield size leading to a worse design than the current one.

6.8.6 Technology Requirements

The following technologies are required or would be beneficial to this domain:

Included in this table are:

- Technologies to be (further) developed
- Technologies available within European non-space sector(s)
- Technologies identified as coming from outside ESA member states.

Equipment and Text Reference	Technology	Suppliers and TRL Level	Technology from Non-Space Sectors	Additional Information
X-Band (Baseline design)				
X-Band transponder	LDPC coding in TC, CCSDS 131.B-1 for TM	Thales-Italy, Current TRL 3, TRL 5 by 2022		Activity in GSTP compendium 2017 for EM.
X-Band Phased array antenna	Radiating cone, BFN	EADS CASA Espacio, Gaia Heritage TRL 5		Cone for 39+/-15 deg (same Gain), BFN for achieving 35 dBW
X-Band with increased data rate option				
X-Band transponder	LDPC coding in TC,	Thales-Italy, Current TRL 3, TRL		Activity in GSTP compendium 2017

Equipment and Text Reference	Technology	Suppliers and TRL Level	Technology from Non-Space Sectors	Additional Information
	CCSDS 131.B-1 for TM	5 by 2022		for EM.
X-Band Phased array antenna	Radiating cone, BFN	EADS CASA Espacio, Gaia Heritage TRL 3		Radiating cone and BFN to be modified for 30 dB gain, 46.9 dBW
K-Band option				
X/X/K transponder (as alternative to K-Band transmitter)		Thales-Italy, Tesat, Kongsberg TRL 3		GSTP activity proposal (STAT id 3811)
K-Band Phased Array Antenna	New PAA Design and Development	TRL 1		PAA to be designed for 46.9 dBW

6.9 SVM Thermal

6.9.1 Requirements and Design Drivers

SubSystem Requirements		
Req. ID	Statement	Parent ID
TCS-010	The TCS shall be composed of only passive thermal hardware (MLI, thermal links, heaters and heat pipes)	
TCS-020	The TCS shall not produce any mechanical vibrations (e.g. no mechanical coolers)	
TCS-050	The SVM shall be thermally decoupled from the PLM in such a way that temperature fluctuations in the SVM do not carry over an influence on the thermal and mechanical stability of the PLM	

6.9.2 Assumptions and Trade-Offs

Assumptions	
1	The thermal design is based upon heritage from the Gaia SVM Thermal Design.
2	Radiator and heater power sizing is based upon equipment dissipations listed in the OCDT model.
3	Radiator coating emissivity assumed to be 0.8 at EOL.
4	A 10 °C margin is considered on top of operating and non-operating temperatures of units for radiator sizing. A margin of 20% is considered for heater power sizing.

6.9.3 Baseline Design

The thermal design of the SVM is based on heritage from the Gaia SVM thermal concept RD[30].

- No active thermal control foreseen
- Internal cavity black painted to promote temperature uniformity within the SVM
- PI heater control on base of SVM bipods to attenuate temperature fluctuations from the SVM towards the PLM
- MLI is foreseen in the following areas:
  o Externally closing gaps between radiator areas
  o Between the SVM and PLM
  o Double blankets on Sun shield + launch adaptor area and bottom of SVM
  o Covering units and the propulsion system where required
- Units mounted on shear panels conductively connected to external radiative surfaces
- Thermal doublers may be used beneath units with large heat fluxes
- Thermal fillers to be used to promote conductive heat flow from units
- Heat is removed via external radiating surfaces with high emissivity finishes

- Heaters and thermistors installed near the unit Temperature Reference Points (TRP).

6.9.3.1 Temperature Requirements

The following operational and non-operation temperature requirements in Table 6-37 have been taken into account when sizing the SVM thermal control system. As the unit temperature requirements have not been individually defined, the reference temperatures are taken from the Gaia mission for typical thermal equipment. The propulsion system has been sized at a higher minimum operational temperature taking into account the freezing temperature of the propellant. An uncertainty margin of +/- 10°C has been included on the temperature requirement.

| | Requirement | | | | Margin | Radiator and Heater Sizing | | | |
| Case | Operating | | Non-Operating | | | Operating | | Non-Operating | |
Sub-system	Max [°C]	Min [°C]	Max [°C]	Min [°C]	+/- [°C]	Max [°C]	Min [°C]	Max [°C]	Min [°C]
Gaia general equipment	55	-15	65	-35	10	45	-5	55	-25
Propulsion System	55	10	55	10	10	45	0	45	0

Table 6-37: Operational and non-operational temperature requirements

* It is assumed that the decontamination is performed at the maximum non-operational temperature of 55 °C for general equipment.

6.9.3.2 Dissipation Requirements

The summary in Table 6-38 shows the dissipation of the SVM units added in OCDT during each mode of S/C operation.

Case / Subsystem	LM [W]	SAM [W]	SM [W]	DM [W]	OCM [W]	STM [W]
AOGNC	0.00	42.60	42.60	51.60	51.60	51.60
COM	0.00	23.47	23.47	23.47	379.41	379.41
CPROP	0.00	4.64	4.64	4.64	55.83	55.83
DH	0.00	0.00	0.00	0.00	0.00	0.00
DET	0.00	0.00	0.00	0.00	0.00	0.00
MEC	0.00	0.00	0.00	0.00	0.00	0.00
PWR	30.00	30.00	30.00	30.00	30.00	30.00

Table 6-38: Unit dissipation for each subsystem in each S/C mode (from OCDT)

6.9.3.3   Radiator Sizing

The total radiative area for the SVM is estimated to be **1.1 m²** for dissipation values indicated for equipment in the OCDT model.

The sizing case for the radiator area is either the Orbit Control Mode (OCM) or Science and Transmitting Modes (STM).

Available external area for radiators is not considered critical on the SVM. However, the PLM radiator baseline will overhang the PLM towards the SVM reducing the available area.

The radiators are sized under the following assumptions:

- Radiator surface emissivity of 0.8
- Radiate all heat from dissipative units at the relevant Tmax per S/C mode
- Radiator has a direct view factor to deep space at 4K (*)
- The radiators do not receive any external heat loads from Solar or Planetary fluxes
- The radiators are constructed from 3mm thick aluminium plates. This is conservative in terms of mass as for room temperature radiators honeycomb panels may also be used to reduce mass.

(*)   The radiators will have a large view factor to the SVM Sun shield, which should be analysed with the construction of a thermal model. A reflective surface finish, for example a SSM layer or OSR tiles, should be considered on the rear of the Sun-shield MLI adjacent to the radiator locations to increase the radiative exchange factors to space and increase the SVM radiator efficiencies.

6.9.3.4   Heater Sizing

The heaters have been sized under the following assumptions:

- Maximum radiator area considered over S/C modes
- Assuring the temperature of units are maintained above the relevant Tmin per S/C mode
- Heater powers incorporate a 20% design maturity margin.

The required heater powers per S/C mode are presented in Table 6-39.

Case / Subsystem	LM [W]	SAM [W]	SM [W]	DM [W]	OCM [W]	STM [W]
Total Heater Power	379	306	306	229	0	0

Table 6-39:   Required SVM heater power per S/C mode

6.9.3.4.1   *Mass budget*

The mass budget breakdown is summarised in Table 6-40 with unit maturity margin applied. The margin philosophy per item has been iterated with the Gaia-NIR system engineering team and it is in line with the CDF margin philosophy.

Item	Mass [kg]	Margin	Estimated Mass including margin [kg]
Radiators (1.1 m²) Aluminum 3mm	32.4	20 %	38.9
Heater lines / Thermistors + harness	0.95	5 %	1.0
Paints and coatings	0.62	5 %	0.65
MLI External SVM MLI Internal between SVM & PLM	6.7	5 %	7.0
Miscellaneous (doublers / fillers / tapes / grounding / thermal links)	3.2	5%	3.4
Total	**43.9**		**51.0**

Table 6-40:   Mass budget for Thermal Control Hardware for the SVM

6.9.4   List of Equipment

The following equipment is used in the SVM thermal subsystem:

- Multi-Layer Insulation (MLI)
- Radiator – Aluminium 3mm (baseline) or honeycomb panel
- Paints and coatings – Black paint for radiators
- Thermistors regular, heaters + harness cables
- Retained test thermo-couples and test heaters
- Thermal fillers or doublers where required
- Thermal links i.e. straps where required
- Tapes, attachments, groundings and glues.

6.9.5   Options

No options considered for the SVM for thermal control.

6.9.6   Technology Requirements

No technology requirements foreseen for the SVM for thermal control.

7 SYSTEMS

7.1 Requirements and Design Drivers

The GaiaNIR high level mission requirements listed in Table 7-1 have been used as a starting point for the CDF Study.

Mission Requirements		
Req. ID	**Statement**	**Parent ID**
MIS-010	The mission shall used NIR detectors to performed high accuracy astrometric and photometric measurements.	See RD[31] for more detailed science requirements
MIS-020	The nominal science operations (lifetime) of GaiaNIR S/C shall last 5 years.	Ability to observe at least the same number of targets as Gaia
MIS-030	The mission and system design shall be compatible with a launch in 2035.	M-Class mission planning constraint
MIS-040	The satellite should be launched by a European launch vehicle.	M-Class mission constraint
MIS-050	The cost to ESA shall not exceed 550M€[2017], including: • Platform, Payload (TBD), System integrator • Launcher • Operations (MOC, SOC) • ESA internal	M-Class mission constraint

Table 7-1: Mission requirements

The above mentioned requirements imply the following major design drivers:

MIS-010 together with the detailed Science requirements in RD[31] drives the choice of the NIR detectors and the payload design.

MIS-020 and **MIS030** drive the programmatic schedule and restrict the nominal mission operational lifetime to 5 years allowing sufficient margin for any new technology development needed.

MIS-040 restricts the available launchers to Ariane 62 and Ariane 64. Preliminary launcher performance and envelope considerations are described in Section 7.2 Launch Vehicle.

MIS-050 severely restricts the trade space of the spacecraft. In order to comply with this requirement, the following have been investigated:

• Significant simplifications to the Gaia S/C and making use of the Gaia lessons learnt regarding S/C design

• Maximise the usage of Gaia components as far as applicable

• Identify potential cost savings, and implement these in the baseline design where suitable.

The main system requirements are as follows:

System Requirements		
Req. ID	Statement	Parent ID
SYS-010	The astrometric measurement principle shall be based upon a continuous scanning or a step-stare mode which discretely approximates continuous scanning of the sky with at least two fields-of-view.	MIS-010
SYS-020	The S/C shall be compatible with an Ariane 62/Ariane 64 launch vehicle.	MIS-030, MIS-040
SYS-030	The GaiaNIR S/C design shall baseline equipment with a TRL of at least 6 at the start of Phase B2. Goal: The GaiaNIR S/C shall maximise reuse of existing Gaia technology	MIS-030
SYS-040	The component of the rotation vector around the S/C X axis shall not be less than equivalent 60 arsec/s (the goal is a nominal value of equivalent 96 arsec/s).	MIS-010

Table 7-2: System requirements

SYS-010 is a consequence of the need of enlarging the astronomic performance of the Gaia mission to include also the NIR astronomical sources while maintaining the Gaia accuracy for the optical reference frame. This is a key driver for the detectors trade-offs (see Chapter 5.2) and the Systems trade-offs (see Section 7.7).

SYS-020 is a consequence of the current estimates for future available launchers Ariane 62, Ariane 64 (see Section 7.2).

SYS-030 is a driving requirement for any proposed new technology development. An overview with the technology developments proposed specifically for GaiaNIR mission is provided in each section .

SYS-040 is driving requirement for the AOCS design (see Chapter 6.5).

7.2   Launch Vehicle

Mission requirements MIS-030 and MIS-040 lead to the SYS-020 system requirement regarding the future launchers to be considered for the GaiaNIR CDF Study: Ariane 62 and Ariane 64. Soyuz was excluded as its availability for a launch in 2035 is highly questionable.

The current Arianespace User Manual for Ariane 62 (RD[32]) indicates the available volume envelope and performance shown in Figure 7-1 and Table 7-3 respectively. The performance of Ariane 62 into an L2 transfer orbit is not stated in the User Manual, but Ariane 62 is expected to be have a better performance than a Soyuz-ST launch vehicle from Kourou, with an expected L2 transfer orbit performance better than 3 metric tons.
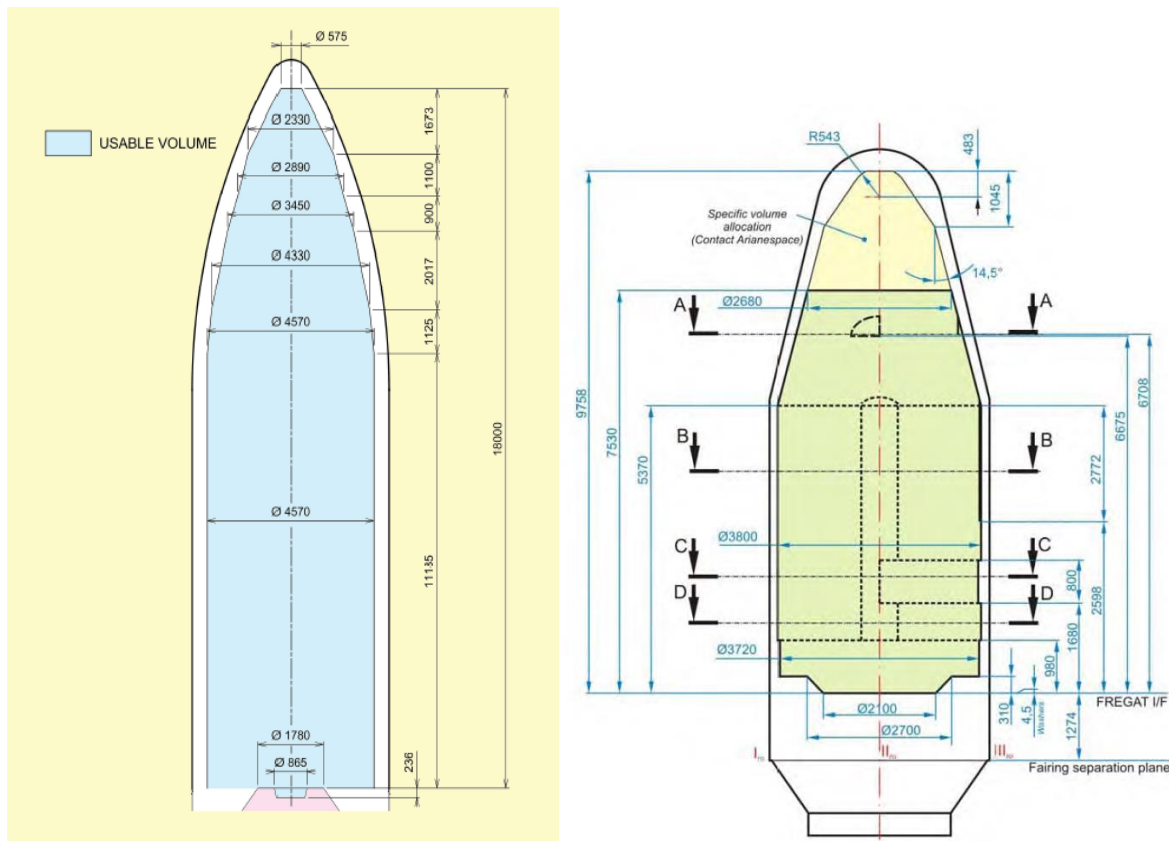
Figure 7-1: Single launch envelope for Ariane 62 (left) and Soyuz ST (right)

Launcher	Max Available Ø [mm]	Max Available Height [mm]	Available Mass [kg] (incl. adapter and via direct ascent)
Soyuz-ST	3720	5370	2250
Ariane 62	4570	11135	2250 – 3000+ (TBC)

Table 7-3: Launcher trade space

7.3   Operational Orbit

The GaiaNIR S/C is inserted in a L2 type orbit that offers high observation efficiency as well as a stable thermal environment and a low radiation dose. Several possibilities for the operational orbit were identified during the CDF Study:

- Large amplitude quasi-Halo orbit
- Small amplitude Lissajous orbit (as Gaia).

A trade-off was performed in order to identify the preferred solution for GaiaNIR. The trade-off is presented in Table 7-4 below:

L2 Orbit	Sun-S/C-Earth angle	Insertion manoeuvre	Insertion ΔV [m/s]	Eclipses	TT&C impact	Example of other missions
Large amplitude quasi-Halo	Large	No operational orbit insertion manoeuvre required	0	Eclipse free	Mechanical steering of the antenna needed	Herschel, JWST, Euclid, LPF
Small amplitude Lissajous	Small	Amplitude reduction manoeuvre required after fast or slow transfer	165	Eclipses after about 5.5 years	Mechanical steering of the antenna can be avoided (use of PAA)	Planck, Gaia

Table 7-4: GaiaNIR orbits trade-off

7.4 Sunshield Trade-offs

For Gaia the 15 deg Sun-S/C-Earth (SSCE) angle was not included in the Sun shield sizing calculations. This implied that for some periods each year, direct Earth and Moon light could impinge on the PLM, with a thermal as well as a straylight impact which meant that the performance and the science data were degraded. This however happened only very rarely, and had insignificant impact on the Gaia mission's observation efficiency.

Considering the Gaia lessons learnt, for GaiaNIR, increasing the SSCE angle to e.g. 27 deg or more by using a large amplitude quasi-halo L2 orbit, the impact of Earth and Moon light on performance and science data would be higher (presumably not linear function) and no longer insignificant. A fine thermal analysis with Earth/Moon light or a related straylight analysis was deemed out of the scope of the GaiaNIR CDF study. For such a high SSCE angle, the Sun shield in the CDF design would therefore also need to function as Earth & Moon shield, with a significantly larger shield as consequence.

The impact of the Sun aspect angle (SAA), SSCE angle, PLM and SVM heights when dimensioning the Sun shield is reflected in Table 7-5 below:

Sun Aspect Angle (deg)	Sun-S/C-Earth Angle (deg)	Max. Earth-Spin axis angle (deg)	PLM Diameter (m)	PLM Height (m)	SVM Height (m)	Total Height (m)	Sunshield Diameter (m)	Case
45	0	45	3.24	2.83	1.17	4.00	**11.2**	Gaia (Sun-Shield)
45	15	60	3.24	1.70	1.17	2.87	**13.2**	Gaia (Sun+Earth-Shield)
45	0	45	3.5	1.33	1.17	2.50	**8.5**	Gaia-NIR (Sun-Shield)
45	15	60	3.5	1.33	1.17	2.50	**12.2**	Gaia-NIR (Sun+Earth-Shield) Small Orbit

Sun Aspect Angle (deg)	Sun-S/C-Earth Angle (deg)	Max. Earth-Spin axis angle (deg)	PLM Diameter (m)	PLM Height (m)	SVM Height (m)	Total Height (m)	Sunshield Diameter (m)	Case
45	27	72	3.5	1.33	1.17	2.50	**18.9**	Gaia-NIR (Sun+Earth-Shield) Large Orbit

Table 7-5: Sunshield sizing for GaiaNIR S/C

Assuming the same operational orbit for GaiaNIR as for Gaia, with a 15 deg. SSCE and 45 deg Sun aspect angle, a Gaia-like size sunshield is considered to ensure feasibility and limit the cost. The relative shield size increase w.r.t. GaiaNIR SVM + PLM height is used to increase the spin axis w.r.t. the Sun (Sun aspect angle) from 45 to 55 degrees (which would improve science - astrometric performance). The SSCE angle as of Gaia implies not designing for a shielding for Earth and Moon light (accepting the same loss of observation efficiency as on Gaia), but accounting for a 3 deg AOCS margin and 0.53 deg Sun width to mitigate straylight issues. The actual Sun aspect angle set for the spacecraft and to be taken into account in the science evaluations is thus 51.47 degrees. A graphical representation of the S/C attitude and relevant angles (15 deg SSCE angle and 45 deg SAA) is shown in Figure 7-2 below:
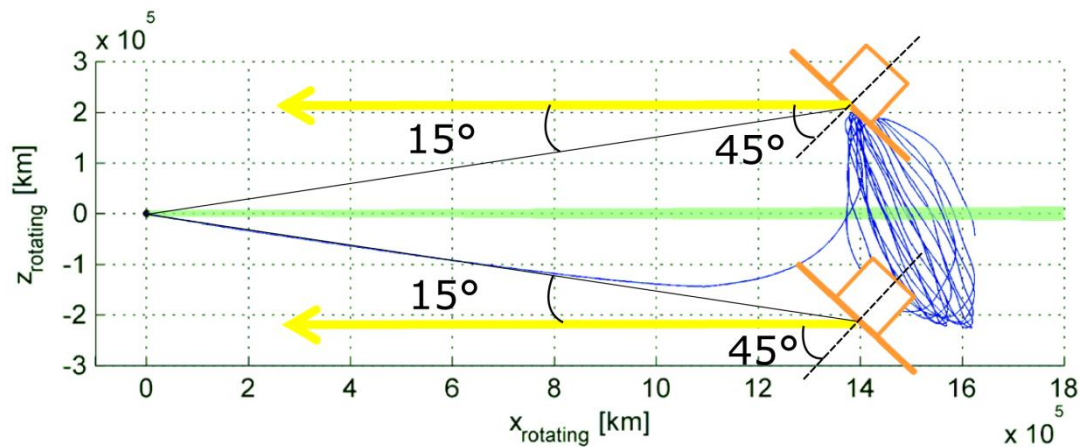
Figure 7-2: GaiaNIR S/C representation with 45 deg SAA and 15 deg SSCE

7.5 Focal Plane Assembly (FPA)

The starting point of the CDF Study was the Focal Plane Assembly (FPA) of Gaia. In Gaia the FPA is common for both telescopes and has the following main functionalities, as presented in RD[34]:

- Metrology Wave-Front Sensing (WFS) and Basic Angle Monitoring (BAM)
- Object detection in the sky mapper (SM1, SM2)
- Astrometry in the astrometric field (AF)
- Low-resolution spectro-photometry using the blue and red photometers (BP and RP)

- Spectrometry using the radial-velocity spectrometer (RVS).

The FPA is shown in Figure 7-4 and carries 106 charge-coupled device (CCD) detectors, arranged in a mosaic of 7 across-scan rows and 17 along-scan strips:
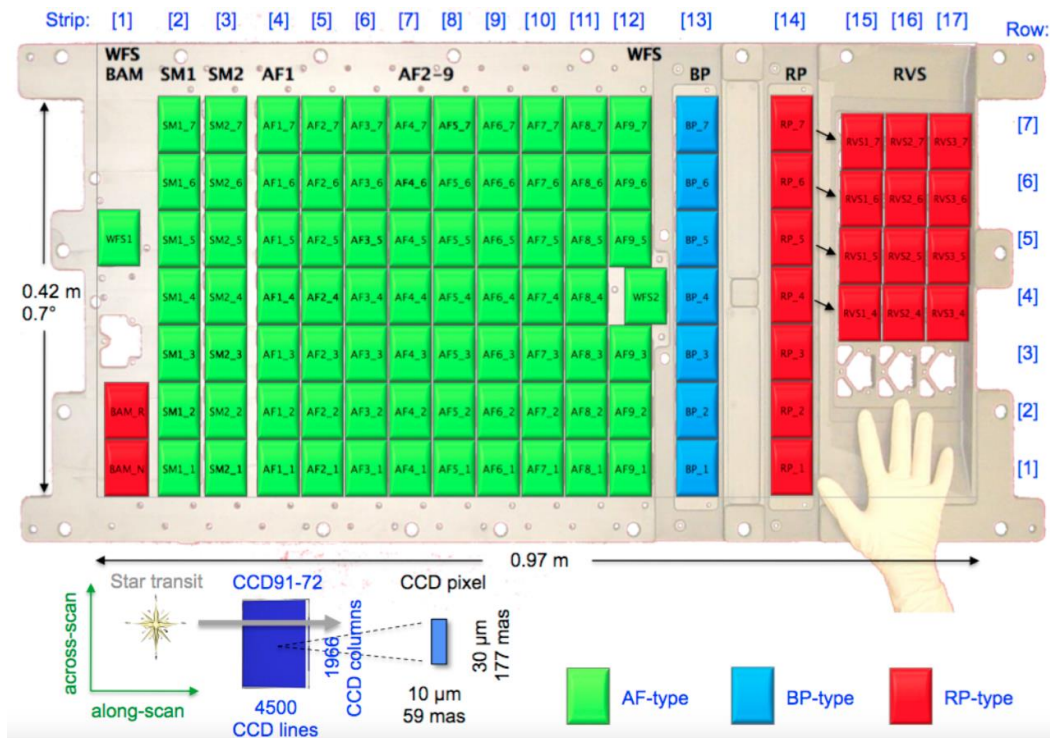
Figure 7-3: Gaia Focal Plane Assembly superimposed on a real picture of the CCD support structure (with a human hand to indicate the scale), with Gaia-specific terminology indicated (e.g. CCD strip and row, TDI line and pixel column)

Even if considered as a starting point for the design for GaiaNIR CDF Study, changing from CCDs to NIR detectors meant that the FPA arrangement had to be reconsidered. Initially, potential FPA arrangement was envisaged with NIR detectors covering all fields as presented in RD[35] and schematically shown in Figure 7-4 below:
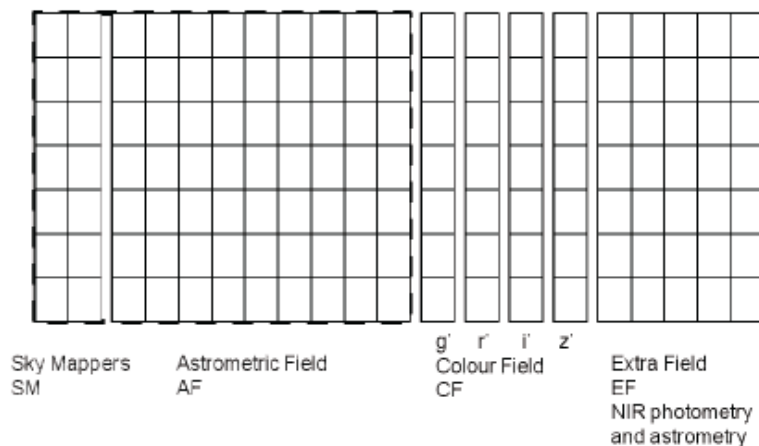
Figure 7-4: Potential FPA Arrangement of GaiaNIR as per RD[35]

Considering the fact that the CDF GaiaNIR is a cost driven study and that the NIR detectors cost more than CCDs detectors, significant modifications compared to Gaia were taking into account for rearrangement of the FPA, excluding the following functionalities compared to Gaia as they were not seen as mission critical:

- Sky mapper (see Appendix B)
- Photometric field and Astrometric field are combined into a single field
- Spectrometry using the radial-velocity spectrometer.

The performance analysis done during the CDF GaiaNIR study lead to a FPA baseline 60 detectors NIR detectors, arranged in 7 across-scan rows and 9 along-scan strips (out of which 8 are for the astrometric/photometric field, divided into 4 photometric fields (4 different cut-off wavelengths) times 2 along-scan strips) as shown in Figure 7-5 below:
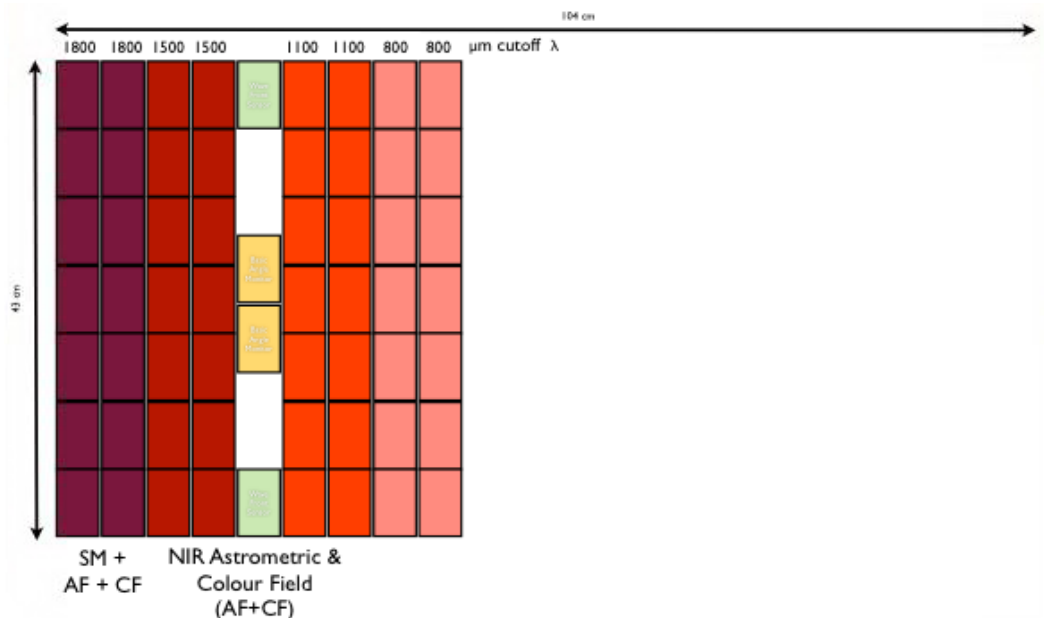
Figure 7-5: GaiaNIR FPA Arrangement

7.6 Telescope Trade-offs

At the beginning of the GaiaNIR CDF Study, a major trade-off regarding the telescope design has been performed. Different options were investigated triggered by the cost reduction exercise of fitting GaiaNIR into an M-class mission:

- 2 telescope and 2 FoVs (as Gaia)
- 1 telescope and 2 FoVs with Hipparcos type design
- 1 telescope and 1 FoV.

The main trade-off considerations are presented in Table 7-6 below:

Telescope type	Complexity	η	Optical quality	BAM	Size / volume	Cost (telescope + BAM + PLM + deployable Sun shield)	Science return
As Gaia	As Gaia with NIR update			As Gaia		Higher than Gaia due to cost of NIR detectors	Better than Gaia due to increases wavebands
1 telescope **2 FoVs with Hipparcos type design**	Gaia-like optics with simplified mirrors:Classical Korsch based on simple conics	50%	For intended FoV 0.6º x 0.47º image quality seems acceptable Image quality defined for longer wavelengths	Possibly simplified compared to Gaia	~½ Gaia	Optics cost lower than Gaia due to reduction in optical elements No sky mapper The cost of the NIR detectors still a driver, as NIR detectors cost more per unit than the Gaia CCDs	Better than Gaia due to increases wavebands, but performance reduced by $1/\sqrt{2}$
1 telescope **1 FoV**	As Gaia but on 1 FoV only			No	½ Gaia	No sky mapper needed to assign a star to a FoV, but for TDI TBC	No absolute astrometry No maintenance of Gaia optical reference frame No improvement in proper motions and parallax Only NIR astrometry relative to Gaia Vis optical reference frame

Table 7-6: GaiaNIR Telescope Trade-off Overview

7.7   System Trade-Offs

7.7.1   System Level Trade-offs

Several system level trade-offs have been performed for the GaiaNIR CDF Study. The main driver for the system trade space is the observation strategy which drives also the choice of the detectors:

- Spinner S/C (Gaia like) with TDI detectors
- Spinner S/C (Gaia like) with "standard" NIR detectors
- Spinner S/C (Gaia like) with "standard" NIR detectors and de-spin mechanism
    - De-spin mechanism for the entire P/L
    - De-spin mechanism in the optical path for the mirror only
- Step&Stare observation strategy with "standard" NIR detectors.

Each system level trade-off is summarised the following sections.

7.7.1.1   Spinner S/C (Gaia like) with TDI detectors

Although not fully investigated during the GaiaNIR CDF Study, no immediate S/C design related showstoppers were identified for a Gaia-like spinning type S/C using TDI NIR detectors. The major open point remains the feasibility of such detectors and the related development costs, which have to be further investigated in a dedicated technology development activity. A high level system budget is shown in Section 7.11 System Options, highlighting the major design implications of embarking TDI NIR detectors on a GaiaNIR type S/C.

Assuming the detectors developments is possible, this solution would be feasible and simpler than the current GaiaNIR baseline (see 7.9), but this baseline is still valid in terms of the design of other subsystems (e.g. thermal design consistent with both options).

7.7.1.2   Spinner S/C (Gaia like) with "standard" NIR detectors

The Gaia-like spinning type S/C embarking "standard" NIR detectors, although at a first glance looking promising, was quickly discarded because of non-compliance with observation requirements (e.g. the integration time of the detectors of ca. 4.4s is not compatible with the S/C Gaia-like spinning type).

7.7.1.3   Spinner S/C (Gaia like) with "standard" NIR detectors and de-spin mechanism

The integration time required by the "standard" NIR detectors led to investigating two different sub-options where the focus is on a de-spin type concept that allows the detectors the necessary time to capture and integrate the image. The mechanism then catches up with the GaiaNIR S/C attitude.

7.7.1.3.1   De-spin mechanism for the entire P/L

The concept of using a de-spin mechanism for the entire P/L was found to have several drawbacks and deemed to be unfeasible for the GaiaNIR CDF Study. The following considerations were made during the investigation:

- The TRL for such a de-spin mechanism is deemed to be currently very low (e.g. TRL=1)
- The high complexity of developing such a mechanism and its overall system impacts such as:
  o Continuous high power demand
  o Heat generation in close vicinity of the optical bench
  o Introducing vibration/jitter.

7.7.1.3.2 *De-spin mechanism in the optical path for the mirror only*

No immediate show stoppers were identified for the Gaia-like spinning S/C with "standard" NIR detectors and a de-spin mirror mechanism concept. The dedicated activity for the mirror de-spin mechanism technology for GaiaNIR is proposed to be further initiated in order to confirm full technical feasibility of the observation strategy. The CDF Study focused on a preliminary assessment of the concept investigating:

- Piezo actuated de-spin mechanisms
- Thermal stability
- Range, accuracy, knowledge and lifetime of the mechanism.

This is selected as the current GaiaNIR baseline. Further details regarding the de-spin mirror mechanism and its impacts are given in the Mechanism and GNC Chapters.

7.7.1.4 Step&Stare observation strategy with "standard" NIR detectors

Two options were considered for the actuators in order to cover the entire Step&Stare trade space:

- Using micro-propulsion thrusters which require:
  o A slew time of ca. 57.1s with a maximum thrust of 1.0 mN and 54.4 kg/year of propellant.
  o A slew time of ca. 40.4s with a maximum thrust of 2.0 mN and 109 kg/year of propellant.
  o Taking into account also the integration time needed for the detectors leads to the need for a mission duration of several decades as minimum to cover the same observation scheme as Gaia, as well as very high propellant loads even for a 5-year mission.
- Using Reaction Wheels and micro-propulsion thrusters, which results in mechanical and thermal noise impacting the quality of the scientific data. For the Reaction Wheels the step time reads in 5.7s (0.1 Nm) and 4.04 s (0.2 Nm). On top of this, it is necessary to take into account the additional time for tranquilisation to cope with sloshing and other possible flexible modes (Gaia sunshield first mode is about 1Hz). Also here the durations are incompatible with a 5-year mission and the required science coverage.

Considering these Step&Stare results, at system level it has been decided to baseline the Gaia-like spinning solution, but with a de-spin mechanism in the optical path for the mirror only.

Taking into account the above presented considerations, Figure 7-6 is graphically summarising the system level trade-offs:
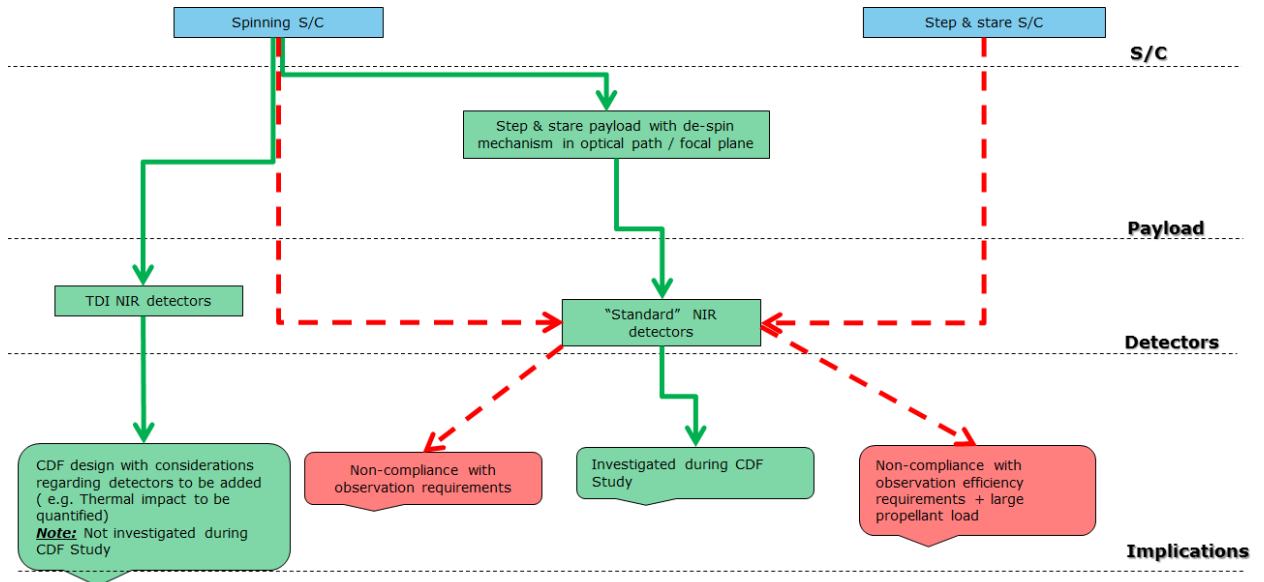
Figure 7-6: GaiaNIR System Level Trade-Offs Summary

7.7.2 Subsystem Level Trade-offs

Throughout the GaiaNIR CDF Study, several subsystem level trade-offs have been performed. An overview of the relevant trade-offs is outlined in Table 7-7 while further details are provided in the corresponding subsystem chapters in the present report.

Guidance Navigation and Control	Micro-propulsion Thrusters vs. RWs Micro-propulsion Thrusters
Communications	X-band vs. X-band + K-band Mechanical steering vs. Fixed Antenna
Propulsion	Mono-propulsion vs. Bi-propulsion
Thermal Control	Payload Cooling: Active vs. Passive vs. Mixed Cooling
Mechanisms	De-spin mechanism for the entire P/L vs. Mirror de-spin mechanism
Detectors	TDI vs. Standards MCT vs. APD

Table 7-7: GaiaNIR Subsystem Level Trade-offs

7.8 Mission Architecture

The key characteristics of the GaiaNIR mission are presented in the Table 7-8 below:

Mission Description	
Launch Vehicle	Dedicated launch with Ariane 62 from Kourou
Launch Date	2035
Transfer	Direct transfer by launcher
Orbit	Small amplitude Lissajous orbit at L2
Operations	Nominal operations: 5 years
	Mission operations centre (MOC) at ESOC
	Science operations centre (SOC) at ESAC
Ground stations	ESTRACK Core ground station 35m antenna network: Cebreros (Spain), New Norcia (Australia) and Malargüe (Argentina)

Table 7-8: GaiaNIR Mission Architecture

7.8.1 Mission phases

The following mission phases and their durations have been defined for GaiaNIR:

- Launch and Early Orbit Phase, duration: < 5 hours
- Transfer and commissioning Phases, duration: 0.5 years
- Nominal Operations Phase, duration: 5 years
- Decommissioning Phase, duration: few days (TBC)

The on-ground phases before and after launch are the Pre-Launch Phase and the Post-Operations Phase, respectively.

7.8.2 System Modes

During the GaiaNIR CDF Study, the system modes have been discussed and established. An overview of all system modes is shown in Table 7-9 below with the relevant equipment switched on or off identified and further used as input for the power subsystem sizing.

Launch Mode	• PLM off • Telecommand on • PCDU on
Sun Acquisition Mode	• PLM off • FPA survival heaters on • Telemetry on • Some thrusters on • PCDU on
Safe Mode	• FPA survival heaters on • SVM survival heaters on • Some thrusters on • PCDU on • Atomic clock switched on
Decontamination Mode	• Both FPA decontamination and survival heaters on simultaneously • Some thrusters on • Telemetry on • PCDU on • MPT off
Orbit Control Mode	• FPA on (incl. Atomic clock switched on) • Some thrusters on • TT&C on • PCDU on • PAA on
Science and Transmitting Mode	• FPA on (incl. Atomic clock switched on) • TT&C on • MPT on • PCDU on • PAA on

Table 7-9: GaiaNIR System Modes

7.9　System Baseline Design

The GaiaNIR design sessions focused on the spinning Gaia-like S/C with "standard" NIR detectors and a mirror de-spin mechanism. A summary of both the PLM and the SVM are provided in the following sections. The starting point for the CDF Study design is the Gaia mission. When considered suitable, Gaia equipment is reused for the GaiaNIR S/C design, otherwise new units are proposed in line with the GaiaNIR S/C needs.

7.9.1　PLM Summary

The starting point for the GaiaNIR PLM design is a Gaia-like optics with simplified mirrors (NIR telescope): classical Korsch based on simple conics. Compared to the Gaia concept (2 telescopes and 2 FoV), the GaiaNIR design makes use of the Hipparcos concept having 2 mirrors at entrance pupil point at different angle and a reduced FoV compared to Gaia. A radial Velocity Spectrometer nor a Sky Mapper were considered required for the GaiaNIR FPA. The need for a Basic Angle Monitoring (BAM) was discussed and acknowledged during the CDF Study design session. Currently the reference Gaia BAM is taken into account but future analysis in line with the new PLM design should be considered.

The following detectors with their associated characteristics were selected for the GaiaNIR mission. A complete detectors trade space is provided in Detectors Chapter 5.2.

- 60 Hawaii-2RG Teledyne NIR detectors
  - Operating temperature 140K
  - FEE operating temperature: 300K
  - Power dissipation
    - Detector: ≤ 4mW at 100KHz
    - FEE: ≤ 300mW at 100KHz
    - Detector: ≤300mW at 10MHz
    - FEE: ≤1W at 10MHz

7.9.2   SVM Summary

The GaiaNIR SVM design is very similar to the Gaia design comprising mechanical, structural, thermal elements supporting the instrument and the spacecraft electronics. However, the obsolescence of reference Gaia equipment should be kept in mind considering that the GaiaNIR launch date is 2035 (equivalents of high-TRL standard SVM equipment will also then be available by then, but very mission specific Gaia equipment like the PAA, cold-gas micropropulsion, BAM and large SiC structure technology may not).

As the GaiaNIR PLM is further consolidation in subsequent design phases, some SVM subsystems will be impacted w.r.t. the Gaia reference design in order to accommodate the PLM, e.g thermal, structures, TT&C and DHS. Details regarding each of the SVM subsystem are provided in dedicated sections of this report.

7.10 System Budgets

7.10.1   Mass Budgets

The total launch mass of the GaiaNIR S/C is 2328.03 kg, including 20% PLM system margin and 10% SVM systems margin, 75 kg light launch vehicle adapter and 362 kg of propellant. The system margin was set to 20% for the PLM due to complete redesign compared to Gaia and 10% for the SVM due to reuse of Gaia reference equipment with some required modifications, which should provide improved confidence on the mass budgets.

The mass of the GaiaNIR S/C is given in below:

PLM Mass Budget		Margin (%)	Mass [kg]
Attitude, Orbit, Guidance, Navigation Control		0.00	0.00
Communications		0.00	0.00
Chemical Propulsion		0.00	0.00
Detectors		15.41	45.91
Data-Handling		20.00	4.80
Mechanisms		15.00	11.50
Optics		0.00	231.21
Power		0.00	0.00
Structures		0.00	260.7
System Engineering		0.00	0.00
Thermal Control		13.01	127.2
Harness	0%		0.00
Dry Mass w/o System Margin			681.30

Table 7-10: Payload Module Mass Budget

SVM Mass Budget		Margin (%)	Mass [kg]
Attitude, Orbit, Guidance, Navigation Control		9.75	23.01
Communications		8.96	32.36
Chemical Propulsion		6.99	122.06
Data-Handling		6.56	20.46
Mechanisms		6.58	202.5
Power		10.00	59.10
Structures		0.00	418.80
System Engineering		0.00	0.00
Thermal Control		16.08	50.92
Harness	5%		46.46
Dry Mass w/o System Margin			975.67

Table 7-11 Service Module Mass Budget

S/C Mass Budget		Mass [kg]
Dry Mass PLM		**681.30**
Dry Mass SVM		**975.67**
System Margin SVM	10%	97.57
System Margin PLM	20%	136.26
Dry Mass incl. System Margin		**1890.80**
CPROP Fuel Mass		114.35
CPROP Oxidizer Mass		188.68
CPROP Pressurant Mass		1.59
AOCS MPT Propellant		57.6
Total Wet Mass		**2253.03**
Launcher Adapter		75.00
Wet Mass + Adapter		**2328.03**

Table 7-12 Combined Mass Budget

Table 7-13 shows the detailed mass budget summary for each subsystem of the S/C, for both PLM and SVM:

	#	Mass (kg)	Total Mass (kg)	Mass margin (%)	Mass incl. margin (kg)
PLM (Payload Module)			**658.23**	**3.51**	**681.30**
OPT			**231.21**	**0**	**231.21**
Mirrors (Mirrors)	1	102.78	102.78	0	102.78
AFP (Astro Focal Plane)	1	109.36	109.36	0	109.36
BAM (Basic Angle Monitoring & Harness)	1	19.08	19.08	0	19.08
STR			**260.70**	**0**	**260.70**
Mirror_Support (Mirror Support Structure)	1	260.70	260.70	0	260.70
DH			**4.00**	**20**	**4.80**
ICU (Instrument Control Unit)	1	4.00	4.00	20	4.80
MEC			**10.00**	**15**	**11.50**
DeScan_mech (DeScan Mechanism)	1	5.00	5.00	20	6.00
M2_RFM (M2 Refocussing Mechanism)	1	5.00	5.00	10	5.50
TC			**112.54**	**13**	**127.18**
MLI (Multi Layer Insulation)	1	41.9	41.9	5	44
TC_MISC (Thermal Hardware Misc.)	1	8.6	8.6	5	9.03
TC_RAD (Radiator)	1	51.78	51.78	20	62.14
TC_RAD_BLK (Radiator Black Paint)	1	1	1	5	1.05
TC_STRAP (Thermal Strap)	1	8.3	8.3	20	9.96
HTR_PLM (Heater PLM)	1	0.96	0.96	5	1.01
DET			**39.78**	**15.41**	**45.91**
Detector_01 (Detector)	60	0.46	27.60	20	33.12

FEE_01 (Front End Electronics)	60	0.14	8.58	5	9.01
SCS_01 (Sensor Chip System)	60	0.06	3.60	5	3.78
SVM (Service Module)			**887.18**	**4.36**	**925.88**
STR			**418.80**	**0**	**418.80**
SVM_Misc (SVM Miscellaneous)	1	10.00	10.00	0	10.00
SVM_Prim_Structure (SVM Primary Structure)	1	236.40	236.40	0	236.40
SVM_Sec_Structure (SVM Secondary Structure)	1	92.60	92.60	0	92.60
Thermal_Tent_GaiaNIR (Thermal Tent Gaia NIR)	1	79.80	79.80	0	79.80
AOGNC			**20.97**	**9.75**	**23.01**
CRS_1 (Coarse Rate Sensor #1)	2	1.40	2.80	10	3.08
STR_AASTR_1 (STR Galileo/Leonardo AA-STR #1)	2	2.40	4.80	10	5.28
SUN_BradTNO_FSS_1 (SUN Bradford TNO Fine Sun Sensor #1)	3	0.36	1.07	5	1.12
IMU_Astrix_200 (IMU Airbus Astrix 200+)	1	12.30	12.30	10	13.53
COM			**29.70**	**8.96**	**32.36**
X_Band_RFDN (X Band Radio Frequency Distribution Network)	1	2.00	2.00	5	2.10
X_LGA_1 (X Band Low Gain Antenna #1)	2	0.25	0.50	5	0.53
X_XPND_1 (X Band Transponder #1)	2	3.50	7.00	10	7.70
PAA (Phased Array Antenna)	1	6.00	6.00	10	6.60
PAA_DCDC_Converter (Phased Array Antenna DCDC Converter)	1	3.50	3.50	5	3.68
PAA_RF_Splitter (Phased Array Antenna RF Splitter)	1	0.20	0.20	5	0.21
PAA_BFN_1 (PAA BFN Module 1)	7	1.50	10.50	10	11.55
CPROP			**114.1**	**6.99**	**122.1**
Cold_Flow_Sensor_01 (Coldgas_Micro_Flow_Sensor)	12	0.43	5.10	5	5.36
Cold_HP_Filter (Coldgas_HP_Filter)	1	0.08	0.08	5	0.08
Cold_HP_T_1 (Coldgas_High_Pressure_Transducer)	2	0.22	0.43	5	0.45
Cold_HPLV_1 (Coldgas_Latch_Valve_HP)	2	0.80	1.60	5	1.68
Cold_LP_Filter_1 (Coldgas_LP_Filter)	2	0.02	0.05	5	0.05
Cold_LP_FVV_1 (Coldgas_LP_FillVent_Valve)	2	0.07	0.14	5	0.15
Cold_LP_T_1 (Coldgas_Low_Pressure_Transducer)	2	0.25	0.50	5	0.53
Cold_LPLV_1 (Coldgas_Latch_Valve_LP)	2	0.34	0.68	5	0.71
Cold_Pipes (Coldgas_Pipes)	1	3.00	3.00	20	3.60
Cold_Thruster_1 (Coldgas_Thruster #1)	12	0.18	2.10	5	2.21
Cold_Tank_1 (Coldgas_Tank #1)	3	22.70	68.10	5	71.51
Cold_HP_FVV (Coldgas_HP_FillVent_Valve)	1	0.21	0.21	5	0.22
Biprop_Pres_Tank (Biprop_Pressurant_Tank)	1	8.20	8.20	5	8.61

Equipment	Qty				
Biprop_Prop_Tank_1 (Biprop_Eurostar2000_Tank #1)	2	10.70	21.40	10	23.54
Biprop_Thruster_1 (Biprop_Thruster #1)	16	0.65	10.40	5	10.92
Biprop_FDV_01 (Biprop_FillDrain_Valve)	13	0.07	0.91	5	0.96
Biprop_Filter_1 (Biprop_Filter)	3	0.07	0.21	5	0.22
Biprop_HP_Trans (Biprop_HP_Transducer)	1	0.22	0.22	5	0.23
Biprop_LV_1 (Biprop_Latch_Valve)	4	0.55	2.20	5	2.31
Biprop_NRV_1 (Biprop_Non_Return_Valve)	4	0.10	0.40	5	0.42
Biprop_Pipes (Biprop_Pipes)	1	5.00	5.00	20	6.00
Biprop_PR (Biprop_PressureRegulator)	1	1.20	1.20	5	1.26
Biprop_LP_Trans_1 (Biprop_LP_Transducer)	2	0.25	0.50	5	0.53
Biprop_PV_01 (Biprop_Pyro_Valve)	11	0.16	1.76	5	1.85
Cold_PR (Coldgas_Pressure_Regulator)	1	1.20	1.20	5	1.26
DH			**19.20**	**6.56**	**20.46**
OSCAR (On board computer OSCAR)	1	5.20	5.20	5	5.46
RTU (Remote Terminal Unit)	1	7.00	7.00	10	7.70
SSMM (Solid State Mass Memory)	1	3.00	3.00	10	3.30
DPU (Data Processing Unit)	1	4.00	4.00	0	4.00
PWR			**53.73**	**10**	**59.10**
BAT (Battery)	1	29.33	29.33	10	32.26
PCDU (Power Conditioning & Distribution Unit)	1	12.00	12.00	10	13.20
SA_2 (SolarArray #2)	1	12.40	12.40	10	13.64
MEC			**190.00**	**6.58**	**202.5**
Dep_SSH (Deploayble Sunshield)	1	134.00	134.00	5	140.70
Rad_HDRM (Radiator Hold Down and Release Mechanism)	1	20.00	20.00	20	24.00
L_Bpod (Launch Bipods)	1	36.00	36.00	5	37.8
TC			**43.87**	**16.08**	**50.92**
MLI (Multi Layer Insulation)	1	6.7	6.7	5	7.04
TC_MISC (Thermal Hardware Misc.)	1	3.2	3.2	5	3.36
HTR (Heater Lines)	1	0.95	0.95	5	1.00
TC_RAD (Radiator)	1	32.4	32.4	20	38.88
TC_RAD_BLK (Radiator Black Paint)	1	0.62	0.62	5	0.65

Table 7-13: Equipment List

7.10.2 Power Budgets

Based on the system modes in section 7.8.2, the power duty cycles for all equipment have been established together with the domain experts. An overview of the power budgets is provided in the table below and detailed power sizing and power demands of each equipment per system mode is provided in Power Chapter 6.6.

Equipment	P_on	P_s tby	P_duty_cyc LM	P_duty_cyc SAM	P_duty_cyc SM	P_duty_cyc DM	P_duty_cyc OCM	P_duty_cyc STM
Biprop_HP_Trans	0.3	0.3	-1	0.05	0.05	0.05	0.7	-1
Biprop_LP_Trans	0.8	0	-1	0.05	0.05	0.05	0.7	-1
Biprop_LV	30	0	-1	0.05	0.05	0.05	0.7	-1
Biprop_Thruster	3.5	0	-1	0.05	0.05	0.05	0.7	-1
Cold_Flow_Sensor	0.15	0	-1	-1	-1	-1	-1	1
Cold_HP_T	0.3	0	-1	-1	-1	-1	-1	1
Cold_HPLV	29	0	-1	-1	-1	-1	-1	0.01
Cold_LP_T	0.8	0	-1	-1	-1	-1	-1	1
Cold_LPLV	29	0	-1	-1	-1	-1	-1	0.01
Cold_Thruster	4.5	0	-1	-1	-1	-1	-1	1
CRS	5	0	-1	1	1	1	1	1
DeScan_mech	0.02	0	-1	-1	-1	-1	-1	1
Detector	0.3	0	-1	-1	-1	-1	1	1
DPU	40	24	-1	-1	-1	-1	-1	1
FEE	0.2	0	-1	-1	-1	-1	1	1
FPA	156.4	0	-1	-1	-1	-1	1	1
HTR	378.8	0	1	0.81	0.81	0.61	-1	-1
HTR_2	438.1	0	0.285	0.285	0.285	1	0.002	-1
ICU	40	15	-1	-1	-1	-1	-1	1
IMU_Astrix_200	32	0	-1	1	1	1	1	1
M2_RFM	1	0	-1	0.5	-1	-1	-1	1
OSCAR	15	10	1	1	1	1	1	1
PAA_BFN_block	43.6	0	-1	-1	-1	-1	1	1
PAA_DCDC_Converters	33	0	-1	-1	-1	-1	1	1
PCDU	30	0	1	1	1	1	1	1
RTU	14	14	1	1	1	1	1	1
SSMM	10	10	-1	-1	-1	-1	-1	1
STR_AASTR	4.5	0	-1	-1	-1	1	1	1
SUN_BradTNO_FSS	0.2	0	-1	1	1	1	1	1
X_XPND	27.3	10	-1	0.1	0.1	0.1	1	1

Table 7-14: Estimated power budget

7.11 System Options

The CDF Study focused on a design for a spinner S/C (Gaia-like) with "standard" NIR detectors and de-spin mirror mechanism in the optical path. The other potential system option deemed feasible during the CDF Study, the spinner S/C (Gaia-like) with TDI detectors was not further investigated due to the lack of maturity of the required

detectors. However, a system level mass budget shown in Table 7-15 and Table 7-16 was put in place highlighting the major areas that are likely to change due to new development of the TDI detectors.

PLM Mass Budget	Margin (%)	Mass [kg]
Attitude, Orbit, Guidance, Navigation Control	0.00	0.00
Communications	0.00	0.00
Chemical Propulsion	0.00	0.00
Detectors	TBD	TBD
Data-Handling	20.00	4.80
Mechanisms	10.00	5.50
Optics	0.00	231.21
Power	0.00	0.00
Structures	0.00	260.7
System Engineering	0.00	0.00
Thermal Control	13.01	127.2
Harness	0%	0.00

Table 7-15: High Level Payload Module Mass Budget for Spinner S/C (Gaia-like) with TDI Detectors Option

Note: The de-scan mechanism is not part of the budget in Table 7-15.

SVM Mass Budget	Margin (%)	Mass [kg]
Attitude, Orbit, Guidance, Navigation Control	9.75	23.01
Communications	8.96	32.36
Chemical Propulsion	6.99	122.06
Data-Handling	6.56	20.46
Mechanisms	6.58	202.5
Power	10.00	59.10
Structures	0.00	418.80
System Engineering	0.00	0.00
Thermal Control	16.08	50.92
Harness	5%	46.46

Table 7-16: High Level Service Module Mass Budget for Spinner S/C (Gaia-like) with TDI Detectors Option

8   GROUND SEGMENT & OPERATIONS

8.1   Requirements and Design Drivers

The primary requirements and design drivers for the Ground Segment and Operations is based on the re-use of the facilities and approaches used for the Gaia mission.

For the GaiaNIR Mission Operations Centre (MOC), considering that the launch date is assumed to be in 2035, the re-use of the Gaia MOC mission control systems and infrastructure is not realistic due to ageing of the systems. The MOC control system for GaiaNIR would be developed new based on the available infrastructure at the time using experience from the Gaia mission.

Based on the current communication requirements, the ESA 35m antenna network would be baselined.

Due to the same operational principle of a spinning satellite with pre-defined scan law, unbiased object detection, iterative ground processing and self-calibrating approach, the same functionality and performance of the Science Ground Segment (SGS) for GaiaNIR mission compared to the Gaia mission would be needed, including the interface to the MOC. The processing of spectroscopic data is however not required for GaiaNIR, since this instrumental function is not foreseen in the GaiaNIR design.

Gaia heritage can be assumed for the SGS data processing and archive design, but - as for the MOC systems - re-use of software and infrastructure is not realistic due to the large time gap. Science Operations Centre (SOC) commanding system, data processing pipelines and mission and science data archives would be developed new for GaiaNIR.

The baseline detector systems of hybrid Mercury-Cadmium-Telluride detectors with CMOS multiplexor (Teledyne Imaging Sensor H2rg), the front-end readout electronics (Teledyne Imaging Sensor SIDECAR) and the implicit non-TDI operation will require a larger traditional calibration component than in Gaia to address non-linear instrumental effects. The large increase of the number of needed geometric calibration parameters will be a challenge for the self-calibration concept.

Operational requirements for Gaia such as regular payload decontamination and refocusing, science and auxiliary instruments operation and on-board processing parameter tuning and maintenance would require a similar level of SGS support for GaiaNIR.

1.1   Assumptions and Trade-Offs

Assumptions	
1	The GaiaNIR MOC is assumed to be implemented at ESOC, Germany.
2	The communications frequency is currently baselined as X-Band for both Science and TT&C usage. X-Band with increased data rate and K-Band (25.5 to 27 GHz) are considered as options.
3	The total Science data to be downlinked is in the order of 301 Gbit/day (including margins).
4	9 to 12 hours of ground station coverage per day is assumed.
5	Maximum downlink bit rate is currently calculated as 9.51 Mbps. (see Service Module Telecommunications section.)

	Assumptions
5	Instrument operational complexity is assumed to be low for routine science data takes. This is however dependent on the instrument design evolution.
6	Use of phased array antenna is assumed. Communication links can be executed in parallel to science observations.
7	The GaiaNIR SGS consists of the GaiaNIR Data Processing and Analysis Consortium (DPAC) with the ESA SOC implemented at ESAC as integral part of DPAC. SOC responsibilities within DPAC are assumed to be unchanged with respect to the Gaia mission.
8	No on-board science data priority scheme with selective downlink and regular data deletion is assumed. All data is marked for downlink and time-ordered as observed.
9	The redundancy factor between number of individual observations and number of fitted parameters in the self-calibrating approach is large enough for the iterative solution to work.
10	No sky-mappers are needed and the FoV assignment is done on-ground from the science data processing.

8.2 MOC and Ground Stations Baseline Design

8.2.1 Ground Stations

The ESTRACK Core ground station 35m antenna network would be used to support the GaiaNIR mission. This includes the use of Cebreros (Spain), New Norcia (Australia) and Malargüe (Argentina). No use of external ground stations is envisaged.

The capability of the 35m antenna network, within the timescale of the GaiaNIR mission (launch 2035), is assumed to support both Ka (32GHz) Far Earth frequency, and K Band (25.5 to 27 GHz) Near Earth frequency. The station upgrades to support K-Band are currently foreseen within the 35m development plan to support the Euclid mission. The 35m ground stations currently all support X-Band and, dependent on the modulation selected, can support downlink data rates of up to 1.2 Mbps for PCM/PSK/PM, 8Mbps for BPSK and 16Mbps for QPSK and GMSK modulation. The current proposed communications design for GaiaNIR includes implementation of the QPSK modulation for the high data rate TM. If higher X-Band data rates (>16 Mbps) are to be supported, ground station TM processor upgrades would be required for the X-Band processors.

The NNO2 4.5m X-Band antenna would be used during the LEOP phase to support the first acquisition of signal activities.

Ranging capability is assumed to be executed in parallel to the data downlink activities, implying that the duration of the ground station passes can be maximised for data downlink without having to reserve windows during the passes for ranging only activities.

8.2.2 MOC Baseline Design

The GaiaNIR S/C would be operated and controlled by ESA from the European Space Operations Centre (ESOC) in Darmstadt, Germany. All operations phases covering LEOP, commissioning, transfer to L2 orbit, routine and de-orbiting phase would be supported from ESOC.

The platform and payload definition at this stage is such that no specifically complex operations are foreseen. The payload operations are assumed to be of low complexity for routine observations. Payload calibration activities are still however to be further defined as the payload design matures. The use of the PAA allows for the science operations to be executed independent of the communication windows, which reduces the mission planning iterations needed for defining the onboard commanding timelines. This reduces complexity on the mission planning process.

The data handling subsystem is sized such that the constraints currently existing on Gaia for data storage and priority downlink would not be experienced on GaiaNIR, allowing for a simpler repetitive operations approach for science data storage and retrieval.

The use of CFDP Class 2 'Reliable Transfer' is assumed as baseline for this type of mission in the 2035 launch time range. Use of the CFDP protocols simplifies and automates the operations from the ground to ensure data completeness.

The robustness of the mission to lost/failed ground station passes, implementation of autonomous operations and the period for survival without ground station coverage are assumed as below allowing for an efficient approach to operations whilst maintaining mission safety.

- S/C to operate nominally without loss of stored science or HK for ~4 days.
- S/C to survive without ground contact for ~6 days in all mission phases.
- S/C design to ensure sufficient autonomy to allow for full autonomous operations for at least ~4 days.

Lessons-learnt from Gaia would be included in the overall MOC design.

8.3 SOC Baseline Design

The SOC baseline design would be based on the Gaia architecture and scope. Within DPAC and removing the spectroscopic data processing, 8 Coordination Units (CUs) and 5 Data Processing Centres (DPCs) would be foreseen to cover the archive and catalogue access and the functional processing needs for the Level 0 to Level 3 processing, which includes the Initial Data Treatment and First Look (IDT/FL), the core Astrometric Global Iterative Solution (AGIS), the photometric processing, complex object processing, variability analysis and astrophysical characterisation. SOC would be responsible for System/IT architecture, mission planning and scheduling, instrument and payload operation including calibration, interface to MOC, AGIS and the mission and science data archives developments at ESAC. Furthermore it will host one of the DPCs dedicated to the IDT/FL and AGIS processing and participate in the data quality assessment, catalogue access and community support.

Mission planning activities would be based as in Gaia on inputs from a pre-defined 5-year full-sky scan law and cadence of regular calibration observations. Redundancy of observations would not require any short-term re-planning due to failed observations.

Instrument and payload operations support cover opto-mechanical performance maintenance through decontamination scheduling, M2 refocusing, de-scan mirror and basic angle monitor performance analysis, as well as parameter tuning and maintenance

in the areas of object detection, spurious object rejection, adaptive window extraction and binning, AOCS feedback and compression/de-compression.

The archives and pipelines would be dimensioned to handle a larger amount of data than foreseen for Gaia (small factor increase), which should not pose any difficulties for the assumed GaiaNIR launch date of 2035.

Lessons-learnt from Gaia would be included in the overall SGS design such as having an effective DPAC project office working early-on in the mission for overall coordination of DPAC activities and interfaces.

9   TECHNICAL RISK

9.1   Reliability and Fault Management Requirements

The following reliability and fault management requirements were proposed for the GaiaNIR mission.

ID	Requirement
REQ-01	The overall reliability of the mission shall be ≥ 85% at end of life.
REQ-02	The lifetime* of S/C shall be compatible with the mission requirement.
REQ-03	Single-point failures with a severity of catastrophic or critical (as defined in ECSS-Q-ST-30C/40C) shall be eliminated or prevented by design.
REQ-04	Single-point failures (other than catastrophic or critical) shall be avoided in the design of the mission units.
REQ-05	Retention of single-point failures of any severity in the design shall be declared with rationale and is subject to formal approval by ESA.
REQ-06	A failure of one component (unit level) shall not cause failure of, or damage to, another component or subsystem within and between mission units.
REQ-07	The failure of an instrument shall not lead to a safe mode of the mission units.
REQ-08	The design shall allow the identification of on-board failures and their recovery by autonomously switching to a redundant functional path. Where this can be accomplished without risk to spacecraft and instrument safety, such switching shall enable the continuity of the mission timeline and performance.
REQ-09	Where redundancy is employed, the design shall allow operation and verification of the redundant item/function, independent of nominal use.
REQ-10	The design and operation of spacecraft shall be compliant with applicable Space Debris rules *(e.g. ESA/ADMIN/IPOL Space Debris Mitigation for Agency Projects)**
REQ-11	The spacecraft design shall be compliant with applicable safety related launch requirements *(e.g. CSG Safety Regulations)*

*see applicable mission success criteria's **Table 9-3**

** depending on the responsible launch authority and/ or launch operator

Table 9-1: Reliability and Fault Management Requirements

The requirements were reviewed during the course of the study and found to be adequate for the GaiaNIR S/C mission.

9.2   Risk Management Process and Scope of Risk Assessment

Risk management is an organised, systematic decision making process that efficiently identifies, analyses, plans, tracks, controls, communicates, and documents risk in order to increase the likelihood of achieving the project/ study goals. The procedure comprises four fundamental steps:

- **Step 1:** Definition of the risk management policy which includes the project success criteria, the severity & likelihood categorisations, and the actions to be taken on risks
- **Step 2:** Identification and assessment of risks in terms of likelihood and severity
- **Step 3:** Decision and action (risk acceptance or implementation of mitigating actions)
- **Step 4:**
- Monitoring, Communication and documentation and risk acceptance.
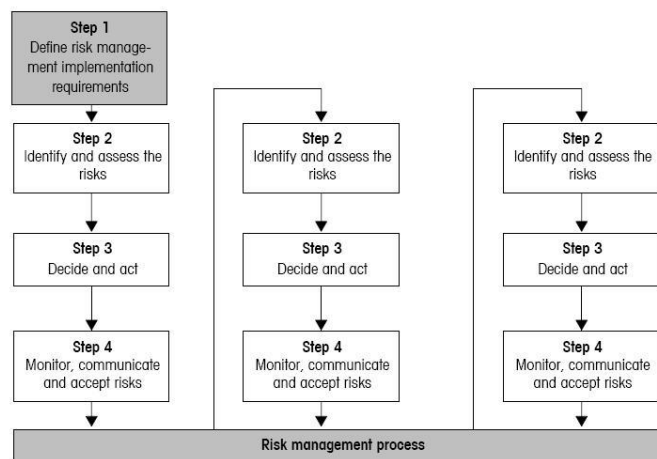
Table 9-2: ECSS-M-ST-80C, 2008 Risk Management Process

The GaiaNIR CDF Study is a pre-phase A feasibility assessment and the results of all 4 steps have to be seen as preliminary. A full documentation of the Risk assessment is premature.

The basis for the preliminary risk assessment is the kick-off documentation/ presentation of the study.. Changes in the kick-off baseline which are caused by identified risks were already seen as mitigation measures.

The scope of the preliminary risk assessment was clearly defined at the beginning and during the study. The risk assessment comprises all mission phases and mission elements.

The preliminary risk assessment for GaiaNIR study considered risk for the following Mission phases

- Mission realisation (project phase)
- Launch preparation and launch
- Lissajous orbit and cruise to/ around L2 (incl. Science operation)
- Disposal manoeuvre

9.3 Risk Management Policy

The CDF risk management policy for GaiaNIR aims at handling risks which may cause serious programmatic/ cost/ schedule/ technological, performance (science)/ technical and safety/ protection* impact on the future project.

* 'Safety' related to the human life and health has a higher priority and importance than 'Safety' related to property and environment. To have a clear split between both safety aspects in the report the term

- *'safety' is used exclusively for risks related to human life and health on ground and in space*
- *'protection' is used exclusively for risks related to equipment, property, and planetary environments (terrestrial, space and specific solar objects)*

9.3.1   Success Criteria

The success criteria with respect to the program, science, technical, safety/ protection safety, schedule, and cost objectives are presented in Table 9-3:

Study/ Risk Domain	Success Criteria
Programmatic	PRO1: GaiaNIR to enlarge the astrometric achievement of Gaia to the astronomical sources which are only visible in NIR in frame of Cosmic Vision 2015-2025: • To maintain the accuracy of the Gaia optical reference frame • To improve the star parallax and proper motion accuracy by revisiting the astronomical sources a number of years after Gaia.
Performance (Science) + Technical	TEC1: The SC operates successfully over the designated mission lifetime of 5.5years TEC2: A reliability of >85% at the end of mission
Safety & Protection	SAF1. Catastrophic hazard (2 Failure/Error Tolerance), • Critical hazard (1 Failure/Error Tolerance) incl. undesired incl. human performance (human related error/failure) SAF2: No SPF can lead to catastrophic hazards; • No performance degradation owing to SPF, and no failure propagation. PRO1: Mission shall be compliant with ESA policy for space debris mitigation
Schedule	SCH1: All architecture elements are available and their FRR successful for the launch (NLT 2035; not binding in terms of specific launch windows) SCH2: The contributions from international partners are available at the relevant milestones of the development schedule SCH3: TRL > 5 (new ISO scale) for all components at the time of mission adoption (est. 2025 to reach NLT 2035) SCH4: Low development risk during Phase B2/C/D
Cost	COS1. CaC for ESA ≤ 770M€* (2015 EC) -> oriented at M4* Class Mission(2014 e.c.).

* The GaiaNIR study has not to be seen as a classical M4 Class Mission; considering the fact of high cost for the NIR detectors the study line for this study was set to 770M€

Table 9-3: Success Criteria

9.3.2   Severity and Likelihood Categorisations

For the GaiaNIR CDF-study, assessment of a 'Preliminary risks' in all project domains like programmatic(pr) , cost(c), schedule(sh), technological readiness (tr), performance(dp)*/technical(dt) and safety(s)/ protection(p) was performed.

Whereby each initial risk in one project domain can be connected or lead to risks (Residual Risks) in other domains as a consequence of its mitigation e.g. the mitigation of technical risks can lead to an impact in other project domains like cost and/ or schedule.

'Performance' is standing for e.g. 'science' incl. 'technological tests' or 'services' (e.g. telecommunication, navigation, cargo)

The severity of the risk scenarios are classified (based on the study baseline) according to their project domains of impact. The consequential severity level of the risks scenarios is defined according to the worst case potential effect with respect to programmatic and science/performance objectives, technical and safety/protection objectives, schedule objectives and/or cost objectives (see Table 9-3).

In addition, identified risks that may jeopardise and/or compromise the GaiaNIR mission will be ranked in terms of likelihood of occurrence and severity of consequence as well for the study baseline as under consideration of possible mitigation actions.

The scoring scheme with respect to the severity of consequence on a scale of 1 to 5 is established in Table 9-4, and the likelihood of occurrence is normalised on a scale of A to E in Table 9-5 and based on recommendations given for the risk assessment in ECSS-M-ST-80C.

Score	Severity	Dependability Performance(Science; dp) & Technical (Dependability) (t)	Safety & Protection (s/p)	Schedule (pr/ sh) incl. technological readiness (pr/ tr)	Cost (pr/ c)
5	Catastrophic	Performance: * Failure leading to the impossibility of fulfilling the mission's performance Technical: failure propagation: * from lower system level to highest system level * from mission to constellation/ campaign level * leading to loss of safety-related barriers	Safety: * Loss of life, life- threatening or permanently disabling injury or occupational illness; * Loss of an interfacing manned flight system Protection: * Severe detrimental environmental effects * Loss of launch site facilities.	Delay results in project cancellation	Cost increase results in project cancellation
4	Critical	Performance: * Failure resulting in a major reduction (70- 90%) in overall performance Technical: * Major damage to flight systems	Safety: * Temporarily disabling but not life- threatening injury, or temporary occupational illness; Protection: * Major detrimental environmental effects. * Major damage to or ground facilities. * Major damage to public or private property	Critical launch delay (24-48 months)	Critical increase in estimated cost (20 -50%)
3	Major	Performance: * Failure resulting in a major reduction (30-70%) in overall performance Technical: * Major degradation of the flight system	Safety: * Minor injury, minor disability, minor occupational illness. Protection: * Minor system or environmental damage	Major launch delay (6-24 months)	Major increase in estimated cost (10 -20%)

Score	Severity	Dependability **Performance**(Science; dp) & **Technical** (Dependability) (t)	Safety & Protection (s/p)	Schedule (pr/ sh) incl. technological readiness (pr/ tr)	Cost (pr/ c)
2	Significant	Performance: * Failure resulting in a substantial reduction (10-30%) in overall performance Technical: * Minor degradation of system (e.g.: system is still able to control the consequences)	Safety: * Impact less than consequences defined for severity level '3-Major'	Significant launch delay (3-6 months)	Significant increase in estimated cost (5 – 10%)
1	Minimum	Performance: * No/minimal consequences (0 - 10%) in overall performance Technical: * No/ minimal consequences	Safety: * No/ minimal consequences * Space Debris Mitigation: casualty risk <10E-4	No/ minimal consequences (1-3 month delay)	No/ minimal consequences (<5%)
0	No	Initial risk fully eliminated	Initial risk fully eliminated	Initial risk fully eliminated	Initial risk fully eliminated

Table 9-4: Severity Categorisation

Score	Likelihood	Definition
E	Maximum	Certain to occur, will occur once or more times per project.
D	High	Will occur **frequently**, about 1 in 10 projects
C	Medium	Will occur **sometimes**, about 1 in 100 projects
B	Low	Will occur **seldom**, about 1 in 1000 projects
A	Minimum	Will **almost never** occur, 1 in 10000 projects

Table 9-5: Likelihood Categorisation

9.3.3   Risk Index & Acceptance Policy

The risk index is the combination of the likelihood of occurrence and the severity of consequences of a given risk item.

Risk ratings of low risk (green), medium risk (yellow), high risk (red), and very high risk (dark red) were assigned based on the criteria of the risk index scheme (see Table 9-6).

The level of criticality of a risk item is denoted by the analysis of the adapted risk index. By policy very high risks are not acceptable and must be reduced (see Table 9-7).

RISK INDEX

Severity Score	* safety related (comp./ funct./ SW/ Human Performanced)					
5	A5	A5*	B5*	C5*	D5*	E5*
5		A5	B5	C5	D5	E5
4	A4		B4	C4	D4	E4
3	A3		B3	C3	D3	E3
2	A2		B2	C2	D2	E2
1	A1		B1	C1	D1	E1
0	no risk					
	A	B	C	D	E
						Likelihood

Safety related (e.g. the 'casualty risk' for controlled re-entry shall be less than 1 in 10000 projects

Table 9-6: generic Risk Index

Risk Index	Risk Magnitude	Proposed Actions (during assessment phase)
C5*, D5*, E5* D5, E5, E4	Very High Risk	**Unacceptable risk:** implement mitigation action(s) - either likelihood reduction or severity reduction through new baseline with appropriate party
B5*, C5, D4, E3	High Risk	**Unacceptable risk:** see above
A5*, B5, C4, D3, E2	Medium Risk	**Acceptable risk for study however unacceptable for project:** therefore implement further reduction action(s) with responsible party/ project partners
A5, A4, B4, B3, C3, C2, D2, D1, E1	Low Risk	**Acceptable risk:** control, monitor; during project seek responsible work package management attention.
A1-3, B2, B1, C1, 0	Very Low ('0' - no) Risk	**Acceptable risk/ no risk:** see above; '0' - no actions to be taken e.g. in case the risk is eliminated

'*' safety related

Table 9-7: Proposed Mitigation Actions

9.4   Risk Drivers

The following risk drivers have been considered in the identification of specific risk items:

- New technologies (TRL)
- Design challenges (mass, volume, power, configuration, lifetime, mission and performance operation, communication)
- Safety, Environmental and Property factors (protection)
- Functional and Reliability issues (science + technical), single point failures (SPFs)
- Major mission events
- Programmatic factors.

9.5   Top Risk Log (preliminary)

Top risk items have been preliminary identified at the mission (ESA) levels. Please refer to Table 9-8 for a complete list of preliminary identified top risks and their corresponding suggested mitigating actions.

The Risk Index results reflecting the initial risk assessment are summarised in Table 9-9a and reflecting the final assessment in Table 9-9b considering mitigation measures as described in the Table 9-8.

The risk numbering (1st column of Table 9-8) is associated to the study internal risk allocation and does not give a ranking according to their importance or any other numerical order.

Risk no./ Title	Risk Classi-fication ----------- Initial Risk Index	Risk Context	Scenario/ *Cause (due to/...)*	Reduc. Action 1 and Remaining Risk / Risk Index	Reduc. Action 2 and Remaining Risk / Risk Index	Reduc. Action 3 and Remaining Risk / Risk Index
				Residual Risk: / Risk Index	Residual Risk: / Risk Index	Residual Risk: / Risk Index
Design & mission realisation						
DI - Gaia 'copy approach'	Program matic/c/ schedule risk(pr/c /sh) **DI_pr** ------------- **E3**	The future GaiaNIR project should be seen as a 'copy' of Gaia project; however between the launch of Gaia (end of 2013) and foreseen start of GaiaNIR mission adoption (2025) is a period of approx. 12 years; for the manufacturing of equivalent parts this period is even longer *Remark: This risk scenario does not address loss of know-how and manufacturing capabilities especially when there is a monopole on certain technologies, e.g. mirror and structure manufacturing (DIVc) and cold gas propulsion (DVIIIb)*	limited applicability of the approach for the program and project planning (even independently from the mentioned period of 12a) might not lead to the expected cost / schedule reduction *due to/ because:...* differences in the programme/ project constellation/ management/ execution (e.g. it is not granted that the prime responsibility for the platform (PF) and payload (PL) will lay in 'one hand' as it was for Gaia; this programme constellation was minimising interface iterations)	Reduction: a) systematic knowledge transfer of information within ESA for programme mgn. related experiences coming from Gaia	Reduction b) it is recommended to keep the 'one hand' approach for the PF and PL prime Risk Reduction via: Likelihood/ severity *Remaining risk: risk scenario remains unchanged with lower likelihood/ severity* **DI_pr** **B5**	Reduction c) PA included in the design and testing loop (especially testing)
DIIb - TRL of NIR detector	Program matic/ schedule risk (pr,sh) **DIIb_pr** ------------- **E5**	other/ not space proven NIR detectors (non-European supplier); *Remark: This risk scenario does not address the expected cost increase caused by change of the type of detector in comparison to Gaia(see OCII)*	Out of 'European control' of possible major project delay *due to/ because:...* low TRL=4 which will stay probably on this level till further developed specifically for GaiaNIR	Reduction: a) orientation of project schedule at the needed time for increase of TRL Risk Reduction via: Remaining risk: **DIIb_pr** **C2**	Reduction: b) timely initiation of an European development (GSDP)* likelihood *remains unchanged with lower likelihood* Residual Risk: further cost/ schedule	

Risk no./ Title	Risk Classi-fication ----------- - Initial Risk Index	Risk Context	Scenario/ *Cause (due to/...)*	Reduc. Action 1 and Remaining Risk / Risk Index Residual Risk: / Risk Index	Reduc. Action 2 and Remaining Risk / Risk Index Residual Risk: / Risk Index	Reduc. Action 3 and Remaining Risk / Risk Index Residual Risk: / Risk Index
				uncertainties – no risk reduction in terms of cost/ schedule; but in terms of better risk control of the process the technical develop-ment should be under European control		
DIId – detector replacement during project implementation	Mainly schedule but also cost risk (sh/c) **DIId_sh** ------------- **D3*** [orange box]	The accessibility/ maintainability of detectors; the need to replace a defect detector even when the detector reliability is seen 'as usual' - this means 'low' – the relatively high numbers of detectors might lead to a 'high' occurrence probability of the risk scenario) Remark: * Severity is estimated as major because of additional cost risk	Significant project delay(additional cost increase) *due to/ because:...* request of a defect detector replacement even	Reduction: a) initial consideration of detector replacement(s) in project planning Risk Reduction via: *Severity(schedule)* Remaining risk: *Remains the same with reduced severity related to schedule* **DIId_sh/c D2** [yellow box]		
DIIIa – PL mecha-nism (data noise)	Performance risk (dp) **DIIIa_dp** ------------- **D4** [red box]	Several mechanism in the PL in constant use before/ after observations	Decreased data accuracy (data noise) *due to/ because:...* movement*/ rotating of mirrors (e.g. micro vibration due to step & stare) and distortion in the system mirror/ mechanism/ counter balance	Reduction: a) Detailed modelling for S/C static and dynamic cases with and implementation of of Gaia lessons learnt Risk Reduction via: Remaining risk: **DIV_dp** **D3**	Reduction: b) rigorous use of rattle-free mechanisms likelihood/ severity *remains unchanged with decreased likelihood/ severity* [orange box]	~~Reduction: c) more detailed functional structural model of PL/ PF than used for Gaia with telescope mech. and mirrors including its environmental test/ qualification~~ ~~Risk Reduction via: Likelihood/ severity~~ ~~Remaining risk: [Risk domain]~~ ~~DIV_C E2~~ [yellow box]

Risk no./ Title	Risk Classi-fication ----------- Initial Risk Index	Risk Context	Scenario/ *Cause (due to/…)*	Reduc. Action 1 and Remaining Risk / Risk Index / Residual Risk: / Risk Index	Reduc. Action 2 and Remaining Risk / Risk Index / Residual Risk: / Risk Index	Reduc. Action 3 and Remaining Risk / Risk Index / Residual Risk: / Risk Index
						~~Residual Risk: Programmatic risk~~ ~~a more detailed S/C-model than it was available for Gaia will lead~~ ~~to a major cost increase which is not any more acceptable under the conside-ration of the risk OCH~~ ~~E4_pr~~ [red box] **Because of the level of the residual risk this mitigation was not taken into account for the study baseline**
DIIIb – PL mecha-nism (TRL)	Techno-logy/ schedule / cost(sh) risk **DIIIb_sh** -------------- **D3** [orange box]	The baseline options for GaiaNIR is a spinning S/C Gaia like with "standard" NIR detectors and a de-scan mirror mechanism in the PL which is not space proven mechanism	Major project delay* *due to/ because:…* TRL increase for specific mirror tracking mechanism *Remark:* *the launch date of 2035 is currently the working assumption for the CDF study; therefore the risk of a delay in the launch is rather seen as a medium risk which however indicates an adequate begin of qualification needed*	Reduction: a) adaptation of project schedule * Risk Reduction via: severity Remaining risk: *risk remains unchanged with lower likelihood* **DV_sh D1** [yellow box]	Reduction: b) early consideration within GSP Risk Reduction via: severity Remaining risk: risk remains unchanged with lower likelihood **DV_sh D1** [yellow box]	
DIIIc – PL mechan ism (SPF/ relia-bility)	protectio n risk(p) **DIIIc_p** -------------- **D5** [red box]	for the de-scan mirror mechanism is a Single Point Failure (SPF) sources (app. every 2 min the mechanisms needs to move back to its initial position; the movements are requested over app. 4 years observation	Loss of mission or critical reduction of science return *due to/ because:…* SPF sources and e.g. unexpected early wear out in several mechanism	Reduction: a) design for minimum risk AND extensive reliability prediction	Reduction: b) consideration in CIL (include PA in the loop) Risk Reduction via: Likelihood Remaining risk: *risk remains unchanged with lower likelihood*	Reduction: c) intensive testing as far it is possible on ground

Risk no./ Title	Risk Classi-fication ---------- - Initial Risk Index	Risk Context	Scenario/ *Cause (due to/…)*	Reduc. Action 1 and Remaining Risk / Risk Index / Residual Risk: / Risk Index	Reduc. Action 2 and Remaining Risk / Risk Index / Residual Risk: / Risk Index	Reduc. Action 3 and Remaining Risk / Risk Index / Residual Risk: / Risk Index
		time)			C5_p D1	
DIVa – Mirror+ struc-ture (data noise)	Performance risk (dp) **DIVa_dp** ----------- -- **D4**	The de-scan mirror mechanism and large structure might be source for increased noise impacting the science data	increased noise in the science data *due to/ because:…* - S/C-internal sources (thermal distortion/ instability of PL/ insufficient thermal decoupling of PL and PF) - complex* PL design (Detector, Mirrors, Focal assemble including mirror mechanism)* - insufficient thermal decoupling between PL and PF** in connection with extreme high accuracy requirements - stray light	Reduction: a) extensive thermal and mechanical analysis Risk Reduction via: Severity	Reduction: b) specification of an extremely stable environment (thermal and particulate contamination), driving shape and material selection (minimise CTE using same material) Risk Reduction via: Likelihood Remaining risk: *risk remains unchanged with lower likelihood/ severity* DIVa_dp. C2	Reduction: c) distortion/ vibration optimisation via functional structural model* of PL with telescope mech. and mirror to be environmental tested/ qualified Risk Reduction via: Likelihood/ Severity
DIVc – Mirror+ struc-ture (know-how)	Schedule risk (sh) **DIVsh_sh** ----------- -- **D3**	Supplier monopole for the Carbon/Selenium based material for mirrors and structures specifically developed for space application	1) Major delay in the project schedule due to loss of know-how and 2) manufacturing capacities or damages during manufacturing *due to/ because:…* - Supplier monopole on the Carbon/Selenium based material for mirrors and structures - failure in the manufacturing process which requires to rebuild the affected component, e.g. in case of cracks in mirrors	Reduction: To 1) no mitigation possible Risk Reduction via: - Remaining risk: *risk remains unchanged* DIVc1_sh D3	Reduction: 2a) to mitigate delay in case of failure in structure and mirror an extensive 'spare part' approach was used in Gaia, e.g. spare blocks for mirrors Risk Reduction via: Likelihood/ severity Remaining risk: *risk remains unchanged with lower likelihood/ severity* DIVc2_sh C2	

Risk no./ Title	Risk Classi-fication ------------ Initial Risk Index	Risk Context	Scenario/ *Cause (due to/...)*	Reduc. Action 1 and **Remaining Risk / Risk Index** **Residual Risk: / Risk Index**	Reduc. Action 2 and **Remaining Risk / Risk Index** **Residual Risk: / Risk Index**	Reduc. Action 3 and **Remaining Risk / Risk Index** **Residual Risk: / Risk Index**
					Residual risk: Significant cost increase **DIVc2_c C2**	
DV – MLI outgass-ing	Performance risk (dp) **DV_dp** ------------- **E4**	The presence of Multi Layer Insulation (MLI) materials is connected with a long-term outgassing process under the given environmental conditions (the more MLI the more water - design inherent /not avoidable)	Critical impact on science data return in terms of accuracy *due to/ because:...* long-term outgassing of MLI	Reduction: a) operational procedures for frequent decontamination including it in the operation concept Risk Reduction via: Severity Remaining risk: *risk remains unchanged with lower severity* **DV_dp E1** *Remark: it's a known problem from Gaia and it is already considered in Gaia design via an adequate functionalities/C decontamination mode; however its use was defined as contingency procedure only*		
DVIIIb – Micro Propulsion (procurment)	Programmatic/ schedule risk (pr) **DVIIIb_pr** ------------- **D3**	There is currently a supplier monopole for the baselined micro propulsion system;	Major delay in the project schedule *due to/ because:...* change in the technology* portfolio of the current monopole-supplier for micro propulsion Remark: * its loss would request a new development/ qualification	Reduction: a) timely conside-ration in the GSP including development of other supplier alternatives Risk Reduction via: Severity Remaining risk: *risk remains unchanged with lower severity* **DVIIIb_pr D1**		

Launch (including preparation) & LEOP & IOT / Space Debris

Risk no./ Title	Risk Classification ----------- Initial Risk Index	Risk Context	Scenario/ *Cause (due to/...)*	Reduc. Action 1 and Remaining Risk / Risk Index Residual Risk: / Risk Index	Reduc. Action 2 and Remaining Risk / Risk Index Residual Risk: / Risk Index	Reduc. Action 3 and Remaining Risk / Risk Index Residual Risk: / Risk Index
LI – Bi-pro-pulsion system	Safety risk (s) **LI_s** ----------- -- **E5-B5**	Chemical propulsion is used for the transfer to L2 and has to be maintained during launch preparation	Loss of life, life-threatening or permanently disabling injury or occupational illness; *due to/ because:...* the uncontrolled release of bipropellant during storage and handling	Reduction: a) obligatory safety & launch regulations for handling of dangerous media Risk Reduction via: Remaining risk: **LI_s** **A5**	Reduction: b) safety submission process between contractor, launch provider & ESA likelihood *Risk remains the same with lower likelihood*	
LIV – New Launcher	Schedule / costs Risk (sh/c) **LIV_sh** ----------- -- **D3**	Study based on the use of a new Launcher 'ARIANE 6.2'; its first flight is scheduled for 2020);	Major delay in schedule *due to/ because:...* delay in the launcher availability and currentlyunknowns regarding the launcher specificifications * Remark: * the performance for L2 of Ariane 6.2 is currently not known (should be same or better than Soyuz, but no guarantees)	Reduction: a) 'worst case' design case based on at least Soyuz perfromance Risk Reduction via: Severity *Remaining risk: risk remains unchanged with lower severity* **LIV_sh** **D1**		
SDI.. – Safety risk	Safety (s) **SDI_s** ----------- -- **C5**	During launch the S/C will cross orbits taken also for manned flight missions; furthermore L2 orbit is not a stable orbit; S/C will return to LEO in a relatively short time frame;	Collision with manned missions *due to/ because:...* system/ functional / operational failure	Reduction: a) mandatory applicability of ESA Space Debris regulation* Risk Reduction via: Likelihood *Remaining risk:* **Protection** – *risk remains unchanged with lower likelihood* **A5_s** *Remark: * compliance e.g. via sufficient*		

Risk no./ Title	Risk Classi-fication ------------- Initial Risk Index	Risk Context	Scenario/ *Cause (due to/…)*	Reduc. Action 1 and **Remaining Risk / Risk Index** Residual Risk: / Risk Index	Reduc. Action 2 and **Remaining Risk / Risk Index** Residual Risk: / Risk Index	Reduc. Action 3 and **Remaining Risk / Risk Index** Residual Risk: / Risk Index
				propellant for disposal manoeuvre to avoid entry in an LEO		
SDII – Spce debris – limitation of in-orbit time	Protection risk (p) **SDII_p** ------------- **D4** 🟥	L2 orbit is not a stable orbit; S/C will return to LEO in a relatively short time frame; The number of space debris has to be limited in LEO by limitation of its remaining time in LEO	Space debris increase *due to/ because:…* S/C longer than 25years in orbit	Reduction: a) mandatory applicability of ESA Space Debris regulation* Risk Reduction via: Likelihood Remaining risk: **Protection** – *risk remains unchanged with lower likelihood* **A5_p** 🟨 *Remark: * compliance e.g. via sufficient propellant for disposal manoeuvre to avoid entry in an LEO*		
SDIII – Space Debris – Debris mitigation	Protection risk (p) **SDIII_p** ------------- **D4** 🟥	Number of space debris has to be limited in LEO by limitation of the probability for an uncontrolled disintegration of the S/C in the LEO	Space debris generation *due to/ because:…* system/ functional / operational failure leading to disintegration of S/C	Reduction: a) mandatory applicability of ESA Space Debris regulation Risk Reduction via: Likelihood Remaining risk: **Protection** – *risk remains unchanged with lower likelihood* **A5_p** 🟨 *Remark: * compliance e.g. via sufficient propellant for disposal manoeuvre to avoid entry in an LEO*		

Risk no./ Title	Risk Classi-fication ---------- - Initial Risk Index	Risk Context	Scenario/ *Cause (due to/...)*	Reduc. Action 1 and Remaining Risk / Risk Index / Residual Risk: / Risk Index	Reduc. Action 2 and Remaining Risk / Risk Index / Residual Risk: / Risk Index	Reduc. Action 3 and Remaining Risk / Risk Index / Residual Risk: / Risk Index
SDIV – Space Debris – Casualty risk	Safety risk (s) **SDIV_s** ----------- -- **C5**	Casualty risk due to uncontrolled re-entry shall not excide an acceptable risk level	Casualties on ground (Earth) *due to/ because:...* re-entering space debris	Reduction: a) mandatory applicability of ESA Space Debris regulation Risk Reduction via: Likelihood Remaining risk: **Safety** – *risk with lower likelihood remains unchanged* **A5_s**		
Cruise and Mission deployment						
CI – Loss of S/C during cruise & operation	Protection risk (p) **CI_p** ----------- -- **C5**	S/C trajectory to L2 and maintaining of Lissajous orbit around L2	Loss of S/C *due to/ because:...* SPF/ e.g. antenna or other failure combinations	Reduction: a) adequate reliability and failure tolerance requirements Risk Reduction via: Remaining risk: **CI_p** **B5**	Reduction: b) tracking of SPF sources via CIL (extensive PA approach) Likelihood *risk remains unchanged with lower likelihood*	
CII – Sun-shield deployment	Protection/ perfor-mance risk (p) **CII_p** ----------- -- **C5**	The full deployment of the sunshield (which curries also the Gaia solar arrays) is needed to guarantee a sufficient power supply and protection against stray light coming from Sun, Earth and Moon	Loss of S/C* *due to/ because:...* SPF/ e.g. antenna or other failure combinations Remark: * worst case	Reduction: a) design to risk approach	Reduction: b) tracking of SPF sources via CIL (extensive PA approach) Risk Reduction via: Likelihood Remaining risk: *risk remains unchanged with lower likelihood* **CII_p** **B5**	Reduction: c) intensive testing + use of Gaia experiences
CIII – Radia-tor deployment	Perfor-mance risk (dp) **CIII_dp** ----------- --	The deployment of the radiators via its release mechanism* *Remark: * the relatively*	Critical reduction of structural integrity of the S/C *due to/ because:...* not being able to withstand the launch loads if not	Reduction: a) design to risk approach	Reduction: b) tracking of SPF sources via CIL (extensive PA approach) Risk Reduction via: Likelihood	Reduction: c) intensive testing

Risk no./ Title	Risk Classi-fication ----------- Initial Risk Index	Risk Context	Scenario/ *Cause (due to/...)*	Reduc. Action 1 and Remaining Risk / Risk Index — Residual Risk: / Risk Index	Reduc. Action 2 and Remaining Risk / Risk Index — Residual Risk: / Risk Index	Reduc. Action 3 and Remaining Risk / Risk Index — Residual Risk: / Risk Index
	C4	*large radiators has to be supported during launch via HDRM to cope with the launch load*	attached to the SVM during launch		*Remaining risk: risk remains unchanged with lower likelihood* **CIII_dp B5**	
Overall cost risks						
OCI – In-creased antenna array	Cost risk (c) **OCI** ------------- -- **E1**	the antenna array will need to be significantly larger in area and mass than the one of Gaia; however it will need more of the same passive elements as on Gaia with a (from risk viewpoint negligible) cost increase (Beam Forming Network (BFN) of this large GaiaNIR PAA would still be very similar to the one on Gaia	Significant cost increase *due to/ because:...* costs for the passive radiating elements, and some delta cost for a larger structure	Reduction: a) *no further mitigation in the frame of the study required* Risk Reduction via: - Remaining risk: **Cost** – *risk remains unchanged* **OCI E1**		
OCII – NIR detect or costs	Cost risk (c) **OCII** ------------- --	The – in comparison to the former Gaia mission – increased costs for the NIR detectors are already accepted in the study baseline and are mentioned here form completeness only	With reference to the remark given to the risk domain 'cost' in the frame of mission success criteria's (tab. 1-3)	Reduction: a) *no further mitigation in the frame of the study required* Risk Reduction via:- Remaining risk: -		

Table 9-8: Risk Log

Severity	A (min.) <or≤ 1/10000 (10^-4) almost never	B (low) ≤ 1/1000 (10^-3).. seldom	C (medi.) ≤ 1/100 (10^-2) .. sometimes	D (high) ≤ 1/10 (10^-1) .. frequently	E (max.) ≤ 1 .. certain
5 (catastr.)				LI_s, SDI/ IV	
			CI_p, CII_p	DIIIc_p	SDII/ III
4 (critical)			CIII_dp		DV_dp
3 (major)				DIId_sh+c, DIIIb_sh, DIVc_sh, DVIIIb_pr, LIV_sh	DI_pr, DII_pr OCII
2 (signif.)					
1 (minor)					OCI
0	no risk				

pr - programmatic/ dt - dep.(tech.) / dp - dep.(perform.)/ p - protection / s -safety/ sh - schedule/ c - cost

Likelihood

Table 9-9a: Top Risk Index – Initial assessment

Severity	A (min.) <or≤ 1/10000 (10^-4) almost never	B (low) ≤ 1/1000 (10^-3).. seldom	C (medi.) ≤ 1/100 (10^-2) .. sometimes	D (high) ≤ 1/10 (10^-1) .. frequently	E (max.) ≤ 1 .. certain
5 (catastr.)	LI_s, SDI/ IV	DIIIc_p, CI_p, CII_p			
	SDII/ III				
4 (critical)		CIII_dp			
3 (major)			DII_pr,	DI_pr, DIIIa_dp, DIVc1_sh	
2 (signif.)		DIVc_sh	DIVa_dp	DIId_sh+c, DIVc2_sh+c, DVIIIb_pr	
1 (minor)				DIIIb_sh, LIV_sh	DV_dp, OCI
0	no risk				OCII

pr - programmatic/ dt - dep.(tech.) / dp - dep.(perform.)/ p - protection / s -safety/ sh - schedule/ c - cost

Likelihood

Table 9-9b: Top Risk Index – Final assessment

9.5.1 Risk Log General Conclusions

- Very high risks and high risks are typical of a phase A project. Areas with lack of definition or little previous experience pose a priori more risk to the mission and therefore are the ones with more risk reduction potential

- Experience shows that all risk items with a critical risk index (red, orange area) must be analysed and proposals for risk treatment actions elaborated

- In the end, ideally all risk items should achieve a level of justifiable acceptance

- The risk management process should be further developed during the project definition phase in order to refine the risk identification/analysis and provide evidence that all the risks have been effectively controlled.

9.6 Risk Log Specific Conclusions and recommendations

The scientific objectives of the GaiaNIR study

- To enlarge the astrometric achievement of Gaia to the astronomical sources which are only visible in NIR in frame of Cosmic Vision 2015-2025:
  - o To maintain the accuracy of the Gaia optical reference frame
  - o To improve the star parallax and proper motion accuracy by revisiting the astronomical sources a number of years after Gaia.

Requires:

- Extreme high precision instruments design and operation over a relatively long lifetime,
- Extremely stable thermal environment and
- Particulate specific care against contamination,

which is driving the selection of configuration and material. Such an ambitious mission has naturally a high risk potential (see Table 9-8 and Table 9-9a).

However this mission can be built up and benefit from comprehensive practical ESA-internal experiences coming from the on-going Gaia mission. Therefore the initially identified risks justified as 'very high' and 'high' could be preliminary mitigated (see Table 9-8 and Table 9-9b) in the frame of the CDF study.

Nevertheless, the GaiaNIR study baselines a complex S/C design with many 'Single Point Failure' sources , mechanisms for sunshield deployment, a de-scan mechanism in the optical path and science operations where certainly ESA-internal experiences are mostly available.

Naturally many risks were identified (yellow/ green see Table 9-8 and orange/ red see Table 9-9a). The majority of this initially identified risks justified as unacceptable could be mitigated (see Table 9-8).

The following risks could not be mitigated to a fully acceptable risk area (yellow/ green – see Table 9-9b), where the final risk mitigation could be done by the future prime/ subcontractor.

- Gaia 'copy approach' (DI) – risk related to programmatic/ cost/ schedule
- PL mechanism (data noise) (DIIIa) – risk related to mission protection
- PL mechanism (SPF/ reliability) (DIIIc) – risk related to mission protection
- Mirror+structure (know-how) (DIVc1) – risk related to schedule
- Loss of S/C during cruise & operation (CI) – risk related to mission protection
- Sun-shield deployment (CII) – risk related to mission protection

For all of these risks (mostly linked to the loss of S/C – 'protection') mitigation measures could be identified. However the currently envisaged mitigation measures available were not seen as effective enough to achieve an acceptable risk area.

The 'Gaia copy approach' has to be seen critically hence the period between the realisation phase of Gaia and GaiaNIR is quite long (over 10 years) which might result in a loss of the available Gaia project experiences. For example where in the 'Gaia

programme' approach the prime role for the payload and platform was in 'one hand' (DI) that is not at all granted for the future GaiaNIR project. However this approach was one of the major conditions for the success of the Gaia project with its extreme complex and demanding S/C design. Also regarding the availability of certain technology, e.g. Carbon/ Selenium technology for structure and mirrors (DIV) or the cold gas propulsion system (DVIIIb), might become a risk driver because of the supplier monopoles.

No overall schedule risk could be identified during the CDF study considering the fact that a sufficient time distance to the ongoing Gaia mission is anyway needed from scientific viewpoint (there is no demand for an immediate start of the project because several years has anyway to go the guarantee a sufficient movement of the stars to compare Gaia and GaiaNIR measurements in terms of 'airspeed' of stars) and no specific launch window is needed in terms of mission objectives.

10   PROGRAMMATICS/AIV

10.1 Requirements and Design Drivers

The GaiaNIR programmatic approach is inherited from its predecessor project, Gaia. As it was demonstrated eventually successful, it is wise to apply it again, with the due adaptations to the new system. Maximum heritage is applied, in order to limit the qualification and delta-qualification activities that by their nature involve impacts in cost and schedule, and increment anyway the programmatic risk.

The required launch date is established for year 2035.

The schedule has been defined backwards from the launch date to demonstrate feasibility and time constraints.

10.2 Options

The baseline assumption is that the Prime Contractor is procuring the complete telescope similarity with any GaiaNIR subsystem. This approach was found successful in other past scientific satellites of the same kind, as Gaia itself.

Another programmatic possibility is to leave to the Prime the full responsibility for the procurement of the PLM, with the exception of an AIT Contractor that would be responsible for the integration and test activities only of the PLM, on the three envisaged models, i.e. Structural Model (SM), Avionics Test Bench (ATB) and Proto Flight Model(PFM). The activities on the SVM would be limited to integration only, as it would be technically recommended that all the mechanical test activities (specifically the environmental tests) are accomplished at integrated GaiaNIR level.

10.3 Technology Requirements

Few on-board items are at a TRL below 6, and need to be brought in line with the minimum programmatic requirement of "all units at TRL >=6 at the beginning of the Implementation Phase (PDR)". They are listed here with their current status:

- Instrument Control Unit, TRL=2
- Data Processing Unit, TRL=2
- De-scan Mechanism, TRL= 4
- Phased Array Antenna, TRL=5

Upgrading the TRL to TRL=6 ranges (best guess) from 1 year for TRL 5, up to more than 12 years for TRL 2. This affects the estimated duration of the GaiaNIR Project (or its recommended beginning).

For information, the TRL definitions are shown in Table 10-1:

TRL	ISO Definition	Associated Model
1	Basic principles observed and reported	Not applicable
2	Technology concept and/or application formulated	Not applicable
3	Analytical and experimental critical function and/or characteristic proof-of concept	Mathematical models, supported e.g. by sample tests
4	Component and/or breadboard validation in laboratory environment	Breadboard
5	Component and/or breadboard critical function verification in a relevant environment	Scaled EM for the critical functions
6	Model demonstrating the critical functions of the element in a relevant environment	Full scale EM, representative for critical functions
7	Model demonstrating the element performance for the operational environment	QM
8	Actual system completed and "flight qualified" through test and demonstration	FM acceptance tested, integrated in the final system
9	Actual system completed and accepted for flight ("flight qualified")	FM, flight proven

Table 10-1: TRL scale

With exception of the De-scan Mechanism, the current status of the few TRL< 6 units is not considered critical and fully in the range of feasibility, with some technology studies already on-going.

10.4 Model Philosophy

The heritage with Gaia allows for the implementation of a very similar model philosophy, where to the PFM S/C, a SM is envisaged in order to early qualify the system under its applicable mechanical environment. The SM will represent the full satellite. It will implement a full flight structure, to be refurbished and reused after SM environmental testing, as PFM structure. On the SM, structural dummies will be integrated in place of the real units; these dummies will represent as a minimum mechanical interface, mass and Centre of Mass (CoM) of the GaiaNIR on-board units. Harness may be represented by dummy cables with the same mass distribution, or by discrete dummy masses loading the harness interfaces on the structure. A partial implementation of the thermal control is necessary, as MLI blankets and other thermal hardware must be installed in order to confirm structural compatibility. Installation may be partial, as long as it is sufficient to verify by test mechanical properties.

The Reaction Control Subsystem (RCS) instead will be the flight one, and will be installed in order to early qualify it with the system environmental tests of the system SM. Besides it will be reused as well on the GaiaNIR PFM, making not necessary to procure and integrate a second RCS S/S.

At the end of the GaiaNIR SM mechanical environment tests, the structural dummies will be removed, then both Structure S/S and RCS will be refurbished, making them ready and already integrated in the starting configuration of the GaiaNIR PFM AIT activities flow.

Beginning from these two subsystems, the GaiaNIR PFM will be integrated, in a process that will build up the system by mounting and testing the distributed hardware like cables and thermal control parts like MLI blankets etc., and the on board avionic units.

For programmatic convenience, the satellite can be functionally and contractually split in two modules, the Service Module (SVM) and the Payload Module (PLM). The SVM provides the S/C services enabling the vehicle flight mission, while the PLM provides the Science Instruments enabling the fulfilment of the scientific mission objectives, and provides the services to the Instruments, like power, data transfer to Ground, commanding functions, thermal control etc.

It may be programmatically convenient to subcontract the design and the AIT of the PLM to a PLM Contractor, sending into parallel design, procurement and AIT activities of the two modules so identified. In such a context, the Prime would be responsible for the overall GaiaNIR design, and the procurement and AIT of the SVM and the whole S/C; included in the Prime/Contractor tasks are the technical and programmatic control of the PLM Subcontractor.

The model philosophy is completed with an Avionics Test Bench, built with avionic unit Engineering Models (EM) or Elegant Breadboard Models, and test harness that depending on the intended depth of testing one wants to achieve, may be fully representative of electrical and EMI properties, including routing and shielding, or just functionally representative (no cable length respected either). The build up of this test model may reflect the technical and programmatic arrangements organising the procurement and AIT by Modules, i.e. SVM ATB and PLM ATB, eventually merging in a S/C ATB managed and tested by the Prime Contractor.

10.5 Schedule

Due to the close similarity with the original Gaia, the schedule is also necessarily very similar. GaiaNIR may take advantage also of the known evolution of the former Gaia schedule, showing a general slippage of the final launch date of about one and a half years, from the assumptions of the PDR times, to the CDR schedule definition that was confirmed eventually, within a reasonable margin of tolerance in the range of a couple of months, fully acceptable.

The GaiaNIR proposed schedule is the following:
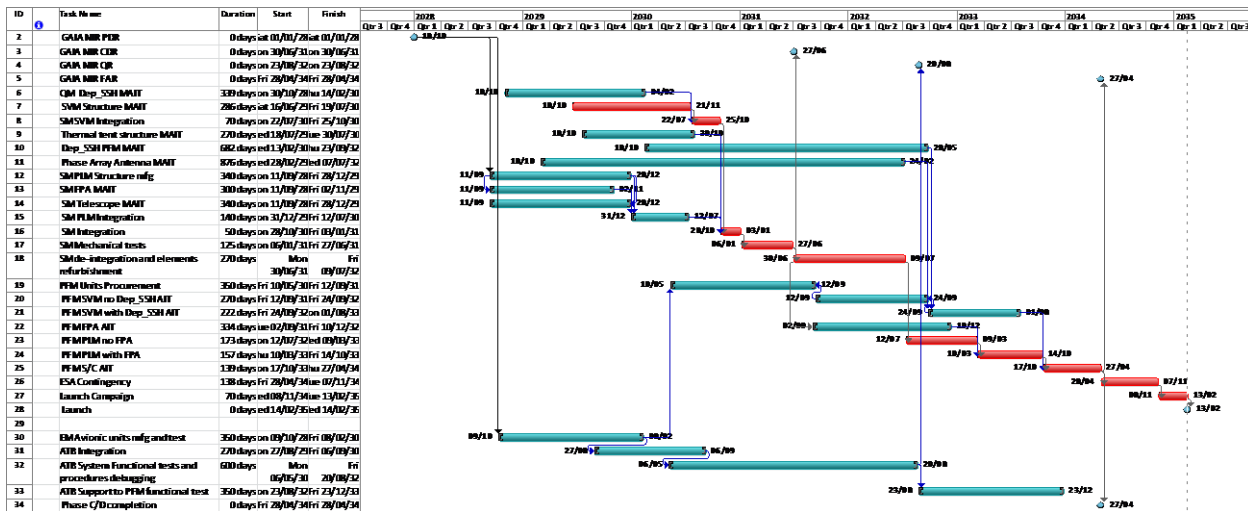
**Figure 10-1: GaiaNIR Proposed Schedule**

No criticality seems present, provided that the implementation phase begins with all products at due TRL (=6). Currently, targeting a launch in 2035, about 9 years are available to achieve that objective.

11 COST

This chapter presents a description of the estimate of the Cost at Completion (CaC) of the CDF concept of the GaiaNIR mission.

11.1 Objective

The first and main objective of the CDF GaiaNIR costing exercise has been to verify the compatibility of the GaiaNIR CaC with respect to the Budget Cap of 550M€ EC 2017.

11.2 Cost Contribution to CDF GaiaNIR Study Preparation: Early Estimate for a Potential Gaia `Re-flight`

In preparation for the CDF GaiaNIR exercise, a preliminary and ROM estimate has been performed in order to investigate the compatibility of a potential Gaia re-flight with the given ceiling price of 550M€. This was done in order to identify the magnitude of savings required for GaiaNIR and to identify key areas for design-to-cost during the rest of the study.

The outcome of the pre-CDF GaiaNIR ROM estimate was that a **`Gaia re-flight` would not be able to fit within the given budget cap**. The main reasons was the impossibility to assume full recurrence of equipment and experience from the Gaia Project, due to:

- The very long gap between the project implementations
- Likely obsolescence of equipment
- Discontinuity of the Industrial set-up from the Gaia project
- Changes in the Geo-industrial scenario, de facto introducing cost items (named GEODIS) for guaranteeing a fair distribution all over Europe of the Project procured items and activities, especially for under-returned member states.

The results led to the conclusion that a major PLM re-design exercise should be performed during the GaiaNIR CDF study, simplifying the Payload concept as much as possible while remaining compatible with the scientific requirements. Furthermore one of the conclusions was that maximum reuse of the existing Gaia architecture would be a significant benefit for the cost and programmatic optimisation.

11.3 Scope and Class of the Estimate

The cost estimates have been performed within the CDF environment by ESA/ESTEC Cost Engineering (TEC-SYC). Thanks to the analogies and similarities with respect to the Gaia project, it has been possible to prepare the cost estimate for GaiaNIR at Class 4 (as described in the ESA Cost Engineering Chart of Services, RD[38]).

The accuracy of the complete estimate is expected to be +/- 20%.

The cost estimate has been based on the CDF proposed design, in accordance with the GaiaNIR CDF team inputs, including risk and programmatic assumptions.

The Estimate of the CDF GaiaNIR includes:

- SC and SVM Development Industrial Cost including Contingency

- PLM Development Industrial Cost including Contingency
- Launch Services
- Mission Operations Cost
- Science Operations Cost
- ESA Internal Cost
- ESA Margins (excluding ESA Program level margins).

Pre-development cost and technology roadmaps have been excluded from this assessment, since they are assumed to be covered by separate budget lines outside the project budget, and moreover require dedicated cost evaluations beyond the scope of the CDF study.

11.4 Estimate Methodology for the Industrial Procurement Cost

The following cost estimating methodologies have been used:

- Product Tree based as much as possible on Gaia, adapted when necessary in accordance with the CDF design

- Escalation with respect to EC 2017 from Gaia most recent available figures (Space Science Advisory Committee, C.E.D.R.E, Financial Proposal); for rough escalation purposes a 1.5% average escalation per year has been used

- Additional cost as GEODIS, Corporate governance, and basic activities recharge have been included in the estimate as defined and agreed during the Cosmic Vision M4 evaluations (RD[41])

- A General Model Philosophy including a Proto Flight Model (PFM), Engineering Model (EM) and Structural Model (SM) as the baseline development assumption, compatible with the CDF GaiaNIR Programmatic evaluation (although a strong heritage from Gaia has been assumed, this cannot be translated into a recurrence/re-built philosophy, due to obsolescence and a too long gap between project implementations. Furthermore, a light model philosophy could not be realistically assumed due to testing and qualification needs down to the single units level.)

- Parametric cost model RACE (RD[39]) for the 1st PFM FPA equipment (one unit includes detector, FEE, and associated cabling), T1 (1st NR FPA equipment), and the 58 fully recurrent units. The algorithms for the recurring unit price have been based on the Wright law (Learning Curve) and by assuming a cumulative learning curve factor of 95%. The ROM estimate, as specified in the cost tables in this report, shows that for the FPA an average value of 1 M€ per FPA Unit needs to be taken into account for the GaiaNIR CDF design.

11.5 Industrial Prime Cost

The GaiaNIR Industrial Prime cost estimate has been based on Gaia references, for all the cost categories and manpower for Project Office, AIV/T, GSE. The same rational has been applied to Spacecraft, Mechanical SVM, Electrical SVM, and PLM activities.

This approach allows to compare the 2-tier Industrial Setup for Gaia with a similar scenario for GaiaNIR. Additional manpower needs and cost imposed by GEO Distribution (GEODIS) has been separately addressed in section 11.6 and completely excluded from the Prime (SC, SVM, PL) cost estimate.

Further cross and sanity checks of the overall Prime manpower assumptions have been performed, by pair-comparing the GaiaNIR case with ARIEL (Cosmic Vision M4) and Gaia.

11.6 GEODIS Strategy

GEODIS has been added on top of the Prime cost for each module and specifically identified in the cost tables as separate items.

As agreed with the customer at the beginning of the study, ARIEL has been taken as the most similar case among the Cosmic Vision M4 cases. The same GEODIS strategy of ARIEL (RD[41])has been assumed compatibly with the CDF GaiaNIR schedule.

11.7 Technical and Schedule Assumptions

The various requirements and assumptions described in the basic study documentation apply to the cost estimates.

All <u>technical details</u> relevant to the various units have been gathered from the CDF GaiaNIR study team, processed by the CDF System team, and reported in the CDF GaiaNIR Workbooks and OCDT Model.

The GaiaNIR implementation schedule duration assumed for cost estimate purposes has been agreed with the CDF GaiaNIR Programmatic chair, as shown below.

	Duration: S/C development B2 KO to FAR				
	Years	Total [months]	Ph. B2 [months]	Ph. C [months]	Ph. D [months]
CDF GAIA NIR	7.58	91	16.0	42.0	33.0

Table 11-1: CDF GaiaNIR-Project implementation duration (Ph B2/CD)

11.8 Cost Risk/Opportunity

A cost risk analysis has been performed by employing triangular cost distributions (Minimum, Most Likely, Maximum) in the tool OpeRa (RD[37]).

As the Most Likely numbers, the point cost estimates have been taken as presented in the detailed estimate tables.

The employed spreads from Minimum to Maximum take into account the uncertainties in the cost estimate relationships, quality of the cost model input parameters, quality and applicability of the references and cost estimate relationships used, and the possible variations in the amount of equipment modifications and qualifications required.

All cost items in the estimate have been correlated amongst each other (i.e. the higher cost of one item increases the chance of a cost increase in the other items as well). The Cost Risk Margin has been established for a 70% confidence level (i.e. the chance that the budget including the Cost Risk Margin is sufficient for the project is 70%, or in other words the chance of a cost overrun is 30%).

This Cost Risk Margin consists of several components:

- Design Maturity Margin (DMM), to account for additional costs caused by unseen complexities that will be revealed as the design gets into more details. This entropic effect is inherent to the design process and therefore has to be provisioned as part of the core estimate. It is allocated 100% to Industry.

- Cost Model Accuracy (CMA), to account for uncertainties in the cost estimates. It includes the contribution of the Inherent Quality of the cost Models (IQM) together with contextual factors such as the Degree of Adequacy (DOA) of the cost models used with respect to the specific context of the cost estimate, and the Quality of the Input Values (QIV). Assuming that industry has better and more detailed cost models than ESA because based on internal costs, 25% of the CMA is accounted for industry and 75% for ESA.

- Project Owned Events (POE), to account for cost risks induced by potential negative events, as well as potential cost reduction opportunities, that may occur or not and that are under the direct responsibility of the Project Manager. POE risks are subject to mitigation measures to be managed at Project level. Assuming that industry has better and more detailed cost models than ESA because based on internal costs, 25% of the POE is accounted for industry and 75% for ESA.

- External to Project Events (EPE), to account for cost risks or opportunities that originate from external influences out of the direct control and responsibility of the Project Manager. The EPE should normally belong 100% to ESA, but ESA regularly transfers the coverage for fair Geo-Return cost impact to Industry.

The various elements of the total Cost Risk Margin are distributed over the Industry and ESA part of the costs. The costs for the Operations are not taken into account as part of the Industrial costs, therefore the risk and opportunities associated are fully assigned to the ESA part of the Cost Risk Margin.

Although the given percentage might appear to be on the low side considering the very early phase (CDF pre-Phase A) of the design, in this case the estimates are fully consistent with the specificities and details available from Gaia, which allowed focusing onto details from the beginning of the CDF Study.

11.9 ESA Internal Cost

ESA Internal Cost has been calculated as Class 5, based on a pro-rata calculation as 19% of the Total Flight Segment Industrial Price. The percentage applied has been extrapolated from Gaia, gathered through the Gaia official documentation available at the time of the estimating exercise.

11.10 Launch Services Cost

The estimate has been based on the agreed and available value from the Cosmic Vision M4 evaluations, assuming that the GaiaNIR will be carried by the Ariane 6-2 launch vehicle.

A specifically developed low-mass adapter has been added as a separate item to the cost estimate, based on Gaia references and according to the CDF study design (also Gaia required such a low-mass adapter, but since the launcher for Gaia-NIR will be different a new low-mass adapter specific for GaiaNIR on Ariane 6.2 is assumed to be required). If at a later stage the performance of Ariane 6.2 proves to be significantly high, a standard adapter as included in the launch price may suffice and the cost for a specifically developed adapter may be excluded from the estimate.

11.11 Operations Cost

Science Operation Centre (SOC) cost have been based on Gaia reference prices, and reduced by roughly 6% overall as discussed and agreed during the study with ESAC.

Mission Operation Centre (MOC) cost have been based on the ARIEL case (Cosmic Vision M4), and properly escalated taking into account 5.5 years routine operations plus commissioning. ROM figures have been discussed and agreed with ESOC, in advance of a more accurate estimate by ESOC at a later stage.

11.12 Cost Estimate and comparison with Gaia

By comparing with the Gaia Project, we can conclude a cost benefit due to:
- Absence of the Radial Velocity Spectrometer (RVS)
- Absence of RVS OMA, Photometer Prism, FPA IM
- Implementation of a single telescope only, leading to a lower SiC structures cost
- One M2 Mechanism only, allowing reduction of the unit cost by a factor 40% ROM
- Mirrors CVD (polishing and coating) cost reduced by a factor 33% ROM (1/3) thanks to
  - A new polishing technique (RD[42])
  - Overall heritage for the mechanical configuration.

On the other hand, cost growth has been expected due to:
- FPA Equipment – detectors price based on EUCLID NISP, leading to a growth of the FPA cost by a factor 60% ROM in spite of the limited number of detectors
- AOCS units as designated by the CDF GaiaNIR AOCS expert (cost based on EUCLID)
- Sub-contracted level activities (GEODIS Modules) for SVM and PLM
- Higher Cost Risk (according to the level of maturity for a CDF pre-Phase A design).

11.13 Conclusions and Recommendations

An important objective of the CDF Study has been the investigation of the compatibility of GaiaNIR with respect to a Budget Cap of 550M€ (EC2017).

A detailed estimate has been performed for the CDF Concept of GaiaNIR. The estimate has been presented in EC 2017.

The main conclusions are:

- This cost and programmatic exercise shows **the unfeasibility of the GaiaNIR mission, as perceived within the CDF Study, with respect to the Ceiling price set at 550M€**.

- Implementation Scheme and ESA responsibilities: focus should be put on the Industrial development cost estimate, where PLM and SVM Expected Industrial prices have been separately identified, not only for the Procurements but also at Cost Risk, GEODIS and Module Prime Level.

In order to allow the implementation for the GaiaNIR within the budget cap of 550M€, one potential solution would be the Implementation of the entire PLM (including the FPA) to National Agencies or within an International collaboration scenario. Furthermore, by removing the entire PLM from under ESA responsibility, the ESA share would potentially fit within the reference budget since also ESA Project cost and associated Risk would slightly decrease from values reported in the tables above.

12   CONCLUSIONS

With respect to the three main science objectives described in 3.3 Science Objectives, the GaiaNIR baseline as designed in this CDF study achieves the following:

- Enlarge the astrometric achievement of Gaia to stars that are only visible in the NIR. The most recent estimate of the total number of stars seen by GaiaNIR (assuming a bandpass of 400 to 1800 nm) and a faint limit of G=21 mag is a factor ~ 2.5 times the number of stars that Gaia sees down to G=21 mag. Assuming that the latter number is 2 billion, this would mean that GaiaNIR sees ~ 5 billion objects in total, 2 billion of which "old" and ~ 3 billion of which "new". These numbers are an all-sky average.
- Maintenance of the accuracy of the Gaia optical reference frame: achieved for the majority of Gaia stars (as most Gaia stars have a SED that covers both the optical and the NIR). In fact, this objective does not even require a GaiaNIR type mission, it would be fulfilled even with a simple repeat of Gaia.
- Improvement of the proper motion of Gaia stars by a factor x14 (at G=15 mag), combining data from both Gaia and Gaia NIR 20 years later, 5 years lifetime each:
  - the 25 microarcsec for Gaia for a 5 years mission is confirmed for G=15 mag (valid for any spectral type, including B1V, G2V, and M6V stars etc.)
  - for the Gaia NIR CDF baseline design, the expected performance is given in the table below: 165 microarcsec (G2V), 81 microarcsec (M0V) and 27 micro arcsec (M3III)
  - rather than a factor x14 when combining Gaia and Gaia NIR data, this results in an improvement by a factor 3, 6 and 14 respectively
  - note that for the modified baseline (optimised pixel pitch) and alternative detector options (see performance chapter), the performance would be even better.

Star magnitude [Gaia-band magnitude]	Gaia NIR with TDI			Gaia NIR baseline		
	G2V	M0V	M3III	G2V	M0V	M3III
7 (bright)	9	9	9	9	9	9
15	48	34	19	165	81	27
21	4129	1881	426	38660*	16843	2919

* Indicates that the detection limit has been reached.

Table 12-1: Summary of the astrometric performance comparison in micro-arcsecs between the Gaia NIR baseline and Gaia NIR with TDI for three stellar types

- With respect to the programmatic objective of making the GaiaNIR proposal fit into a M-class cost envelope, the CDF conclusion is negative (further details in the separate cost report).

The step & stare spacecraft solution was found to be unfeasible due to the far too-long time required between each observation step (leading to mission duration of over a

century to cover the same amount of sky with similar repeats as Gaia) and the prohibitive amount of propellants needed.

The alternative concept enabling the use of conventional NIR detectors that was identified during the study uses a de-spin Mirror Mechanism on a Gaia-like slow-spin spacecraft concept. No immediate show-stoppers were found for this concept, although there remain many related questions to be answered that were beyond the scope of this study.

No immediate show stoppers were identified for a Gaia-like slows-spin solution using TDI NIR detectors, apart from the fact that the technical feasibility of such detectors is questionable, and that the technology would most likely specifically need to be developed for the GaiaNIR mission, possibly at great expense.

12.1 Areas of Concern

The resulting CDF GaiaNIR design however inevitably exhibits the following unfavourable system-level characteristics:

- A total CaC well over the 550 M€[2017] limit set
- The incorporation of equipment with a TRL well below 6:
  - o De-spin (or de-scan) Mirror Mechanism: the basic piezo actuator technology is available, but there are several basic design options that need to be explored, after which Breadboard(s) and an Engineering Model need to be developed and tested to reach TRL 6 and have sufficient confidence in this critical item to allow phase B2/C/D implementation of the GaiaNIR mission.
  - o Instrument Control Unit (ICU): all required components are available, but needs development up to EM level to reach TRL 6.
  - o Data Processing Unit (DPU): all required components are available, but needs development up to EM level to reach TRL 6.
  - o Detectors: the Hawaii-2rg detectors are high-TRL, but for improved performance modifications would be required. If a European equivalent detector would be needed, then considerably more pre-developments would be required (see the Technology Requirements section in the Detectors chapter).
- The inclusion of a de-spin Mirror Mechanism that will inevitably result in thermal and mechanical noise.
- The launch mass is currently within the expected mass envelope of Ariane 62 according to the launch performance information available from Arianespace when performing the GaiaNIR CDF Study (the launch performance of Ariane 62 to L2 via direct ascent assumed to be at least 3 metric ton, including launcher adapter); Arianespace has however only informally stated an L2 launch performance "equal or better than Soyuz" – as the CDF GaiaNIR design has launch mass somewhat higher than what can be carried by Soyuz, this might become a concern.

The first issue only appears to be resolvable through significant cost sharing between ESA and National Agencies and/or international cooperation (as is however typical for other ESA Science missions).

The second issue can likely be resolved through sufficient pre-development, which however comes at a cost (even though formally outside the GaiaNIR project budget) and entails technical, programmatic and cost related risks.

The seriousness of the third issue is currently unclear. The Gaia PLM performance has proven to be extremely susceptible to what in other missions would be considered minute vibrations and temperature variations. Determination of the impact of the use of a de-spin Mirror Mechanism on the scientific performance of GaiaNIR (apart from the conclusion that from an AOCS point of view it appears feasible) will require a very detailed evaluation that was beyond the scope of the CDF study.

The last issue has a high chance of being resolved by a sufficiently favourable Ariane 62 launch performance guarantee in the near future. The use of the higher-performance Ariane 64 is an option, but would result in a significantly higher launch price.

Other areas of concern are:

- The dependence of Gaia heritage; the retention of the related equipment lines (such as for micro propulsion, PAA technology, BAM technology and large SiC structures) and knowledge and experience (for instance in the area of Science Operations) up until the implementation of GaiaNIR can at this moment not be guaranteed
- Optical filters may need to be introduced for the detectors; the consequences require further study
- The calibration of the GaiaNIR data can be expected to be more complex than for Gaia; this requires an in-depth study.

12.2 Cost Limitation Measures

To limit the GaiaNIR total mission budget while maintaining sufficient scientific performance, the following measures were taken into account in the CDF GaiaNIR baseline concept in relation to the Gaia mission concept:

- Exclusion of a Radial Velocity Spectrometer; incorporated on Gaia but not deemed necessary for GaiaNIR
- Use of a single telescope with two Fields of View (FoV); Gaia involved two telescopes with each a different FoV
- Exclusion of a Sky Mapper; incorporated on Gaia but not necessary for GaiaNIR
- Limitation of the number of NIR detectors to the minimum deemed necessary for sufficient scientific performance.

A specifically developed low-mass adapter has been taken into account, but if the performance of Ariane 6.2 proves to be significantly high, a standard adapter as included in the launch price may suffice.

12.3 Satisfaction of Requirements

As depicted in the tables hereunder, not all requirements have been met. Further analyses are required to increase the level of confidence on the preliminary results established in the course of the CDF study.

12.4 Compliance Matrix

Mission requirements		
Req. ID	**STATEMENT**	**Compliance**
MIS-010	The mission shall use NIR detectors to perform high accuracy astrometric and photometric measurements.	Compliant
MIS-020	The nominal science operations (lifetime) of GaiaNIR shall be 5 years.	Compliant; sufficient propellant load
MIS-030	The mission and system design shall be compatible with a launch in 2035.	Compliant
MIS-040	The satellite should be launched by a European launch vehicle.	Compliant; Ariane 6.2 baseline
MIS-050	The cost to ESA shall not exceed 550M€[2017], including: • Platform, Payload, System Integrator • Launcher • Operations (MOC, SOC) • ESA internal activities	Not compliant; total cost estimate significantly higher

Table 12-2: Mission requirements compliance matrix

System requirements		
Req. ID	**STATEMENT**	**Compliance**
SYS-010	The astrometric measurement principle shall be based upon a continuous scanning or a step-stare mode which discretely approximates continuous scanning of the sky with at least two fields-of-view.	Compliant, but feasibility of baseline design with de-spin Mirror Mechanisms TBC, requiring more detailed analyses
SYS-020	The S/C shall be compatible with an Ariane 62/Ariane 64 launch vehicle.	Compliant; Ariane 62 if L2 performance sufficiently better than Soyuz
SYS-030	The S/C shall maximise reuse of existing Gaia technology with a TRL of at least 6 at the start of Phase B.	Compliant
SYS-040	The component of the rotation vector around the S/C X axis shall not be less than equivalent 60 arcsec/s (the goal is a nominal value equivalent to 96 arcsec/s).	Compliant; Gaia-like 60 arcsec/s baseline

Table 12-3: System requirements compliance matrix

12.5 Further Study Areas

The following activities are identified as important next steps for the GaiaNIR mission development, considering that implementation is still about a decade away:

• (re-)Evaluation of the science case, based on the results from the current CDF study

- Detailed analyses of thermal and mechanical disturbances that can be expected from use of a de-spin Mirror Mechanism, and the consequences for the scientific performance
- Detailed analysis of the calibration of GaiaNIR data, also taking into account the lack of a Sky Mapper
- Predevelopment of Detectors, de-spin Mirror Mechanism and DPU.

12.6 Final Considerations

Ultimately, there seem to be two principal solutions for the GaiaNIR mission, both involving significant low-TRL equipment, high development and implementation risk, and potentially costly pre-developments:

- A Gaia-like slow-spin concept with a de-spin Mirror Mechanism and conventional, non-TDI detectors (the main design of this CDF study)
- A Gaia-like slow-spin concept with TDI detectors (the characteristics of which have been assessed by the current CDF study to a much lesser degree, as this was determined both before and during the study not to be the main concept of interest).

For either case a total mission budget well over the limit for an M-class mission is to be expected; to make the mission fit within the budget constraint while maintaining sufficient scientific performance will require significant sharing of the cost with National Agencies and/or through international cooperation.

This Page Intentionally Blank

13   REFERENCES

13.1.1.1   Chapter 1 Introduction References

RD[1]   GaiaNIR; Combining optical and Near-Infra-Red (NIR) capabilities with Time-Delay-Integration (TDI) sensors for a future Gaia-like mission, Hobbs et al., Lund Observatory, arXiv:1609.07325v1 [astro-ph.IM], 23 Sep 2016, https://arxiv.org/abs/1609.07325v1

13.1.1.2   Chapter 5.1 Optics References

RD[2]   J.J Arnoux et al. Optical design of the Hipparcos telescope. SPIE Vol. 655 Optical system design (1986)

RD[3]   J. de Bruijne, D. Hobbs, A. Mora. On the need of a Sky Mapper for Gaia-NIR, Gaia-CZ-TN-ESA-JDB-112-01, 26/09/2017

RD[4]   A. Mora et al, Gaia on-board metrology: basic angle and best focus, arXiv:1407.3729v1 [astro-ph.IM] 14 Jul 2014

RD[5]   T. Steinmetz et al. Absolute long distance measurement with sub-micrometer accruacy for formation flight applications, Executive summary, ESTEC Contract No. 20184/06/NL/HE Nov. 2009

RD[6]   A.L. Verlaan, High Accuracy Absolute Long Distance Measurements (HAALDM) using fs laser metrology, Executive summary, Dec 2008 ESA Contract no. 20183/06/NL/HE

13.1.1.3   Chapter 5.2 Detectors References

RD[7]   http://www.teledyne-si.com/pdf-imaging/H2RG%20Brochure%20 %20September%202017.pdf

RD[8]   http://www.teledyne-si.com/pdf/SIDECAR%20ASIC%20Dev%20Kit%20Brochure%20%20Jan_2017 _V1.0.pdf

RD[9]   "Detecting stars, galaxies, and asteroids with Gaia", J. H. J. de Bruijne et al. A&A 576, A74 (2015), DOI: 10.1051/0004-6361/201424018

RD[10]   " Detectors for the James Webb Space Telescope Near-Infrared Spectrograph I: Readout Mode, Noise Model, and Calibration Considerations", Bernard J. Rauscher, Ori Fox, Pierre Ferruit, DOI : 10.1086/520887

13.1.1.4   Chapter 5.3 Calibration References

RD[11]   Lennart Lindegren, et al., 2017: *Gaia Data Release 1. Astrometry: one billion positions, two million proper motions and parallaxes*, Astronomy & Astrophysics, Volume 595, id. A4, 32 pp. (http://adsabs.harvard.edu/abs/2016A%26A...595A...4L)

13.1.1.5   Chapter 5.4 Performance References

RD[12]   https://www.cosmos.esa.int/web/gaia/science-performance

RD[13]   Gaia Mission paper (https://arxiv.org/abs/1609.04153,
https://www.aanda.org/articles/aa/abs/2016/11/aa29272-16/aa29272-16.html)

RD[14]   GaiaNIR Preliminary Detector Study, ESA-SCI-FV-GNI-TN-0001

13.1.1.6   Chapter 5.7 PLM Thermal References

RD[15]   M. Donabedian, *Thermal Uncertainty Margins for Cryogenic Sensor Systems,*
1991, AIAA 26th Thermophysics Conference

RD[16]   M. Donabedian, Chapter 19 of the Thermal Control Handbook, Vol II:
Cryogenics, *Thermal Control Margins, Risk Estimation, and Lessons Learned*

RD[17]   Gaia.ASF.DDD.PLM.00001 Gaia FPA Mechanical and Thermal Design Report,
19/01/2010, issue 5 rev 0, section 3.3, p25 - Thermal Requirements

13.1.1.7   Chapter 6.4 Propulsion References

RD[18]   Gaia.ASF.BG.SAT.00003: Gaia Spacecraft Mass and Mass Properties Budget
Report

13.1.1.8   Mechanisms References

RD[19]   Mechanisms for Gaia deployable sunshield, Esmats 2005, Eduardo Urgoiti,
Gerard Migliorero

13.1.1.9   Chapter 6.5 GNC References

RD[20]   GaiaNIR – Scientific requirements Document, Gaia-NIR-SCI-REQ-01, ESA, issue
1D, 2017-09-14

RD[21]   Requirements on the attitude noise (2), L. Lindegren, Gaia{LL{048,,Rev. 1 (20
December 2003)

RD[22]   GaiaNIR – A future all sky astrometric mission, David Hobbs's presentation at
the GaiaNIR CDF KO, 19/09/2017

RD[23]   Spacecraft System Design Report, Gaia.ASF.ADD.SAT.00001, Astrium, issue 2,
20/04/2007

RD[24]   Mass and Mass Properties Budget Report, Gaia.ASF.BG.SAT.00003, Astrium,
issue 7, 06/05/2013

RD[25]   Gaia attitude control design: milli-arcsec relative pointing performance using
micro-thrusters and instrument in the loop, P. Chapman, T. Colegrove, E. Ecale,
B. Girouart, Proceedings of the 8th International ESA Conference on Guidance,
Navigation and Control System, 5-10 June 2011

13.1.1.10   Chapter 6.8 SVM Telecomms References

RD[26]   ECSS-E-ST-50C Rev. 2, *Radio Frequency and Modulation*, 4 October 2011,
complemented with CCSDS 131.2-B.1, *Flexible advanced coding and modulation
scheme for high rate telemetry applications,* March 2012.

RD[27]   ECSS-E-50-04C, *Telecommand protocols synchronization and channel coding*, 31 July 2008 complemented with CCSDS 231.B-3, *TC synchronization and channel coding*, September 2017.

RD[28]   ECSS-E-50-01C*, Telemetry synchronization and channel coding,* 31 July 2008.

RD[29]   ECSS-E-50-02C, *Ranging and Doppler Tracking*, 31 July 2007, complemented with CCSDS 4.1.4-B-2, *Pseudo-Noise (PN) Ranging Systems*.

13.1.1.11   Chapter 6.9 SVM Thermal References

RD[30]   Gaia.ASD.RP.MSM.00051 Issue 2, Gaia M-SVM Thermal Design Description.

13.1.1.12   Chapter 7 Systems References

RD[31]   Mission Requirements Document , Gaia-EST-RD-00533, Issue 3, Revision 1, 21st May 2013

RD[32]   Ariane 6 User Manual, Issue 0, Revision 0,February 2017

RD[33]   Soyuz User Manual, Issue 2, Revision 0, March 2012

RD[34]   The Gaia Mission, A&A 595, A1(2016), 10.1051/0004-6361/201629272

RD[35]   Combining optical and Near-Infra-Red (NIR) capabilities with Time-Delay-Integration (TDI) sensors for a future Gaia-like mission, Dr. David Hobbs, 23 Sept 2016.

13.1.1.13   Chapter 9 Technical Risk References

RD[36]   Space Project Management, Risk Management, ECSS-M-ST-80C, 31 July 2008.

13.1.1.14   Chapter 11 Cost References

RD[37]   TEC-SYC Cost Risk Procedure, TEC-SYC/5/2010/PRO/HJ, February 2010

RD[38]   ESA Cost Engineering Charter of Services, Issue 4, TEC-SYC/12/2009/GRE/HJ

RD[39]   Guidelines for the use of TRLs in ESA programmes, TEC-ESSB-HB-E-002, issue 1, rev.0, 21 August 2013

RD[40]   The RACE Model, a tool for fast and early cost estimates in the CDF, M.O. van Pelt

RD[41]   M4 Mission Selection Review Programmatic Panel Report, ESA-SCI-F-ESTEC-RP-2017-004

RD[42]   Manufacturing and testing of a brazed optical quality SiC mirror, TEC-MMO/2016/374

13.1.1.15   Appendix B Sky Mapper References

RD[43]   EADS Astrium, 29 September 2011, "VPU Algorithms Requirements Specifications", Gaia.ASF.SP.PLM.00073 (issue 5, revision 2)

This Page Intentionally Blank

14 ACRONYMS

Acronym	Definition
AC	ACross-scan direction
ACC	Accelerometer
AF	Astronomic Field
AFP	Astronomic Focal Plane
AGIS	Astrometric Global Iterative Solution
AHFD	Attitude High Frequency Disturbance
AIT	Assembly Integration Test
AIT/V	Assembly, Integration and Test/Verification
AIV	Assembly Integration Verification
AL	Along-scan direction
AME	Attitude Measurement Error
AOCS	Attitude and Orbit Control Subsystem
APA	Amplified Piezo Actuator
APD	Avalanche Photodiode
APE	Absolute Pointing Error
APSK	Amplitude Phase Shift Keying (modulation)
ARW	Angular Random Walk
ASIC	Application Specific Integrated Circuit
ATB	Avionics Test Bench
AVM	Avionics Model
BAM	Basic Angle Monitoring
BAV	Basic Angle Variation
BCDR	Battery Charge and Discharge Regulator
BFN	Beam forming network (part of Phased Array Antenna RF stage)
BoL	Beginning of Life
BPSK	Binary phase shift keying
CaC	Cost at Completion
CAD	Computer Aided Design
CAN	Controller Area Network

Acronym	Definition
CCD	Charge Coupled Device
CCSDS	Consultative Committee on Space Data Systems
CDF	Concurrent Design Facility
CDMU	Command & Data Management Unit
CDR	Critical Design Review
CDS	Correlated Double Sampling
CER	Cost Estimation Relationship
CFDP	CCSDS File Delivery Protocol
CFRP	Carbon Fibre Reinforced Polymer
CHC	Charge Handling Capacity
CMA	Cost Model Accuracy
CMOS	Complimentary Metal Oxide Semiconductor
CoM	Centre of Mass
CPS	Chemical Propulsion Subsystem
CPU	Central Processing Unit
CRS	Coarse Rate Sensor
CSG	Guyanne Space Centre
CSW	Central Software
CTE	Coefficient of Thermal Expansion
DHS	Data Handling System
DMM	Design Maturity Margin
DOA	Degree of Adequacy of the cost model
DoD	Depth of Discharge
DPAC	Data Processing and Analysis Consortium
DPU	Data Processing Unit
DR	Data Release
DSA	Deployable Sunshield Assembly
DSP	Digital Signal Processing
ECC	Error Check and Correction
ECSS	European Cooperation for Space Standardisation (Standards)
EFL	Effective Focal Length

Acronym	Definition
EGSE	Electrical Ground Support Equipment
EIRP	Equivalent Isotropically Radiated Power
EM	Engineering Model
EMC	Electro Magnetic Compatibility
EMI	Electro Magnetic Interference
EoL	End of Life
EPE	External Project Events
EPS	Electrical Power Subsystem
EQM	Engineering and Qualification Model
ESOC	European Space Operations Centre
FAR	Flight Acceptance Review
FDIR	Fault Detection, Isolation and Recovery
FDV	Fill and Drain Valve
FEE	Front End Electronics
FGYR	Fine Gyro
FL	First Look
FM	Flight Model
FOG	Fibre Optic Gyro
FOS	Folding Optics Structure
FoV	Field Of View
FPA	Focal Plane Assembly
FPGA	Field Programmable Gate Array
FRR	Flight Readiness Review
FSS	Fine Sun Sensor
FVV	Fill and Vent Valve
FWC	Full Well Capacity
G/S	Ground Station
GEO	Geosynchronous Earth Orbit
GMSK	Gaussian Minimum Shift Keying
GNC	Guidance Navigation and Control
GPU	Graphical Processing Unit

Acronym	Definition
GS	Ground Segment
GSE	Ground Support Equipment
GSP	General Studies Program
HAWAII	HgCdTe Astronomical Wide Area Infrared Imager
HDRM	Hold Down and Release Mechanism
HPLV	High Pressure Latch Valve
HW	Hardware
ICU	Instrument Control Unit
IDT	Instrument Data Treatment
IGM	Inertial Guidance Mode
IMU	Inertial Measurement Unit
IQM	Inherent Quality of the cost Model
ISO	International Standard Organisation
ITU	International Telecommunications Unit
JWST	James Webb Space Telescope
L2	Lagrange Point 2
LC	Launch Campaign
LCL	Latching Current Limiter
LEO	Low Earth Orbit
LEOP	Launch and Early orbit phase
LGA	Low Gain Antenna
LoS	Line of Sight
LP	Low Pressure
LPF	Lisa Pathfinder
LPLV	Low Pressure Latch Valve
LSF	Line Spread Function
LVA	Launch Vehicle Adapter
LVDS	Lox-Voltage Differential Signalling
M2MM	Mirror 2 Moving Mechanism
M4MM	Mirror 4 Moving Mechanism
MAIT	Manufacturing Assembling Integrating Testing

Acronym	Definition
MCT	Mercury Cadmium Telluride
MEMS	Micro Electro-Mechanical Systems
MFS	Mass Flow Sensor
MIB	Minimum Impulse Bit
MIPS	Millions of Instructions Per Second
MLI	Multi-Layer Insulation
MM	Mass Memory
MMPU	Modular Medium Power Unit
MMU	Mass Memory Unit
MOC	Mission Operations Centre
MPE	Micro-Propulsion Electronics
MPPT	Maximum Power Point Tracker
MPS	Micro-Propulsion System
MPT	Micro-Propulsion Thruster
MRE	Mean Rate Error
MTF	Modulation Transfer Function
NCR	Non-Conformance Report
NIR	Near Infrared
NM	Normal Mode
NNO	New Norcia (Perth Australia)
NRV	Non Return Valve
OBC	On-Board Computer
OCDT	Open Concurrent Design Tool
OCM	Orbit Control Mode
OGS	Operational Ground Segment
OSR	Optical Solar Reflector
OTS	Off The Shelf
PA	Product Assurance
PAA	Phased Array Antenna
PCB	Printed Circuit Board
PCDU	Power Conditioning and Distribution Unit

Acronym	Definition
PDR	Preliminary Design Review
PF	Platform
PFD	Power Flux Density
PFM	Proto-Flight Model
PI	Principal Investigator
PL	Payload
PLM	Payload Module
POE	Project Owned Events
POG	Pyrolitic Oriented Graphite
PPA	Parallel Prestressed Piezo Actuator
PSA/WCA	Parts Stress Analysis/Worst Case Analysis
PSF	Point Spread Function
PSK	Phase Shift Keying (modulation)
QE	Quantum Efficiency
QIV	Quality of the Input Values
QM	Qualification Model
QPSK	Quadrature Phase Shift Keying
RCS	Reaction Control Subsystem
RCT	Reaction Control Thruster
REQ	Requirement
RF	Radio Frequency
RFDN	Radio Frequency Distribution Network
RMS	Root Mean Square
ROM	Rough Order of Merit
RPE	Relative Performance Error
RRW	Rate Random Walk
RTD	Resistance Temperature Detector
RTU	Remote Terminal Unit
RVS	Radial Velocity Spectrometer
RW	Reaction Wheel
S/C	Spacecraft

Acronym	Definition
S/S	Sub-system
S3R	Sequential Switching Shunt Regulator
SA	Solar Array
SAA	Solar Aspect Angle
SAM	Sun Acquisition Mode
SAR	Solar Array Regulator
SBM	Stand-By Mode
SDRAM	Synchronous Dynamic Random Access Memory
SED	Spectral Energy Distribution
SEE	Single Event Effect
SFCG	Space Frequency Coordination Group
SGS	Science Ground Segment
SiC	Silicon Carbide
SIDECAR	System for Image Digitization, Enhancement, Control and Retrieval
SLI	Single Layer Insulation
SM	Structural Model
SNR	Signal to Noise Ratio
SOC	Science Operations Centre
SoC	System-on-Chip
SPF	Single Point Failure
SpW	Space Wire
SRM	Survival Mode
SRR	System Requirements Review
SSCE	Sun-S/C-Earth
SSM	Second Surface Mirror
SSMM	Solid State Mass Memory
STM	Structural Thermal Model
STR	Star Tracker
SVF	Software Validation Facility
SVM	Service Module
SW	Software

Acronym	Definition
tbc	to be confirmed
tbd	to be determined
TBTV	Thermal Balance / Thermal Vacuum
TC	Telecommand
TCM	Transfer Correction Manoeuvre
TCS	Thermal Control System
TDI	Time Delayed Integration
TID	Total Ionising Dose
TM	Telemetry
TRL	Technology Readiness Level
TRP	Technology Research Program
TRSP	TRanSPonder
TSM	Transition Mode
TT&C	Tracking, Telemetry and Command
TVAC	Thermal Vacuum
UART	Universal Asynchronous Receiver Transmitter
WA	Walking Actuator

A   GAIA LESSONS LEARNT

A.1   Background & Lessons Learnt from Gaia

A.1.1   Lessons Learnt from Gaia

The design of Gaia is driven by the payload. There are two separate lines of sight, which is achieved by using two telescopes set at a fixed "basic angle", requiring an extremely accurate knowledge of this basic angle. Therefore a Basic Angle Monitoring device is required. In addition, an extremely stable environment in terms of thermal, micro-vibration and particulate contamination, is needed. These are drivers for the shape of the spacecraft and the material selection (minimise CTE using same material, avoid any mechanism, etc.).

The focal length of two the telescopes dictates the number of mirrors and folding optics structure (FOS). The scanning law and TDI read out of the CCD detectors requires a spinning spacecraft. This requires a spin symmetrical design, impacting all design aspects (e.g. communications, AOCS, propulsion). A spinner and two apertures also result in the need for a large circular sun shield around the entire S/C.


Payload Module (PLM)

In-orbit bipods decoupling the PLM from the SVM after release of the launch bipods in parallel

Some PLM electronic units are accomodated in the SVM structure:
Video **P**rocessing **U**nits
Clock **D**istribution **U**nit

The central cone is the main load path from the launcher ring interface to the PLM bipods

Service Module (SVM)
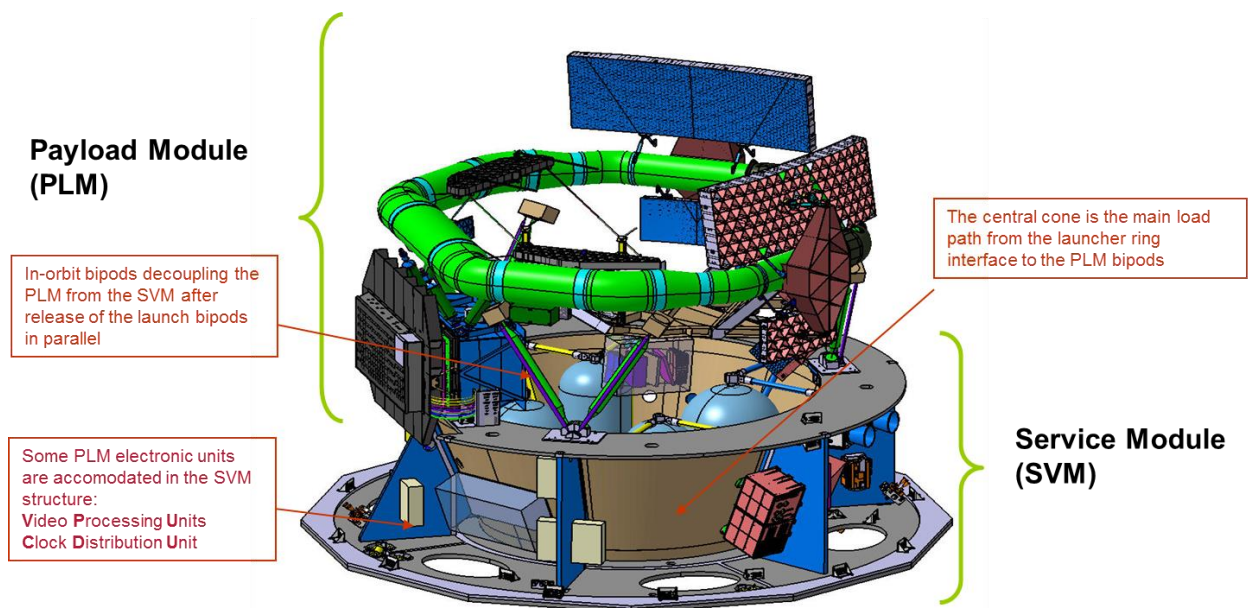
Figure A-1: Gaia SVM and PLM overview

Generic issues

At the start of the definition phase special care shall be taken of the requirement documents. They need to be of high quality and very detailed. Poorly written or unnecessary requirements can result in major cost contributors. A critical review of requirements shall be a priority in the study phase, involving project teams that have experience with similar missions.

The impact of accuracy requirements at the limits of technical capability shall not be underestimated. Verification of these requirements is very difficult and costly,

sometimes even impossible. This can be due to limitations of test facilities or environmental disturbances greater than the value to be measured.

It should be clearly planned how to test requirements that cannot be directly measured on ground. The impact of testing compromises shall be fully understood.

For mission critical performances, such as the Basic Angle Variation, an independent party shall model and verify the expected parameter's behaviour, to minimise the risk of (modelling) errors. This entails shadow engineering of the highest calibre and capability, and presumes a fully detailed sharing of engineering information between the industrial consortium, its subcontractors and ESA. A trustworthy relationship between the parties (covered by the appropriate non-disclosure agreements) must be established as a top priority from the moment of kick-off of the engineering development activities.

The Payload shall be understood as an integral part of the S/C, as Gaia is built around the payload. This understanding allows for an efficient AIT sequence rather than the more traditional PI led payload procurement: The Gaia "payload" is not a bolt on instrument that can "easily" be procured by a third party.

Optical performance

Significant straylight scattered from the edge of the deployable sunshield was unanticipated prior to launch and only discovered in flight. This has proved to be a limiting factor for the detectable in-flight stellar magnitude lower limits, in both astrometric and RVS photometric channels. The original scientific requirements cannot be met. A more thorough and co-engineering system approach is mandatory in future to avoid these types of issues. The project system engineer must ensure an adequate and thorough sharing of information and regular concurrent engineering sessions to avoid specialist experts only having visibility within their own disciplines and particular areas of responsibility. The root cause of the straylight issue on Gaia was solar illumination of nomex fibers at the edge of the MLI thermal blankets of the deployable sun shield. These fibers were known to both the thermal, optical and mechanical/mechanisms teams pre fight. But no one "joined the dots" at system level and asked was this a potential straylight problem?

A second, and also unanticipated, source of straylight was due to diffuse light from the Galactic plane scattering off the inside of the top cover of the payload thermal tent. This thermal tent inner surface is black MLI and therefore was not considered as a significant optical scattering surface in the straylight analysis. This was an unfortunate oversight. However a fortunate synergistic effect – in flight, ended up working to the advantage of mitigating the optical performance impact. Due to the low temperature of the inner surface of the top cover MLI, water ice from outgassing of the spacecraft (expected) deposited itself there, and (counterintuitively) reduced the level of scattered light towards to focal plane. This was due to the effective reduction in the specular scattering component, by the behaviour of the sublimated ice as an effective diffuser (Lambertian type). This optical scattering property was verified under vacuum conditions on representative samples in the TEC-Q laboratories of ESTEC, and this experimental proof directly enabled the decision to avoid a dangerous and risky operation of using solar illumination to bake out the inside of the roof of the thermal

tent in flight. Once again a system engineering lesson learnt – all disciplines must interact and communicate and share detailed information during all development phases of the mission.

TT&C

Early testing of transponder EM with the ESOC Ground Segment is very valuable. It enabled to identify spurious issues and problems with Gaia phase noise/GMSK demodulator in Coherent Mode.

The "RF suitcase" is best to incorporate EM of CDMU or functional breadboard to drive TRSP: rather than relying on simulated hardware, which can be very different from the actual flight hardware, it is best to use as representative hardware as possible to identify potential problems early on.

The Mission Timeline shall allow for ample margin for the tele-command capacity, especially for long autonomous operation timeline uploads. Gaia was limited to 2400 TCs, which required cumbersome workarounds in order to upload multi day sequences.

Software

The fidelity of the software validation facility (SVF) shall be improved and tests on the real HW shall be maintained, especially in those cases where the SVF lacks representativeness.

Stress tests on the SW proved a good tool to unveil operational faults or mission inefficiencies.

The traffic scenario shall be agreed early and be maintained by the project/prime with ESOC and Science involvement. The traffic scenario shall be used to drive budgets, SW design/sizing, and mission tests.

Flexibility is needed to adjust the SW development plan during the mission development.

Comprehensive end-to-end tests shall be included in the complete SW, after the incremental development, and the number of operational test scenarios shall be increased.

Thermal Control:

This shall be extensively stressed during TVAC and simulations. The TVAC shall be performed at S/C level, not only at unit or (sub)module level. The TCS shall be modelled in the SVF. Also, an Operational Simulator shall be used to maximise the results of verification and validation.

Test scenarios shall also focus on identifying wiring errors, such as swapping of heaters, etc.

Electrical

Mixing of the Low-Voltage Differential Signal (LVDS) transponder and receiver device supply voltages between units, on the same interface, shall be avoided. SpaceWire (SpW) grounding specifics shall be optimised and agreed early. Also, double insulation

shall be tackled early in the design phase and monitored throughout the development of the units and at S/C level.

The Part Stress Analysis (PSA)/Worst Case Analysis (WCA) and radiation analysis, as well as the resulting circuit provisions, shall be thoroughly reviewed and examined at PDR, or at the very latest at CDR.

An early understanding and agreement on slow power-up tests, ideally in time for EGSE specification, is beneficial.

Mechanical

The structural verification approach and the test results need to be approved by the launcher authority. An early involvement in the definition and information about possible changes is beneficial and can limit the repeating of tests. This allows timely implementation of constraints from the launcher authorities for analyses, test definition, and test results.

AOCS and Propulsion

The Gaia AOCS is innovative as it used the payload star mappers integrated into the AOCS in order to meet the very stringent AOCS requirements.

Running a real application code in a functional validation bench proved to be very useful for securing the CSW schedule.

CPS should be integrated very early on the structure which would then be delivered to the prime with hundreds of wires for the propellant lines thermal control. Later, the power sub-system responsible is supposed to connect them to the correct PCDU LCLs. If the wires are not well labelled, or if the definition of the connections is not coordinated or maintained, the connection becomes complex and time consuming.

For the MPS, the following recommendations are given:

1. Allow for cross strapping of MPEs
2. Test in operational conditions and perform long duration test to identify MFS offset drift
3. Allow for calibration in operational conditions
4. Ensure that the changes made to MPS system for Microscope, LPF and Euclid are implemented to enhance the MPS robustness

AIT:

It is of utmost importance to test in the <u>relevant</u> environment. This is also the lesson learnt from the problem encountered in Kourou. There, oscillation on the power lines was detected, once all the thrusters were operating and they could reach their operating temperature.

TBTV test scenarios shall cover the full in-flight temperature range for a sufficiently long duration. This is to ensure reaching thermal equilibrium. This will lead to on/off toggling of heaters, which can induce disturbances on the electrical system.

In the MPS case, the relevant environment should cover temperature, fluidic supplies (He vs GN), presence of the full MPS system (all thrusters connected to the electronics and operating at the same time) and presence of vacuum wherever possible.

Emphasis shall be given to operational and system wide end-to-end tests.

During AIT, support from the engineering team is crucial to ensure an efficient transfer of knowledge, treatment of NCRs and test result handling. Industry usually starts its launch campaign preparation late because many more important activities have to be completed and for S/C standard production a few months of preparation are sufficient. Launch campaign preparation of S/C prototypes for scientific missions is not comparable. To limit stress and difficulties, ESA may take the lead in starting launch campaign preparation.

Validation & Verification

It is very useful to put a working team in place on the verification matrix to ensure it is always up to date and ready to support major reviews. This was very useful for Gaia and prevented the usual inconclusive rush at CDR and FAR.

This Page Intentionally Blank

B   ON THE NEED OF A SKYMAPPER ON GAIANIR

B.1   Abstract

This document explains the roles of the Gaia Sky Mapper (SM) for on-board and on-ground processing and argues that a spinning GaiaNIR could be designed in a simpler way, without special optical provisions to enable FoV discrimination. Special data treatment on board remains, however, needed for FoV discrimination / tagging, for fine pointing performance and control (rate measurement and control, using the payload in the loop), and for window propagation of objects.

B.2   Introduction

In an attempt to reach an as-simple-as-possible design for GaiaNIR, the need of a Gaia-like Sky-Mapper (SM) function has been challenged. This note assesses the roles of the Sky Mapper in Gaia and concludes that significant simplifications could be made in a spinning GaiaNIR design.

B.3   SM in Gaia

In Gaia, a Sky Mapper functionality has been implemented (see RD[43] for details). The Sky Mapper function has three elements, one optical, one at detector level, and one at (application) software level in the Video-Processing Unit (VPU). The Sky Mapper serves both on-board functions (Section B.3.1) and on-ground functions (Section B.3.2).

B.3.1   On-Board

From the optics perspective, Gaia's Sky Mapper uses dedicated optical masks, which are located between M2 and M3 in the optical path and mechanically attached to the folding optics structure (FOS). These masks ensure that SM1 only sees light from telescope 1 and that SM2 only sees light from telescope 2. This allows unambiguous, on-board FoV discrimination: stars detected in SM1 must come from telescope 1 while stars detected in SM2 must come from telescope 2.

From the detector perspective, the Sky Mapper consists of two CCDs per CCD row (so there are 14 SM CCDs in total). These CCDs are conventionally named SM1 and SM2. Both CCDs are normal, broadband CCDs, identical to those in the main astrometric field (AF). However, these CCDs are operated differently: the SM CCDs are read out "full frame" (while still operating in TDI) while the AF CCDs are read out in window mode, reading only the areas of interest where stars are located ("windows").

The "full-frame" sample stream from the SM CCDs is processed in real time in the VPU using a mixed hardware (FPGA) – software solution. The following operations are performed on the CCD sample stream:

- FoV discrimination: this is "automatic" as a result of the optical design;
- Pre-processing for on-board operations: correct for column-response non-uniformity, dark-signal-non-uniformity, dead columns, etc.;
- Object detection and object characterisation: a thresholding algorithm finds point sources and determines their AL coordinate, AC coordinate, and background-subtracted flux (this step requires buffering the readout for several TDI lines).

For saturated samples, a special branch is active to detect bright stars. On-board object detection is a critical requirement since there is no suitable (i.e., sufficiently complete and with sufficient spatial resolution) input catalogue that could be uploaded. This applies both to Gaia and GaiaNIR;

- The algorithm also filters objects based on their PSF shape: it keeps point sources (stars) while discarding cosmic rays, solar proton events, extended sources such as galaxies, blurred moving objects, etc.;

- Priority assignment: the object priority is programmable to some degree but the default priority is based on flux (so bright stars have priority over faint ones). Prioritisation is important when scanning dense areas on the sky, in which Gaia's capability to window stars is exhausted;

- Prediction of where (AC) and when (AL) the detected star will cross the readout register of the first CCD (actually all CCDs in the focal-plane assembly) of the astrometric field (AF1). This is referred to as "window propagation". Since, as a result of the precession of the spin axis, stars generally have a small AC velocity while they traverse the focal plane (with this velocity normally being different for the two FoVs but the same within a given FoV; see Annex A), the prediction of the AC coordinate requires knowledge of the FoV. The instantaneous AC velocity used in the propagation is received from the AOCS (CSW in the CMDU).

Note: in principle, the SM CCD measurements could be used in the astrometric solution but in practice, the SM data do not carry significant astrometric weight:

1. The SM CCDs are at the edge of the FoVs and have poor optical quality (wave-front error and optical distortion);
2. They have a reduced integration time (2.8 s versus 4.4 s for AF CCDs) because of the permanent activation of a TDI gate (itself needed to limit optical distortions and to reduce the active CCD area that is sensitive to prompt-particle events that generate false detections);
3. They have reduced AL resolution: all samples are binned 2×2 pixels (AL×AC) on chip to make the real-time processing feasible;
4. They have a larger read noise (12 e- versus 5 e- for AF CCDs) because all 1966 pixels in the read-out register have to be read during the TDI line period (982.8 µs).
5. They are poorly geometrically calibrated (e.g., they do not have periodic charge injection for radiation-damage mitigation, they have a different sky background, etc.).

Therefore, it would be advantageous for GaiaNIR to replace the SM CCDs with normal, full-capability astrometric-field CCDs and ideally have them located in the superimposed part of the focal plane to collect as much source flux as possible.

In the first AF CCD (AF1), the pixels predicted to contain the light of objects detected in SM are read at the predicted moment in time. The windows that are read out are two-dimensional so that the fine centroid, both AL and AC, of the image can be determined. Combined with the SM centroid measured earlier, the actual AL and AC speed of the object is determined. These measurements are delivered at 1 Hz to the AOCS through two circular buffers (one for each FoV), each with 60 slots to allow averaging / Kalman filtering. In the AOCS, these measurements are used for AL and AC rate control. Note:

in fine-pointing mode, the Fibre-Optics Gyroscopes (FOGs) in Gaia are used only for FDIR.

The AF1 measurement (the flux in particular) is also used as object confirmation stage: in case the predicted window is empty (most likely because the SM detection was a star-like prompt-particle event; alternatively, the object could have been a fast-moving asteroid), the detection is suppressed so to not waste on-board storage space and downlink TM bandwidth. In Gaia, the fraction of non-confirmed detections is significant (~10% for class1, i.e., G = 13–16 mag, and ~20% for class 2, i.e., G = 16–21 mag). Therefore, object confirmation is a relevant requirement.

In short, the on-board needs of the SM for Gaia are to:

- Provide object detection;
- Provide object characterisation (PSF shape and flux) and prioritisation;
- Provide FoV discrimination;
- Provide window propagation through the focal plane, in particular in the AC direction (the AL propagation is directly linked to the spin rate [control] and hence "trivial");
- Provide AL and AC rate measurements to the AOCS control loop.

B.3.2   On-Ground

The SM data of detected and confirmed objects are transmitted to ground as two-dimensional windows (with reduced spatial resolution for faint stars) with a FoV tag. On ground, the 2D-nature of the SM data is used in various places in the science ground segment (e.g., the on-ground attitude reconstruction, the source environment analysis, etc.). In none of these cases, however, the (systematic) absence of 2D SM data would lead to critical problems (e.g., the attitude reconstruction is largely based on Calibration Faint Stars [CFSs] combined with the 2D AF windows of bright stars, etc.). The FoV tag, on the contrary, is crucial in the ground processing. It is used in the initial-data-treatment (IDT) cross-matching (including the new-source creation), the scientific first look (FL, in particular in the one-day iterative solution, ODAS), and in the astrometric global iterative solution (AGIS), e.g., since optics-related calibrations (e.g., PSF) are FoV dependent and since the attitude calibration requires the FoV index.

B.4   A Simpler and Better SM in GaiaNIR?

We now address the question whether – assuming that for a spinning GaiaNIR design, the Gaia SM functionality shall be maintained – it is possible to remove the SM optics and to upgrade the SM CCDs to normal AF CCDs in the superimposed part of the focal plane. This would simplify the optical design as well as improve the quality of the end-of-life astrometry through the addition of more, high-quality data.

B.4.1   On-Board

Conceptually, all required SM functionality could be achieved through on-board processing, primarily making use of the scanning-law-induced FoV-dependent AC rates at which objects transit the focal plane (see Annex A for details). The AC rate of objects can either be measured between adjacent detector transits (as used for Gaia, and assumed as baseline below) or within the transit of a single detector, assuming

intermediate, non-destructive readouts of the signal can be made (which is possible with MCT-type detectors). The following, detailed remarks can be made:

Detection, object characterisation (PSF shape and flux), and prioritisation: these aspects would work as in Gaia, requiring "full-frame" readout of the first detector strip.

Window propagation: if the full focal plane could be read as well as processed each TDI line, window propagation would not be needed. In that case, all detector data could continuously be readout "full frame" and processed to detect objects (similar to the Gaia SM data). In case on-board (CPU) resources do not allow this (which is deemed very likely), some kind of windowing is needed: the notion of an object traversing the focal plane with a given AL and AC velocity allows knowing which pixels to read at which time and suppresses the need to process these pixels on board in real time to detect objects. Since the AL window propagation is directly linked to the spin rate (control), and to first order independent of the FoV, this propagation is easy. For the AC propagation, however, a FoV dependency exists. One could then either rely on the measured AC motion of each object or on the known AC motion of the parent FoV (which is supplied by the AOCS to the VPU at 1 Hz). In the first case, the key question is whether the noise on the measured AC motion of individual objects allows sufficiently accurate AC propagation over the time it takes to cross the focal plane (for Gaia, this is ~90 s). In the second case (which is how Gaia works), the FoV tag of the object is required; this is addressed below.

Object confirmation: in case a confirmation of each detected object is required, the second detector strip could be used. Confirmation would then work very similar to Gaia, meaning that the FoV tag is needed for AC window propagation; this is addressed below.

Provision of AL and AC rate measurements to the AOCS control loop: for making rate measurements, it is highly advantageous to work with the notion of objects and associated windows since that avoids on-board cross-matching of detections from adjacent detector strips. The AL and AC rate measurements would work as in Gaia, using the measured on-board AL and AC centroid differences between (2D) star images acquired in two adjacent strips. For the AC rates to enter the correct AOCS buffer (FoV1 or FoV2), the FoV tag of each object is required; this is addressed below.

FoV tagging: as shown in Annex A, the AC rates of both FoVs are generally discrepant except for two "short" intervals during each revolution (6 hours for Gaia). For those periods, during which the AC rates are (nearly) indistinguishable, on-board FoV tagging would remain ambiguous. However, this ambiguity would neither impact the window propagation, nor the confirmation of detected objects, nor the AC rate control since the AC velocities of objects will still be estimated correctly and since FoV assignment errors during these time intervals (FoV1 instead of FoV2 and FoV2 instead of FoV1) will statistically cancel each other so that the AOCS buffers of both FoVs both remain filled with sufficient measurements. The ambiguity is of course transmitted to ground, where it needs to be resolved (see Section B.4.2). Two alternative concepts to unambiguously resolve the FoV-tag ambiguity are discussed in Annex B and Annex C. Both, however, involve "blocking of light" / using "half of the light" and therefore reduce the science performance.

We finally would like to mention an interesting possibility: intra-detector readouts. Individual pixels of "classical" MCT-type detectors (say "CMOS Hawaii-like readout circuitry") can be read out at any time during integration, in non-destructive mode. If this concept could be generalised to TDI operation (which remains to be proven), then one could conceptually perform several functions within the first detector strip. The idea would be to read the detector multiple times, for instance once per second, while the charge is building up. This would (assuming a Gaia-like integration time of 4 s) give four measurements over the first transit, the first one based on the integrated signal over the first second, the second one based on the integrated signal over the first two seconds, etc. The final 2D image, which has the highest SNR, would be used for object detection. The confirmation could be derived from the consistency in the charge build-up over time during the detector transit, both flux- and location-wise. The AL and AC motion could be derived as the slopes of two straight-line fits to the four, 2D intermediate positions. The FoV tagging would be derived from the AC velocity. Key questions that remain to be studied are whether this is technically feasible and whether the SNR of such intermediate readouts of faint sources would be sufficiently high.

B.4.2   On-Ground

As explained in Section B.4.1, on-board FoV tagging based on AC rates is reliable most of the time but leads to ambiguities during "short" intervals of time. These intervals occur twice per spin period and have known start and end times. In the science ground segment, special provision needs to be made to deal with such ambiguous-FoV data. In the IDT cross-matching and ODAS/FL, prior knowledge can be inserted to resolve ambiguous cases: by the time GaiaNIR makes it measurements, a good fraction of its targets will be known from other surveys such as Gaia, EUCLID, WFIRST, LSST, etc. This should be sufficient for the daily processing chains (IDT, FL, ODAS). For AGIS, the few affected transits can initially be discarded such that an astrometric fit can be produced for each source. The ambiguous data points can then be added, one by one, using trial and error (FoV1 or FoV2) by minimising the astrometric residuals.

B.5   Conclusions

A simplified Sky Mapper concept for GaiaNIR is feasible, which relies for FoV tagging primarily on the AC rates of the objects. During the "short", predicted intervals of time where such a tagging gives ambiguous FoV identification, on-board processing (in particular window propagation) and attitude (rate) control is not affected. On-ground processing can deal with such ambiguities, without data loss or degradation, but at the expense of improved complexity of the science ground segment.

This Page Intentionally Blank

C GAIANIR TELESCOPE OPTICAL DESIGN RAY TRACE PRESCRIPTION (CODE-V)

Gaianir_shift

```
            RDY              THI      RMD        GLA        CCY  THC  GLC
 OBJ:      INFINITY        INFINITY                         100  100
   1:      INFINITY        0.000000                         100  100
     SLB: "Ref"
   2:      INFINITY        0.000000  REFL                   100  100
     SLB: "Dummy"
     XDE:   0.000000  YDE:   0.000000  ZDE:   0.000000  BEN
     XDC:    100       YDC:    100     ZDC:    100
     ADE:   0.000000  BDE:  22.500000  CDE:   0.000000
     ADC:    100       BDC:    100     CDC:    100


   3:      INFINITY      -2500.000000                       100  100
 STO:      INFINITY        0.000000                         100  100
     SLB: "Stop"
     XDE:   0.000000  YDE: 300.000000  ZDE:   0.000000  DAR
     XDC:    100       YDC:    100     ZDC:    100
     ADE:   0.000000  BDE:   0.000000  CDE:   0.000000
     ADC:    100       BDC:    100     CDC:    100


   5:      INFINITY        0.000000  REFL                   100  100
     SLB: "Flat"
     ASP:
     K  :   0.000000  KC :    100
     CUF:   0.000000  CCF:    100
     A  :0.000000E+00  B  :0.000000E+00  C  :0.000000E+00  D  :0.000000E+00
     AC :    100       BC :    100     CC :    100     DC :    100
     XDE:   0.000000  YDE:   0.000000  ZDE:   0.000000  BEN
     XDC:    100       YDC:    100     ZDC:    100
     ADE:   0.000000  BDE: -22.500000  CDE:   0.000000
     ADC:    100       BDC:    100     CDC:    100


   6:      INFINITY        0.000000                         100  100
   7:      INFINITY        0.000000                         100  100
     SLB: "Flat+1"
   8:      INFINITY      2500.000000                        100  100
   9:    -5880.00000    -2480.000000  REFL                  100  100
     SLB: "M1"
```

```
    ASP:
    K  :  -0.983957   KC :       0
    CUF:   0.000000   CCF:     100
    A :0.000000E+00   B :0.000000E+00   C :0.000000E+00   D :0.000000E+00
    AC :     100      BC :     100      CC :     100      DC :     100


10:    -1404.00000    1226.000000  REFL                       100   100
    SLB: "M2"
    ASP:
    K  :  -3.906141   KC :       0
    CUF:   0.000000   CCF:     100
    A :0.000000E+00   B :0.000000E+00   C :0.000000E+00   D :0.000000E+00
    AC :     100      BC :     100      CC :     100      DC :     100


11:       INFINITY     0.000000                              100   100
12:       INFINITY  1285.000000                              100   100
    SLB: "Pickup"
    XDE:   0.000000   YDE:    0.000000   ZDE:    0.000000   BEN
    XDC:      100     YDC:      100      ZDC:      100
    ADE:   0.000000   BDE:    0.000000   CDE:    0.000000
    ADC:      100     BDC:      100      CDC:      100


13:    -1894.00000   -1375.005853  REFL                       100   100
    SLB: "M3"
    ASP:
    K  :  -0.608476   KC :       0
    CUF:   0.000000   CCF:     100
    A :0.000000E+00   B :0.000000E+00   C :0.000000E+00   D :0.000000E+00
    AC :     100      BC :     100      CC :     100      DC :     100


14:       INFINITY    27.856685                              100   100
15:       INFINITY     0.000000                              100   100
    XDE:   0.000000   YDE:    0.000000   ZDE:    0.000000
    XDC:      100     YDC:      100      ZDC:      100
    ADE:  -0.354350   BDE:    0.000000   CDE:    0.000000
    ADC:      100     BDC:      100      CDC:      100


>  16:       INFINITY     0.000000  REFL                       100   100
    SLB: "Fold1"
    XDE:   0.000000   YDE:    0.000000   ZDE:    0.000000   DAR
    XDC:      100     YDC:      100      ZDC:      100
    ADE:   0.000000   BDE:    9.900000   CDE:    0.000000
    ADC:      100     BDC:      100      CDC:      100
```

```
17:       INFINITY       0.000000                          100    100
   XDE:   0.000000  YDE:   0.000000  ZDE:   0.000000
   XDC:   100       YDC:   100       ZDC:   100
   ADE:   0.354350  BDE:   0.000000  CDE:   0.000000
   ADC:   100       BDC:   100       CDC:   100


18:       INFINITY     200.000000                          100    100
   XDE:   0.000000  YDE:   0.000000  ZDE:   0.000000
   XDC:   100       YDC:   100       ZDC:   100
   ADE:   0.000000  BDE:   0.000000  CDE:   0.000000
   ADC:   100       BDC:   100       CDC:   100


19:       INFINITY       0.000000                          100    100
   XDE:   0.000000  YDE:   0.000000  ZDE:   0.000000  DAR
   XDC:   100       YDC:   100       ZDC:   100
   ADE:   0.000000  BDE:   0.000000  CDE:   0.000000
   ADC:   100       BDC:   100       CDC:   100


20:       INFINITY       3.946592                          100      0
   XDE:   0.000000  YDE:   0.000000  ZDE:   0.000000
   XDC:   100       YDC:   100       ZDC:   100
   ADE:   0.000000  BDE:  20.000000  CDE:   0.000000
   ADC:   100       BDC:   100       CDC:   100


21:       INFINITY    1305.556107                          100      0
   XDE:   0.000000  YDE:   0.000000  ZDE:   0.000000
   XDC:   100       YDC:   100       ZDC:   100
   ADE:   0.000000  BDE:   0.000000  CDE:   0.000000
   ADC:   100       BDC:   100       CDC:   100


22:       INFINITY   -2003.219029   REFL                   100    100
   SLB:  "Fold2"
   XDE:   0.000000  YDE:   0.000000  ZDE:   0.000000  BEN
   XDC:   100       YDC:   100       ZDC:   100
   ADE:  -2.000000  BDE:  12.000000  CDE:   0.000000
   ADC:   100       BDC:   100       CDC:   100


23:       INFINITY      -4.861247                          100      0
IMG:      INFINITY       0.000000                          100    100
   XDE:   0.000000  YDE:   0.000000  ZDE:   0.000000  DAR
   XDC:   100       YDC:   100       ZDC:   100
   ADE:   0.841480  BDE:  -0.000829  CDE:   0.000000
```

```
      ADC:        0    BDC:        0    CDC:      100
```

SPECIFICATION DATA

```
   EPD    1600.00000
   DIM          MM
   WL        900.00
   REF           1
   WTW           1
   INI         ies
```

XAN	0.31800	0.31800	0.31800	0.00000	0.00000
	0.00000	-0.31800	-0.31800	-0.31800	0.01800
YAN	0.00000	0.23500	0.47000	0.00000	0.23500
	0.47000	0.00000	0.23500	0.47000	0.00000
WTF	1.00000	1.00000	1.00000	1.00000	1.00000
	1.00000	1.00000	1.00000	1.00000	1.00000
VUX	0.00000	0.00000	0.00000	0.00000	0.00000
	0.00000	0.00000	0.00000	0.00000	0.00000
VLX	0.00000	0.00000	0.00000	0.00000	0.00000
	0.00000	0.00000	0.00000	0.00000	0.00000
VUY	0.00000	0.00000	0.00000	0.00000	0.00000
	0.00000	0.00000	0.00000	0.00000	0.00000
VLY	0.00000	0.00000	0.00000	0.00000	0.00000
	0.00000	0.00000	0.00000	0.00000	0.00000
POL	N				

APERTURE DATA/EDGE DEFINITIONS

```
   CA APE
   REX S4            800.000000
   REY S4            125.000000
   REX S5            875.000000
   REY S5            125.000000
   ADY S5            300.000000
   REX S9            800.000000
   REY S9            270.000000
   ADY S9            435.000000
   REX S10           165.000000
   REY S10            65.000000
   ADY S10            80.000000
   REX S13           200.000000
   REY S13           120.000000
   REX S16            95.000000
   REY S16            35.000000
```

```
ADY S16                -45.000000
REX S22                160.000000
REY S22                120.000000
ADX S22                -80.000000
ADY S22               -120.000000
REX S24                250.000000
REY S24                200.000000
ADX S24                -69.000000
ADY S24               -186.000000


No refractive materials defined in system


No solves defined in system


No pickups defined in system



ZOOM DATA

                        POS 1        POS 2        POS 3        POS 4        POS 5        POS 6


  BDE S2            22.50000     -22.50000      22.50000     -22.50000      22.50000     -22.50000
  BDC S2                 100          100           100          100           100          100
  YDE S4           300.00000     570.00000     300.00000     570.00000     300.00000     570.00000
  YDC S4                 100          100           100          100           100          100
  BDE S5           -22.50000      22.50000     -22.50000      22.50000     -22.50000      22.50000
  BDC S5                 100          100           100          100           100          100
  ADY S5           300.00000     570.00000     300.00000     570.00000     300.00000     570.00000
  BDE S16            9.90000       9.90000      10.10000      10.10000      10.00000      10.00000
  BDC S16                100          100           100          100           100          100


   This is a non-symmetric system.  If elements with power are

   decentered or tilted, the first order properties are probably

   inadequate in describing the system characteristics.




         POS 1      POS 2      POS 3      POS 4      POS 5      POS 6

INFINITE CONJUGATES

   EFL    35173.0197 35173.0197 35173.0197 35173.0197 35173.0197 35173.0197

   BFL       7.2458     7.2458     7.2458     7.2458     7.2458     7.2458

   FFL    -0.3504E+06-0.3504E+06-0.3504E+06-0.3504E+06-0.3504E+06-0.3504E+06

   FNO     -21.9831   -21.9831   -21.9831   -21.9831   -21.9831   -21.9831

   IMG DIS  -4.8612    -4.8612    -4.8612    -4.8612    -4.8612    -4.8612
```

```
    OAL     -1809.8655  -1809.8655  -1809.8655  -1809.8655  -1809.8655  -1809.8655


PARAXIAL IMAGE

    HT          0.0000      0.0000      0.0000      0.0000      0.0000      0.0000

    ANG         0.0000      0.0000      0.0000      0.0000      0.0000      0.0000


ENTRANCE PUPIL

    DIA      1600.0000   1600.0000   1600.0000   1600.0000   1600.0000   1600.0000

    THI      2500.0000   2500.0000   2500.0000   2500.0000   2500.0000   2500.0000


EXIT PUPIL

    DIA       159.4623    159.4623    159.4623    159.4623    159.4623    159.4623

    THI      3512.7275   3512.7275   3512.7275   3512.7275   3512.7275   3512.7275

    STO DIA  1600.0000   1600.0000   1600.0000   1600.0000   1600.0000   1600.0000
```